U.PORTO

DOUTORAMENTO

PROGRAMA GRADUADO EM ÁREAS DA BIOLOGIA BÁSICA E APLICADA (GABBA)

Mechanisms regulating myonuclear positioning and its impact on muscle function

Mafalda Azevedo

D

2020

U.PORTO

Mafalda Azevedo. Mechanisms regulating myonuclear positioning and its impact on muscle function

D.ICBAS **2020**

Mechanisms regulating myonuclear positioning and its impact on muscle function

Mafalda Azevedo

SEDE ADMINISTRATIVA

INSTITUTO DE CIÊNCIAS BIOMÉDICAS ABEL SALAZAR

FACULDADE DE CIÊNCIAS

FACULDADE DE MEDICINA

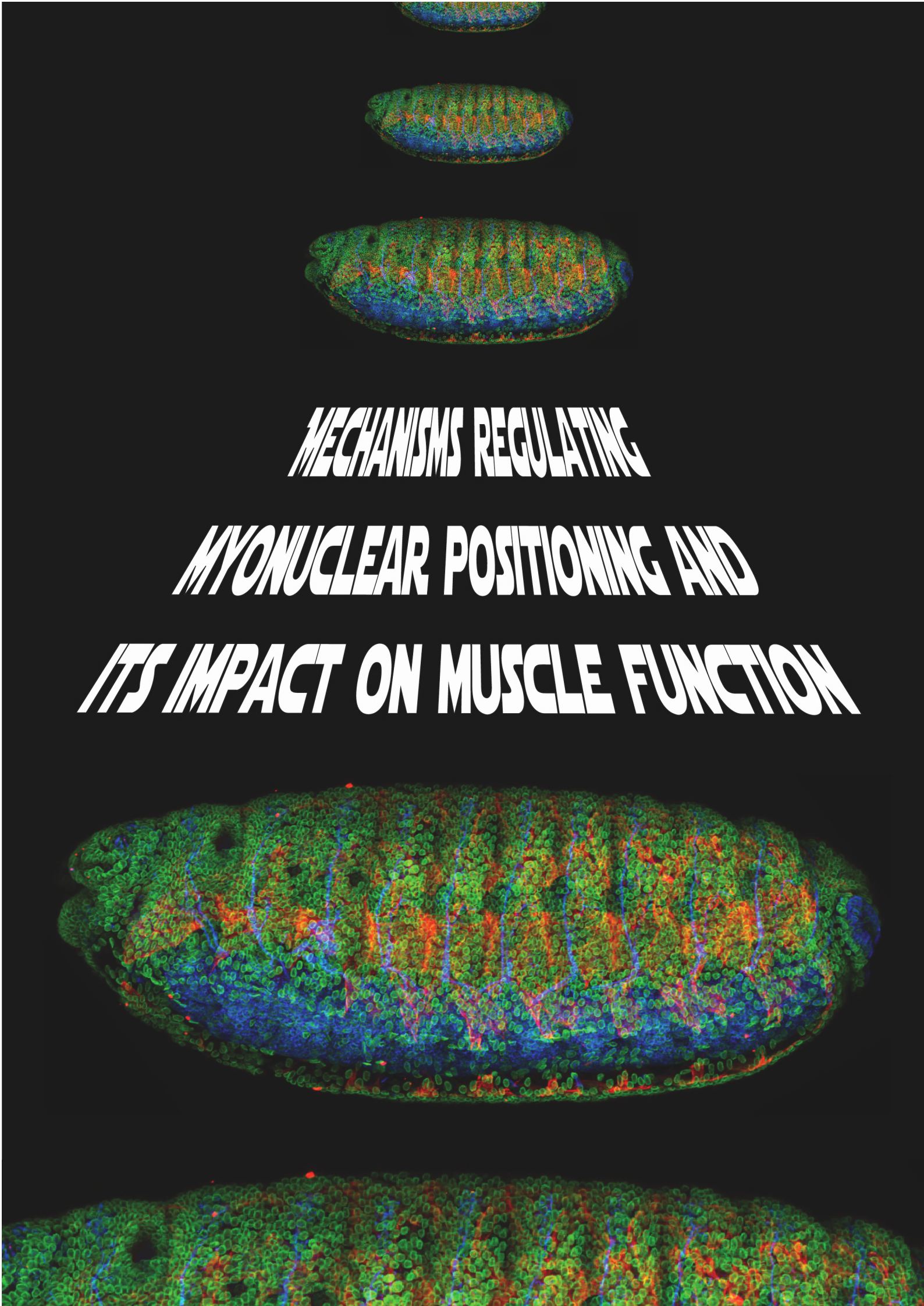
MAFALDA MARIA COELHO AZEVEDO

MECHANISMS REGULATING MYONUCLEAR POSITIONING AND ITS IMPACT ON MUSCLE FUNCTION

Tese de Candidatura ao grau de Doutor em Áreas da Biologia Básica e Aplicada submetida ao Instituto de Ciências Biomédicas Abel Salazar da Universidade do Porto.

Orientador – Mary K. Baylies
Categoria – Professora Catedrática
Afiliação – Memorial Sloan Kettering Cancer Center e Weill Cornell Graduate School of Medical Sciences, Cornell University

Coorientador – Hélder Maiato
Categoria – Investigador Coordenador
Afiliação – Instituto de Biologia Molecular e Celular/Instituto de Investigação e Inovação em Saúde, Universidade do Porto



MECHANISMS REGULATING MYONUCLEAR POSITIONING AND ITS IMPACT ON MUSCLE FUNCTION

This work was conducted at the Memorial Sloan Kettering Cancer Center, New York, NY, USA.



Mafalda Azevedo was supported by a fellowship (SFRH/BD/52041/2012) awarded by the Doctoral Program in Basic and Applied Biology (GABBA) of the Abel Salazar Institute of Biomedical Sciences, University of Porto and funded by the Portuguese Foundation of Science and Technology (FCT). This work was funded by grants from the National Institutes of Health (NIH [GM078318, AR108981]) and National Cancer Institute (P30 CA 008748).











Acknowledgements

First and foremost, I would like to thank Mary Baylies for welcoming me in her lab and for being an inspiring role model as a scientist. Thank you for everything you taught me and for helping grow as a scientist and as a person. I am very glad I had you as my mentor and supervisor.

I would like to thank Helder Maiato for agreeing to be my co-supervisor, letting me join his lab for a few months while I waited for a visa and allowing me to have a little fly bay there. Thank you for all the support.

A special thanks to the GABBA family. Firstly, to the GABBA scientific committee for accepting me in the program and allowing me to have this fantastic opportunity. Secondly, a big thank you to everyone in the 16th edition of GABBA – Ana Luísa Neves, André Sousa, Catarina Seabra, Iliona Wolfowicz, Joana Nabais, Lara Cravo, Paula Voabil, Raquel Sousa, Ricardo Sousa, Samuel Chiquita e Vera Lemos – for all the amazing support throughout the years.

To my true mentor in the lab and friend, Jon Rosen, thank you! I am deeply grateful for everything I learned from you, thank you for your endless patience, your friendship and for always inviting me to spend Thanksgiving with your family.

Thank you to all the past and present members of the Baylies lab and in special to my Iberian half, Carol, for making me roll my eyes so many times and for being an amazing friend and labmate. Thank you for all the fun times, in lab or not, for always wanting to go to karaoke and have a great time. Thank you, Steffi, for the great science discussions, for teaming up with me to keep things organized, for your friendship and for all the help you have been giving me with the final experiments. To David, a big thank you for all the interesting discussions we've had over the years, for helping me so much during my project and for all the great parties. Silvia and Rishi are not official members of the lab, but it is almost as if they were. Rishi, I am very thankful for your help with my project and for always keeping the plants happy. To Silvia, I am incredibly grateful I met you and became such good friends with you. Thank you for everything, for always being there, for all the support you have given me and for all the good times and conversations we had.

To my Portuguese community in New York, in special to Ana Vasconcelos, Rita Nobre, Marlene Quintas and Daniela Freitas, for always being there in the good and not-so-good moments, and for making home feel a little less far.

To the little family I got to keep from my time at IPATIMUP, Patrícia Oliveira, Diana Martins, Catarina Salgado, Rita Nobre (again!), Ana Justino and Bárbara Sousa, for helping me keep my sanity in moments of need, for always being available to help, for all the friendship and sushi eating.

To my amazing friends Ana Cunha, Flávia Martins, Mónica Carvalho, Susana Pereira and Maria João Saraiva, thank you for so many years of laughter, friendship and good times. Thank you so much for always listening, for always supporting me, for being optimistic and for being present even when an ocean was in between us.

To Adam Paré for the unconditional support, love, friendship and patience.

Lastly, I would like to thank my family, especially my Parents, my brothers and my grandparents, for believing in me and supporting me at all times. I am eternally grateful for everything you have done for me, not only during the PhD, but during my whole life.

Por último, gostaria de agradecer à minha família, em especial aos meus Pais, aos meus irmãos e aos meus avós, por acreditarem em mim e me terem apoiado sempre. Estou-vos eternamente grata por tudo o que fizeram por mim, não só durante o doutoramento, mas ao longo da minha vida.

Table of Contents

Summary ..... **xi**

Resumo xiii

List of publications xv

List of abbreviations xvii

Chapter 1 - General Introduction **19**

Part I - Acting on identity: myoblast fusion and the formation of the syncytial muscle fiber *21*

Abstract 23

Introduction 25

Preparing for fusion: specification of muscle cells 27

Making larval muscle: myoblast fusion in the drosophila embryo 31

Making adult muscle: myoblast fusion in the drosophila pupa 39

Making muscle in vertebrates: myoblast fusion 41

Conclusion 45

Part II - Getting into position: nuclear movement in muscle cells *47*

Abstract 49

The nucleus in skeletal muscle 51

Myonuclear positioning 55

Box 1 69

Outstanding questions 71

Concluding remarks 73

Chapter 2 - Goals **75**

Chapter 3 - General Materials and Methods **79**

Imaging approaches to investigate myonuclear positioning in Drosophila *81*

Abstract 83

Introduction 85

Materials 89

Methods 95

Notes 107

Chapter 4 - Results **109**

Part I - Robo1 regulates myoblast fusion and myonuclear positioning independently of its ligand Slit *111*

Introduction 113

Materials and methods 117

Results 123

Discussion 143

Future perspectives 149

Part II - The Drosophila *Ninein homologue Bsg25d cooperates with Ensconsin in myonuclear positioning* *151*
Abstract 153
Introduction 155
Materials and methods 159
Results 167
Discussion 183
Supplemental material 189
Part III - Additional unpublished results *197*

Chapter 5 - Final Remarks **209**
Summary of findings *211*
Conclusions *213*

Bibliography **215**

Annex - Publications **237**

SUMMARY

Skeletal muscle cells are syncytial cells that attach to tendon cells via the myotendinous junction for proper function. Muscle cells acquire nuclei via several rounds of myoblast fusion events. The multiple nuclei within myofibers are distributed evenly along the periphery of the muscle cell. The positioning of myonuclei within the cell is a dynamic process, that depends on the cell's fate and developmental stage, and that is adjusted for optimal cell function. This pattern is established in embryonic myotubes, where myonuclei move via microtubules and microtubule-associated proteins to achieve their distribution. Improper positioning of myonuclei is often associated with muscle dysfunction and disease. Several mechanisms required for regulating myoblast fusion and nuclear position have been identified using the fruit fly, *Drosophila melanogaster*. The conservation of the myofiber between the fly and vertebrates, the availability of advanced genetic tools, and the ability to visualize dynamic processes using fluorescent proteins *in vivo* makes the fly an excellent system to study these mechanisms.

In this Thesis, in Chaper 1 (General Introduction) we start by extensively reviewing the mechanisms that regulate myoblast fusion and myonuclear positioning. In Chapter 3 (General Materials and Methods) we describe the tools and techniques used to investigate myonuclear positioning and muscle function in the *Drosophila* embryo and larva.

To achieve Goal 1 described on Chapter 2 (Goals) of analyzing the input of tendon cells in myonuclear movement and positioning, in Part I of Chapter 4 (Results) we investigate the role of muscle-tendon interactions in aspects of intracellular muscle organization, such as myonuclear positioning, by focusing on the Slit-Robo pathway. We describe two novel roles for Robo1 in *Drosophila* myogenesis and show that *robo1* is involved both in regulating myoblast fusion and myonuclear positioning in the LT muscles in a Slit-independent fashion. In embryos lacking *robo1*, fusion events take longer, actin foci have less actin, the LTs contain fewer nuclei, and LT myonuclei are mispositioned. We also investigated the possibility of an interaction of Robo1 with known regulators of myonuclear positioning and showed that Robo1 does not participate in the cortical pulling pathway. Moreover, we describe a setback and the measures we took to overcome that. Nevertheless, the main conclusions mentioned above remain valid.

For our Goal 2, we were interested in exploring the impact of myonuclear positioning on cytoskeletal organization and muscle structure and function by analyzing mutants with myonuclear positioning defects and assessing larval muscle organization and locomotion. In Part II of Chapter 4 (Results), we describe the mechanistic interaction of Ensconsin and Bsg25D, which defines a novel relationship between these two proteins. Loss of *Bsg25D* enhances myonuclear positioning defects in embryos sensitized by partial Ens loss. Bsg25D overexpression results in severe positioning defects in immature myotubes and fully differentiated myofibers, with the presence of ectopic microtubule organizing centers, disrupts astral microtubules, reduces muscle stiffness, and decreases larval crawling velocity. We show that misexpression of Bsg25D disrupts the microtubule cytoskeleton organization, with disastrous consequences for myonuclear positioning and muscle function.

Lastly, we present preliminary data on genes that were analyzed during the course of the graduate studies and provide future directions for the next experiments.

Our data sheds light into the importance of muscle-tendon interactions during muscle development, as well as the proper organization of the microtubule cytoskeleton for optimized muscle function. Further studies in this field to identify new players required for myoblast fusion and myonuclear positioning will provide valuable insight into the mechanisms that regulate these processes.

RESUMO

As células do músculo esquelético são sincícios que se ligam às células do tendão para o funcionamento muscular adequado. As células do músculo adquirem núcleos através de vários ciclos de eventos de fusão de mioblastos. Os múltiplos núcleos nas fibras musculares são distribuídos uniformemente ao longo da periferia da célula. O posicionamento dos núcleos é um processo dinâmico que depende do estadio de desenvolvimento da célula e é ajustado para um funcionamento celular ideal. Este padrão é estabelecido nos miotubos embrionários, onde os mionúcleos se movem por acção dos microtúbulos e proteínas associadas para obter sua distribuição final. O posicionamento inadequado dos mionúcleos está frequentemente associado a disfunção e doenças musculares. Vários mecanismos necessários para regular a fusão de mioblastos e a posição nuclear foram identificados usando a mosca da fruta, *Drosophila melanogaster*. A conservação da miofibra entre a mosca e os vertebrados, a disponibilidade de ferramentas genéticas avançadas e a capacidade de visualizar processos dinâmicos utilizando proteínas fluorescentes *in vivo* tornam a mosca um excelente sistema para estudar esses mecanismos.

Nesta Tese, no Capítulo 1 (Introdução Geral), começamos por rever extensivamente os mecanismos que regulam a fusão de mioblastos e o posicionamento mionuclear. No Capitulo 3 (Materiais e Métodos Gerais) descrevemos as ferramentas e técnicas utilizadas para investigar o posicionamento mionuclear e a função muscular no embrião e larva de *Drosophila*.

Para atingir o Objetivo 1 descrito no Capitulo 2 (Objectivos) de analisar a acção dos tendões no movimento e posicionamento mionucleares, na Parte I do Capítulo 4 (Resultados) investigamos o papel das interacções músculo-tendão na organização intracelular do miotubo, particularmente no que toca ao posicionamento mionuclear com foco na via de sinalização Slit-Robo. Descrevemos duas novas funções para o Robo1 durante a miogénese na *Drosophila*. Demonstramos que o Robo1 está envolvido tanto na regulação da fusão de mioblastos quanto no posicionamento nuclear nos músculos LT de maneira independente do Slit. Em embriões sem Robo1, a fusão de mioblastos demora mais tempo, os focos de actina têm menos actina, os músculos LT contêm menos núcleos e os mionúcleos estão incorrectamente posicionados. Também investigamos a possibilidade da interação do Robo1 com conhecidos reguladores do posicionamento mionuclear e demonstramos que o Robo1 não participa nas mesmas vias de sinalização já descritas. Além disso, descrevemos

um contratempo e as medidas que adoptámos para o ultrapassar. No entanto, as principais conclusões mencionadas permanecem válidas.

Para cumprir o Objetivo 2, estávamos interessados em explorar o impacto do posicionamento mionuclear na organização do citoesqueleto e na estrutura e função muscular, através da análise de mutantes com defeitos no posicionamento mionuclear e avaliação da organização e função do músculo da larva. Na Parte II do Capítulo 4 (Resultados), descrevemos o mecanismo de interacção do Ensconsin e do Bsg25D, definindo uma nova relação entre estas duas proteínas. A perda de Bsg25D aumenta os defeitos de posicionamento mionuclear nos embriões sensibilizados pela perda parcial de Ensconsin. A sobreexpressão de Bsg25D resulta em graves defeitos de posicionamento nos miotubos e miofibras, que manifestam a presença de centros organizadores de microtúbulos ectópicos, sem microtúbulos astrais, com rigidez muscular reduzida e diminuição da mobilidade da larva. Demonstramos que a expressão incorreta de Bsg25D desregula a organização dos microtúbulos, com consequências desastrosas para o posicionamento mionuclear e a função muscular.

Por fim, apresentamos dados preliminares sobre genes que foram analisados durante o doutoramento e fornecemos orientações futuras para as próximas experiências.

Os nossos dados revelam a importância das interacções músculo-tendão durante o desenvolvimento muscular, assim como da correcta organização do citoesqueleto para o bom funcionamento dos músculos. Estudos futuros com o objectivo de identificar novas proteínas envolvidas na fusão de mioblastos e no posicionamento nuclear vão, por certo, trazer conhecimento valioso acerca dos mecanismos responsáveis por regular estes processos.

Publications included in this Thesis (in order of appearance):

Deng, S., Azevedo, M. and Baylies, M., 2017. *Acting on identity: Myoblast fusion and the formation of the syncytial muscle fiber*, **Semin. Cell Dev. Biol.**; 72:45–55. doi:10.1016/j.semcdb.2017.10.033.

Azevedo, M. and Baylies, M.K., 2020. *Getting into position: nuclear movement in muscle cells.* **Trends in Cell Biology**, *accepted*.

Azevedo, M., Schulman, V.K., Folker, E., Balakrishnan, M. and Baylies, M., 2016. "Imaging Approaches to Investigate Myonuclear Positioning in *Drosophila*". *The Nuclear Envelope: Methods and Protocols.* Ed. Shackleton, S., Ed. Collas, P., Ed. Schirmer, E.C. New York: Springer. 1411:291-312. doi:10.1007/978-1-4939-3530-7.

Rosen, J.N., Azevedo, M., Soffar, D.B., Boyko, V.P., Brendel, M.B., Schulman, V.K., Baylies, M.K., 2019. *The* Drosophila *Ninein homologue Bsg25D cooperates with Ensconsin in myonuclear positioning*, **J. Cell Biol.** 218:524–540. doi:10.1083/jcb.201808176.

Other manuscripts to which the candidate contributed during the doctoral work:

Manhart, A., Azevedo, M., Baylies, M. and Moligner, A., *Reverse engineering forces responsible for dynamic clustering and spreading of multiple nuclei in developing muscle cells*. Submitted to **Molecular Biology of the Cell**.

AEL	After Egg Laying
AFM	Atomic Force Microscopy
AMP	Adult Muscle Progenitor
ARIH1	Homolog of *Ari-1*
BSA	Bovine Serum Albumin
CNM	Centronuclear Myopathy
CRISPR	Clustered Regularly Interspaced Short Palindromic Repeats
DFM	Direct Flight Muscle
DLM	Dorsal Longitudinal Muscle
DNA	Deoxyribonucleic acid
DO	Dorsal Oblique
DVM	Dorsal-Ventral Muscle
ECM	Extracellular Matrix
EDMD	Emery-Dreifuss Muscular Dystrophy
FC	Founder Cell
FCM	Fusion Competent Myoblast
GEF	Guanine nucleotide Exchange Factor
GFP	Green Fluorescent Protein
IFM	Indirect Flight Muscle
INM	Inner Nuclear Membrane
KASH	Klarsicht, Anc-1 and Syne Homology
LINC	Linker of The Nucleoskeleton and Cytoskeleton
LT	Lateral Transverse
MAP	MT-associated Protein
MRF	Myogenic Regulatory Factor
MTJ	Myotendinous Junction
MTOC	Microtubule Organizing Center
MT	Microtubule
NE	Nuclear Envelope
NM-MHC-IIA	Non-muscle Myosin IIA
NMJ	Neuromuscular Junction
NPC	Nuclear Pore Complex
NPF	Nucleation-promoting Factor
ONM	Outer Nuclear Membrane
PBS	Phosphate-buffered Saline
PFA	Paraformaldehyde
PNS	Perinuclear Space
RTK	Receptor Tyrosine Kinase
SH	*src* Homology
SMC	Smooth Muscle Cell
SR	Sarcoplasmic Reticulum
SUN	Sad1 and Unc-84
UAS	Upstream Activation Sequence
VCA	Verprolin, cofilin, acidic
VL	Ventral Longitudinal
WASp	Wiskott-Aldrich Syndrome protein
WBD	WASp-binding Domain
WH1	WASp Homology-1
WRC	WAVE/SCAR Regulatory Complex

Chapter 1
General Introduction

Part I. Acting on Identity: Myoblast Fusion and the Formation of the Syncytial Muscle Fiber

Part II. Getting into position: myonuclear movement in muscle cells

Part I

ACTING ON IDENTITY: MYOBLAST FUSION AND THE FORMATION OF THE SYNCYTIAL MUSCLE FIBER

Su Deng[1], Mafalda Azevedo[1,2], Mary Baylies[1]

[1]Program in Developmental Biology, Sloan Kettering Institute, New York, NY 10065, United States
[2]Graduate Program in Basic and Applied Biology (GABBA), Institute of Biomedical Sciences Abel Salazar, University of Porto, Porto, Portugal

Seminars in Cell & Developmental Biology 2017 Vol. 72 45-55

ABSTRACT

The study of *Drosophila* muscle development dates back to the middle of the last century. Since that time, *Drosophila* has proved to be an ideal system for studying muscle development, differentiation, function, and disease. As in humans, *Drosophila* muscle forms via a series of conserved steps, starting with muscle specification, myoblast fusion, attachment to tendon cells, interactions with motor neurons, and sarcomere and myofibril formation. The genes and mechanisms required for these processes share striking similarities to those found in humans. The highly tractable genetic system and imaging approaches available in *Drosophila* allow for an efficient interrogation of muscle biology and for application of what we learn to other systems. In this article, we review our current understanding of muscle development in *Drosophila*, with a focus on myoblast fusion, the process responsible for the generation of syncytial muscle cells. We also compare and contrast those genes required for fusion in *Drosophila* and vertebrates.

INTRODUCTION

From *Drosophila* to human, skeletal muscles develop and mature through similar steps: cells of the mesoderm are first specified to be skeletal muscle cells, which then undergo cell–cell fusion to add mass to these cells. After fusion is completed, sarcomeres assemble to provide contractile force, and the muscle cell builds connections with its surrounding tissues, such as tendons and motor neurons. Many of the genes that are critical for these steps are conserved across species. This also holds true for *nautilus*, which is the fly ortholog of vertebrate MYOD and a key regulator of myogenic differentiation in *Drosophila* ([1]; reviewed by [2]). As discussed below, Nautilus interacts with other transcription and chromatin regulators, and determines muscle identity, morphology, and size (reviewed in [3]).

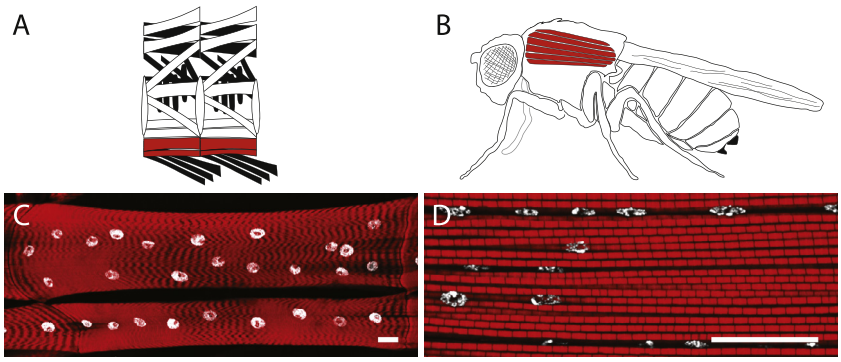


Figure 1.1.1 – Larval and adult *Drosophila* muscles. A) Schematic representation of the larval muscles. The Ventral Longitudinal (VL) muscles 3 (top) and 4 (bottom) are highlighted in red. **B)** Schematic representation of the adult muscles. The Dorsal Longitudinal Muscles (DLMs) that compose the major portion of the Indirect Flight Muscles are highlighted in red. **C)** Representative image of the 3rd instar larval VL muscles 3 and 4. **D)** Representative image of the DLMs where it is possible to observe multiple myofibrils and nuclei. **C** and **D)** Actin labeling in sarcomere, red; Nuclei, white. Scale bars, 25 μm.

During *Drosophila*'s life cycle, two periods of myoblast fusion occur to form the larval muscle system and adult muscle system, respectively (Fig. 1.1.1). The larval body wall muscles form during the embryonic stage. These muscles have been intensively studied as they represent muscle at its simplest: a single muscle fiber forms a single muscle. The adult muscle system forms during the pupal stage of development. In contrast to the larva, each single adult muscle is composed of multiple muscle fibers and thus more closely resembles the muscle organization found in vertebrate skeletal muscle (reviewed by [3,4]). This pertains in particular to the indirect flight muscles, the largest and best-studied muscle set of the adult fly. In

this review, we first give a brief overview of muscle specification (Fig. 1.1.2) and then focus on a discussion of the current studies in myoblast fusion both in *Drosophila* (Fig. 1.1.3, Table 1.1.1) and vertebrates (Table 1.1.2).

PREPARING FOR FUSION: SPECIFICATION OF MUSCLE CELLS

Muscle specification in the *Drosophila* embryo forms the larval muscles

The body wall or skeletal muscles are derived from somatic (*Drosophila*) or paraxial (mammals) mesoderm, respectively. In *Drosophila*, the allocation of somatic mesoderm depends on the communication between the mesoderm and the ectoderm [5–7], as well as the combination of transcription factors that are expressed in the mesoderm (reviewed in Baylies [3,8]). After the allocation of the somatic mesoderm, the bHLH protein Lethal of Scute (L'sc) is expressed in clusters of promuscle cells (Fig. 1.1.2A), under the control of the Receptor Tyrosine Kinase (RTK) pathway [9]. In each cluster, a combination of the Notch and RTK- Ras signaling pathway activities restricts the expression of L'sc to one cell—the muscle progenitor cell (Fig. 1.1.2B, C) [9–11]. Each progenitor cell then undergoes an asymmetric division to form either two founder cells (FC) or a single FC and an adult muscle progenitor (AMP) (Fig. 1.1.2D) [12,13]. The cytoplasmic membrane-associated protein Numb plays a critical role in determining muscle fate. Numb antagonizes Notch-mediated lateral inhibition and allows the expression of muscle identity proteins in the muscle progenitor cells [13]. Different combinations of identity transcription factors expressed in each muscle progenitor, such as Slouch, Eve, Krüppel, Apterous, and the MyoD ortholog, Nautilus, in conjunction with chromatin regulators such as Sin3a [14] determine the different cell identities of each FC, and hence, the final muscle pattern (Fig. 1.1.2E, [3]. After L'sc is restricted to the progenitor cell, the remaining cells in the promuscle cell cluster adopt a fusion competent myoblast (FCM) fate. The specification of FCMs is controlled by Notch-mediated lateral inhibition as well as by the transcription factors Lame duck and Tramtrack [15].

Completion of FC and FCM specification allows for fusion between the two cell types, generating syncytial muscle cells (Figs. 1.1.2E and 1.1.3). Throughout the period of fusion, the transcriptional profiles in both FCs and FCMs are dynamically regulated [16–19]. With the completion of each round of fusion, the fused FCM nuclei undergo progressive reprogramming, such that FCM-specific genes are suppressed, and the transcriptional pattern of the FC nucleus is adopted. The nucleus from the FC retains the expression of identity transcription factors after fusion. Additional experimental evidence suggests that the nucleus from the FC remains transcriptionally different from other nuclei in the same muscle fiber [16]. Fusion

events between FCs and FCMs are completed at late stage 15 (~13.5 h AEL) [20,21]. Myotubes derived from myoblast fusion differentiate into fully striated, functional larval muscles (Fig. 1.1.1A, C). These muscles grow without additional fusion events throughout the larval stage.

Muscle specification in the *Drosophila* pupa forms the adult muscles

Compared to the larval muscle, less is known about the specification process of adult *Drosophila* muscles. The prominent muscle groups in the adult *Drosophila* include the Direct Flight Muscles (DFM), the Indirect Flight Muscles (IFM), the jump muscles, the abdominal muscles, and the leg muscles. Based on morphology and gene expression, these adult somatic muscles can be divided into two types: tubular and fibrillar muscles. The *Drosophila* abdominal, jump, leg and direct flight muscles are tubular muscles with aligned myofibrils that rely on glycolytic metabolism, while the Indirect Flight Muscles (IFMs) are fibrillar muscles with distinct, unaligned myofibrils (Fig. 1.1.1D) and are primarily oxidative [22]. The IFMs are composed of 7 pairs of dorsal-ventral muscles (DVMs) and 6 pairs of dorsal longitudinal muscles (DLMs) (Fig. 1.1.1B). DVMs and DLMs have different orientation and attachment sites and are generated from fusion between myoblasts and templates with different origins (reviewed in [3]). The specification of DFMs requires the homeodomain transcription factors Cut and Apterous [23]. The specification of IFMs depends on the transcriptional regulators Vestigial [24] and Scalloped [25]. In addition, Spalt major in the IFMs directs the fibrillar muscle fate [26]. Readers are directed to reviews on the specification of adult muscle for more detail [3,27,28].

Muscle specification in vertebrates

Similar to *Drosophila*, the specification of muscle progenitor cells in vertebrates also requires a combination of signals from adjacent tissues (reviewed in [29,30]). Extracellular signals induce the expression of Paired Box (Pax) 3 and Pax7 in the somites [31]. Pax genes have dual roles: they enhance the proliferation of muscle precursor cells [32], and they activate the expression of MyoD and Myf5, two members of the myogenic regulatory factor (MRF) family ([33,34]; reviewed in [30]). MRFs are a family of four transcription factors: MyoD, Myf5, myogenin, and MRF4. MRFs activate the expression of genes required for muscle differentiation. MyoD and Myf5 are the first MRFs expressed in muscles and function redundantly to trigger myoblast

specification [35]. Myogenin functions after muscle progenitor formation and regulates terminal differentiation of committed myoblasts [36] but can also function upstream of MyoD to direct the specification of some myogenic cells [37]. In addition to MRFs, other transcription factors are required for muscle differentiation, such as the Myocyte enhancer factor 2 (Mef2), which plays a conserved role in muscle cell differentiation from *Drosophila* to human [38–40]. After the specification of myogenic cells, two waves of myogenesis take place to form the final vertebrate muscle pattern. The first wave generates primary myofibers. The primary fibers function similarly to FCs in *Drosophila* and determine the shape and identity of muscles (slow or fast). The second wave generates secondary myofibers that align alongside the primary myofibers and adds mass to the muscles [41]. The formation of both types of myofibers requires fusion of myoblasts. *In vitro* experiments suggest that the fusion process occurs in two periods: the first involves the fusion of individual myoblasts to form the nascent myotubes; the second period involves fusion between the myotube and additional myoblasts (reviewed in [42]).

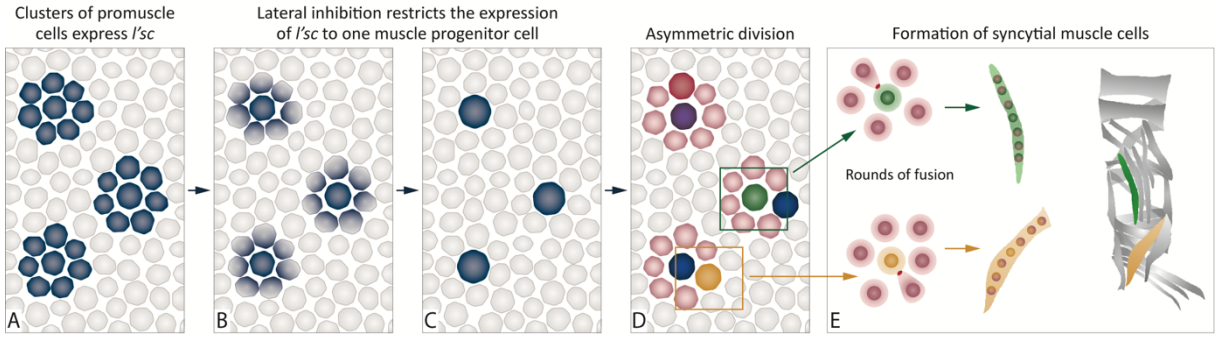


Figure 1.1.2 – Specification, Fusion and Differentiation of Muscle Cells. A) Expression of L'sc occurs in clusters of mesodermal cells with competency to become muscle progenitor cells. **B** and **C)** The activity of the Notch and RTK-Ras pathways restricts the expression of L'sc to a single muscle progenitor cell of a particular identity. **D)** The remaining cells from the initial cluster of promuscle cells become FCMs (pink). The muscle progenitor cells undergo asymmetric division to form either two founder cells (red and purple) or one founder cell (green or yellow) and an adult muscle progenitor (blue). **E)** Founder cells shown in panel 2D express different identity genes and undergo several rounds of fusion (actin foci, red) to form syncytial muscle cells with different characteristics. The green founder cell expresses *apterous* and forms muscle LT1 and the yellow founder cell expresses *nautilus* to form muscle VA1 (modified from [3]). The myotubes maturate by attaching to tendon cells and developing sarcomeres (not shown). The final position of these muscles is highlighted in the hemisegment schematic on the right.

Recognition and adhesion

Myoblast fusion begins with cell–cell recognition and adhesion (Fig. 1.1.3A, Table 1.1.1). In *Drosophila*, recognition and adhesion between the FC and FCMs are mediated by cell-specific immunoglobulin super family (IgSF) members. The IgSF members expressed in the FC are Dumbfounded (Duf) and Roughest (Rst) [43]. Duf and Rst are transmembrane proteins that function redundantly to mediate recognition and adhesion [44]. In the FCMs, Sticks and Stones (Sns) and Hibris (Hbs) are the counterparts of Duf and Rst [45,46]. Hbs can partially compensate for Sns function, but its activity is less efficient than Sns [47]. Expression of Rst is also detected in a subset of FCMs; however, its function in the FCM is unclear [44]. The interaction between Duf-Sns and Rst-Hbs is required for cell recognition and adhesion. Ectopic expression of Duf induces myoblast aggregation and adhesion but is insufficient to trigger fusion [43]. The interaction between Duf/Rst-Sns/Hbs is also required in other developmental events such axon guidance and eye development [48,49], and this "cassette" of transmembrane proteins is referred to as an "adhesion module" in these contexts. If the FC/myotube and FCMs are not in direct contact before adhesion, cell migration is required to bring the two types of cells into close proximity [42,50]. An intriguing recent development in the understanding of fusion-related adhesion is the identification of N-cadherin as a contributor to myoblast fusion in the *Drosophila* embryo. N-cadherin is a member of the cadherin family of adhesion proteins. N-cadherin is present, but not restricted at the fusion site [51]. One possible function of N-cadherin is to mediate cell adhesion through the formation of cellular junction-like structures at the fusion site [52]. For membrane fusion to proceed, however, N-cadherin needs to be removed from the fusion site [52]. Kette and Schizo/Loner, upstream regulators of Arp2/3-mediated actin rearrangements (see Actin rearrangement section below), are reported to facilitate removal of N-cadherin [51–53]. Notably, N-cadherin loss of function does not result in fusion defects in the *Drosophila* embryo [51,54], suggesting potential redundant functions with other members of the cadherin family.

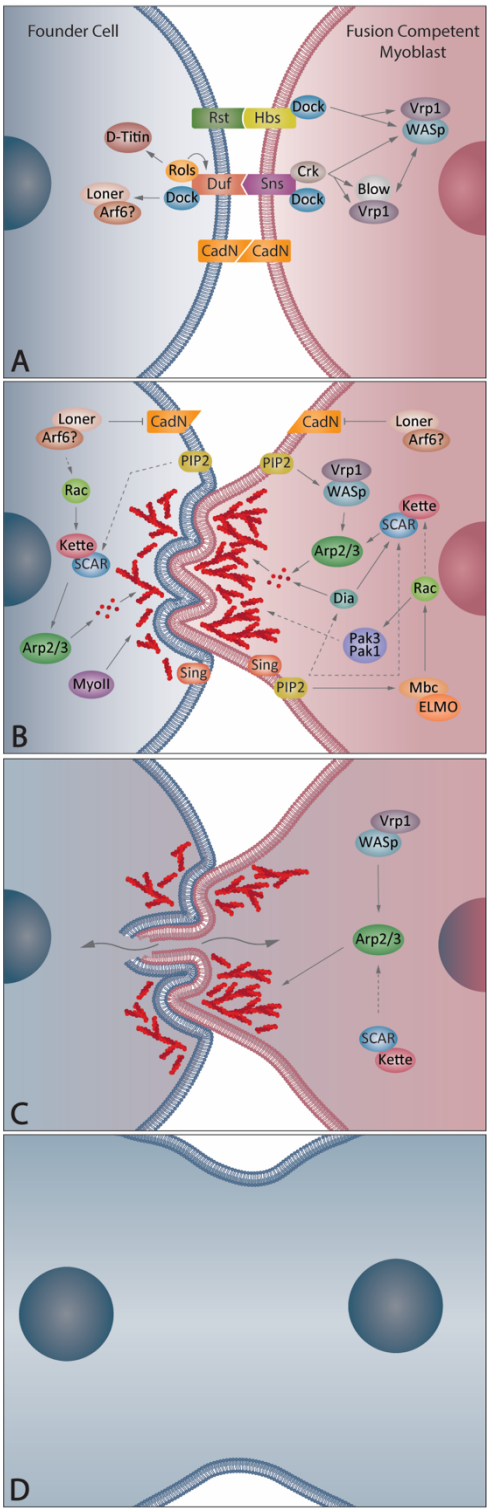


Figure 1.1.3 – Schematic representation of myoblast fusion. In the *Drosophila* embryo, fusion of an individual founder cell (FC) with multiple fusion competent myoblasts (FCMs) gives rise to a single multinucleated muscle cell; the number of FCM fusion events determines the number of nuclei in the mature muscle cell. **A)** Recognition and Adhesion: FC and FCM express different membrane proteins that allow the two cells to recognize and adhere to each other. When in contact, each cell initiates the fusion process by recruiting several proteins to the fusion site. **B)** Actin Focus Formation: Through the activity of the fusion machinery on both the FC and the FCM, actin (red) monomers are assembled into filaments and form a dense F-actin focus on the FCM side and a thin layer on the FC side. The FCM actin focus invades the FC with multiple finger-like protrusions. N-cadherin is removed from the membrane to allow for the next steps of fusion. **C)** Pore Formation. The formation of a fusion pore in the membrane occurs, allowing for the exchange of cytoplasm between both cells. The repression of the FCM transcriptional profile begins (FCM pink nucleus turns blue). **D)** Post Fusion. After one fusion event, the resulting cell has one additional nucleus that has the transcriptional profile of the FC (blue nuclei). At this moment, the cell either prepares for another round of fusion or stops fusing with FCMs.

Actin rearrangements at the fusion site

After the cells adhere to one another, signals from these trans- membrane recognition and adhesion molecules cause the actin cytoskeleton in both the FC and FCM to undergo remodeling, resulting in a filamentous-actin (F-actin)-based focus structure in the FCM and a thin sheath of F-actin on the opposing inner membrane in the FC (Fig. 1.1.2B). The actin focus in the FCM mediates the formation of invasive finger-like membrane protrusions [55]. This actin structure in the FCM is thought to provide the necessary force to push the lipid bilayers of the cells into close proximity. In response to the mechanical forces generated by the invasive protrusions from the FCM, non-muscle Myosin II (MyoII) is recruited to the fusion site in the FC/myotube. The

accumulation of MyoII generates cortical tension, facilitates cell membrane juxtaposition, and promotes fusion pore formation (see below) [56].

A major regulator of the actin focus during myoblast fusion is Arp2/3. Arp2/3 is a multi-subunit protein complex that binds to actin filaments and polymerizes new actin filaments at a 70° angle from the pre-existing actin filament. Arp2/3 is activated by the nucleation-promoting factors (NPFs), Wiskott-Aldrich Syndrome protein (WASp) and SCAR (also known as WAVE). Signal transduction from the membrane to these actin cytoskeleton regulators is partially mediated by the activity of Crk, as well as Dreadlock (Dock), the *Drosophila* homolog of Nck. Both Dock and Crk are adapter proteins with *src* homology 2 (SH2)/SH3 domains. Dock can interact with all four IgSF transmembrane proteins that have SH2 or SH3 domains, but it only genetically interacts with Duf, Sns, and Hbs [57]. In addition, rescue experiments using a series of *sns* deletions and site-directed mutations suggest that Sns functions through interacting with a complex array of proteins [58]. In the FCMs, the Dock SH3 domain biochemically and genetically interacts with WASp, as well as the WASp regulator, Verprolin 1 (Vrp1, also known as Solitary (Sltr) and D-Wip) [57]. In both the FC and FCMs, Dock biochemically and genetically interacts with the Arp2/3 NPF SCAR. Through a similar mechanism as Dock, Crk biochemically interacts with Sns. In a FCM, Crk physically interacts with the WASp regulatory proteins Vrp1 and Blow [59]. Thus, the adaptor proteins Dock and Crk function as links that relay signals from the membrane to the actin cytoskeleton.

In the FC, another adaptor protein that links activity at the membrane to the actin cytoskeleton is Rolling pebbles (Rols, also known as Antisocial (Ants)/Rols). Rols is recruited to the fusion site by Duf. In a positive feedback loop, Rols replenishes Duf at the membrane, and thus enables additional rounds of fusion [60]. Rols interacts with two proteins that regulate the actin cytoskeleton organization: Myoblast city (Mbc) [61,62] and D-titin [60]. Mbc is the *Drosophila* homolog of the mammalian protein DOCK1, which mediates actin rearrangements by acting as a guanine nucleotide exchange factor (GEF) for the small GTPase Rac. However, recent data suggest that the downstream target of Rols is not Mbc: rescue experiments suggest that the activity of Mbc is not required in the FC for the initial fusion event [63]. Another actin cytoskeletal protein that can bind to Rols is D-titin [60]. D-titin is recruited to the fusion site by Rols and mediates myoblast fusion in a mechanism that remains unclear. D-titin is also involved in maintaining myotube morphology [60,64].

While Mbc appears not to be required by the FCs initially, Schizo/Loner, another GEF that regulates actin rearrangements, is required in FCs to mediate fusion.

Schizo/Loner is recruited to the fusion site by Duf and Rst [65]. Domain analysis suggests that the function of Schizo/Loner is to recruit and activate the small GTPase

Table 1.1.1 – List of gene products required in *Drosophila* myoblast fusion.

Protein	Localization	Function	References(s)
Arp2/3	Cytoplasm	Actin polymerization	[50]
Blown fuse (Blow)	Cytoplasm	Regulation of WASp activity	[66,67]
Crk	Cytoplasm	Adaptor protein	[68,69]
Diaphanous (Dia)	Cytoplasm	Actin polymerization	[70]
Dumbfounded (Duf)	FC- Membrane	Recognition and Adhesion	[43]
Hibris (Hbs)	FCM- Membrane	Recognition and Adhesion	[45]
Kette	Cytoplasm	SCAR activation	[50]
Schizo/Loner	Cytoplasm	Rac localization and N-cadherin removal	[51,71]
Myoblast City (Mbc)	Cytoplasm	Regulation of Rac activity	[72]
Myosin II (Myo II)	FC- Cytoplasm	Cortical tension generation on the FC/myotube	[56]
N-cadherin	Membrane	Adhesion	[51]
PI(4,5)P2	Membrane	Actin cytoskeleton remodeling	[73]
Rac	Cytoplasm	SCAR activation	[74]
Rolling pebbles (Rols)	Cytoplasm	Adaptor protein involved with Duf recycling	[61,62]
Rst	FC- Membrane	Recognition and Adhesion	[44]
SCAR	Cytoplasm	Arp2/3 activation	[50]
Singles Bar (Sing)	Membrane	Vesicle trafficking	[75]
Sticks and Stones (Sns)	FCM- Membrane	Recognition and Adhesion	[46]
Veprolin1 (Vrp1)	Cytoplasm	Regulation of WASp activity	[67,76]
WASp	Cytoplasm	Arp2/3 activation	[77]
WHAMY	Cytoplasm	Actin polymerization	[78]

dARF6 at the fusion site. Schizo/Loner and dARF6 control the membrane localization of Rac [71]. However, *arf6* maternal/zygotic null mutants do not have a myoblast fusion defect [79], and the fusion phenotype in a dominant negative *dARF6* background is not as severe as that in the *schizo/loner* mutant. Together these data suggest that the downstream target of Schizo/Loner is another GTPase or that there is redundancy with other dARF family members such as dARF1 [71].

Once activated, the small GTPase Rac regulates the function of SCAR and is critically important in both FCs and FCMs to mediate fusion. The activity of SCAR is controlled by the pentameric WRC complex (the WAVE/SCAR regulatory complex). The WRC is composed of Kette/Nap1, Sra1, Abi, Hspc300, and SCAR itself [80]. Rac activity is essential for the localization of the WRC to the fusion site, as well as activation of SCAR via the release of the SCAR VCA domain from an inhibited state [81,82]. As part of the WRC, Kette is also essential for myoblast fusion as it controls the localization and stability of SCAR [50]. It has not been reported whether loss of function in the other WRC components, Sra1, Abi and Hspc300, lead to a fusion phenotype. This may be due to a lack of appropriate mutant alleles, as well as a maternal supply of protein/mRNA in the embryo that masks the role of these proteins during the time period in which fusion takes place. Nevertheless, overexpression of WRC components in muscle cells results in fusion block and suggests a potential role of other WRC components during fusion [83].

In the FC, SCAR activates its downstream target Arp2/3, and rearranges the actin cytoskeleton into a thin sheath along the fusion site [55]. In the FCM, SCAR activity is also regulated by Rac. However, Rac localization and activation is regulated through Mbc [63]. Mbc is recruited to the fusion site by the phospholipid PI(4,5)P2 (PIP2). When PIP2 activity is sequestered via overexpression of the pleckstrin homology domain of phospholipase C-gamma ($PH^{plcgamma}$), Mbc is concentrated in the cytoplasm instead of at the fusion site, leading to mislocalization of active Rac [73]. Mbc interacts with ELMO using its SH3 domain and forms the Mbc/ELMO complex. The GEF activity of Mbc/ELMO is tightly regulated during myoblast fusion, and it controls the level of active Rac. Both overexpression and loss of function of Mbc/ELMO cause defects in myoblast fusion, which are reminiscent of constitutively active Rac and Rac mutants, respectively [84]. When activated by Mbc/ELMO, Rac, in turn, binds to the WRC and regulates Arp2/3 activity at the fusion site.

In addition to SCAR, the other NPF, WASp, also regulates Arp2/3 at the fusion site. Unlike SCAR, which functions both in FCs and FCMs, WASp activity is only required in the FCM [67]. The activity of WASp is regulated by Blown Fuse (Blow) and Vrp1. The WASp homology-1 (WH1) domain in WASp can bind to the WASp-binding domain (WBD) in Vrp1 [85]. The interaction between WASp and Vrp1 is required to stabilize and localize WASp at the fusion site [67]. This interaction is disrupted when Blow competes with WASp for Vrp1 WBD binding [67]. Thus, after cell recognition and adhesion, a signal is transduced from the membrane via the adaptor protein Crk, which recruits Blow and Vrp1 to the fusion site. At the fusion site, the WASp-Vrp1 complex promotes actin polymerization by regulating Arp2/3 activity. Blow suppresses WASp activity by competing with WASp for Vrp1 binding and by dissociating the WASp-Vrp1 complex. Since the binding affinity between Blow-Vrp1 is lower than WASp-Vrp1, dissociated WASp interacts with Vrp1 again and promotes another round of branched actin polymerization [67]. It has been reported that in FCs, the function of WASp and SCAR is redundant, as overexpression of WASp in the FCs can partially restore fusion in *kette* mutant background [52]. FCM-specific reduction of the WASp level in a *kette* mutant background rescues fusion defects. It has been proposed that a particular ratio of active WASp and SCAR needs to be maintained for fusion to occur [52].

Recent studies have indicated that in addition to the branched actin network generated by Arp2/3, the linear actin filament nucleated by Diaphanous (Dia) also plays a role during myoblast fusion [70,86]. Dia is a member of the formin family of actin polymerization proteins. Dia is enriched at the actin focus during the formation

of *Drosophila* somatic musculature and dorsal pharyngeal musculature. Dia loss of function blocks myoblast fusion [70]. Interestingly, overexpression of active Dia also leads to fusion defects [70,86], suggesting that the activity of Dia is highly regulated. Notably, in addition to Dia, the WASp family member WHAMY can also promote the assembly of linear actin filament. It has been reported that WHAMY synergizes with WASp during myoblast fusion [78]. Altogether, these data suggest that a balance between linear and branched actin filament is required at the fusion site for fusion to occur.

Fusion pore formation

A critical step in cell fusion is the formation of fusion pores that allow for cytoplasmic continuity between the fusing cells (Fig. 1.1.3C). Studies from virus-cell fusion and *C. elegans* epithelial cell fusion have identified fusogens that mediate fusion pore formation ([87]; reviewed in [88]). A fusogen is a transmembrane protein that localizes to the fusion site and its presence is essential and sufficient to trigger membrane fusion [88]. Despite the identification of many gene products that are required for myoblast fusion in both *Drosophila* and vertebrates, no fusogen has been identified in these systems to date. Therefore, the mechanism that brings the membranes in close proximity to allow pore formation during myoblast membrane fusion remains a critical, open question.

It has been proposed that the actin cytoskeleton plays a crucial role in forcing the juxtaposition of the FC/FCM cell membranes, leading to the formation and expansion of fusion pores (reviewed by [89–91]). During *Drosophila* embryonic myoblast fusion, the F-actin focus in the FCM forms podosome-like structures at the fusion site, which provide an invasive force on the apposing FC and pushes the cell membranes of the FCM and FC into closer proximity. The F-actin focus later evolves into a single-channel fusion pore on the membrane of the fusing cells [55]. Studies aimed at investigating the function of actin regulators during pore formation have been performed. In these studies, the exchange of fluorescent proteins between the FCM and the FC were measured as a reporter of cytoplasmic continuity in various fusion mutant backgrounds. From these experiments, it has been proposed that SCAR-regulated actin remodeling is required for the initiation of fusion pore formation [82]. The function of WASp and its regulators is required for the formation of invasive structures [55,59,67]. Therefore, it is believed that WASp-regulated actin remodeling is required for pore formation [55,59,67] and expansion [82]. Notably, the actin focus

resolves prior to fusion, suggesting that actin and other proteins located at the fusion site need to be removed, allowing fusion to occur. Thus far, the removal of proteins associated with the actin cytoskeleton at the fusion site has not been well studied. One potential protein involved in this process is Schizo/Loner, which has been reported to remove N-cadherin from the fusion site to permit fusion [51]. In addition, the transmembrane protein *singles bar* (*sing*) is required during myoblast fusion. *sing* mutant embryos display a cell fusion block with accumulation of vesicles at the fusion site, suggesting a potential role of Sing in vesicle trafficking during fusion [75].

Other studies suggest alternative models of fusion pore formation [66,89,92]. Electron microscopy images have shown the presence of prefusion complexes at the fusion site. These prefusion complexes contain electron-dense, paired vesicles at the apposed plasma membranes. It has been suggested that these paired vesicles resolve into membrane plaques. Subsequently, the juxtaposed plasma membranes vesiculate and form sacs that enclose the extracellular space. Multiple fusion pores are observed in these situations [66]. Similar membrane structures and multiple fusion pores at the fusion site have also been reported during myoblast fusion which leads to the formation of the *Drosophila* adult flight muscle [92]. These data emphasize the requirement for the delivery and the clearing of vesicles at the fusion site as critical for mem- brane breakdown [66]. These data also suggest that instead of one fusion pore, multiple pores are formed to facilitate fusion. It is still unclear whether these differences of fusion pore number arise from different fixation methods, context or other variables (reviewed in [91]).

MAKING ADULT MUSCLE: MYOBLAST FUSION IN THE *DROSOPHILA* PUPA

The *Drosophila* adult muscles form during metamorphosis in the pupal stages. During the first few hours of metamorphosis, most of the *Drosophila* larval body wall muscles are destroyed through histolysis, but a few muscles, such as the Dorsal Oblique (DO1-3) muscles, escape degradation and serve as templates for some adult muscles, notably the Dorsal Longitudinal Flight muscles [93]. The growth of adult muscles is achieved through hundreds of cell–cell fusion events, in which a pool of myoblasts fuse with either template myotubes or muscle precursor cells [93].

The pathways that regulate myoblast fusion to form the *Drosophila* adult muscles are not fully understood. Based on our current knowledge, the mechanisms that regulate myoblast fusion during adult myogenesis are similar to those that regulate embryonic myogenesis. Fusion occurs between the adult muscle progenitors (AMPs) and myoblasts that migrate from the imaginal discs to form the adult abdominal muscles, the leg muscles, and the DVMs. The DLMs are formed through fusion between myoblasts and the muscle templates that are preserved during histolysis [93]. The AMPs associated with the wing imaginal disc go through two phases of amplification during adult muscle development. The initial phase is a symmetrical division which is regulated by Notch signaling and leads to increased AMP numbers. The second phase is an asymmetrical division that is regulated by Notch and Wnt signaling and results in AMP self-renewal and the generation of myoblast progeny required for the later fusion events [94]. It has been proposed that during muscle injury, the AMPs could function similarly to satellite cells, whose progeny fuse with myotubes to repair muscles [94]. A recent study has shown that dIlp6 signals from a muscle niche can activate dormant AMPs through the Insulin-Notch-dMyc cascade [95].

Similar to embryonic myoblast fusion, the transmembrane proteins Duf, Rst, Sns, and Hbs are required to mediate cell recognition and adhesion [96]. After adhesion, the fusing myoblast flattens on the myotube, such that the cell membranes are in tight apposition [92]. Actin accumulates primarily at the myoblast side of the fusion site, after receiving signals from the cell membrane, and forms a focus-like structure. As with embryonic myogenesis, actin rearrangements during adult myogenesis require the function of Arp2/3, as well as the actin NPFs WASp and SCAR. Loss of function studies revealed that WASp is required for fusion pore initiation [97].

Similar to embryonic myoblast fusion, the MARVEL domain protein Sing is expressed in adult muscles, and its activity is required for adult myoblast fusion [98].

Despite these similarities, however, there are differences between *Drosophila* embryonic and adult myogenesis. In embryos, FCMs and FCs are positioned relatively close to one another prior to fusion. The FCMs in contact with FCs/myotubes are responsible for the early fusion events. The FCMs that are located more internally migrate prior to making contact and fusing with the FCs/myotubes [20,21]. During adult myogenesis, myoblasts often need to migrate long distances from the imaginal discs to the muscle template/myotubes. More importantly, during migration, these myoblasts maintain a semi-differentiated state via the Notch signaling pathway. Each myoblast expresses the Notch ligand Delta and represses the differentiation of its neighboring cells. Notch signaling decays when myoblasts reach the vicinity of the myotubes, and this allows for the terminal differentiation of the myoblasts and the expression of FCM markers such as Sns [96].

During adult muscle formation, the adhesion between myoblasts and myotubes also requires filopodia that emanate from the myotube surface. The filopodia are actin-based structures that bring the myoblasts and myotubes into close proximity. The formation and maintenance of filopodia requires the activity of Enabled and IRSp53 [99]. The requirement for these two proteins during embryonic myoblast fusion has not been reported. In addition, reducing WASp and SCAR activity simultaneously in embryos abolishes actin focus formation [73]. However, double knockdown of WASp and SCAR during adult muscle formation results in enlarged actin foci, suggesting novel roles of the NPFs during *Drosophila* adult myoblast fusion [97].

MAKING MUSCLE IN VERTEBRATES: MYOBLAST FUSION

Compared to *Drosophila*, the vertebrate muscle is a more complex system, both in terms of its structure and the regulatory mechanisms required during development. Over the past few decades, researchers have identified numerous genes that are required for myoblast fusion in vertebrates (reviewed in [42,100]). Nevertheless, how these different proteins coordinate fusion remains unclear. The morphological steps that are required for myoblast fusion and many of the genes necessary for the process are conserved between *Drosophila* and vertebrates. Therefore, we review recent updates in vertebrate fusion-related genes based on their localization and which steps they are involved in during fusion (Table 1.1.2).

Similar to the process of *Drosophila* myoblast fusion, the myotube-myoblast fusion during muscle development in vertebrates is also asymmetric and requires recognition molecules located on the cell membrane. One pair of membrane proteins required for fusion is Integrin vLA-4 and its receptor VCAM-1. Integrin vLA-4 is expressed in myotubes and VCAM-1 in myoblasts. Interactions between vLA-4 and VCAM-1 are required for the alignment of the secondary myofiber with the primary myofiber, as well as for the second phase of muscle cell fusion [101]. In addition to vLA-4 and VCAM-1, the transcription factor NFAT2C also mediates cell recognition by regulating the expression of IL-4. IL-4 is a cytokine that functions as a secreted myoblast recruitment factor [102]. Another pair of membrane proteins required for fusion is the immunoglobin superfamily proteins Jamb and Jamc. In zebrafish, Jamb and Jamc are expressed in fast-muscle myoblasts. The physical interaction between Jamb and Jamc is required for myoblast fusion during the formation of fast-twitch muscles. Loss of function of either protein severely impairs myoblast fusion [103,104]. In addition, it has been shown that Nephrin, an ortholog of the *Drosophila* transmembrane protein Sns, localizes on myoblasts and mediates cell recognition [105]. In zebrafish, Kirrel, an ortholog of Nephrin, is localized to membranes of myoblasts and is required for fusion [106]. After recognition, adhesion molecules such as M-cadherin [107], N-cadherin [108], and integrin family members [109] mediate the adhesion and alignment of the myoblasts. It has been reported that the G-protein coupled receptors BAI1 and BAI3 also play a role during fusion, through signal transduction from the membrane to the cytoskeleton via the Dock1/Rac1 pathway [110,111].

Unlike in *Drosophila*, an actin focus structure has not been reported during vertebrate myoblast fusion. Nevertheless, actin cytoskeletal rearrangements play a critical role in vertebrate muscle formation. Similar to *Drosophila mbc* mutants, *Dock1*-null mice embryos exhibit severely impaired myoblast fusion and skeletal muscle content is reduced [112]. Dock1 is the mammalian ortholog of Mbc, and it functions as a GEF protein that activates Rac GTPase. In a conditional *Rac1* knockout

Table 1.1.2 – List of gene products required for vertebrate myoblast fusion.

Protein	Location and function	Animal model	Reference(s)
Adam12	Membrane Mediates myoblast adhesion Interaction with the actin-binding protein α-actinin-2 promotes myoblast fusion	Mouse	[113,114]
BAI1	Membrane Mediates recognition of phosphatidylserine on apoptotic cells Regulates myoblast fusion through Dock1/Rac1 pathway	Mouse	[110]
BAI3	Membrane Interacts with the scaffold protein ELMO to regulate myoblast fusion, possibly through the ELMO/DOCK/Rac1 pathway	Chicken	[111]
Caveolin-3	Membrane Involved in myoblast fusion (unclear role) Contradictory fusion phenotypes in different experimental models	Mouse	[115,116]
Cdc42	Cytoplasm Required for actin rearrangement at the fusion site	Mouse	[117]
CKIP-1	Cytoplasm Regulates myoblast fusion by interacting with both phosphoinositides on the membrane and Arp3/3 subunit	Mouse Zebrafish	[118]
Crk Crkl	Cytoplasm Adaptor proteins Crk/Crkl genetically interact with DOCK1/DOCK5 to regulate myoblast fusion	Zebrafish	[119]
DOCK1	Cytoplasm Required for myoblast fusion by activating Rac1	Zebrafish Mouse	[112,119]
DOCK5	Cytoplasm Function redundantly with DOCK1 Also involved in post-fusion myofiber development	Zebrafish Mouse	[112,119]
EHD2	Membrane and cytoplasm Regulates myoblast fusion by mediating endocytic recycling of membrane proteins, such as Myoferlin	Mouse	[120]
Gm7325 Myomixer Minion Myomerger	Membrane Interacts with Myomaker to induce fusion Functions in cell recognition (proposed)	Mouse	[121–123]
JAM-B JAM-C	Membrane Both physically interact to mediate fusion Facilitate myocytes recognition and adhesion (proposed)	Zebrafish	[103]
Kirrel	Membrane Required for fast muscle precursor fusion	Zebrafish	[106]
M-cadherin	Membrane Mediates myoblast adhesion Promotes fusion by activating the Rac1 pathway	Mouse	[124]
MOR23	Membrane Regulates cell adhesion during myoblast fusion	Mouse	[125]
Myoferlin	Membrane Regulates myoblast fusion through unclear mechanism, potentially by activating as a scaffold protein that links fusion proteins with the membrane	Mouse	[126]
Myomaker	Membrane Muscle-specific protein that induces fusion during muscle development and repair Mediate cell recognition (proposed)	Mouse Zebrafish Chicken	[127–130]
N-WASP	Cytoplasm Required in both fusing partners	Mouse	[131]
Rac1	Cytoplasm Required for proper recruiting of Arp2/3 to the contact site	Mouse Zebrafish	[106,117,132]

	Regulates actin remodeling during fusion Unlike in *Drosophila*, constitutively active Rac1 in zebrafish leads to myoblast hyperfusion	Chicken	
Stab2	Membrane Involved in the phosphatidylserine-dependent fusion of myoblasts during muscle development and regeneration	Mouse	[133]
Talin 1/2	Cytoplasm Regulates myoblast fusion, potentially by mediating the interaction between integrins and the cytoskeleton	Mouse	[134]
VLA4 VCAM1	Membrane VLA-4 and its counter receptor VCAM-1 are involved in secondary myogenesis	Mouse	[101]
β-1 integrin	Membrane Involved with membrane breakdown during myoblast fusion	Mouse	[109]

mouse model, the recruitment of Arp2/3 and F-actin to the cell-contact site is reduced, resulting in impaired myoblast migration and fusion [117]. Experiments using C2C12 mouse myoblast cell culture suggest that Nap1, the mammalian ortholog of Kette and the downstream target of Rac1, is also required for regulating WAVE dependent actin remodeling during myoblast fusion [135]. Moreover, a recent study reported the requirement of the non-muscle myosin IIA (NM-MHC-IIA) during myoblast fusion. NM-MHC-IIA is involved in the formation of the cortical actin wall in the FC/myotube in the rat L6 myoblast cell culture, providing structural and mechanical support to facilitate membrane alignment and fusion pore formation [136]. Together, these data suggest a conserved role of actin during muscle development.

It has been a major challenge to identify muscle-specific genes that ensure that fusion occurs only between myoblasts rather than other cell types. The first such gene found in vertebrates is Myomaker/Tmem8c. Myomaker is a transmembrane protein that is specifically expressed in the muscles during muscle development and regeneration [127–130,137]. In humans, reduced Myomaker function is linked to Carey-Fineman-Ziter syndrome [138], a congenital myopathy. Myomaker is required for fusion and is localized to the adhesion site. Expressing Myomaker in fibroblasts is sufficient to induce fusion between fibroblasts and myoblasts, but it is not sufficient to induce fibroblast–fibroblast fusion [129]. These reports suggest that additional proteins on the myoblasts are required to interact with Myomaker to induce fusion.

Recently, Gm7325, the potential counterpart of Myomaker, has been identified by three different labs, and was given the name Myomixer [121], Myomerger [122] and Minion [139]. Gm7325 is an 84 amino acid microprotein with a similar expression pattern to Myomaker. The function of Gm7325 is required for Myomaker-induced fusion, as simultaneous expression of Myomaker and Gm7325 induces fusion between non-muscle cells [121,122,139]. The mechanism by which Myomaker and Gm7325 regulates fusion is not well understood. A physical interaction between Myomaker and Gm7325 has been reported [121], but remains controversial

[122,130]. In Gm7325- and Myomaker- deficient myoblasts, cell fusion is blocked at different fusion stages. Based on whether the cell membranes align in the deficient myoblasts, it has been proposed that Myomaker is necessary for cell recognition, while Gm7325 is required for downstream events such as actin cytoskeleton remodeling [139].

Cell fusion in vertebrates is required not only during early embryonic myogenesis, but also during muscle regeneration after damage. As with *Drosophila* AMPs, a pool of myoblasts remains undifferentiated during vertebrate myogenesis. These myoblasts are satellite cells that associate with myofibers. Satellite cells contribute to post-natal muscle growth, as well as to muscle repair. The specification of satellite cells is critically dependent on Pax7, as no satellite cells are found in *Pax7* mutant mice [140]. With intact muscles, satellite cells are mitotically quiescent and express Pax7 and Myf5, but not Myogenin or MyoD (reviewed in [141]). Upon muscle injury, myofiber necrosis triggers inflammatory responses, which induce satellite cells to proliferate [142]. After proliferation, the majority of satellite cells differentiate and start to express MyoD and myogenin [143]. These cells later fuse with damaged myofibers or fuse with each other to generate new muscle fibers [144]. Thus far, the process of satellite cell fusion is mechanistically similar to myoblast fusion during primary and secondary myofiber formation.

CONCLUSION

Myoblast fusion in organisms ranging from the fly to human occurs through conserved steps: cell recognition, membrane apposition, actin rearrangement, pore formation, and cytoplasmic continuity. The investigation of myoblast fusion in *Drosophila* continues to provide valuable insights to vertebrate muscle development. However, there are many questions that remain unanswered: How do muscles control the number of fusion events during development and during repair? How do the nuclei added to a myotube adopt the program of the growing myotube? How are movement and transcriptional diversity among the added myonuclei controlled? And when considering the mechanisms of fusion, how are the ratios of linear and branched actin filaments controlled at the actin focus? What are the actin depolymerization factors that resolve the actin focus after fusion pore formation? What causes pore formation between the engaged cells? The knowledge gained from answering these questions in model systems such as *Drosophila* will illuminate how the key steps of fusion are controlled and how the syncytial muscle cell develops and is maintained.

Part II

GETTING INTO POSITION: NUCLEAR MOVEMENT IN MUSCLE CELLS

Mafalda Azevedo[1,2] and Mary K. Baylies[1,3]

[1]Program in Developmental Biology, Sloan Kettering Institute, New York, New York, United States of America
[2]Graduate Program in Areas of Basic and Applied Biology (GABBA), Abel Salazar Biomedical Sciences Institute, University of Porto, Porto, Portugal
[3]Cell and Developmental Biology, Weill Cornell Graduate School of Medical Sciences, Cornell University, New York, New York, United States of America

Keywords
nuclear positioning; muscle; *Drosophila*; Cytoskeleton, LINC complex; muscle disease

Accepted in Trends in Cell Biology

ABSTRACT

The positioning of nuclei within the cell is a dynamic process, that depends on the cell's fate and developmental stage, and that is adjusted for optimal cell function. This is especially true in skeletal muscle cells, which contain hundreds of myonuclei distributed evenly along the periphery of the muscle cell. Mispositioned myonuclei are often associated with muscle dysfunction and disease. Different mechanisms governing myonuclear positioning are now emerging, with several of the new genes implicated in nuclear movement linked to human muscle disease. Here we discuss the recent advances in myonuclear positioning and its implications for muscle size and function from the view of Drosophila. Additionally, we highlight similarities and differences to mammalian systems and provide connections to human muscle disease.

THE NUCLEUS IN SKELETAL MUSCLE

In most textbooks, the nucleus is depicted at the center of the cell. However, nuclei adopt different localizations, depending on the cell's fate, developmental stage, or specific function (e.g. neurons, epithelia, and skeletal muscle cells). Importantly, in all cell types and cell states, nuclear positioning is an active process and is continuously adjusted for optimal cell function. Changes in nuclear positioning are often associated with cellular dysfunction and disease [145,146]. The position of nuclei in skeletal muscle cells (myofibers) is of particular interest, since these cells are multinucleated, with up to hundreds of nuclei (myonuclei), evenly distributed along the cell surface. Mislocalized myonuclei have been associated with a variety of muscle diseases [147] that are characterized by reduced muscle size, muscle weakness, and decreased muscle function [148]. Many genetic mutations lead to the development of diseases displaying these characteristics, including those in nuclear proteins which are associated with centronuclear myopathy (CNM) and Emery-Dreifuss muscular dystrophy (EDMD)[148–150]. While mispositioned myonuclei are typical for many muscle diseases, it is still unclear whether these diseases share a common mechanism or are the result of distinct mechanisms that lead to myonuclear mispositioning. A better understanding of the mechanisms underlying the positioning of myonuclei is required to understand and treat these severe disorders (see Box 1).

From the first observation of a nucleus in 1700 [151], our knowledge of nuclear composition, organization, and positioning has continuously evolved. In addition to containing the genomic DNA, nuclei across species and different cell types share many structural similarities. The nucleus is delimited by the nuclear envelope (NE), composed of two lipid bilayer membranes that separate the nucleoplasm from the cytoplasm (Fig. 1.2.1). The inner nuclear membrane (INM) and outer nuclear membrane (ONM) have distinct compositions and functions, and only associate where there is a nuclear pore. Nuclear pore complexes (NPCs) allow for the communication between the cytoplasm and nucleoplasm. The nuclear lamina is intimately associated with the INM and is composed of a thin meshwork of intermediate filaments, mostly A and B-type lamins, that associate with heterochromatin and provide structural support to the nucleus [152]. LINC (Linker of the Nucleoskeleton and Cytoskeleton) complexes support the structure of the nucleus as well as its interaction with

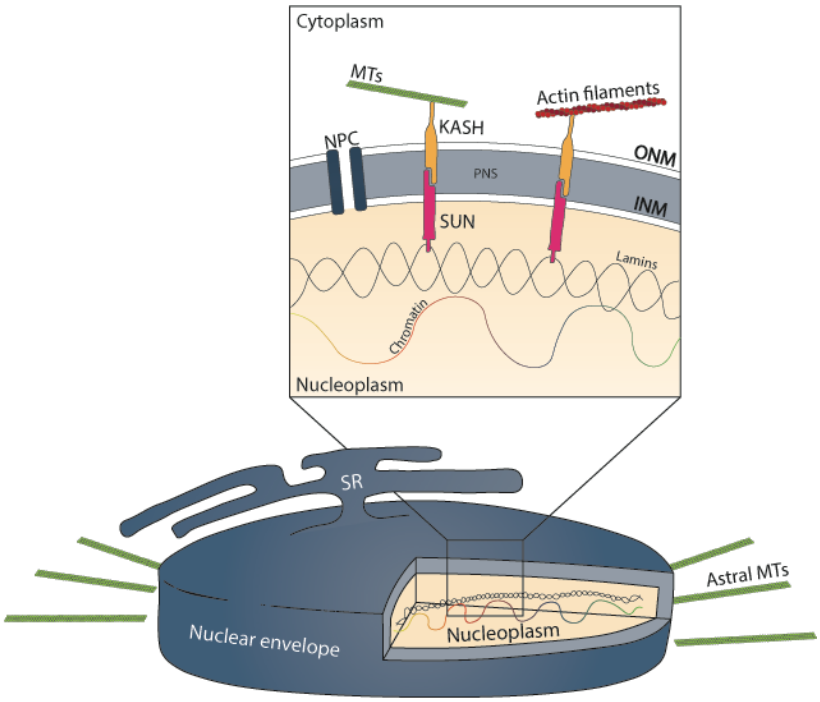


Figure 1.2.1 – Schematic representation of the components present at the nuclear envelope of a *Drosophila* larval myonucleus. Astral MTs represent the microtubules nucleating from the nuclear envelope in larval muscle. The box highlights a zoomed region of the nuclear envelope. Representative KASH and SUN proteins are shown in orange and magenta, respectively. NPC: nuclear pore complex. MTs: microtubules. PNS: perinuclear space. ONM: outer nuclear membrane. INM: inner nuclear membrane. SR: sarcoplasmic reticulum.

cytoskeletal components [152,153]. LINC complexes are located throughout the NE and consist primarily of transmembrane SUN and KASH proteins. SUN (Sad1 and UNC-84) proteins are INM components that associate with the nuclear lamina and other components through their N-terminal domains. The C-terminal domain of SUN proteins projects into perinuclear space (PNS) and associates with KASH proteins. KASH (Klarsicht, Anc-1 and Syne Homology) proteins are present at the ONM and interact with SUN proteins at the PNS through their C-terminal domains. The KASH N-terminal domain links to the cytoplasmic cytoskeletal networks, including the microtubules and actin filaments. By connecting nuclear and cytoplasmic components, the LINC complexes are essential for maintaining the integrity of the nucleus, as well as its position within the cell (Fig. 1.2.1) [152,153].

Multinucleated skeletal muscle cells develop through a series of steps that are conserved across invertebrate and vertebrate species. First, muscle progenitors (myoblasts) are specified in the embryonic mesoderm. This is followed by a series of cell-cell fusion events. Each fusion event adds a nucleus and cytoplasmic mass, leading to the formation of syncytial myotubes (Fig. 1.2.2A; for additional information

on muscle cell fusion see [154,155]). Myoblast fusion in the Drosophila embryo requires two types of myoblasts: founder cells (FCs) and fusion-competent myoblasts (FCMs). The FC contains all the information that determines an individual muscle cell's identity. Each FC fuses with a specific number of FCMs (2-25) and establishes a unique muscle with a specific size, shape, tendon attachment and innervation [3,156]. Each embryonic muscle is composed of a single muscle cell with a relatively small number of nuclei, which is ideal for investigating molecular events underlying myogenesis in great detail. In mammals, muscles are more complex, consisting of bundles of muscle cells. In addition, mammalian myoblasts appear to be equivalent and fuse to form syncytia that contain up to 100s of nuclei [157]. Nevertheless, myonuclei in both systems undergo a similar series of stereotyped movements during myogenesis and assume positions which maximize their internuclear distances at the surface of mature myofibers.

Over the past several years, researchers have defined different mechanisms that ensure the proper localization of myonuclei through their interactions with the cytoskeleton and the LINC complexes. In this review, we highlight the latest findings on the molecular mechanisms of myonuclear positioning, the relationship between nuclear scaling and positioning in muscle cells, and the functional consequences of myonuclear mispositioning. We focus specifically on the Drosophila melanogaster somatic musculature and highlight similarities and differences to the mammalian systems.

MYONUCLEAR POSITIONING

Drosophila melanogaster presents an excellent *in vivo* system to study muscle development, particularly the mechanisms of myonuclear positioning and the interactions of muscle with other cell types, such as the tendons and motor neurons. The fly embryo consists of 12 segments, each hemisegment containing 30 skeletal muscles. The plethora of genetic tools permits the visualization of nuclei from individual muscle cells, both in fixed and live samples at different developmental stages. Therefore, the movements of myonuclei in four dimensions can be readily assessed throughout muscle development.

Based on work with the *Drosophila* lateral transverse (LT) and ventral longitudinal (VL) muscles, the steps required for proper nuclear positioning were initially described by Metzger *et al*, [158]. Here, we review this process and subdivide it into four significant steps: 1) cluster formation; 2) cluster spread; 3) myonuclear dispersion; and 4) myonuclear spacing and anchoring (Fig. 1.2.2). Steps 1 through 3 are assessed during embryonic development, whereas step 4 is usually analyzed in the mature myofibers of the fly larva. In mammalian muscle, similar movements have been observed [157,159]. Nuclear positioning in both systems is controlled molecularly by a variety of proteins from different groups, mainly microtubules (MTs), MT motor and non-motor proteins (also known as MT-associated proteins, MAPs), actin and actin-associated proteins, and LINC complex proteins. Most proteins play a role in distinct myonuclear movement steps throughout myogenesis, which has been demonstrated in various cellular and animal models, as well as in several human diseases. For a list of proteins and their functions in myonuclear positioning that are included in this review we refer the reader to Table 1.2.1. Below we describe the most recent findings for each step of myonuclear positioning.

2.1 Cluster formation

Cluster formation in Drosophila has been investigated primarily in the four finger-shaped LT muscles. The LT muscles establish dorsal-ventral orientation; LT muscles 1, 2, and 3 contain between six and eight myonuclei, while LT 4 has between four and six nuclei. The first myonuclear movements in the LTs occur while the myotubes are still undergoing fusion events (stage 14; 10h20 after egg laying (AEL); Fig.1.2.2A and

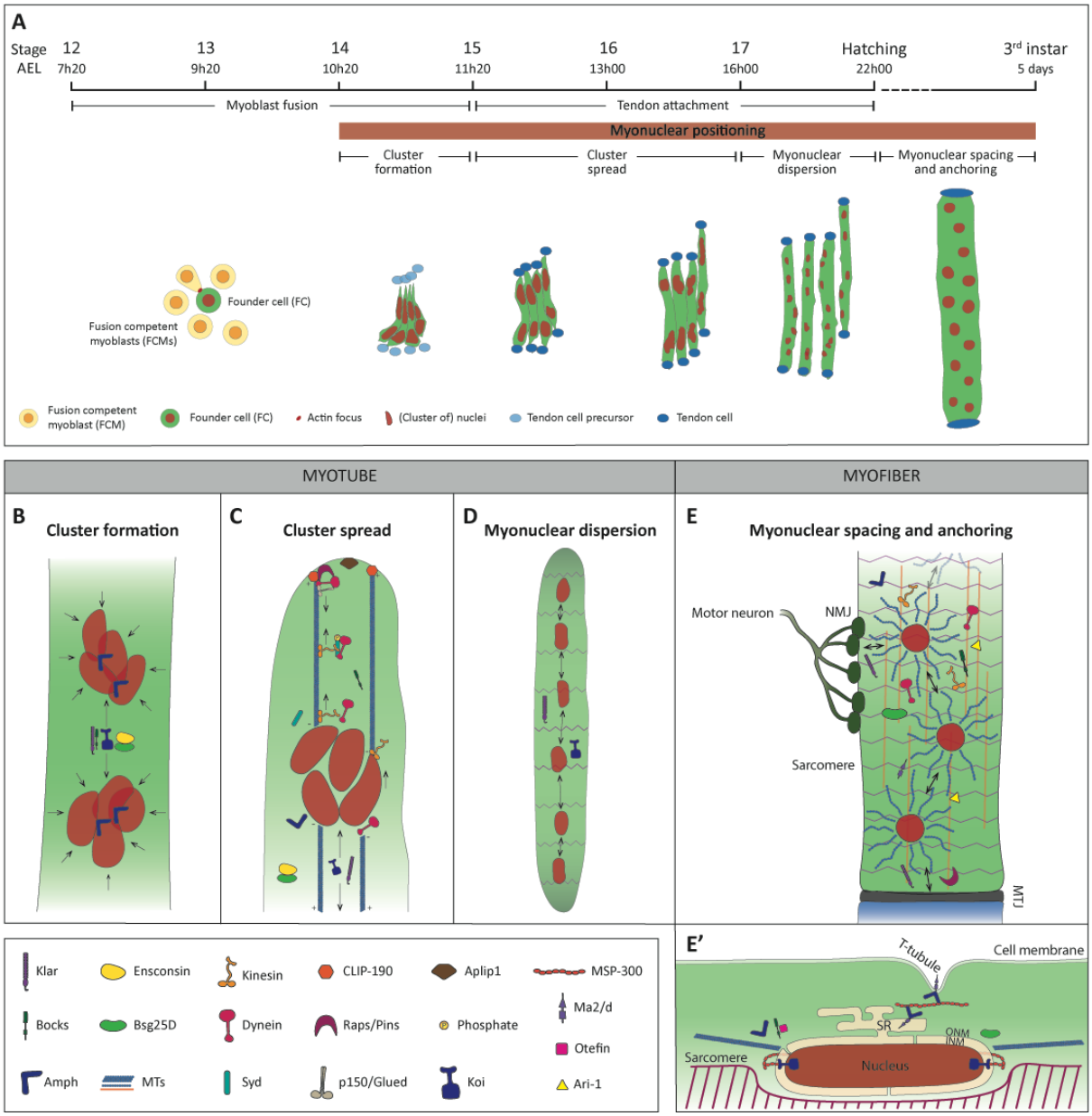


Figure 1.2.2 - Figure legend on the next page.

B). As each fusion event occurs, the added nucleus moves to the cell center, becoming part of a cluster. Two closely apposed nuclear clusters can be identified in the ventral center of the LTs at this stage. However, it was not entirely clear how myonuclei associate with a cluster.

Recently, a number of proteins present at the NE have been implicated in the initial myonuclear cluster formation. These include Bocks and Klar, the Drosophila homologs of Emerin and the LINC protein Nesprin-4, respectively, and Koi, the Drosophila SUN2 protein [160,161]. In addition, Amphiphysin, a BAR domain protein linked to vesicle trafficking, is implicated in nucleus-nucleus interactions to maintain cluster cohesion. Although the mechanism of Amphiphysin remains unknown, the

Figure 1.2.2 – Schematic representation of myonuclear positioning during embryonic and larval *Drosophila melanogaster* development. A) *Drosophila* myogenesis consists of multiple steps, including myoblast fusion, tendon attachment, and myonuclear positioning. The latter is further divided into cluster formation (B), cluster spread (C), myonuclear dispersion (D), and myonuclear spacing and anchoring (E and E'). Development and myonuclear positioning from Stages 12 to the end of stage 17 are shown using the embryonic lateral transverse (LT) muscles as examples. From hatching to 3rd instar larva, the muscle represented is a larval ventral longitudinal (VL) muscle. AEL – After Egg Laying. Stage and times correspond to those observed at 25°C. B) Close-up of the two clusters of myonuclei present in the embryonic LT muscle. Arrows indicate the forces required to maintain the integrity of the two clusters and those to keep them separated. C) Close-up of a single cluster within an embryonic LT muscle as it moves towards the end of the myotube. Arrows indicate the pulling and pushing forces clustered myonuclei experience as they move. D) View of a single embryonic LT muscle showing the presence of sarcomeres, which together with the neuromuscular junction (not shown), indicate that the muscle can experience coordinated contraction. In this panel, the double arrows represent the movements of myonuclei to be equidistant from each other. E) View of a larval VL myofiber and its interaction with two cell types: motor neuron (dark green), forming the neuro muscular junction (NMJ), and tendon (bottom of the muscle, blue), forming the myotendinous junction (MTJ). The two populations of microtubules (MTs) can be observed: longitudinal MTs run along the length of the myofiber (orange lines) and astral MTs surround the nucleus and extend in multiple directions (blue). The double arrows indicate the distance between myonuclei and the edges of the myofiber. E') Longitudinal cross-section of a larval VL nucleus for a more detailed view of the localization of proteins involved in myonuclear spacing and anchoring. SR – Sarcoplasmic reticulum; ONM – Outer Nuclear Membrane; INM – Inner Nuclear Membrane. Note: protein localization in panels B-E' represents the function in specific processes or mechanisms, rather than the precise described localization of each protein in the cell.

authors suggest that it could be microtubule independent [160]. Mutations in Emerin and Nesprin-4 are linked to Emery-Dreifuss muscular dystrophy (EDMD), and Amphiphysin is implicated in Centronuclear Myopathy (CNM), indicating that the crucial roles of these proteins in myonuclear positioning are highly conserved.

One cytoskeletal element involved in cluster formation in Drosophila is Ensconsin (Ens)/MAP7. Ens loss results in the formation of a single cluster instead of two clusters [158]. Recently, Bsg25D, the Drosophila homolog of Ninein, was described to physically interact with and positively regulate Ens activity during myonuclear positioning. Loss of Bsg25D in developing myotubes affects nuclear positioning in embryos that have been sensitized by the partial loss of Ens. However, muscle-specific Bsg25D overexpression leads to a phenotype similar to that of Ens loss. While in mature myofibers Bsg25D and Ens regulate perinuclear MT organization (see below), the mechanisms by which they act during the formation of the initial nuclear clusters remain unclear [162]. To this end, work in mammalian cell culture provides insights. In mammalian myotubes generated in 2D tissue culture, myonuclei are found in the cell center, forming a single cluster. Upon fusion, the newly added myonucleus rapidly moves towards the center in a microtubule-dependent way. Several key players,

including a dynein/dynactin complex, Cdc42, Par6 and Par3, have been shown to be involved in this process in vitro [157,163]. It remains to be tested whether similar mechanisms are at play in early Drosophila myotubes.

An interesting distinction between fly and mammalian muscle with regards to clustering is that, in the latter, myonuclei cluster initially in the cell center during regeneration upon injury, with subsequent movement to the periphery at a later timepoints [164]. Muscle repair in mammals is promoted by adult muscle stem cells, called satellite cells, that become activated, proliferate, and subsequently fuse to the regenerating myofiber [165]. Recently, a satellite-like cell population has also been identified in the adult Drosophila muscles. These cells, upon muscle injury, are capable of proliferating and fusing to existing myofibers. However, instead of appearing in the cell center, these new myonuclei were only detected at the muscle cell surface [166]. It would be interesting to investigate the myonuclear movements in Drosophila muscle undergoing repair to better understand this process and compare it with observations in mammalian muscles.

2.2 Cluster spread

In Drosophila embryonic LT muscles, the second step of nuclear positioning involves the movement of the two adjacent nuclear clusters towards the ends of the muscle cell (stages 15-16; 11h20-13h00 AEL; Fig.1.2.2A and C). This step is perhaps the most well-studied in the Drosophila myonuclear positioning field. Quantification of the cluster distance from the muscle ends relative to muscle length at stage 16 has proven to be effective at assessing even small differences in cluster spread [160,162,167–171]. The activities of the MT motor proteins, Kinesin-1 and cytoplasmic Dynein, as well as their associated proteins, Ens/MAP7, Bsg25D, CLIP-190, Glued, Pins/Raps, Syd, and Aplip1, are necessary for the movement for the nuclear clusters [158,162,167–170]. Both Kinesin-1 and Dynein exert forces directly on the nuclei, and from the cell cortex via the MTs, with the latter being termed as the cortical pulling mechanism [167,168]. The localization of both motor proteins was shown to be essential for their correct activity during this step. The proposed mechanism has Syd, a homolog of the mammalian JIP3, mediating the formation of a complex between Kinesin-1 and Dynein, and promoting the Kinesin-1- and JNK signaling-dependent transportation of Dynein along the MTs to the cell cortex. The MTs are stably connected to the cell cortex through CLIP-190. Once Dynein is

anchored at the muscle end via Raps/Pins, it becomes active to pull myonuclei. The authors further hypothesize that, while

Table 1.2.1 - Summary of proteins involved in myonuclear positioning and the consequences of their removal for muscle function.

Mammalian	**Drosophila**	***Role in* Drosophila**	***Muscle Function Consequences (Human disease*; Drosophila)***	***References***
Nesprin-4	klarsicht/klar	Cooperates with bocks; cluster formation (separation of nuclei into distinct clusters); myonuclear dispersion (sarcomere assembly); myonuclear spacing and anchoring (regulates myonuclear distances to the NMJ and near the MTJ)	EDMD; affects larval muscle function	[160,161,172,173]
Emerin	bocksbeutel/ bocks	Cooperates with klar; cluster formation (separation of nuclei into distinct clusters); cluster spread (via the cortical pulling pathway); myonuclear spacing and anchoring (in combination with Ote, it regulates klar expression at the NE; regulates astral MTs)	EDMD; affects larval muscle function	[160,161]
SUN2	klaroid/koi	Cluster formation (separation of nuclei into distinct clusters); cluster spread; myonuclear dispersion (sarcomere assembly; regulates klar expression at the NE)	EDMD disease modifier	[161,172,174, 175]
Amphiphysin	Amphiphysin/ Amph	Cluster formation (maintains nuclei within clusters); myonuclear spacing and anchoring (necessary for the proper localization of Ma2/d; regulates astral MTs)	CNM; affects larval muscle function	[160,176]
MAP7	Ensconsin/Ens	Positively regulated by Bsg25D; cluster formation; cluster spread; myonuclear spacing and anchoring	Affects larval muscle function	[158,162]
Ninein	Blastoderm-specific gene 25D/Bsg25D	Positively regulates Ens; cluster formation; cluster spread; myonuclear spacing and anchoring (regulate astral MTs and MT stability)	Affects larval muscle stiffness and function	[162]
Kinesin/Kif5b	Kinesin/Khc	Cluster spread (force exertion of nuclei leading edge and via the cortical pulling pathway); myonuclear spacing and anchoring (regulates myonuclear distance near the NMJ)	Not reported	[167,168,173]
Dynein	Dynein/Dhc	Cluster spread (force exertion of the nuclear lagging edge and via the cortical pulling pathway); myonuclear spacing and anchoring (regulates myonuclear distance near the NMJ)	Affects larval muscle function	[167,168,173]
CLIP1/2	CLIP-190	Cluster spread (via the cortical pulling pathway; connects the MTs to the cell cortex)	Affects larval muscle function	[167–169]
Dynactin 1, p150 subunit	Glued/p150	Cluster spread (via the cortical pulling pathway; forms a complex with Dynein)	Affects larval muscle function	[167,168]
G-protein-signaling modulator 2	Partner of inscuteable/ pins/raps	Cluster spread (via the cortical pulling pathway; anchors Dynein at the muscle ends); myonuclear spacing and anchoring (regulates the myonuclear position near the MTJ)	Not reported	[169,173]
JIP3	Sunday driver/Syd	Cluster spread (via the cortical pulling pathway; mediates the formation of a Kinesin-Dynein complex)	Affects larval muscle function	[169]
JIP1	Aplip1	Cluster spread (regulates nuclear translocation via changes in nuclear shape and the cortical pulling pathway; regulates the MT networks)	Not reported	[170]
SYNE-1/SYNE-2	Muscle-specific protein 300kDa/ MSP-300	Myonuclear spacing and anchoring (provides elasticity to the perinuclear shield; maintenance of nuclear shape; attachment of the MT asters to the NE; necessary for the proper localization of Ma2/d)	Autosomal-Dominant EDMD, EDMD-like phenotypes, Arthrogryposis (SYNE-1), Autosomal Recessive Cerebellar Ataxia type 1	[172,176,177]

			(SYNE-1); affects larval muscle function, control of glutamate receptor density at the NMJ	
Spectraplakin	short stop/ shot	myonuclear spacing and anchoring (provides rigidity to the perinuclear shield)	Not reported	[178]
EB family member 1	Eb1	myonuclear spacing and anchoring (provides rigidity to the perinuclear shield)	Not reported	[178]
Emerin	Otefin/Ote	myonuclear spacing and anchoring (in combination with bocks, it regulates klar expression at the NE)	X-EDMD	[161,179]
	Muscle-specific α2/δ/ Ma2/d	myonuclear spacing and anchoring (necessary for the SR-nucleus association)	Affects larval muscle function	[176]
ARIH1	Ariadne 1/ Ari-1	myonuclear spacing and anchoring (proper localization of MSP-300; mono-ubiquitinates koi)	SMC dysfunction (e.g. thoracic aortic aneurysms)	[180,181]

***where known**

Kinesin-1 and Dynein have roles in nuclear dynamics, Syd may also organize a population of both motors near the nucleus before transportation to the cell cortex [169]. The cortical pulling pathway is the most complete mechanism described to date in *Drosophila*. However, new components are still being discovered, suggesting that other proteins may be involved in this step via this pathway.

Ens is an important regulator of myonuclear positioning through its genetic and physical interaction with the motor protein Kinesin-1 [158]. Given the strong clustering phenotype it produces, Ens is also a potential candidate for the cortical pulling pathway [158]. However, despite being required for Kinesin-1 recruitment to MTs in other cellular contexts, the molecular mechanism of Ens' action during myonuclear movements in *Drosophila* is unclear [158,182,183]. Ens also interacts genetically and physically with Bsg25D to regulate cluster spread [162]. However, there a lack of evidence, such as genetic interactions with motor proteins, to implicate Bsg25D's direct participation in the cortical pulling pathway. These data suggest that alternative pathways involving these proteins remain to be uncovered.

Several NE components are involved in cluster spread. *bocks* genetically interacts with both Kinesin-1 and Dynein to affect the spreading of myonuclear clusters, suggesting that Bocks regulates myonuclear positioning through the cortical pulling pathway [160]. Moreover, recent work indicates that *bocks* genetically interacts with *klar* to properly move the myonuclear clusters [161]. This particular result could be a consequence of defective cluster formation and/or indicate that *bocks* has roles in more than one mechanism regulating myonuclear positioning. Other proteins associated with the LINC complexes also play a role in cluster spread. In particular,

embryos that have homozygous mutations or knockdown constructs for *klar* or *koi* fail to establish the appropriate distance between the nuclear clusters [172,174].

As the clusters migrate towards the muscle ends, dynamic movements of individual myonuclei have also been noted within each cluster. These movements include nuclear rotations and shape changes, and involve Kinesin-1 and Dynein acting directly on individual myonuclei in a polarized manner: while Kinesin-1 exerts forces on the leading edge, Dynein acts on the nuclear lagging edge [168]. More recently, Aplip1, the *Drosophila* JIP1, was also shown to be involved in regulating nuclear cluster translocation via changes in nuclear shape [170]. The forces that determine nuclear shape and orientation are independent of the cortical pathway and required to keep nuclei from changing directions.

An additional aspect of nuclear movement during cluster spread was revealed in Rosen *et al* [162]. Detailed time-lapse analyses showed that, while the nuclear clusters were overall moving towards the cell poles (positive movement), this trajectory was frequently disrupted by short-term movements in the opposite direction (negative movement). At the end of cluster spread, the final position of nuclear clusters resulted from the ratio of positive and negative movements. Strikingly, in different genotypes (e.g. *Bsg25D* overexpression and *Ens* loss) the quantification of this movement ratio at stage 15 was highly predictive of the final separation of nuclear clusters at stage 16 [162]. Together with the nuclear rotations and shape changes described above, these suggest that both, the manner in which the clusters move and the interactions between myonuclei within clusters, are essential for proper cluster spread. A better understanding of the mechanisms that regulate myonuclear dynamics and their impact on nuclear activity is needed.

As many of the proteins involved in the spreading of the myonuclear clusters in *Drosophila* are associated with the MT network, several studies have examined the MT network integrity and MT dynamics. Analysis of the MT-plus end binding protein EB1 has been used to probe how MT dynamics are affected in response to mutations in genes essential for cluster spread. Current data suggest that the MT network is not perturbed by the absence of most genes discussed in this section, with the exceptions of CLIP-190 and Aplip1 [162,167,169,170]. While CLIP-190 is necessary to facilitate the MT-cortex interactions that allows Dynein to move nuclei towards the muscle ends, the mechanism by which Aplip1 regulates the MT networks remains unknown.

In the *Drosophila* embryo, myonuclear cluster spread and the establishment of the myotendinous junctions (MTJs) occur simultaneously [184] (Fig. 1.2.2A). The MTJ, a specialized junction that connects muscles to tendons, is essential for structural

support and force transmission. While the mature MTJ is necessary for proper muscle contraction without detachment and allows the muscle cells to recover their shape after contraction [185–188], it is still unknown if and how the interactions between muscles and tendons influence myonuclear cluster movements. In mammalian muscle *in vitro*, there is no evidence of the two distinct clusters spreading as described in the *Drosophila* embryo, as myonuclei align in a single file and then spread. While these *in vitro* data are compelling, 2D muscle cell cultures lack extracellular cues provided by tendons and other cells types, which could be the reason for this observation. Nevertheless, the spreading of myonuclei in mammalian and *Drosophila* myotubes has several players in common. In mammals, MTs form a bipolar network around myonuclei that is required for proper myonuclear distribution. Similar to the fly, these networks seem to be minimally affected by depletion of Kinesins. Further, Kinesins and Dynein motors, Ens/MAP7, and MTs were shown to be necessary for nuclear three-dimensional rotation and translocation, resulting in the proper distribution of nuclei [158,189–191]. Due to the complexity of skeletal muscles and the intimate interactions with a variety of different cell types, i*n vivo* systems are essential to understanding myogenic processes. Our understanding of the roles that these interactions play in the regulation of myonuclear positioning is still limited, in particular concerning cluster spread, which could be highly dependent on structural cues and stability provided by stable cell-cell contacts.

2.3 Myonuclear dispersion

During stage 17, the last stage of the *Drosophila* embryonic development (16h00 AEL; Fig. 1.2.2A and D), the myonuclei dissociate from their cluster and disperse along the entire cell. During this stage, the myotubes mature into myofibers through the development of distinct structural and functional features: 1) the sarcomeres, highly conserved contractile units, that are linked to form longitudinal myofibrils and allow for muscle contraction; and 2) the neuromuscular junction (NMJ), through which the motor neurons signal for muscle contraction. While these and other structural changes occur (e.g. maturation of the MTJs), the *Drosophila* embryo starts to experience coordinated muscle contractions at this stage. It is tempting to hypothesize that any of the structural changes mentioned above, as well as muscle activity could promote/cause the dispersion of nuclei along the myofiber. However, we have observed that myonuclear dispersion occurs even in the absence of muscle

contractions (unpublished observations), suggesting that a different mechanism is driving this aspect of nuclear positioning.

An alternative mechanism that could promote myonuclear dispersion is the assembly of the sarcomeres and the formation of myofibrils. Before sarcomere assembly, Zasp, a protein present at the sarcomere Z-line, colocalizes with F-actin in puncta at the vicinity of the nucleus in a LINC-dependent manner [174]. This accumulation of Zasp, and the subsequent sarcomere and myofibril formation, only occurs after nuclear positions are determined. Additionally, embryos with defects in nuclear positioning or reduced expression of the LINC complex components, Klar and Koi, show poorly assembled sarcomeres and unstable, incomplete, and/or torn myofibril networks [172,174]. These data indicate that proper nuclear positioning and the presence of LINC complexes are required for stable sarcomere assembly. While this does not exclude the possibility that sarcomerogenesis contributes to nuclear dispersion, it is unlikely that it drives these nuclear movements.

A final attractive hypothesis is that nuclear dispersion is linked to the re-organization of the cytoskeleton. The cytoskeleton is a structural complex present in all cells, and it is composed of different classes of filamentous proteins: MTs, actin, and intermediate filaments. An interesting feature of skeletal muscle development is the drastic reorganization of the cytoskeleton, particularly of the MT networks. In myoblasts, MTs nucleate at a single centrosome, which is composed of two centrioles plus several proteins and constitutes the microtubule organizing center (MTOC). During most embryonic nuclear movements, the MT network appears to consist mostly of longitudinal MTs that run along the length of the myofiber. In addition, live imaging of EB1 comets to visualize growing MTs near myonuclei suggests that there is an increase in MT nucleating at the nuclear membranes throughout development (unpublished data). In differentiated myofibers of the *Drosophila* larva, at least two networks of MTs can be observed: longitudinal MTs that run along the length of the myofiber, as well as MTs nucleating from the nuclear membranes (astral MTs). Astral MTs result from the redistribution of the MTOCs [192]. It is not entirely clear when these MT rearrangements occur or whether they can drive the myonuclear dispersion observed in *Drosophila* embryonic muscles. It is further unclear if MAPs play a role in this process. Although Ens is essential for cluster spread in *Drosophila* LT muscles, a certain degree of myonuclear dispersion can be observed in *Ens* mutant embryos [158]. Similarly, despite the severe defects in cluster spreading, individual myonuclei and some dispersion can be observed in embryos lacking Dynein [167]. The partial recovery of nuclear positioning under these conditions suggests that cluster spread

and nuclear dispersion have distinct regulation and that additional regulators of myonuclear dispersion remain to be discovered.

Similar to fly muscles, mammalian muscle cells also relocate their MTOC to the nuclear envelope. However, these rearrangements occur in post-mitotic myoblasts, prior to fusion [157,192]. After fusion, the myonuclei cluster in the cell, then align along the long axis of the cell, before spreading in a MT-dependent way that involves Dynein and Kinesin-1 [159]. Results from mammalian muscle cells and a computational model suggest that MAP7/Ens and Kinesin cooperate to slide antiparallel MTs nucleating from neighboring nuclei [158,193]. Another mechanism proposed to explain myonuclear dispersion in cultured mammalian myotubes involves Nesprin 1 or 2, as part of the LINC complex, recruiting motor proteins to the NE. The authors identified the nucleus as a Kinesin-1 cargo, with Nesprins 1 and 2 working as cargo adaptors. According to their model, nuclear dispersion is achieved by using the antiparallel MT network created by the multiple myonuclei [189,194]. Hence, it appears that MTs and MAPs are involved in nuclear dispersion in *Drosophila* and mammalian muscle fibers. However, further experiments exploring the rearrangements and dynamics of the cytoskeleton are required to better understand myonuclear dispersion.

2.4 Myonuclear spacing and anchoring

At the end of *Drosophila* embryogenesis, the muscles become fully functional and contract in a coordinated manner, allowing the embryo to hatch into a first instar larva. Subsequent larval development (five days at 25℃) is characterized by dramatic muscle growth and continuous muscle activity manifested as locomotion. At this stage, the ventral longitudinal (VL) muscles have been the most studied group of myofibers for this process due to their location, size, shape, and nuclear arrangement [195–197]. VL muscles have a rectangular, flat shape with disc-shaped nuclei peripherally positioned on one side of the cell [196] (Fig. 1.2.2A, E and E'). Due to their simple morphology, they allow for the precise analysis of many muscle cell features, including protein localization, cytoskeletal networks organization, and myonuclear positioning. While the size of individual muscle fibers increases up to 50-fold during larval growth, the number of myonuclei remain the same [198]. To support this rapid growth, the myonuclei increase their DNA content through endoreplication, in a way that linearly scales with the muscle size [196,198]. Although little is known about myonuclear movements after the embryo hatches, the positions that myonuclei adopt along the length of the myotubes at the end of embryonic development are

maintained in larval muscles. To maintain proper spacing, the myonuclei have to continuously adjust their positions along the growing cell. To withstand the forces produced during muscle contraction, each nucleus also needs to be anchored at its position.

Myonuclei are protected from intrinsic and extrinsic forces by a flexible perinuclear shield. This shield, which consists of nuclear, cytoskeletal and LINC complex components, is involved in nuclear spacing as well as anchoring. Some components provide elasticity, such as the Nesprin 1 homolog MSP-300, while others provide rigidity, such as the MT network which is stabilized by Shot, the *Drosophila* spectraplakin, and EB1 [178,199]. In the absence of this shield, myonuclei show changes in morphology, have reduced levels of nuclear proteins, such as lamins and HP1, and positioning defects [178]. In addition to protecting the integrity of the nucleus itself, components of the perinuclear shield also connect to other muscle cell structures, like the T-tubules and the sarcoplasmic reticulum [176].

Further support for the roles of the LINC components in myonuclear spacing and anchoring has been generated by examining mutations in parkin-like E3 ubiquitin ligase Ariadne-1 (Ari-1). The authors showed that Ari-1 mono-ubiquitinates Koi, a central member of the LINC complex. Mutations in *ari-1* resulted in *Drosophila* larval muscles with myonuclei clusters and morphology defects. Additionally, the authors identified rare variants of the human homolog of *ari-1* (ARIH1) which is associated with conditions resulting from smooth muscle cell (SMC) dysfunction, such as thoracic aortic aneurysms. Excitingly, the *Drosophila* defects could be rescued with human ARIH1, while the rare variants found in patients could not. Due to the presence of abnormal nuclear morphology in SMCs from patients, the authors concluded that ARIH1 is crucial for myonuclear anchoring to the cytoskeleton [180,181]. Collectively, these data reinforce the importance of appropriate myonuclear positioning and anchoring through these complexes and the use of simpler models, like *Drosophila,* to study mechanisms of human muscle dysfunction.

The spacing of myonuclei in *Drosophila* VL muscles is far from random. A recent *in silico* study proposes that myonuclei maximize their distances with each other by pushing on neighboring myonuclei and the cell membrane via the astral MTs at the NE (Fig. 1.2.2E) [200]. These data are supported by various *in vivo* observations. Loss of *bocks* and *Amph* resulted in changes in the polarization of the perinuclear MTs, and, in some cases, the absence of the MT asters. These MT changes were associated with defects in myonuclear spacing [160]. Similar to the embryo, Bsg25D and Ens also interact to position myonuclei in the larvae. Muscle-specific *Bsg25D* overexpression

also shows severe myonuclear positioning defects in larval VL muscles, a phenotype that can be rescued by Ens expression. Similarly, increased levels of Bsg25D fully disrupts astral MTs in all myonuclei and result in the formation of ectopic MTOCs where Bsg25D and Ens colocalize. An interesting characteristic of polymerized tubulin is its ability to undergo posttranslational modifications, which are associated with MT stability. Tubulin acetylation in particular is associated with increased binding of motors to MTs [201]. Bsg25D overexpression causes a decrease in acetylated tubulin, a marker of MT stability found in the longitudinal MTs, which might indicate a loss of MT stability [162]. The stiffness of the muscles was also decreased in Bsg25D overexpression larvae, which the authors attribute to changes in MT organization [162]. These studies clearly highlight the importance of the MT cytoskeleton, in particular the astral MTs in establishing and maintaining nuclear spacing in the mature myofiber.

Mammalian myofibers *in vivo* are rod-shaped and display peripheral nuclear localization around the perimeter of the cell. An *in vitro* mammalian model has recently been developed in which mammalian myotubes mature into a myofiber in culture, complete with myofibrils. Coupled with a theoretical modeling, this *in vitro* model has revealed that centrally located myonuclei move to the cell periphery in the maturing myofiber. The authors found that this movement was due to centripetal forces generated by myofibril contraction and crosslinking around the nuclei. This process is dependent on the Cdc42-regulated organization of desmin. The nuclear dispersion also relies on the stiffness of nuclei, and the activity proteins like Amphiphysin-2 and the Arp2/3 complex proteins, which regulate the deformation and squeezing of nuclei to the muscle periphery [202–204]. Additionally, peripheral nuclear positioning depends on the local accumulation of fibronectin deposited by myofibroblasts [204]. Since several muscle disorders show centrally located myonuclei, understanding how making myonuclei peripheral and possibly keeping them anchored in place are key to discover the mechanisms behind these diseases and generate therapies that help prevent or revert this process.

An important feature of myonuclear spacing and anchoring is that myonuclei in *Drosophila* and mammalian mature myofibers diversify and adopt specific characteristics dependent on their position within the cell specifically their proximity to MTJs and NMJ [173,196,200]. In *Drosophila* larval myofibers, internuclear distances near the NMJ depend on Kinesin-1 and Dynein, and the distance between myonuclei and the NMJ is regulated by Klar [173]. Nuclei that are closer to the NMJ are overall larger and have higher DNA copy number than other nuclei. The opposite is true for

the nuclei near MTJ; they are smaller in size with fewer copies of DNA [196]. Additionally, there are more nuclei near the MTJ and their positions within muscle cells appear to be regulated by Klar and Pins, as well as in response to mechanical stimuli [173,200]. Similarly to what is observed in *Drosophila* myofibers, mammalian muscle *in vivo* also displays two very clear populations of myonuclei that aggregate near NMJs and MTJs [159,205]. These data argue for the similarities between animal models and the important relationships that the muscle establishes with other cell types. However, a better understanding of these relationships using mammalian *in vivo* models or *in vitro* co-cultures models will better clarify the importance of these interactions and the impact that they have on myonuclear spacing and anchoring within the myofiber.

BOX 1

Nuclear mispositioning and muscle disease

Nuclear mispositioning is a hallmark of several muscle diseases, including EDMD and CNM [149,150]. Nevertheless, it was unclear whether mispositioning is a cause or consequence of muscle disease. The analysis of ens mutations in Drosophila suggested a causal link between aberrant nuclear position and muscle dysfunction [158]. Following this study, other genes, such as *Dynein* and *Bsg25D*, were found to have mispositioned myonuclei and larval movement defects [162,167–169,172]. Recently, mutations associated with EDMD and CNM in Drosophila showed similar phenotypes [160]. However, it remains an outstanding question why mispositioned myonuclei in these mutants lead to deficits in muscle function. Several hypotheses merit investigation.

One hypothesis relates specific nuclear localization to specific function within the muscle cell. It has been long recognized that myonuclei in mammals are clustered at the NMJ and express unique RNAs [159,205]. These observations were further developed in *Drosophila*, where changes in nuclear and nucleolar size, DNA content, and transcriptional activity were associated with different regions of the muscle cell (NMJ, MTJ, others) [196]. Together, these data suggest that myonuclei in these regions are distinct and produce unique products required for optimal muscle function. Hence myonuclear mispositioning would lead to alterations in region-specific transcriptional programs. This hypothesis could be tested using single nuclear sequencing approaches to define unique transcripts for myonuclei in each region.

A second related hypothesis considers myonuclear position within its cytosolic context, also known as its myonuclear domain [196]. Each myonucleus has MT arrays that maintain the position of individual myonuclei [162,196,200]. These arrays may also function to traffic RNAs and proteins within the domain. One can speculate that RNAs and proteins may not be properly trafficked within the myonuclear domain in the positioning mutants, thus reducing muscle homeostasis. An extreme case can be seen with Bsg25D: misexpression of Bsg25D leads to missing myonuclear MT arrays, mispositioned myonuclei, and decreased muscle size [162]. Future studies in which fluorescently-tagged RNA transcripts or proteins are followed by time-lapse imaging

in Bsg25D and other positioning mutants will provide further insight to the mechanisms required for nuclear positioning and function.

Translating these findings into treatments for patients suffering from skeletal muscle diseases remains a critical challenge. Clearly, identifying additional mutated gene(s) associated with muscle diseases, such as EDMD and CNM, will enlarge our understanding of disease mechanisms and contributions of myonuclear positioning to disease. Likewise, assessing the extent of global (muscle) and local (myonuclear domain) transcriptional changes in patient samples with aberrant myonuclear positioning will provide possible therapeutic targets and approaches. Lastly, a better understanding of the dynamics of myonuclear positioning in the context of satellite cell mediated repair may offer new insights to disease treatment.

OUTSTANDING QUESTIONS

- Do muscle diseases share a common mechanism or result from different mechanisms?
- Are the mechanisms that drive nuclear clustering and positioning during development and regeneration the same?
- How do muscle cell interactions with other cells types (e.g. tendons and motor neurons) affect myonuclear positioning?
- How does position dictate nuclear identity?
- How are myonuclear positions maintained during myofiber growth and contraction?
- What are the mechanisms that drive even myonuclear dispersion within the muscle cell?
- How do nuclear clusters maintain their cohesion during cluster spread?
- When do the rearrangements of the microtubule network occur during fly myogenesis?

CONCLUDING REMARKS

Myonuclear positioning is a complex sequence of steps involving many molecular players active at multiple processes. Here we subdivide the *Drosophila* myonuclear positioning into four steps and describe the most recent mechanisms including those players. Overall, the major molecular components are nuclear components, LINC complexes, cytoskeletal and motor proteins. These processes and the genes that regulate them appear to be highly conserved from fly to mammal. Most importantly, in all models, mispositioned nuclei are associated with a decrease in muscle function (Table 1.2.1). Nevertheless, several aspects of myonuclear positioning remain to be addressed, including the impact of muscle cell interactions with other cells types, the links between myonuclei as they move, and the movement of myonuclei during growth and regeneration (see Outstanding Questions). The use of multiple models – *Drosophila*, mammalian *in vitro* and *in vivo* – and approaches – genetic, biochemical, mathematical modeling – will surely uncover the answers.

Myonuclear mispositioning has been shown to be a hallmark of numerous muscular disorders. For example, centronuclear myopathies are a diverse group of disorders associated with mutations in several different genes [206]. Similarly, Emery-Dreifuss muscular dystrophy represents a genetically heterogeneous disease. For both of these examples, novel mutations are still being discovered [206,207]. These new mutations open new ways to explore muscle biology as well as offer targets for precise and individualized therapies. From studies using *Drosophila* to study myonuclear positioning, at least a dozen genetic mutations have been identified to affect muscle function, some of which involve genes directly linked to disease [158,160,167,169,171,172,176,196]. These studies confirm the contribution of proper myonuclear positioning for muscle function and the validity of this model for exploring the mechanisms behind myonuclear position and muscle loss of function (see Box 1). Nevertheless, it is the collective data from studies in both the fly and mammals that will clarify the importance of myonuclear positioning.

Chapter 2
Goals

GOALS

In skeletal muscle, nuclei reside above the sarcomere at the periphery of the muscle fiber and are positioned to maximize their internuclear distance. Mechanisms for anchoring nuclei along the myofiber have been identified. However, it is unclear how the majority of the myonuclei become spaced throughout the myofiber during development. For proper function, the muscles develop an intimate relationship with other cell types. Tendon cells provide connection between the muscle and the skeleton through an interface called myotendinous junction (MTJ). These cells provide signaling information that modify different aspects of muscle biology, including muscle type and shape. Muscle-tendon interactions are required to provide a strong, yet adaptive, connection between the skeleton and the muscle. The MTJs in *Drosophila* are structurally and functionally analogous to human MTJs: both rely on Integrin signaling to anchor muscles to tendon cells through an intervening ECM. Studies in *Drosophila* have provided insight into the crosstalk between tendon and muscle that sets up and subsequently matures the MTJ. Little is known about how the established MTJ influences overall muscle cytoarchitecture, and specifically myonuclear position, during muscle development.

Mispositioned myonuclei are a hallmark of many muscle disorders, such as Emery-Dreifuss Muscular Dystrophy and Centronuclear Myopathies, and have been used diagnostically for decades. Assessing the contribution of myonuclear positioning to disease in *in vivo* mammalian muscle is difficult due to the inability to follow individual nuclei in undergoing ongoing muscle repair, since during this process post fusion myonuclei move to the center of the muscle. Additionally, little regeneration is thought to occur in some muscle diseases, such as myotonic dystrophy and centronuclear myopathies; nonetheless an abundance of clumped, centronucleated myonuclei is found in these patients. Therefore, it is of the utmost importance to understand the mechanisms that drive proper myonuclear positioning and muscle function.

This Thesis presents the results obtained during the doctoral work divided into three parts. The main goals were to:

Main goal 1: Analyze the input of tendon cells in myonuclear movement and positioning by manipulating the MTJ to determine how tendons influence myonuclear positioning and lead to a fine tuning of muscle architecture.

Main goal 2: Determine the impact of myonuclear positioning on cytoskeletal organization and muscle structure and function by analyzing mutants with myonuclear positioning defects and assessing larval muscle organization and locomotion.

To accomplish these goals, an *in vivo Drosophila* model was used. It provides a simple and rapid system to investigate basic mechanisms of myonuclear positioning and its effects on muscle function/physiology. Previous data indicate a striking correlation between aberrantly placed and clumped nuclei and a decrease in muscle function. Given the conservation of genes and mechanisms from fly to mammal, there is a strong suggestion that aberrant myonuclear positioning could indeed contribute to the muscle deficits associated with muscle disease.

Chapter 3
General Materials and Methods

IMAGING APPROACHES TO INVESTIGATE MYONUCLEAR POSITIONING IN *DROSOPHILA*

Mafalda Azevedo[1,2], Victoria K. Schulman[2,3], Eric Folker[2,4], Mridula Balakrishnan[2,5], and Mary Baylies[6,7]

[1]Graduate Program in Basic and Applied Biology (GABBA), Institute of Biomedical Sciences Abel Salazar, University of Porto, Porto, Portugal.
[2]Program in Developmental Biology, Sloan Kettering Institute, Baylies Lab, Box 310, 1275 York Avenue, New York, NY, 10065, USA.
[3]Department of Genetics, Yale University School of Medicine, 333 Cedar Street, New Haven, CT, 06520, USA.
[4]Biology Department, Boston College, 140 Commonwealth Avenue, Chestnut Hill, MA, 02467, USA.
[5]Weill Graduate School at Cornell Medical College, 430 East 67th Street, New York, NY, 10021, USA.
[6]Program in Developmental Biology, Sloan Kettering Institute, Baylies Lab, Box 310, 1275 York Avenue, New York, NY, 10065, USA. m-baylies@ski.mskcc.org.
[7]Weill Graduate School at Cornell Medical College, 430 East 67th Street, New York, NY, 10021, USA. m-baylies@ski.mskcc.org.

in Sue Shackleton et al. (eds.), The Nuclear Envelope: Methods and Protocols, Methods in Molecular Biology, 1411 (2016) 291–312

ABSTRACT

In the skeletal muscle, nuclei are positioned at the periphery of each myofiber and are evenly distributed along its length. Improper positioning of myonuclei has been correlated with muscle disease and decreased muscle function. Several mechanisms required for regulating nuclear position have been identified using the fruit fly, *Drosophila melanogaster*. The conservation of the myofiber between the fly and vertebrates, the availability of advanced genetic tools, and the ability to visualize dynamic processes using fluorescent proteins *in vivo* makes the fly an excellent system to study myonuclear positioning. This chapter describes time-lapse and fixed imaging methodologies using both the *Drosophila* embryo and the larva to investigate mechanisms of myonuclear positioning.

Keywords *Drosophila*, Muscle, Nuclear movement, Embryo, Larvae

INTRODUCTION

The skeletal muscle provides an important system in which to study mechanisms of myonuclear positioning. Myofibers, the cellular units of the skeletal muscle, are multinucleated and position their myonuclei to reside above the sarcomeres at the cell periphery and along the length of the fiber to maximize internuclear distance. Moreover, mispositioned myonuclei correlate with muscle disease [208], and recent data suggest that mispositioned myonuclei may cause muscle weakness [158,167,169], illustrating the functional importance of proper positioning.

To identify the cellular mechanisms of myonuclear movement in vivo, we have utilized the musculature of *Drosophila* embryos and larvae [158,167–169,209]. *Drosophila* muscles share the conserved myofiber structure found in vertebrates: *Drosophila* myofibers are multinucleated, maintain particular sizes and shapes, attach to particular tendon cells, become innervated by specific motoneurons, build sarcomeres, and are essential for locomotion (reviewed in [3,90]). The *Drosophila* system also offers unparalleled genetic approaches to manipulate genes of interest within the whole organism or specifically within muscle tissue. In addition to their powerful genetics, *Drosophila* embryos are also amenable to drug treatments commonly used to manipulate cell biological processes in culture, providing additional opportunities to probe the cellular machinery responsible for myonuclear movement [209]. Lastly *Drosophila* embryos are amenable to time-lapse microscopy without perturbing development such that cell biological processes, including myonuclear dynamics, can be assessed [168].

There are 30 individual muscles per abdominal hemisegment of the *Drosophila* embryo (Fig. 3.1.1). Formation of these individual body wall myofibers depends on the specification and fusion of two myo- blast cell types: founder cells (FCs) and fusion-competent myoblasts (FCMs). Each FC contains the information necessary to direct the formation of a specific muscle. FCs can be identified by the expression of identity genes, such as the transcriptional regulators *even- skipped* and *apterous* [17,210,211]. The combination of identity genes and chromatin regulators expressed by a particular FC regulates the final morphology of the specific muscle. In contrast, FCMs are more naïve cells. Upon fusion to an FC, FCMs become reprogrammed to the specific developmental program of the FC, as evidenced by the observation that each newly incorporated FCM nucleus begins to express the same combination of identity genes as the FC [3]. Myoblast fusion is an iterative process; depending on the

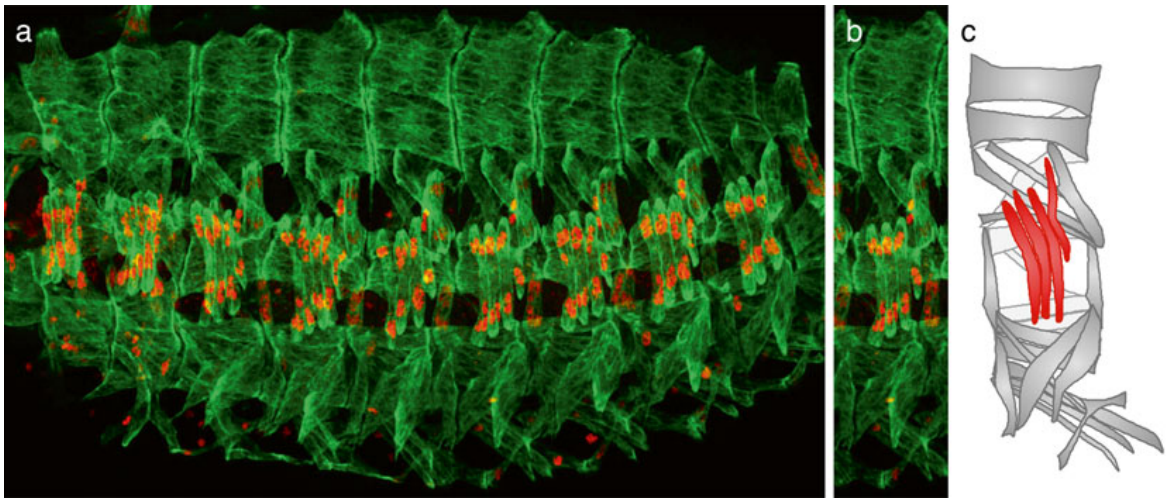


Figure 3.1.1 The *Drosophila* embryonic musculature. The *Drosophila* embryo is divided in hemisegments, each containing 30 muscles. (**A**) Stage 16 embryo showing the musculature in green (Tropomyosin) and the nuclei of the lateral transverse (LT) muscles in red (DsRed). (**B**) Image of a single hemisegment. (**C**) Schematic representation of all the muscles present in one hemisegment; the LT muscles are highlighted in *red*. For additional detail *see* Dobi et al. [7]

particular muscle, body wall muscles in *Drosophila* embryos contain between 2 and 25 myonuclei. As myoblast fusion concludes, the polarized syncytial myotube extends processes toward specific tendon cells and forms stable myotendinous junctions. Specific motoneurons innervate each muscle, leading to coordinated contraction at the final stage of embryogenesis [90,212].

Although mispositioned nuclei are observed in all muscles when certain genes are disrupted, myonuclear positioning has been best characterized in the lateral transverse (LT) muscles of the developing embryo. We have shown that LT myonuclei undergo not one but a series of movements to maximize internuclear distance *in vivo* (Fig. 3.1.2; [158,167–169]). Post-fusion (stage 14), the myonuclei are located in a single group within the myotube. Over the course of development, these nuclei segregate into smaller groups that follow characteristic migration patterns (stages 15, 16) before evenly distributing throughout the myofiber at the end of embryonic stage 17 [3,90,158,167–169,209]. During larval development, in which the muscles grow up to 40-fold [198], the myonuclei in the individual muscles maintain regular spacing along the muscle fiber. These myonuclei are positioned above the sarcomeres along the periphery of the muscle fiber (Fig. 3.1.3; [158]).

To date, there are several mechanisms required for the different movements of myonuclei in *Drosophila*. These mechanisms require microtubules; microtubule-associated proteins, such as Ensconsin; the microtubule motor proteins, kinesin and dynein; and motor protein adaptors, such as kinesin light chain, dynein light chain,

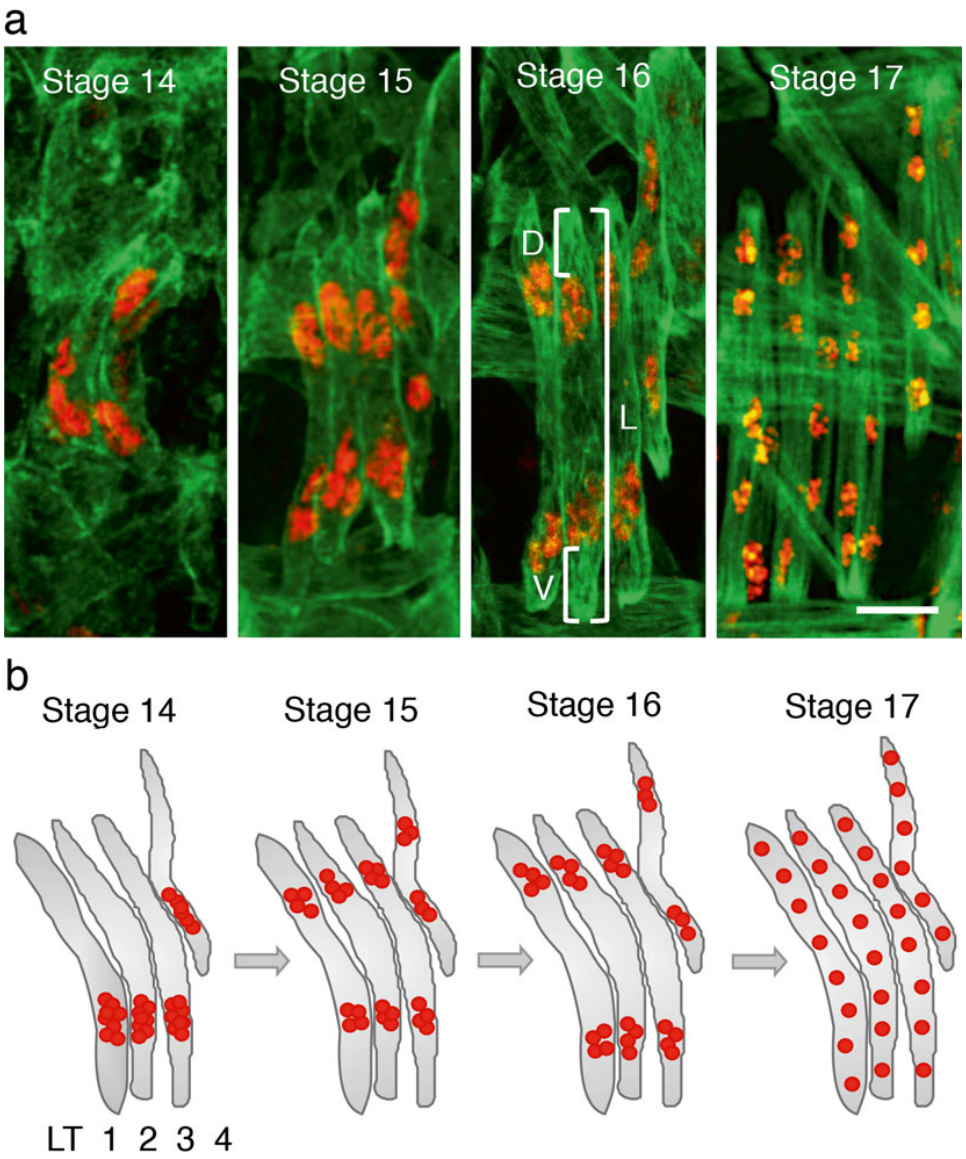


Figure 3.1.2 Myonuclear positioning in the LT muscles during embryonic development. (**A**) Myonuclear position from stage 14 to stage 17. In the images of stages 14–16, the LT muscles are stained with Tropomyosin (*green*) and DsRed (*red*) to show the muscle structure and the nuclei, respectively. In the stage 17 image, the LT muscles are labeled with *Tropomyosin-GFP* (*green*) and the nuclei are labeled with *apterousME::NLSdsRed* (*red*) (*see* Table 2). At stage 16, image measurements are taken: D represents the dorsal measurement, V represents the ventral measurement, and L represents the total length of the muscle. Scale bar, 10 μm. (**B**) Schematic representation of myonuclear movements from stage 14 to stage 17 as shown in panel (**A**). LT muscles 1–3 have 6–8 nuclei each, whereas LT4 has 4–6 nuclei.

p150/Glued, cytoplasmic linker protein-190 (CLIP190), Sunday driver (Syd or JNK-interacting protein 3 (JIP3)), and JNK signaling [158,167–169]. We refer the reader to [90] in which we discuss our current thinking about the different mechanisms at work during each stage of myonuclear movement. To identify these mechanisms, we have developed various techniques to define and quantify myonuclear position in

Drosophila [158,167–169]. This chapter describes these methodologies in both fixed and live *Drosophila* embryonic and larval preparations.

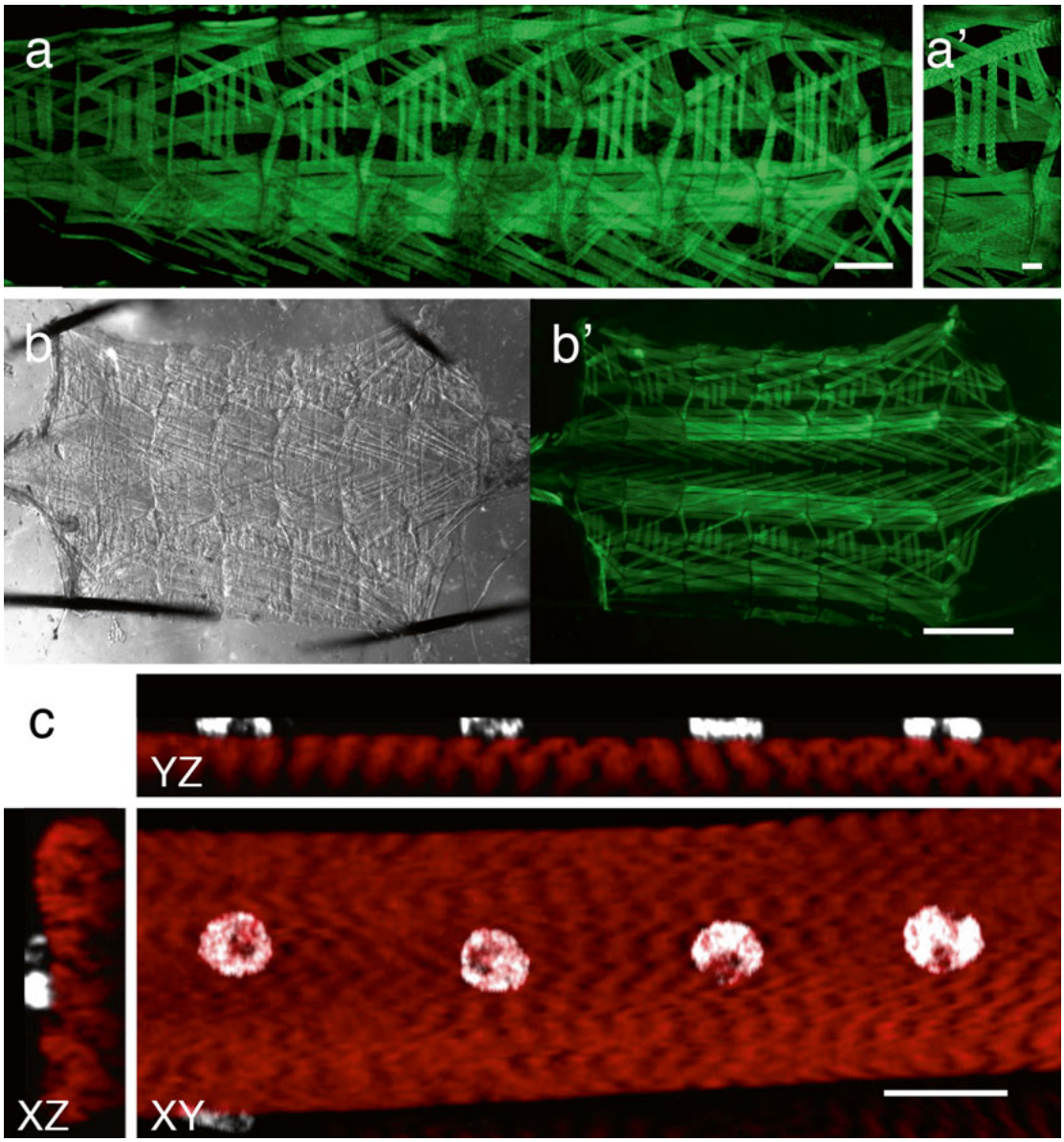


Figure 3.1.3 Larval musculature and myonuclear positioning in a 3rd instar larva. (**A**) Image of a live *Drosophila* 3rd instar larva expressing *Tropomyosin-GFP*, a GFP gene trap that labels all muscles. Note the repeated muscle pattern in each hemisegment. Scale bar, 100 μm. (**A'**) Higher magnification of one hemisegment. Scale bar, 25 μm. (**B**, **B'**) Dissected flat prep of a larva carrying *Tropomyosin-GFP* with all the muscles exposed. Scale bar, 50 μm. (**B**) Bright field image. (**B'**) Wide field fluorescence image. (**C**) Orthogonal view of a ventral longitudinal 4 muscle (VL4). *Red*, actin; *white*, nuclei. Scale bar, 25 μm

MATERIALS

2.1 Imaging of Fixed Embryonic Muscles

2.1.1 Embryo Collection and Fixation (Fig. 3.1.4)

1. Embryo laying pot: 100 ml plastic beaker punched with holes to allow air exchange and prevent condensation. To make holes use a hot syringe needle with gauge (Sub-Q 26G5/8).
2. Embryo collection plates (apple juice plates): Microwave 1500 ml of ddH_2O, 50 g of granulated sugar, and 45 g of agar until a homogeneous solution is formed. Add 500 ml of cold apple juice, cool solution to 65˚C, and add 40 ml of 10 % Tegosept in 100 % ethanol. Pour solution into petri dishes (60×15 mm); make approximately 200 plates. Secure these plates to the laying pots with rubber bands.
3. Yeast paste: Distill water plus dry baker's yeast and stir to make a paste. Store at 4˚C.
4. Paintbrush (size 0).
5. Collection baskets: Cut the top off of a 15 ml Falcon tube at approximately the 12 ml line and cut out the center of the tube cap.
6. Nylon membrane (pore size, 140 μm) screwed onto the collection basket with the cap.
7. 3 % sodium hypochlorite (50 % bleach).
8. Small funnel.
9. Eppendorf tubes (1.5 ml).
10. Heptane.
11. Methanol.
12. PFA: 4 % EM grade paraformaldehyde diluted in PBS (phosphate-buffered saline).
13. Platform shaker.
14. Vortex with 1.5 ml Eppendorf tube adaptor.
15. PFA/heptane waste receptacle.
16. Methanol/heptane waste receptacle.
17. Glass Pasteur pipets.

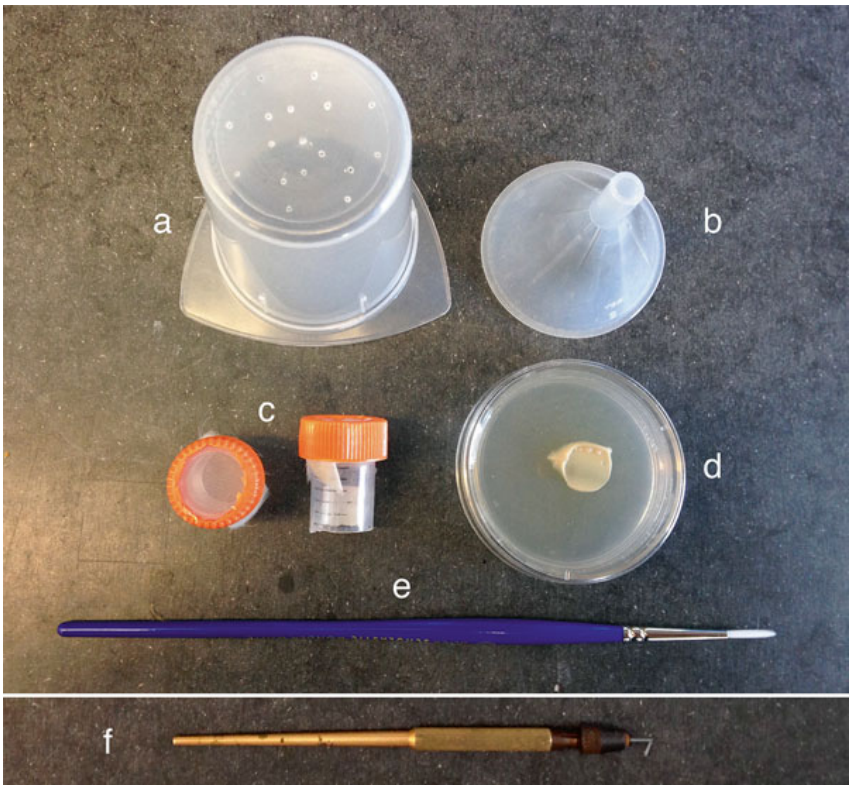


Figure 3.1.4 Materials used for embryo collection. (**A**) Embryo laying pot perforated on the *bottom*. (**B**) Small funnel. (**C**) Collection baskets: *top* and *side* views. (**D**) Yeasted apple juice plate. (**E**) Paintbrush. (**F**) Embryo hook.

2.1.2 Embryo Staining

1. 3 % Triton X-100: For 200 ml, add 6 ml of Triton X-100 and 194 ml ddH_2O.
2. 10× PBS (phosphate-buffered saline; 0.01 M KH_2PO_4, 0.1 M Na_2HPO_4, 1.37 M NaCl, 0.027 M KCl, pH 7.0).
3. PBT (phosphate-buffered saline containing 0.3 % Triton): For 100 ml, add 10 ml 10× PBS, 10 ml 3 % Triton X-100, and 80 ml ddH_2O.
4. PBT-BSA (phosphate-buffered saline containing 0.3 % Triton and 0.1 % BSA): For 100 ml, add 10 ml 10× PBS, 10 ml 3 % Triton X-100, 1 ml 10 % BSA, and 79 ml ddH_2O.
5. Primary and secondary antibodies of interest. Refer to Table 1 for a suggested list of antibodies and probes routinely used to label *Drosophila* muscle and nuclei.
6. Three-dimensional rotating mixer such as a Nutator.
7. Eppendorf tubes (0.5 ml).
8. Glass Pasteur pipets.

Table 3.1.1
Antibodies and probes used to probe *Drosophila* myonuclear positioning[a]

Primary Antibodies[b]	**Expression Detected**	**Company, reference #**
Muscle markers		
Tropomyosin	Actin cytoskeleton	Abcam, ab50567
Myosin Heavy Chain (MHC)	Myosin, Actin motor protein	DSHB, EB165-s
Nuclear Markers		
Lamin Dm0	Nuclear envelope	DSHB, ADL67.10
Lamin C	Nuclear envelope	DSHB, LC28.26
Specific Muscle Nuclear Markers		
Even-skipped	DA1	[213]
Vestigial	DA1, DA2, DA3, LL1, VLs1-4	[214]
Others		
DsRed	Red fluorescent protein	Clontech, 632496
GFP	Green fluorescent protein; useful to identify the present of fluorescent balancers (e.g.: DGy, CTG)	Clontech, 632381 Invitrogen, A-11120
α-tubulin	Microtubules	Sigma, T9026
Secondary Antibodies	**Expression detected**	**Company, reference #**
Alexa Fluor 488-conjugated		Life Technologies
Alexa Fluor 555-conjugated		Life Technologies
Alexa Fluor 647-conjugated		Life Technologies
Probes antibodies	**Expression detected**	**Company, reference #**
Alexa Fluor 546- conjugated Phalloidin	F-actin	Life Technologies, A22283
Hoechst	DNA	Invitrogen, 33342

[a]We refer the reader to several papers for reagents that probe specific proteins involved in myonuclear positioning [158,172,209].
[b]See Notes 1 and 2.

2.1.3 Embryo Mounting

1. Microscope slides.

[a]We refer the reader to several papers for reagents that probe specific proteins involved in myonuclear positioning [2–6, 22]
[b]*See* **Notes 1** and **2**

2. Scotch tape.
3. Cover slips: size 22×40 mm with thickness 0.16–0.19 mm.
4. Mounting medium, such as ProLong Gold antifade reagent or Vectashield.
5. Razor blades.
6. Metal washers (any hardware store).

2.1.4 Embryo Imaging

All images in the lab are acquired on a Leica SP5 laser-scanning confocal microscope equipped with a 20× 0.7NA HC PL Apochromat oil objective, 63× 1.4NA HCX PL Apochromat oil objective, and LAS AF 2.2 software. Equivalent microscopes and software may be used.

2.2 Time-Lapse Imaging of Embryonic Muscles

2.2.1 Embryo Collection and Mounting (Fig. 3.1.5)

Materials described in Subheading 2.1.1, plus:

1. Plain-tipped applicator (wooden stick).
2. Halocarbon oil 700.
3. Air-permeable Teflon membrane mounted on a circular Perspex frame (designed by E. Wieschaus; [215,216]).

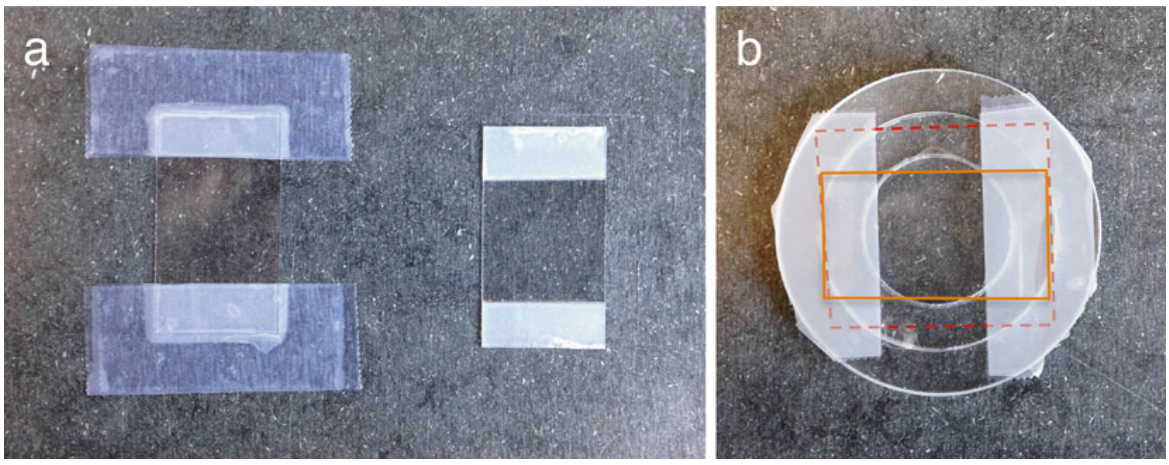


Figure 3.1.5 Materials used for mounting embryos. (**A**) Cover slip with a Scotch tape bridge used to mount fixed embryos for imaging. The image shows a cover slip with two pieces of tape on both ends, before the excess is removed (*left*) and after (*right*). (**B**) Frame used to mount embryos for time-lapse imaging. The image shows an air-permeable Teflon membrane (*red dashed line box*) mounted on a circular Perspex frame. Two pieces of tape provide support for a cover slip bridge where the embryos are placed (*center of the frame*). The orange solid line box represents the cover slip; it is placed on top of both sides of the tape as shown in the image.

4. Cover slips: size 22×40 mm with thickness 0.16–0.19 mm.

2.2.2 Embryo Imaging

Mounted embryos are imaged on a Leica SP5 laser-scanning confocal microscope equipped with a 63× 1.4NA HCX PL Apochromat oil objective and LAS AF 2.2 software (for imaging nuclear clusters or individual nuclei [168]) or on a Zeiss AxioPlan2 epifluorescence imaging system with light microscopy with a 40× Plan-NeoFluar 0.75NA objective and AxioVision Rel 4.8 software (for myonuclear movement in the whole embryo; [158]). Equivalent microscopes and software may be used.

2.3 Imaging of Formalin-Fixed Larval Muscles

2.3.1 Larvae Collection

1. Laying pot as described in Embryo Collection and Fixation from Imaging of Fixed Embryonic Muscles section (*see* Fig. 3.1.4).
2. Lightly yeasted apple juice plates (*see* Subheading 2.1.1, step 2).
3. 15 % sucrose solution: sucrose diluted in water.
4. Embryo hook or straight forceps (tip dimensions, 0.1×0.06 mm).
5. Dissection microscope equipped with fluorescence.
6. Paintbrush.

2.3.2 Larvae Dissection and Fixation

1. Dissection pins (diameter, 0.1 mm).
2. Two pairs of straight forceps (tip dimensions, 0.1×0.06 mm).
3. Dissection plate: petri dish (150×15 mm) coated with a thick layer of Sylgard.
4. Vannas spring scissors (sharp tips; non-serrated; cutting edge, 3 mm; tip diameter, 0.05 mm).
5. Cold HL3.1 buffer: 70 mM NaCl, 5 mM KCl, 0.2 mM $CaCl_2$, 20 mM $MgCl_2$, 10 mM $NaHCO_3$, 5 mM trehalose, 115 mM sucrose, and 5 mM HEPES; pH 7.3 [217].
6. 1× PBS.
7. Formalin solution, 10 %. 8. Glass Pasteur pipets.

2.3.3 Larvae Staining and Mounting

As in Subheadings 2.1.2 and 2.1.3, plus:

1. Straight forceps (tip dimensions, 0.1×0.06 mm).
2. Kimwipes tissues.
3. Dissection scope.

2.3.4 Heat-Fixed Larvae

1. Water (distilled) at 65˚C.
2. Halocarbon oil or 50 % glycerol.
3. Microscope slides.
4. Cover slips: size 22×40 mm with thickness 0.16–0.19 mm.

2.3.5 Larval Imaging

Images are acquired using the 40× 1.25–0.75NA HXC PL Apochromat oil objective of a Leica SP5 laser-scanning confocal microscope and the LAS AF 2.2 software. Equivalent microscopes and software may be used.

2.4 Fly Stocks

The *Drosophila* community has developed a rich collection of genetic reagents to probe various cellular processes, including myonuclear positioning. In addition to classic mutations, there is a wide range of available fly stocks that allow tissue-specific manipulation of a gene of interest. Spatial and temporal manipulation is accomplished using the bipartite GAL4/UAS system [218]. Reagents useful for the study of myonuclear positioning are listed in Table 3.1.2. New reagents are constantly being developed, particularly with the development of CRISPR genome-editing approaches in *Drosophila*. We refer the reader to FlyBase (http://flybase.org/), a community resource that provides a comprehensive, searchable compendium of genes, mutations, expression patterns, available stocks, and references.

METHODS

3.1 Imaging of Fixed Embryonic Muscles

3.1.1 Embryo Collection

1. Set up a laying pot with 60 females/female virgins and 30 males at 22 ˚C (room temperature), 25 ˚C, or 29 ˚C, depending on the experiment (*see* **Note 3**).
2. Label and change the apple juice plates on laying pots, keeping the old ones for embryo collection.
3. Pour enough 50 % bleach to cover embryos on each plate and remove dead flies with a paintbrush. Dechorionate embryos for 4 min at room temperature. During this period, label 1.5 ml Eppendorf tubes and add 500 µl heptane to each.
4. Gently disturb the embryos on the plate with a paintbrush and transfer them to a collection basket using a small funnel. Rinse the plate with water to collect any remaining embryos and transfer them to the collection basket. Rinse the embryos in the collection basket liberally with additional distilled water to remove any traces of bleach.
5. Move the embryos to the Eppendorf tube containing the heptane with the paintbrush.

3.1.2 Embryo Fixation

1. Thaw an aliquot of 4 % PFA.
2. Add 500 µl of PFA to the Eppendorf tube containing the heptane and embryos.
3. Using a platform shaker set at 250 rpm, incubate the embryos for 20 min at room temperature.
4. Remove both the PFA and heptane phases, leaving the embryos in the Eppendorf tube.
5. Add 500 µl of fresh heptane and 500 µl of 100 % methanol (for an alternative fixation method to label fixed embryos with phalloidin, *see* **Note 4**).
6. Vortex for 1 min at room temperature. Embryos that have been devitellinized will fall to the bottom of the tube, whereas those that remain at the interface or float are not devitellinized and should be discarded.

***Table 3.1.2 – Drosophila* stocks useful for the study of myonuclear positioning**

Fly Stock	Use	Reference(s)
GAL4 Lines	Available from stock centers/*Drosophila* labs	
twist-GAL4	Somatic mesoderm expression from gastrulation to stage 14	[219]
Mef2-GAL4	Somatic mesoderm expression from stage 7 and throughout larval and adult development	[220]
24B-GAL4	Somatic mesoderm expression from stage 7	[218]
MHC-GAL4	Somatic muscle expression – stage 13 throughout larval and adult development	[61]
G7-GAL4	Muscle expression in larvae	[221]
Alpha-GAL4	Muscle expression in larvae	K. Broadie lab, Vanderbilt University
apterousME-GAL4	LT muscle specific expression in embryo	[50]
5053-GAL4	VL1 muscle specific expression in embryo	[222]
Rp298-GAL4	Founder cell/myotube specific expression in embryo/pupa	[223]
sns-GAL4	Fusion competent myoblast in embryo/pupa	[58]
UAS Lines	Available for gene of interest at *Drosophila* stock centers (i.e. Bloomington or Vienna Stock centers) or from individual *Drosophila* labs	
UAS-RNAi	Examples: UAS-DhcRNAi, UAS-SydRNAi	[167,169]
UAS-fluorescent reporter lines targeted to nuclei or other organelle	Examples: UAS-cytoplasmic GFP, UAS-nuclear localized GFP; UAS-laminGFP labels nuclear envelope; UAS-EB1-GFP labels microtubule plus ends	[167,168]
Fluorescent Reporter lines		
apterousME::NLSdsRed	Labels all myonuclei in the LT muscles	[50,158]
Tropomyosin-GFP	GFP Gene trap in Tropomyosin. Labels all muscles	*Drosophila* FLYTRAP Collection
Zasp66-GFP	GFP Gene trap in Zasp66. Labels all muscles	*Drosophila* FLYTRAP Collection
Gene mutants	Available for gene of interest at stock centers or from *Drosophila* labs: (http://flybase.org/)	

7. Remove all liquid.

8. Rinse embryos in methanol three times. To rinse: add solution, invert tube, let settle, remove, and repeat.

9. Add fresh 100 % methanol for storage at −20 ˚C. Embryos can be stored and used reliably for up to 6 months.

3.1.3 Embryo Staining

1. Transfer embryos to a 0.5 ml Eppendorf tube and remove excess methanol.
2. Rinse three times with PBT-BSA.
3. Add fresh PBT-BSA and incubate for 30 min on Nutator at room temperature. BSA serves to reduce nonspecific binding of antibodies.
4. Add primary antibodies diluted in PBT-BSA (Table 3.1.1). As an example, use antibodies directed to tropomyosin or myosin heavy chain to visualize muscles and DsRed to label the nuclei of the lateral transverse (LT) muscles expressing the *apterousME::NLSdsRed* (Figs. 3.1.1 and 3.1.2). Incubate primary anti- bodies with the embryos on the Nutator for 1 h at room temperature or overnight at 4 ˚C.
5. Remove primary antibodies and store at 4 ˚C (most can be reused up to three times).
6. Rinse embryos with PBT-BSA three times.
7. Wash embryos with PBT-BSA three times for 10 min at room temperature on the Nutator.
8. Remove PBT-BSA and add secondary antibodies (Table 3.1.1), diluted in PBT-BSA, to the embryos and incubate on the Nutator for 1 h at room temperature. As fluorescent antibodies are light sensitive, cover them with aluminum foil. From this point forward, keep them covered as much as possible until the staining protocol is finished.
9. Remove and discard secondary antibodies.
10. Rinse embryos with PBT (no BSA) three times.
11. Wash embryos with PBT three times for 10 min on the Nutator at room temperature.

3.1.4 Embryo Mounting

1. While washing the embryos (**step 12** above), prepare slides for mounting. To mount embryos, first make a "tape bridge," comprised of two superimposed pieces of Scotch tape, on two opposite sides of the cover slip (Fig. 3.1.5a).
2. Label the slide with date, genotype or cross, and the antibodies used.
3. Place a metal washer on the slide and rest the cover slip on the washer with the tape bridge facing up.
4. Cut 1 cm off of the end of a p200 pipet tip for each sample so that embryos can be pipetted without damage.
5. Remove PBT from the last wash (**step 12** above).
6. Add 80 μl of ProLong Gold antifade reagent to embryos using the truncated p200 tip (ProLong Gold is extremely viscous) and slowly mix them together.

7. Transfer embryos to the cover slip. Remove any visible bubbles.
8. Place a new cover slip over the tape bridge and line up both cover slips to form a sandwich.
9. Store overnight in the dark until the ProLong Gold sets.
10. Remove the washer and tape the cover slip sandwiches to the slide. These slides are ready to be imaged.
11. Slides can be stored at −20 ˚C for up to 6 months.

3.1.5 Confocal Microscopy

While the data indicate that similar movements and mechanisms are active in other *Drosophila* muscle subsets, our lab has focused on studying myonuclear movements in a subset of muscles, the lateral transverse muscles (LT). Hence, the methodology for confocal imaging described below is focused on this subset.
1. On the confocal microscope, identify an embryo at the correct stage (stages 14–16) positioned with its lateral side facing up using the low-magnification objective. Staging is done based on overall embryo shape, the intensity of DsRed and tropomyosin signal when used, gut morphology, and the morphology of the trachea [20,158,167]. At stage 16, a control LT muscle shows two clusters of nuclei (3–4 nuclei in each cluster) near each longitudinal pole of the muscle.
2. After finding a correctly staged embryo for imaging, move to a higher magnification objective, such as the 63× objective, and increase the zoom to 1.5×. On the computer, position the embryo in a horizontal position with four hemisegments visible in the imaging field. Choose hemisegments 3–7 for imaging (*see* **Note 5**).
3. To set the *Z*-stack, begin by selecting the first slice in which the LT muscles are visible, and after moving through the muscle, stop and select the last slice in which these muscles are no longer visible. The recommended step size is 0.5 μm. The total size of the stack will vary between embryos, but the step size should be kept constant. The gain for each channel should be adjusted according to the intensity of the corresponding signal.

3.1.6 Image Analysis

Multiple software packages, including Volocity Visualization Software 6.1.1 (Improvision), Imaris (Bitplane), and Adobe Photoshop CS4, are used for image processing. ImageJ (NIH) software is used for measurements. With the appropriate

plug-in (*bioformats_package*), however, files from Leica or Zeiss confocal microscopes can be opened directly in ImageJ, and all rendering, processing, and analysis can be done within ImageJ. Therefore, the instructions below will refer to ImageJ software:

1. Open your files by dragging them into ImageJ toolbar.
2. For the nuclear positioning analysis, select the extended focus view to visualize whole muscles. Select: Image>Stacks>Z Project and select Standard Deviation as the projection type (*see* **Note 6**). Adjust the number of slices to be included in the final projection.
3. Merge channels by selecting Image>Color and Merge Channels.
4. Brightness and contrast, as well as other settings, can be adjusted by selecting Adjust under the Image menu (Image>Adjust>Brightness/Contrast).
5. For analysis, position the image with the anterior side of the muscle set to the left and dorsal to the top of the viewing field. The image can be rotated by selecting Transform under the Image menu (Image>Transform>Rotate).
6. For measuring nuclear positioning, turn on the segmented line option. To do this, go to the ImageJ toolbar, right-click on the line option (represented as a straight diagonal line) and select Segmented Line.
7. Three different measurements are made for each muscle (Fig. 3.1.2a): Dorsal (D)— Distance from the dorsal end of each muscle to the nearest edge of the closest nucleus; Ventral (V)— Distance from the ventral end of each muscle to the nearest edge of the closest nucleus; and Length (L)—Length of each muscle following the curvature of the muscle. The edges of the nuclei and ends of the myofibers are defined by a clear change from signal to background within the relevant viewing channel. Each LT muscle is considered individually in all cases. To register each measurement, hit the M key (a new window will pop up when this is assessed for the first time).
8. For the analysis, a total of three measurements (dorsal, ventral, and length) per muscle, from four muscles per hemisegment in four hemisegments per embryo, are measured in each of ten embryos per genotype.
9. Copy all measurements to an Excel sheet. To calculate the dorsal and ventral distances, represent each value as a percent of the total muscle length to account for variation in muscle size. This will provide a quantification of the proximity of each cluster to each end of the muscle, which can be compared to control values. To calculate the nuclear spread, use the measurement values in the following formula: $\frac{Length-Dorsal-Ventral}{Length}$. This quantifies the distance that both clusters have traveled relative to each other and to the muscle length.

10. For statistical analysis, use either Excel or an advanced statistical software, such as SPSS (Statistical Package for the Social Sciences, IBM) or GraphPad Prism. The standard statistical test used is the Student's *t*-test.

3.2 Time-Lapse Imaging of Embryonic Muscles

3.2.1 Embryo Collection and Mounting

1. Follow **steps 1–4** from Subheading 3.1.1.
2. Place the collection basket on a small petri dish and fill it up with water so that the embryos are floating.
3. Dip a wooden stick into halocarbon oil and use the halocarbon oil on the end of the stick to collect the floating embryos from the collection basket. Then transfer them to an air-permeable Teflon membrane mounted on a circular Perspex frame (Fig. 3.1.5b). Place two pieces of tape on each side of the embryos to create a bridge that will prevent embryo damage. Place a cover slip on top of both pieces of tape.

3.2.2 Confocal Microscopy

1. For time-lapse imaging of whole embryos, *Z*-stacks are taken with optical sections set at 3 μm on the Zeiss AxioPlan2. To set the stack, the first slice is set when the LT nuclei are in view in multiple hemisegments. The final slice is set below the nuclei. A frame rate of 20 s is used. Only a single Z-section with the greatest number of nuclei in focus is selected for each time point. Images are processed using ImageJ and compiled into a video using QuickTime [158] (*see* **Note 7**).
2. For time-lapse imaging of myonuclear clusters and individual myonuclei, *Z*-stacks of two hemisegments are imaged simultaneously, using a high-magnification objective, such as the 63× 1.4 NA HCX PL Apochromat oil objective (*see* Subheading 2.2.2) and increasing the zoom to 2–2.5×. Set the stack starting slightly above the nuclei and finishing slightly below the nuclei. Set the step size to 0.5 μm and the time interval to be between 20 s and 3 min [168] (*see* **Note 7**).
3. Depending on the types of nuclear movement analyzed, collect data from 10 h (whole embryo) to 60 min (individual nuclear movements). Record a minimum of five time-lapse series per genotype.

3.2.3 Image Analysis

1. Quantification of myonuclear movements and myonuclear morphology changes are completed manually using measurement functions in ImageJ (NIH) as described in Subheading 3.1.6.
2. *Nuclear translocation speed:* The velocity at which myonuclear clusters in the LT muscles separate during stage 15 is assessed by measuring the distance between the dorsal and ventral clusters of nuclei at *t*=0 h and at *t*=1 h and determining the increased distance between the two clusters. By tracking individual nuclei as they moved relative to a fixed position in the embryo over the course of 10 min, the speed of individual myonuclei is determined. One hundred individual myonuclei from five different embryos are assayed for each genotype.
3. *Nuclear rotations:* The number of LT myonuclei that rotate is determined by examining the time-lapse videos. A myonucleus that rotates, stops, and then rotates again is counted as one rotating myonucleus. Two hundred and fifty myonuclei are normally examined.
4. *Nuclear translocation directionality:* The leading edge of a myonucleus is defined as the edge of the myonucleus furthest in the direction of translocation. A myonucleus is judged to have changed direction if it persistently moves a distance of at least one nuclear radius in the opposite direction from its previous direction of translocation. Two hundred and fifty myonuclei are examined.
5. *Nuclear shape changes:* The aspect ratios of moving myonuclei are determined by dividing the length of the dorsal-ventral axis of a myonucleus by the length of the anterior-posterior axis of a myonucleus using ImageJ software (NIH). Aspect ratios are considered to change if a difference of ≥0.7 was observed in these measurements. Two hundred and fifty myonuclei are examined with at least ~80 % exhibiting the changes in noted behavior.

3.3 Imaging of Formalin-Fixed Larval Muscles

3.3.1 Larval Collection (Fig. 3.1.4)

1. Set up a laying pot with 60 females/female virgins and 30 males at 22 ˚C (*see* **Note 3**).
2. Label and change the apple juice plates on laying pots, keeping the old ones for embryo collection.
3. Day 0: Under the dissection scope, select stage 16/17 embryos and transfer them to a half-yeasted plate with the help of an embryo hook. Arrange the embryos in a

line next to a very thin layer of yeast. This will make it easier to find the 1st instar larvae on the next day.
4. Day 1: Within 24 h, transfer the hatched larvae to a vial with food and store the vial at 25 ˚C for an additional 3 days or 22 ˚C for 4 days.
5. On day 4 or day 5 (depending on the temperature), larvae will be 3rd instar larvae. Pour room temperature 15 % sucrose solution in the vial. Gently disturb the food at the bottom of the vial with a spatula. The larvae will float and can be collected using a paintbrush. In the event that some larvae are stuck in the food, release by gentle agitation. Transfer the larvae to an apple juice plate.
6. If larvae expressing a fluorescent protein that was not previously visible in the embryo are desired, select the appropriate larvae under the fluorescence scope before starting dissecting.
7. Prepare separate Eppendorf tubes with PBS for each genotype/cross and keep them in ice.

3.3.2 Larval Dissection and Fixation with Formalin

1. Before starting the dissections, gather at least six dissection pins on the dissection plate.
2. Transfer one larva to the dissection plate and add a drop of cold HL3.1 buffer using a glass pipet. This “relaxing buffer” will slow larval movements.
3. Orient the larva with its dorsal side up (identified by visualization of the main trunks of the trachea) and pin both the anterior and posterior ends of the larva to the plate. Specifically, after securing one end, use the other pin to stretch the larva to its normal length, being careful to not overstretch it, before securing the other end.
4. Using the scissors, make small incisions perpendicular to the length of the larva close to each pin (cutting both trunks of the trachea). Then, cut along the larval body, ideally between the two main trunks of the trachea, to expose the inner organs.
5. With forceps, gently remove the gut, trachea, and neurons, being careful to not damage muscles.
6. Pin each corner of the larval body to the plate, making it flat. Once more, stretch out the tissue, but avoid overstretching. The flatter the larva during preparation, the easier the image acquisition later.
7. Remove the HL3.1 buffer, add a few drops of 10 % formalin, and incubate for 20 min at room temperature.
8. Rinse with cold PBS three times.

9. Add fresh PBS and remove pins.
10. Transfer to an Eppendorf tube with cold PBS.
11. Store at 4 ˚C for a maximum of 1 week (for optimal staining results). Do not store dissected larvae at −20 ˚C as this will damage the structure of the muscle.

3.3.3 Larval Staining and Mounting

1. Staining larvae is similar to staining embryos (*see* Subheading 3.1.3), except when using fluorescence-conjugated probes such as phalloidin or Hoechst. If these types of probes are used, there is only one incubation of 1 h at room temperature followed by PBT washes. If antibodies are also used, incubate with primary antibodies first, as in the embryo staining protocol, followed by incubation with appropriate secondary antibodies and the aforementioned probes.
2. After completing the staining, transfer a maximum of six larvae to a microscope slide.
3. Under a dissection scope, position larvae with the head at the top and flatten them by exposing the muscles facing up. Spread out the larvae evenly on the slide. While doing this, do not let larvae dry out. Add more PBT if necessary.
4. Remove any excess PBT by absorbing it with a Kimwipes.
5. Place a drop of ProLong Gold antifade reagent on top of each larva and remove any visible bubbles.
6. Cover with a cover slip and let it dry at room temperature in the dark. Note that there is no bridging of the cover slips for the mounting of larvae.
7. Slides can be stored at −20 ˚C for up to 6 months.

3.3.4 Confocal Microscopy

1. For formalin-fixed larval muscles, we image the ventral lateral muscles 3 and 4 (VL3 and VL4) because they are easily observed and are more resistant to damage during dissection. For simplicity, it is recommended to focus on VL4, with its single row of myonuclei, rather than VL3, which contains two rows of nuclei.
2. A VL4 muscle should fit in the imaging field on the micro- scope computer. Set the *Z*-stack, starting a little above the muscle and finishing just prior to the slice when other muscles first become apparent. Set the Z-step size to 0.5 μm. Image six muscles from each of five larvae per genotype.

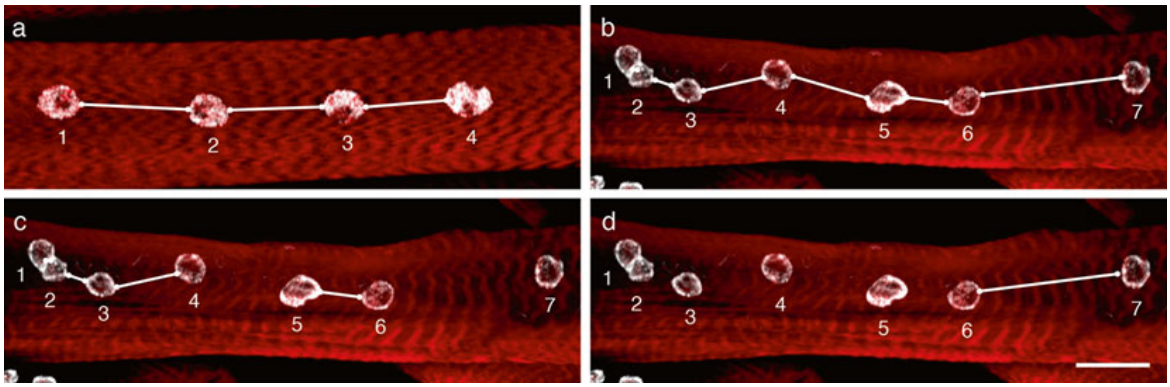


Figure 3.1.6 Myonuclear positioning measurements in larval muscles. In a control VL4 muscle (**A**) and in a VL4 muscle with disrupted myonuclear positioning (**B–D**), white lines represent different measurements made to deter- mine myonuclear positioning defects. (**A**) Internuclear distance. Nuclei are approximately equidistant. (**B**) Internuclear distance. The distance between nuclei is variable. (**C**) Nearest neighbor. Two different scenarios: the nearest neighbor of nucleus 5 is nucleus 6 and vice-versa; the nearest neighbor of nucleus 4 is nucleus 3 but the opposite is not the case. Nucleus 2 is the nearest neighbor to nucleus 3. (**D**) Largest gap. In this muscle, the largest gap between two nuclei is the distance between nuclei 6 and 7. Scale bar, 25 μm.

3.3.5 Image Analysis

As for embryo image analysis (*see* Subheading 3.1.6), different software packages can be used. All the instructions herein will refer to ImageJ software (NIH):

1. Follow **steps 1–4** from Confocal Microscopy in the Imaging of Fixed Embryonic Muscles (*see* Subheading 3.1.6).

2. For assessing myonuclear position in larvae, different types of measurements are made: muscle length, internuclear distance (Fig. 3.1.6a, b), nearest neighbor (Fig. 3.1.6c), largest gap (Fig. 3.1.6d), and myonuclear number.

3. Muscle length: Use the straight line option on the ImageJ toolbar and hit the M key to open a new window with the values.

4. Internuclear distance: Measure the distance between every nucleus. In control muscles or muscles without nuclear clumping, the resulting standard deviation will be very small compared to the measurements from muscles with nuclear clumping.

5. Nearest neighbor: Measure the distance to the nearest edge of the closest nucleus from each nucleus. Assume distance equals 0 when two nuclei are touching. The closer the nuclei, the lower the final average will be.

6. Largest gap: Measure the longest distance between two nuclei within a given muscle. For more severe defects in myonuclear positioning, this distance is bigger, whereas in muscles with control-like nuclear distribution, this value is smaller.

7. Number of nuclei per muscle: A control VL4 muscle contains 7–9 nuclei.

8. Copy all measurements to an Excel sheet. To calculate each of the parameters mentioned above, always consider the length of the muscle and express values as a percentage of muscle length.
9. For statistical analysis, either use Excel or a more advanced statistical software, such as SPSS (Statistical Package for the Social Sciences, IBM) or GraphPad Prism. The standard statistical test used is the Student's *t*-test.

3.4 Heat-Fixed Larvae

An alternative method of fixing larvae for microscopy is heat fixation (adapted from [224]). For this approach, use larvae at any developmental stage. Since there is no staining with this protocol, larvae expressing fluorescent markers in both the muscles and the nuclei are ideal (*see* Table 3.1.2):
1. Pick a larva using forceps. Be careful not to damage muscles.
2. Dip the larva in water at 65 ˚C for 1–2 s.
3. Mount 5–6 larvae in halocarbon oil or 50 % glycerol in a microscope slide.
4. Cover with a cover slip.

NOTES

1. For antibodies with high levels of nonspecific background staining, preabsorption using fixed control embryos is recommended. For example, some antibodies listed in Table 1, such as anti-Eve, are preabsorbed to obtain better results [209].
2. Due to the formation of the embryonic cuticle at stage 17, antibodies can only penetrate the embryo from the initial stages of embryogenesis until stage 16. For visualizing myo- nuclear position as well as muscle structure at stage 17, fluorescently tagged proteins that label the myonuclei and the muscles must be examined (*see* Table 2).
3. Although the ideal number of flies in a laying pot is 60 females/ female virgins and 30 males, laying pots can be set up with as few as 25 females/female virgins and 15 males. Using a large number of flies in a laying pot is important when collecting large amounts of embryos.
4. For labeling fixed embryos with phalloidin, an alternative fixation method in which methanol is substituted with ethanol should be used. After fixing in heptane and PFA, add 100 % ethanol, vortex for 45 s, discard the ethanol, add 100 % ethanol, vortex for 45 s, collect embryos to a new tube, and store in fresh 90 % ethanol at −20 °C.
5. When imaging embryos, it is recommended to focus on hemisegments 3–7 because these hemisegments are develop- mentally more similar in age and are less prone to variations in muscle structure.
6. When rendering a *Z*-stack in ImageJ, a number of projection types are available (average intensity, maximum intensity, minimum intensity, sum of slices, standard deviation, and median). The type selected depends on what is being measured. Maximum intensity is suggested if the user is measuring that particular signal. We use standard deviation as it renders an excellent image of the sarcomeric structure in the muscle; however, we are measuring distances between the nuclei.
7. While acquiring time-lapse images, check every 10 min to adjust focus as embryos will move and the nuclei will shift out of focus. However, note that adjusting this focus means restarting the time-lapse sequence. This cannot be done within a time-lapse. After a few adjustments, the focal plane will essentially stabilize, and it can be left for hours to get the desired time-lapse sequence.

Chapter 4
Results

Part I. Robo1 regulates myoblast fusion and myonuclear positioning independently of its ligand Slit (unpublished data)

Part II. The Drosophila Ninein homologue Bsg25D cooperates with Ensconsin in myonuclear positioning

Part III. Additional unpublished results

Part I

ROBO1 REGULATES MYOBLAST FUSION AND MYONUCLEAR POSITIONING INDEPENDENTLY OF ITS LIGAND SLIT

Mafalda Azevedo[1,2], Jonathan N. Rosen[1], Su Deng[1],
David B. Soffar[1], Rishi Ravichandran[1] Stefanie Windner[1], Mary K. Baylies[1,3]

[1] Program in Developmental Biology, Sloan Kettering Institute, New York, New York, United States of America

[2] Graduate Program in Areas of Basic and Applied Biology (GABBA), Abel Salazar Biomedical Sciences Institute, University of Porto, Porto, Portugal

[3] Cell and Developmental Biology, Weill Cornell Graduate School of Medical Sciences, Cornell University, New York, New York, United States of America

Unpublished data

INTRODUCTION

Mammalian skeletal muscle is a composite tissue that consists primarily of contractile myofibers, which rely on interactions with other tissues to optimally function. Blood vessels provide muscle cells with oxygen and nutrients, motor neurons innervate the muscle and signal through neurotransmitters to stimulate contraction, and tendons and muscles establish a specialized junction called a myotendinous junction (MTJ), which is essential for force transmission and structural support during contraction [185,186]. However, it is not well understood how these interactions with other tissues influence aspects of myofiber intracellular organization and muscle function.

Mammalian skeletal muscle and *Drosophila melanogaster* embryonic body wall muscle share several characteristics, including formation of a highly organized syncytium, achieved through myoblast fusion followed by myonuclear movements, as well as establishment of specialized attachment to tendon cells and innervation by specific motor neurons [157,225]. Due to its simplicity, where each muscle is a single cell, and the high degree of conservation between vertebrates and *Drosophila*, the fly embryo is an ideal model to investigate these aspects of muscle development and intracellular organization.

Drosophila embryonic myogenesis involves a series of conserved events that are essential for the formation of fully functional, contractile myofibers. In fruit flies, myoblast fusion occurs during embryogenesis from stages 12 to 15 (7-13 h After Egg Laying (AEL)[226]). Each fusion event can be divided into three steps: cell-cell recognition and adhesion, actin focus formation, and fusion pore formation (reviewed in Kim et al. 2015 and Deng et al. 2017). Each event adds volume and an additional nucleus to the growing myotube. Two cell types are required for muscle formation in *Drosophila*: founder cells (FCs) and fusion-competent myoblasts (FCMs). Each FC, which determines muscle identity, fuses with multiple FCMs to form a syncytial cell [3]. FCs and FCMs express sets of transmembrane receptors that allow these two cell types to recognize and adhere to one another: FCs express *dumbfounded* (*duf*) and *roughest* (*rst*), and FCMs express *sticks and stones* (*sns*) and *hibris* (*hbs*). Adhesion of the FCM to the initial FC or growing myotube via these transmembrane receptors activates pathways that promote actin polymerization and the formation of a filamentous (F)-actin focus present primarily within the FCM [50,154]. The FCM invades the FC with podosome-like protrusions [55], and membrane pore formation

subsequently occurs, allowing for the mixing of the cytoplasm and the addition of the FCM nucleus to the FC/developing myotube. After a fusion event, the myotube will either prepare for the next fusion event or stop fusing through mechanisms that are not clearly understood. As each myotube accumulates nuclei through successive fusion events, the nuclei undergo a series of movements that will ultimately place them in their final position within the muscle cell.

The process of myonuclear positioning has been best characterized during fly muscle development in the *Drosophila* embryonic lateral transverse (LT) muscles. Beginning at stage 14 (10-11 h AEL), while fusion events are still occurring, LT muscle nuclei form two clusters that are in close proximity to each other. During stage 15 (11-13 h AEL), these nuclear clusters move away from each other toward opposite muscle poles, and at the same time, the muscle cells extend filopodia and elongate towards tendon cells, establishing an attachment. By stage 16 (13-16 h AEL), the LTs are firmly attached to tendon cells and the clusters of nuclei position close to the ends of the myotubes. By the start of stage 17 (16-24 h AEL), when the tendon attachment is mature, coordinated muscle contraction begins, and nuclear clusters dissociate, now spreading along the myotube to maximize their internuclear distance [158,184,227]. The end result is a multinucleated myofiber with nuclei evenly distributed along the periphery of the muscle cell. This subcellular pattern of nuclear localization is shared between mammalian and *Drosophila* mature muscle cells and is thought to be essential for muscle function. Certain muscle diseases, such as Emery-Dreifuss muscular dystrophy (EDMD) and centronuclear myopathies (CNM), are characterized by the presence of abnormally positioned myonuclei, and show muscle weakness and skeletal muscle wasting [148]. A better understanding of how nuclear positioning is regulated at a molecular level is critical to understanding the mechanisms of myofiber organization and how mispositioned nuclei contribute to deficits in muscle function.

Previous reports showed that myonuclear positioning and muscle function depend on the activity of the microtubule motor proteins Kinesin and Dynein and their associated proteins, including Clip190, Glued, Partner of inscrutable (Pins/Raps), Sunday driver (Syd), and Aplip1 [167–170]. Myonuclear position also requires other microtubule-associated proteins, including the microtubule-binding protein 7 (MAP-7)/Ensconsin [158] and its binding partner Bsg25D/Ninein [162], and the cooperation between microtubules and the KASH proteins, Klarsicht and MSP-300 [172]. A cortical pulling pathway, mediated by Dynein and Kinesin, is essential for myonuclear positioning, in which coordinated activity of both motors along the microtubule

network allows for the movement of the clusters of nuclei towards the muscle poles [168]. In addition, EDMD and CNM disease-associated genes were identified as regulators of distinct mechanisms of myonuclear positioning. EDMD-associated genes regulate the separation of an initial cluster into two clusters and CNM-linked genes are necessary to maintain clustering as the nuclei move towards muscle ends [160]. However, these cell-intrinsic mechanisms regulate myonuclear positioning at a time when muscle cells are actively interacting with cells in their environment, including interactions with tendon cells to form strong and stable MTJs which allow the muscles to withstand strong contraction without detaching from the tendon and to recover their shape after contraction [187,188]. How these interactions influence myonuclear positioning have not yet been explored.

MTJ formation involves the guidance, elongation, and attachment of muscle cells with their target tendon cell. Several axon guidance pathways have been involved in this process, including the Slit-Robo pathway [187,228]. Initially identified in a large screen for genes that regulate axonal midline crossing [229], *roundabout* (*robo1*) was later found to encode a repulsive guidance receptor that binds to Slit [230] and is conserved among various species [231,232]. The Robo family is part of the immunoglobulin superfamily of cell adhesion receptors and in *Drosophila* there are three *robo* genes: *robo1*, *robo2,* and *robo3* [230,233]. While most roles for Robo have been described as dependent on Slit, some studies have identified Slit-independent functions in different organisms [234–237]. During nervous system development, the Slit-Robo pathway is essential for axon guidance, controlling the crossing and recrossing of the midline, where Slit is expressed [230–232,235]. In muscle development, this pathway performs a dual role of promoting repulsion from the midline during early ventral mesodermal migration and later on, attraction towards tendon attachment sites [228,230]. Since muscles require interaction with tendon cells to properly develop and become functional (i.e. contract), we explored the possibility that muscle-tendon interactions also regulate intracellular muscle organization, such as myonuclear positioning. We focused our studies on the Robo-Slit pathway, a paradigm of muscle-tendon signaling.

Here we describe two novel roles for Robo1 in *Drosophila* myogenesis. We show that *robo1* is involved both in regulating myoblast fusion and myonuclear positioning in the LT muscles in a Slit-independent fashion. In the absence of *robo1*, fusion events take longer, actin foci contain less actin, the LTs acquire fewer nuclei, and LT myonuclei are mispositioned. We investigated the possibility of an interaction of Robo1 with known regulators of myonuclear positioning and showed that Robo1 does

not participate in the cortical pulling pathway. As we were completing the final experiments for this work, we found that many of our *robo1* stocks were not as assumed. Data obtained and the conclusions drawn using these stocks will be presented chronologically and labeled with an asterisk (*). This issue led to a re-examination of the phenotypes, that is included at the end of this chapter. Nevertheless, the main conclusions—that a *slit*-independent *robo1* activity is required for myoblast fusion and myonuclear position—remain valid. This study sheds further light into the importance of muscle-tendon interactions during muscle development and reveals novel *in vivo* roles for Robo1 in myoblast fusion and myonuclear positioning.

MATERIALS AND METHODS

Drosophila genetics

All *Drosophila melanogaster* stocks were grown on standard cornmeal medium at 25°C. The following stocks were used: *apterousME-NLS::dsRed* (or *apRed*; always referred to as control) [50], *ens^{swo}* [158], *Khc^{8}* [238], *Dhc64c$^{4-19}$* [239], *Mef2-Gal4* [220], *twist-actin::GFP* [240], *UAS-robo.myc* (gift from the Bashaw lab [241]), *sns-GAL*4 (gift from the Abmayr lab [58]) and *duf-GAL4* [70]. From the Bloomington *Drosophila* Stock Center: *robo1$^{1/1}$* (8755 [232]), *robo1$^{2/2}$* (*) (8756 [232]; later identified as having the *robo1^{1}* mutation), *sli$^{2/2}$* (3266), and UAS-GFP RNAi (41551). From the Vienna *Drosophila* Resource Center: *UAS-robo RNAi KK108817* (100624). To visualize nuclei in the LTs, stocks were crossed with *apRed* [50] which fluorescently labels nuclei. The GAL4-UAS system [218] was used for expression and "rescue" studies. Embryos were staged according to [226].

Viability assay

Viability assays were done at 25°C essentially as previously described (Schulman et al. 2014). In brief, stage 16 embryos were selected over multiple days without bleaching and transferred to a fresh apple juice plate. The number of hatched/unhatched embryos was counted the day after and 1st instar larvae were transferred to a vial with food. The number of pupae and adults was counted later on. A minimum of 51 embryos was collected over the course of several days.

Fluorescent antibody staining

Embryos were prepared for staining as previously described [50]. Embryos were incubated in primary antibody for 1 hour at room temperature or overnight at 4°C and used at the following dilutions: rat anti-Tropomyosin (50567, Abcam, Cambridge, UK, 1:500), rabbit anti-DsRed (632496, Clontech, Mountain View, CA, 1:400), chicken anti-GFP (13970, Abcam, 1:500), mouse anti-βPS-integrin (CF.6GG11, Developmental Studies Hybridoma Bank [DSHB], 1:50), mouse anti-Robo (13C9, DSHB, 1:100), mouse anti-c-Myc (9E10, DSHB, 1:50), mouse anti-α-Tubulin (T9026, Sigma, St. Louis, MO,

1:500), mouse anti-Dynein Heavy Chain (2C11-2, DSHB, 1:50), mouse anti BP-102 (anti-CNS axons, DSHB, 1:15). In addition, we used 467-conjugated anti-goat HRP (Jackson Immunoresearch, 1:300). Alexa fluor-conjugated secondary antibodies (Invitrogen, Carlsbad, CA) were applied 1:400 for one hour at room temperature. Fluor-conjugated phalloidin (Life Technologies, Carlsbad, CA) were added with the secondary antibody at 1:100. Samples were mounted in ProLong Gold antifade reagent (Invitrogen).

Fixed sample imaging and analysis

Z-stacks of fixed samples were acquired using a Zeiss LSM700 laser-scanning confocal microscope using a Plan-Apochromatic 20x/0.8-NA M27 objective and PlanNeo 40x/1.3-NA oil-immersion objective and processed in FIJI/ImageJ (NIH).

For analysis of nuclear spread at stage 16, embryos of all genotypes carrying *apRed* were used in order to visualize the nuclei in the LT muscles. The segmented line function in FIJI was used to measure the distances from the dorsal-most nucleus to the dorsal myotube pole, the ventral-most nucleus to the ventral myotube pole, and the total myotube length. Nuclear spread was calculated by subtracting the first two values from the third and expressing the difference as a percentage of total myotube length. Only muscles that attached were considered for this analysis. We find that our controls show a maximum value of 69.36% [and our most severe mutants, i.e, Bsg25D overexpression, 26.7% [162]]. Due to increased levels of attachment defects in *robo1*$^{2/2}$ embryos, which difficulted measuring nuclear spread, we performed all experiments with the *robo1*$^{1/1}$ mutant allele. For statistical purposes, the mean of four lateral transverse muscle measurements (whenever possible) from a maximum of four hemisegments per embryo was considered a sample. Embryos were fixed over the course of multiple days and then pooled for staining and analysis. A minimum of 4 embryos was used for quantification. Student's t-tests were used to statistically compare samples.

For the quantification of defects in stage 16 LT muscles, we examined a minimum of three hemisegments per embryo, using Z-stacks of fixed images of control and *robo1*$^{1/1}$ embryos. We classified defects in three categories: no defects, attachment defects, and guidance defects. Attachment defects were defined as loss of the elongated shape of at least an LT muscle per hemisegment. Guidance defects were defined as the loss of the dorsal to ventral orientation of at least one LT muscle per hemisegment. A minimum of 91 hemisegments from 21 embryos were analyzed.

For βPS-integrin intensity analysis, we used embryos that were fixed over the course of several days and then pooled for staining. We measured the signal intensity at the LT muscle ends, using the rectangle tool in FIJI, including integrin signal from both inside and outside the muscle. The background intensity value was subtracted from the absolute βPS-integrin intensity value for each measurement. A minimum of 106 muscles was used in this quantification. To create the intensity distribution graph, the average of each measurement for all muscles was considered. For the purpose of comparing intensities between the genotypes analyzed, the 80th percentile was calculated for all muscles analyzed and a Student's t-test was performed.

Microtubule density was calculated essentially as previously described in [167]. For statistics, we used the Tubulin/Tropomyosin ratios from multiple cells (n>20) from at least four embryos. Student's t-tests were performed using GraphPad Prism or Microsoft Excel.

For the Dynein intensity analysis, the background intensity value was subtracted from the absolute Dynein intensity value. Statistical analysis considered multiple measurements from one embryo as a sample. A minimum of 55 muscles from seven embryos was used.

To measure actin intensity in the actin foci, we used the straight-line function from FIJI to draw a line parallel to the orientation of the fusing FCM and including the whole actin focus. The average of each measurement for all muscles was used to create the distribution graph. The peak values were considered to statistically compare amount of actin between genotypes, using a Student's t-test. A minimum of 17 foci from 13 embryos was used.

Unfused myoblasts and nuclei counting

Single slices from Z-stacks of fixed stage 16 embryos labelled with tropomyosin were analyzed and the number of unfused myoblasts was classified into three categories: no visible unfused myoblasts, between one and five unfused myoblasts, and more than five unfused myoblasts. A minimum of 24 embryos was used. Each category for each genotype was represented in a pie chart as a percentage of the total number of embryos analyzed.

For counting nuclear number in the LTs, embryos carrying *apRed* were collected and dechorionated using 50% bleach for four minutes at room temperature. After being rinsed, embryos were quickly heat fixed in water at 65°C and mounted in halocarbon oil on a glass slide. The number of nuclei was counted per hemisegment

in stage 17 embryos, when it is possible to identify individual myonuclei. A minimum of 18 hemisegments was analyzed. A Student's t-test was used to compare genotypes for statistical significance.

Western Blotting

To compare Robo1 protein expression in control, mutant, and rescue genotypes, stage 16 embryos were selected and lysed in lysis buffer (150mM NaCl, 2mM MgOAc, 20mM Tris, pH 7.5, 5% Glycerol, 0.5% NP40, 2m DTT, and one Complete Mini tab [Roche, Basel, Switzerland]). Following Bradford assay to determine protein concentration (Bio-Rad Laboratories, Hercules, CA), 20μg of lysate per genotype was loaded onto a 7.5% SDS-PAGE protein gel. The gel was transferred onto a nitrocellulose membrane overnight, blocked with 5% milk and incubated overnight with mouse anti-Robo (13C9, DSHB, 1:1000) and mouse anti-α-Tubulin (T9026, Sigma, St. Louis, MO, 1:1000) antibodies. The membrane was then incubated with HRP-conjugated secondary antibodies against mouse (1:5000, Jackson ImmunoResearch, West Grove, PA) prior to development using chemiluminescence (Kindle Biosciences, Greenwhich, CT). Above experiment was repeated three times.

Time-lapse imaging

Embryos subjected to time-lapse imaging of myoblast fusion were prepared as published [167] and carried *twist-actin::GFP*. Time-lapse series of myoblast fusion events were acquired on a Zeiss LSM700 using a Plan-Apochromatic 20x/0.8 M27 objective or Leica SP5 using a 40x. Stacks were acquired every minute for a minimum of 30 minutes. Duration of actin focus was determined by the presence of actin accumulation in a focus for a certain number of frames. For statistical purposes, embryos were divided in two groups, stage 12/13 and stage 14/late 15, and compared using a Student's t-test. A minimum of 31 foci from three embryos was analyzed.

DNA extraction and sequencing

For genomic extraction, 5-10 flies of each line were homogenized in 100 µl of chilled 0.1M Tris-EDTA (TE) pH 9. 100 µl of chilled 2% SDS and 100 µg / ml Proteinase K were added to the homogenate, and the homegenate was then incubated at 50ºC for 3 hours. The cell debris was then centrifuged for 10 minutes, and a phenol/chloroform

extraction was performed on the recovered supernatant. The genomic DNA was precipitated from the extraction using 0.4 volumes of 5M Ammonium Acetate and 2 volumes of 100% Ethanol. Precipitates were centrifuged for 10 minutes at 15000 RPM, then washed with 70% Ethanol, dried, and resuspended in sterile water. Genomic extractions were quantified and diluted to 50 ng / µl.

Robo1-1 mutant stocks were analyzed by PCR-amplifying the genomic DNA region around the putative C1231T (Q411term) mutation using forward primer AACTACCTTGCATGGCCTCC and reverse primer AGCTTCCTTGGATGATGCTGT. The 405 bp products were column purified (Qiagen 28706) and sequenced (Eton Biosciences) with the forward primer.

RESULTS

Robo1 acts on myonuclear positioning in a Slit-independent fashion

To test the hypothesis that muscle-tendon interactions affect muscle intracellular organization, and specifically myonuclear positioning, we performed a screen using mutants defective for known regulators of MTJ formation (see Chapter 4 Part III). From this screen emerged *robo1,* which encodes a transmembrane protein present in muscles [228]. Using immunofluorescence, we first confirmed that in control embryos, Robo1 is present at the myotendinous junction (Fig. 4.1.1A), consistent with its role in muscle attachment to the tendon cell. We then examined the muscle pattern in control and homozygous *robo1*$^{1/1}$ mutant embryos, which entirely lack Robo1 protein (Fig. 4.1.1B), as shown previously [232]. In agreement with previously published data [242,243], muscle attachments defects were detected in stage 16

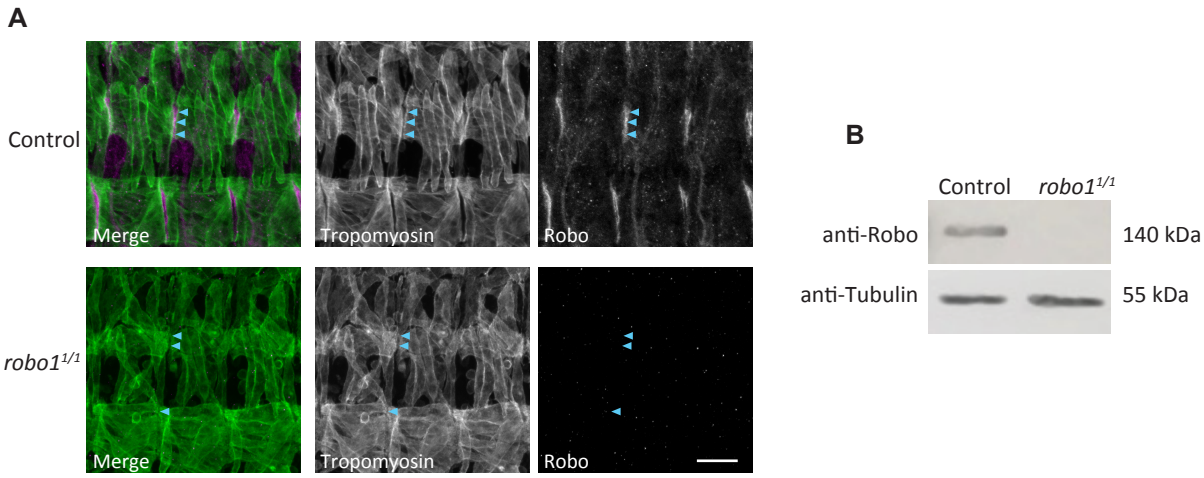


Figure 4.1.1– *robo1*$^{1/1}$ embryos are protein null. A) Representative images of stage 16 embryos highlight the localization of Robo1 at muscle attachment sites in control embryos and its absence in *robo1*$^{1/1}$ embryos. The blue arrowheads indicate tendon attachment sites. Tropomyosin highlights the muscles. Scale bar, 20 μm. **B)** Western Blot showing the absence of Robo protein in *robo1*$^{1/1}$ mutant embryos.

robo1$^{1/1}$ mutant embryos (Fig. 4.1.2A). We found that 35% of *robo1*$^{1/1}$ hemisegments showed defects in guidance and/or attachment of the LT muscles, whereas 65% of *robo1*$^{1/1}$ hemisegments exhibited no obvious muscle attachment defects (Fig. 4.1.3A). Those muscles that were attached were similar in length to control muscles, suggesting that these *robo1* mutant muscles did attach to the correct tendon cell (Fig. 4.1.3B). However, when we examined the MTJs of the LT muscles (Fig. 4.1.21A, bottom panel), we observed reduced expression of an essential MTJ adhesion

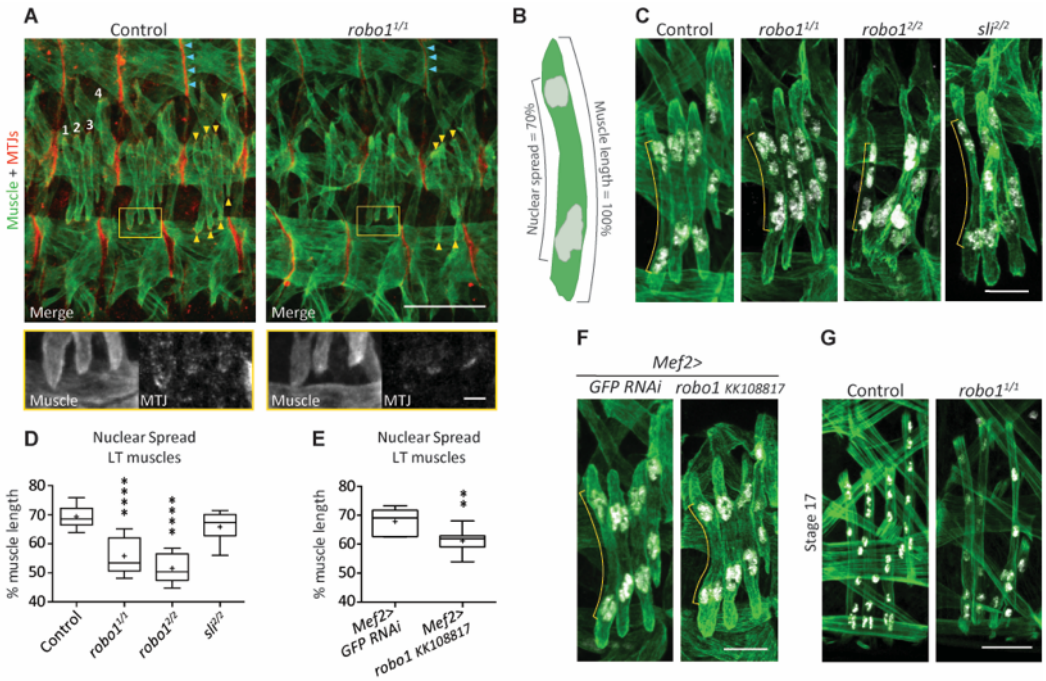


Figure 4.1.2 - Loss of *robo1* leads to decreased nuclear spread in a Slit-independent fashion. A) The top panel shows representative images of part of the musculature (tropomyosin, green) and myotendinous junctions (MTJ; β1PS-integrin, red) of control and *robo1*$^{1/1}$ embryos. In the control image, the numbers in white identify the Lateral Transverse muscles (LTs) 1-4. The yellow arrowheads indicate tendon attachment sites of the LT muscles. The blue arrowheads indicate places of tendon attachment at the segment border. The yellow boxes indicate the ventral tips of LTs 1-3 from one hemisegment which are zoomed in on the bottom panel. Scale bar, 50μm. The bottom panel (grey scale) shows the presence of β1PS-integrin at the tips of the LTs, indicating a weaker MTJ in *robo1*$^{1/1}$. Scale bar, 5μm. **B)** Schematic representation of a LT muscle depicting nuclear spread and muscle length measurements as percentages. Note that 70% nuclear spread is the average for a control LT muscle. **C)** Representative images of LTs in control, *robo1* mutant alleles 1 and 2 (*), and *slit* mutant embryos. Images show the position of the dorsal and ventral myonuclei clusters at stage 16. The yellow line represents the distance between myonuclei clusters (nuclear spread). Scale bar, 20μm. **D)** Quantification of nuclear spread as a percentage of the total muscle length. Crosses indicate the average for each genotype. Genotypes were compared to control using Student's t-test. Control, 69.36±3.65, n=10. *robo1*$^{1/1}$, 55.79±6.28, n=10, ****p<0.0001. *robo1*$^{2/2}$ (*), 51.58±4.90, n=7, ****p<0.0001. *slit*$^{2/2}$, 65.83±5.05, n=8, not significant. **E)** Quantification of nuclear spread as a percentage of the total muscle length. Crosses indicate the average for each genotype. *robo RNAi* was compared to *GFP RNAi* using a Student's t-test. *Mef2>GFP RNAi*, 68.07±4.37, n=7. *Mef2>robo KK108817*, 61.25±3.76, n=10, **p=0.0035. **F)** Representative images of the LTs in embryos expressing either *GFP* or *robo RNAi* specifically in the muscle. The yellow line represents the distance between myonuclei clusters (nuclear spread). Scale bar, 20μm. **G)** Representative images of stage 17 embryos, where the nuclei (white) in both control and *robo1*$^{1/1}$ muscles have spread along the muscle cell (actin, green). Scale bar, 20μm.

receptor, β1PS-integrin (Fig. 4.1.4A,B) [244], suggesting that the muscle attachments may be weaker in those muscles compared to controls. It is in these muscles that we assessed myonuclear positioning.

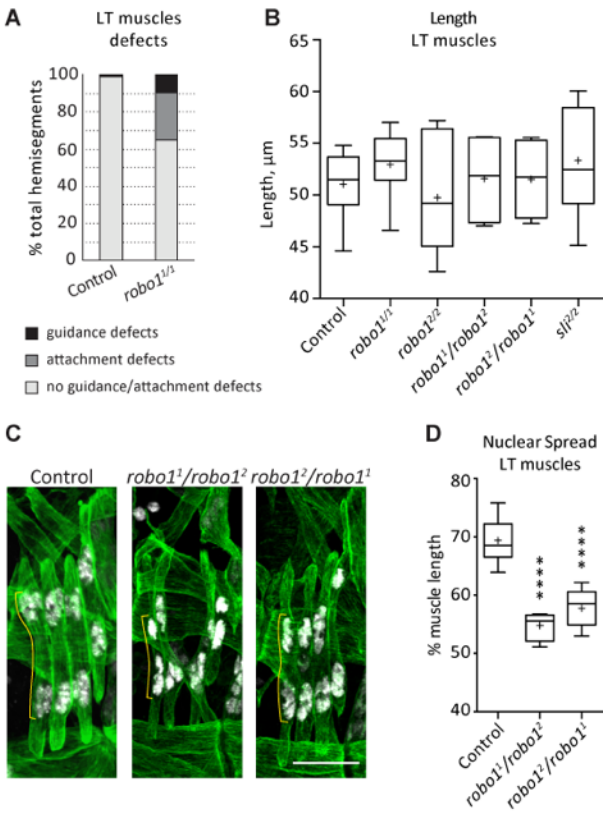


Figure 4.1.3 – *robo1* transheterozygotes show significant nuclear positioning defects in LT muscles. A) Quantification of guidance and attachment defects in the LT muscles at stage 16 control and *robo1*$^{1/1}$ embryos. Control, n=155 hemisegments from 36 embryos. *robo1*$^{1/1}$, n=91 hemisegments from 21 embryos. **B)** Quantification of the length of *robo1* mutant and transheterozygote embryonic LTs, and *sli* mutant LTs. Crosses indicate the average for each genotype. All genotypes were compared with the control using a Student's t-test. All comparisons were not significant. Control, 51.04±3.28 µm, n=10. *robo1*$^{1/1}$, 52.95±3.08 µm, n=10. *robo1*$^{2/2}$(*), 49.76±5.78 µm, n=7. *robo1*^{1}/*robo1*^{2}(*), 51.59±4.57 µm, n=4. *robo1*^{2}/*robo1*^{1}(*), 51.57±3.78 µm, n=5. *sli*$^{2/2}$, 53.34±5.23 µm, n=8. **C)** Representative images of the LTs in control and transheterozygote stage 16 embryos using *robo1* alleles 1 and 2 (*) show the position of the dorsal and ventral myonuclei clusters. The yellow line represents the distance between myonuclei clusters (nuclear spread). Scale bar, 20 µm. **D)** Quantification of the nuclear spread of the genotypes shown on panel A. Crosses indicate the average for each genotype. Genotypes were compared to the control using a Student's t-test. Control, 69.36±3.65, n=10. *robo*^{1}/*robo*^{2} (*), 54.77±2.51, n=4. *robo*^{2}/*robo*^{1} (*), 57.92±3.36, n=5. **** p<0.0001.

We examined the position of nuclei in the LT muscles at stage 16, when the two clusters of nuclei have nearly completed their initial migration towards the muscle poles. These nuclear clusters are positioned close to the dorsal and ventral ends of each muscle cell [167–169]. Considering only those muscles that attached to the correct tendon cells, we quantified the distance between the two clusters of nuclei as a percentage of the muscle length (here referred to as Nuclear Spread; described in detail in the Materials and Methods section and in [162]) (Fig. 4.1.2B). Control embryos had an average nuclear spread of 69.4±3.6%. Compared to controls, we

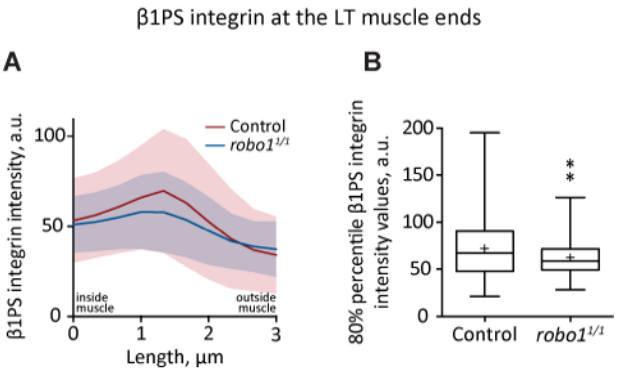


Figure 4.1.4 – *robo1* LT muscle ends have decreased amounts of β1PS integrin. A) Quantification of the intensity of β1PS-integrin signal along the tips of the LTS in control and *robo1*$^{1/1}$ muscles. **B)** Quantification of the values corresponding to the 80% percentile for control and *robo1*$^{1/1}$ embryos. Crosses indicate the average for each genotype. Both genotypes were compared with the control using a Student's t-test. Control, 71.87±31.43, n=254. *robo1*$^{1/1}$, 62.27±19.44, n=106. ** p=0.0037.

observed that *robo1* loss using two different mutant alleles, *robo1*$^{1/1}$ and *robo1*$^{2/2}$ (*), resulted in significantly decreased nuclear spread (Fig. 4.1.2C,D). Additionally, *robo1* transheterozygotes (i.e. ♀*robo1*^{1} x ♂ *robo1*^{2}= *robo1*^{1}/*robo1*^{2} (*) and ♀*robo1*^{2} x ♂ *robo1*^{1}= *robo1*^{2}/*robo1*^{1} (*)) displayed defects similar to *robo1*$^{1/1}$ and *robo1*$^{2/2}$ (*) homozygous mutants (Fig. 4.1.3C,D). However, as we later found out, these two stocks have the same mutation, but most likely different genetic backgrounds (see section Understanding the genetic background of the *robo*^{1} stocks). Similarly, muscle-specific knockdown of *robo1* using *Mef2*-GAL4 to drive the expression of a *robo1* RNAi resulted in significantly decreased nuclear spread in the LT muscles (Fig. 4.1.2E,F), which further confirmed a role for *robo1* in myonuclear positioning. Together, these results indicated that Robo1 is required for myonuclear positioning in the LT muscles and suggested that myonuclear positioning depends on stable MTJs promoted by Robo1.

Next we investigated whether Robo1 regulates myonuclear positioning through interacting with its established ligand, Slit [230], which is secreted by tendon cells [228,242,245]. While *slit* is maternally deposited, zygotic *slit* expression starts at 4 to 6 hours of development at 22°C, and zygotic loss of function leads to the described nervous system, mesoderm, and muscle-tendon defects at stages 12-16 [228,230,242,243,246,247]. Using *sli*$^{2/2}$ mutant embryos, we observed orientation defects in the LT muscles (data not shown) as described previously [245]. We measured nuclear spread in muscles from homozygous *sli*$^{2/2}$ embryos (Fig. 4.1.2C,D) and observed that nuclear spread in the attached muscles is similar to control. We

concluded that Robo1 regulates nuclear positioning through a Slit-independent mechanism.

During stage 17 of embryonic development, nuclei leave their clusters and spread along the muscle cell (Fig. 4.1.2G, control). The mechanisms regulating nuclear spreading at stage 17 differ from those at stages 14-16 and remain unknown [158]. To test whether Robo1 is required for myonuclear movement at this stage, we examined stage 17 embryos and found that nuclei were correctly spread out along the muscle cell (Fig. 4.1.2E). Together, these data indicated that Robo1 is required for the initial movement of the nuclear clusters towards the poles of the LT muscles, similar to genes like *Kinesin* and *Dynein* [162,167–169]; however, as was seen in these mutations that affect nuclear positioning at stages 14-16, Robo1 does not affect the subsequent movements required for final myonuclear positioning in the embryo (stage 17; Metzger et al. 2012; Schulman et al. 2014).

Microtubule and Dynein intensity in LTs is unaffected by the absence of Robo1

Previous studies identified the cortical pulling pathway, a mechanism that relies on the presence of microtubules and the appropriate localization of the minus end microtubule motor protein, Dynein, as necessary to properly position myonuclei in the embryonic LTs [167–169]. During myonuclear positioning, Kinesin, the plus end microtubule motor, walks along microtubules, bringing Dynein to the muscle cortex. Once anchored at the tip of the muscles, Dynein walks on microtubules pulling the cluster of nuclei towards the end of the muscle [167,169]. To determine whether Robo1 is regulating myonuclear positioning through this pathway, we first examined whether its absence perturbs the microtubule networks. We quantified tubulin intensity at the LT muscle ends, using previously published methods [162,168,170]. We observed no significant differences between control and *robo1*$^{1/1}$ embryos (Fig. 4.1.5A,B). This indicated that loss of Robo1 does not significantly perturb microtubule density at the LT muscle ends.

Knowing that the localization of Dynein at LT muscle poles is necessary for proper nuclear positioning through the cortical pulling pathway, we next investigated whether Robo1 plays a role in myonuclear positioning through the mislocalization of Dynein. We quantified the presence of Dynein at LT muscle ends and did not find significant differences between control and *robo1*$^{1/1}$. These data suggested that *robo1* does not influence Dynein localization in the LT muscle ends (Fig. 4.1.5C,D). As a

further test, we examined whether we could detect genetic interactions between *robo1* and *Dhc* (Dynein heavy chain) in doubly heterozygous embryos; analogous

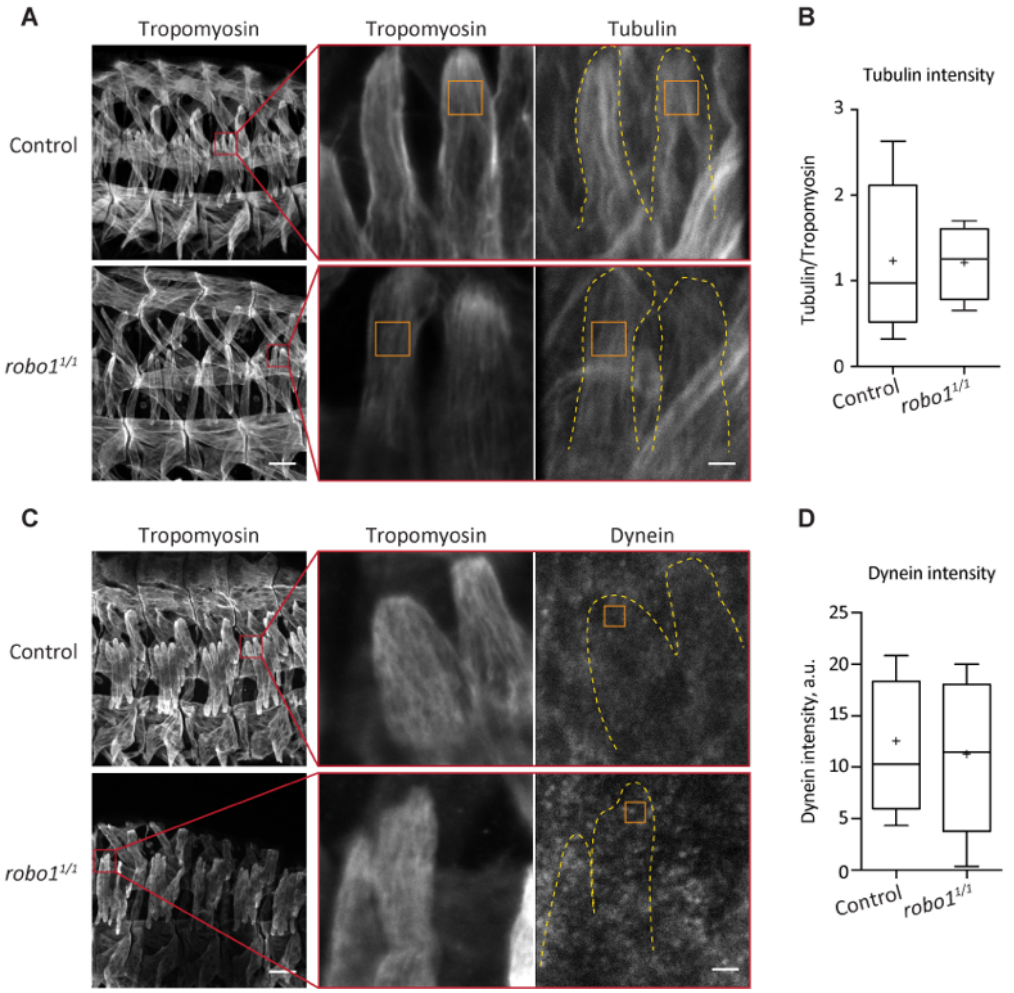


Figure 4.1.5 - Microtubule and Dynein intensity in LTs is unaffected by the absence of Robo. A) Representative images of stage 16 control and *robo1*$^{1/1}$ embryos. The red box represents the area of the LTs used for measuring of tubulin intensity and is zoomed in on the right for each genotype. The orange box exemplifies where the intensity measurement was taken within a muscle. The yellow dashed line outlines the LT tips. The Tropomyosin intensity was used to normalize the Tubulin intensity across all muscles. Scale bars, 20μm and 2μm. **B)** Quantification of the normalized Tubulin intensity shows no significant differences between control and *robo1*$^{1/1}$ muscles. Crosses indicate the average for each genotype. Statistical comparison was made using a Student's t-test. Control, 1.23±0.85, n=52 muscles from 8 embryos. *robo1*$^{1/1}$, 1.22±0.44, n=21 muscles from 4 embryos. *p*=0.9704. **C)** On the left panel, Tropomyosin highlights the musculature of control and *robo1*$^{1/1}$ embryos at stage 16. The red box represents the region in the LTs used for Dynein intensity measurements and is zoomed in on the right. The orange box demonstrates where the measurement was taken within a muscle. The yellow dashed line outlines the tips of the LT muscles. The Dynein background intensity was subtracted from the Dynein intensity in all muscles. Scale bars, 20 μm and 2 μm. **D)** Graph shows the quantification of the Dynein intensity in control and *robo1*$^{1/1}$. Crosses indicate the average for each genotype. Statistical comparison was done using a Student's t-test. Control, 12.57±6.19, n=95 muscles from 15 embryos. *robo1*$^{1/1}$, 11.30±7.13, n=55 muscles from 7 embryos. *p*=0.6743.

genetic interaction experiments have identified functional relationships between other genes in myonuclear positioning [162,167,169,170]. When we analyzed the nuclear spread in *robo1*$^{1/+}$;*Dhc64c*$^{4\text{-}19/+}$ doubly heterozygous embryos, we found no significant defects compared to each single heterozygote, suggesting no genetic

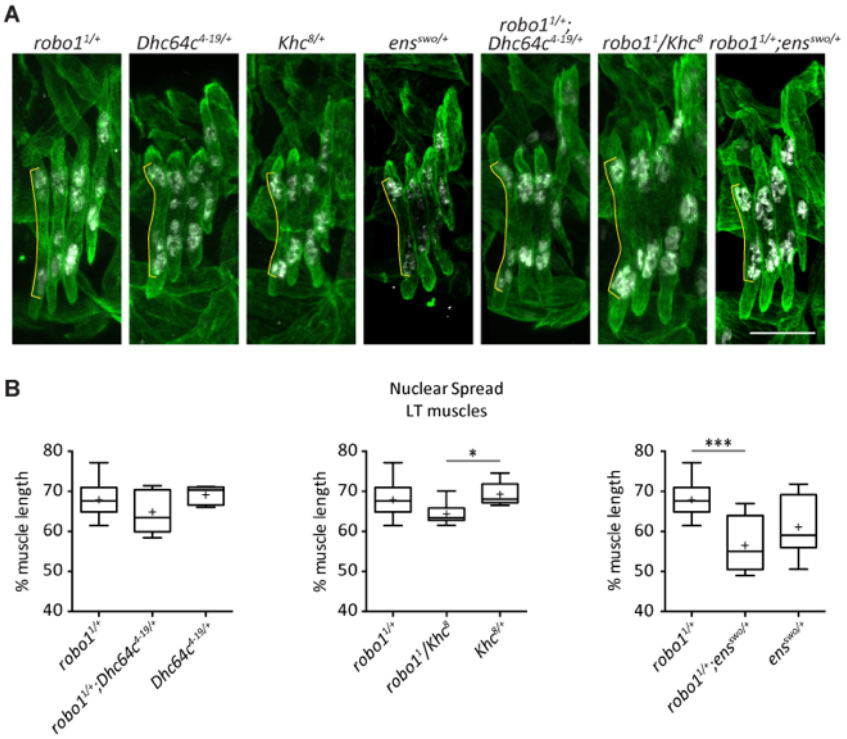


Figure 4.1.6 – *robo1* does not genetically interact with *Khc*, *Dhc* or *ens*. A) Representative images of stage 16 *robo1*, *Dhc*, *Khc* and *ens* single and double heterozygous embryos. The yellow line represents the distance between myonuclei clusters (nuclear spread). Scale bar, 20 μm. **B)** Quantification of nuclear spread as a percentage of the total muscle length. Crosses indicate the average for each genotype. Each double heterozygote was compared to the corresponding single heterozygotes using a Student's t-test. *robo1*$^{1/+}$, 68.06±4.06, n=20. *Dhc64c*$^{4\text{-}19/+}$, 69.15±2.39, n=5. *Khc*$^{8/+}$, 69.28±3.01, n=6. *ens*$^{swo/+}$, 61.08±7.43, n=7. *robo1*$^{1/+}$; *Dhc64c*$^{4\text{-}19/+}$, 64.86±5.45, n=5. *robo1*^{1}/*Khc*^{8}, 64.37±2.98, n=6. *robo*$^{1/+}$; *ens*^{swo}, 56.50±7.54, n=4. * p=0.0175. *** p=0.0002.

interaction in this assay (Fig. 4.1.6A,B). As Kinesin regulates myonuclear positioning through the cortical pulling pathway, we also tested for a possible genetic interaction between *robo1* and *Khc* (Kinesin heavy chain). We observed no significant differences between the heterozygotes *robo1*$^{1/+}$ or *Khc*$^{8/+}$ and the doubly heterozygous *robo1*$^{1/+}$; *Khc*$^{8/+}$ embryos (Fig. 4.1.6A,B). Another gene that plays an essential role in positioning myonuclei is *ensconsin*, which encodes the Microtubule-associated Protein 7 (MAP7) [158]. Absence of *ensconsin* results in severe nuclear positioning defects with all nuclei remaining as a single cluster until the beginning of coordinated muscle contraction [158,162]. When we tested for possible genetic interactions between *ens* and *robo1*, we found that these two genes do not interact in the double heterozygote

assay (Fig. 4.1.6A,B). Although negative results in genetic interaction assays cannot definitively rule out functional interactions between the encoded proteins, it should be noted that *Dhc*, *Khc* and *ens* heterozygotes have all demonstrated genetic interactions with key interactors in other studies [158,162,167–169], demonstrating

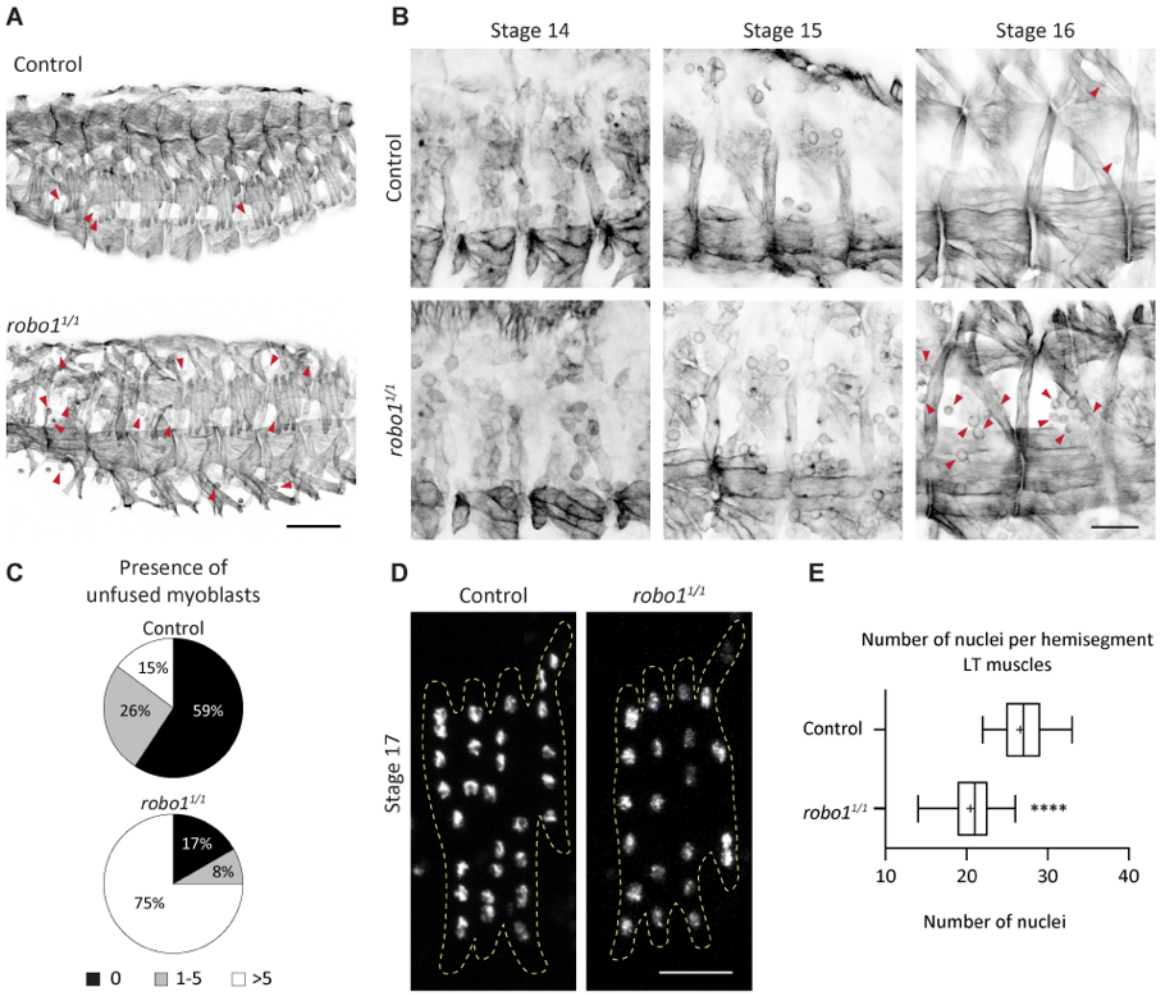


Figure 4.1.7 - Loss of *robo* results in the increased presence of unfused myoblasts and fewer nuclei in Lateral Trans- verse muscles (LTs). A) Representative image of a stage 16 *robo1*$^{1/1}$ mutant embryo shows the increased presence of unfused myoblasts (red arrowheads) in comparison with the control embryo. Scale bar, 50 μm. **B)** Internal zoomed in view of the embryos. In control embryos, the presence of myoblasts decreases over time (compare stage 14 with stage 16). However, *robo1*$^{1/1}$ embryos show a continued presence of unfused myoblasts (red arrowheads). Scale bar, 20 μm. **A and B)** Tropomyosin highlights the muscles. **C)** Quantification of the presence of unfused myoblasts at stage 16 in control and *robo1*$^{1/1}$ embryos. Embryos were divided in three categories: no unfused myoblasts, one to five unfused myoblasts and more than five unfused myoblasts. Control, n=27 embryos. *robo1*$^{1/1}$, n=24 embryos. **D)** Representative images of a single hemisegment showing the individual nuclei present in the LT muscles in both control and *robo1*$^{1/1}$ embryos. The yellow dashed line outlines the LT muscles. Scale bar, 20 μm. **E)** Quantification of the number of nuclei in the LTs per hemisegment. Crosses indicate the average for each genotype. Statistical analysis was done using a Student's t-test. Control, 26.64±2.60, n=45. *robo1*$^{1/1}$, 20.48±2.60, n=33. ****p<0.0001.

that these alleles are capable of dosage-sensitive interactions when tested with functional partners. Collectively, our data suggested that Robo1 does not regulate myonuclear positioning through the cortical pulling pathway or other Kinesin/Ens/MT-based pathways, implying a new mechanism.

Loss of *robo1* results in the increased presence of unfused myoblasts and fewer nuclei in LTs

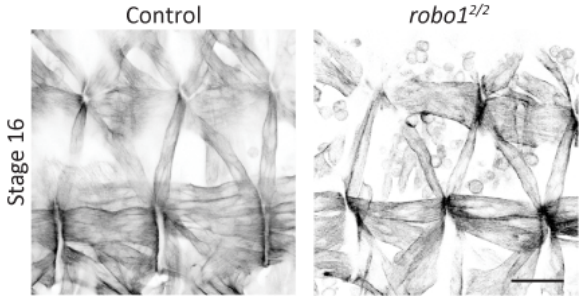


Figure 4.1.8 - *robo1*$^{2/2}$(*) shows unfused myoblast at stage 16. Representative images of the embryonic internal view show that unfused myoblasts are present in *robo1*$^{2/2}$. Tropomyosin highlights the muscles. Scale bar, 20 μm.

While assessing the nuclear positioning defects in *robo1*$^{1/1}$ embryos, we observed that these embryos also showed increased presence of unfused myoblasts (Fig. 4.1.7A, indicated by red arrowheads). In both *robo1*$^{1/1}$ and control embryos, unfused myoblasts were readily detected at stages 14 and 15, when myoblast fusion occurs (Fig. 4.1.7B). However, at stage 16, when fusion is complete [20], 75% of *robo1*$^{1/1}$ embryos exhibited >5 unfused myoblasts, compared to only 15% of control embryos (Fig. 4.1.7C). We observed the presence of unfused myoblasts in *robo1*$^{2/2}$ (*) embryos as well (Fig. 4.1.8), although, as we mention earlier, we later found out the two alleles carry the same genetic alteration. The excess of unfused myoblasts at stage 16 in *robo1*$^{1/1}$ mutants could be explained by the specification of extra FCMs earlier in mesodermal development, defects in the removal of unfused myoblasts, or fewer events of myoblast fusion to myotubes. If either of the first two possibilities were true, the LT myotubes would have the correct number of, or possibly more, myonuclei. To interrogate these possibilities, we counted the number of myonuclei per hemisegment in control and *robo1*$^{1/1}$ LT muscles at stage 17, a stage at which it is possible to resolve and count individual myonuclei because they have spread out from their clusters, and *robo1*$^{1/1}$ LT muscles show nuclear positioning like control (Fig. 4.1.2G and Fig. 4.1.7D, E). On average, *robo1*$^{1/1}$ LT myotubes had 6 fewer nuclei per hemisegment. These data indicated that loss of *robo1*$^{1/1}$ leads to fewer fusion events, resulting in LT muscles with fewer nuclei, and suggested that *robo1* regulates myoblast fusion.

Robo1 acts on fusion independently of Slit activity

To determine whether Robo1 acts during fusion through activation by Slit, we examined embryos lacking Slit (Fig. 4.1.9A). Upon inspection of *sli*$^{2/2}$ embryos, we observed that, similar to control embryos, only 6% showed more than five unfused myoblasts at stage 16 and 71% of the embryos showed no unfused myoblasts (Fig. 4.1.9B). Therefore, it was not surprising to see that at stage 17, the nuclear number present in the LTs was also comparable to the control (Fig. 4.1.9C,D). Given the lack of *slit* maternal compensation at these stages [246,247], our data suggested that Slit is not involved in myoblast fusion and that, similar to nuclear positioning, Robo1 acts during fusion in a Slit-independent fashion.

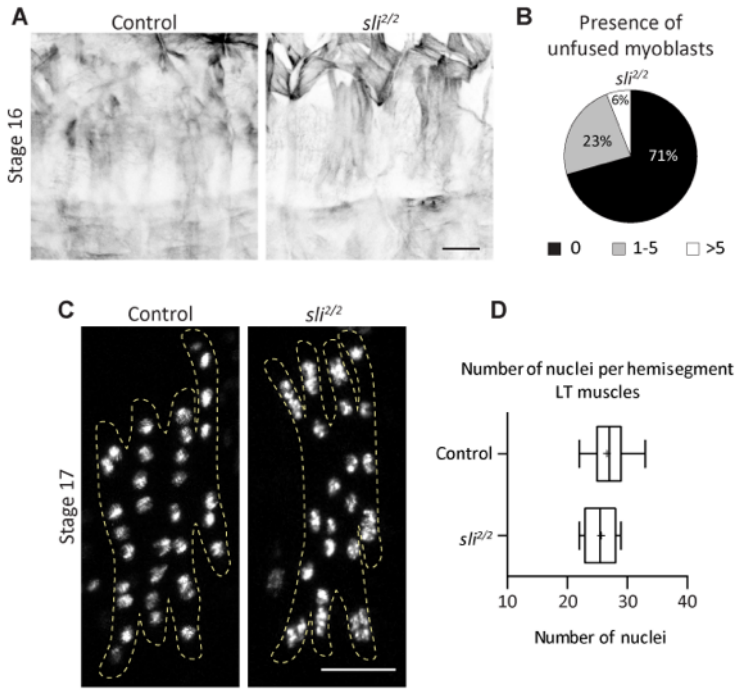


Figure 4.1.9 - Robo acts on myoblast fusion independently of Slit activity. A) Representative images of stage 16 control and *slit* mutant embryos. Embryos depleted of *slit* do not show an increased presence of unfused myoblasts indicating that Slit activity is not necessary for fusion. Tropomyosin highlights the muscles. Scale bar, 20 μm. **B)** Quantification of the number of unfused myoblasts at stage 16 in *sli*$^{2/2}$ embryos is divided in three categories: no unfused myoblasts, one to five unfused myoblasts and more than five unfused myoblasts. n=34 embryos. **C)** Representative images of control and *sli*$^{2/2}$ hemisegments showing individual nuclei present in the LT muscles. The yellow dashed line outlines the four LTs. Scale bar, 20 μm. **D)** Quantification of the number of nuclei in the LTs per hemisegment. Crosses indicate the average for each genotype. Statistical comparison was done using a Student's t-test. Control (same as in Fig. 5C), 26.64±2.60, n=45. *sli*$^{2/2}$, 25.65±2.37, n=20. A Student's t-test was used to compare the samples and the result was not significant, p=0.1484.

Robo1 regulates the duration of fusion and the amount of actin present in the actin focus

The presence of an actin-rich focus at the fusion interface is one of the hallmarks of *Drosophila* myoblast fusion. Actin foci form invasive structures, called podosome-like structures, that are essential for fusion and precede pore formation [50,55,76,156,248,249]. The presence and subsequent dissolution of the actin focus corresponds to a single fusion event (Richardson et al. 2008). Since several

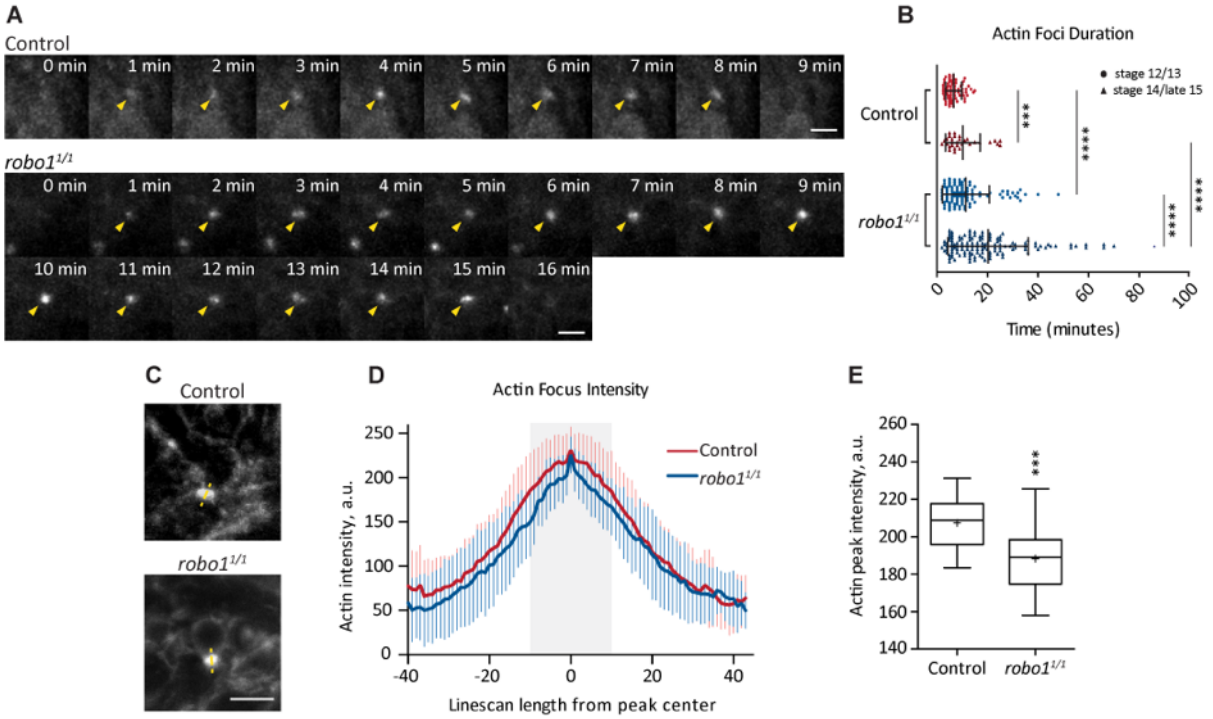


Figure 4.1.10 - Robo1 regulates the duration of fusion and the amount of actin present in the actin focus. A) The top panel shows the actin focus over time in a control embryo lasting approximately 8 minutes. In the bottom panel, a series of still frames of a *robo1*$^{1/1}$ embryo shows the extended duration of the actin focus presence for approximately 15 minutes. *twist-Actin::GFP* was used to visualize actin foci. Scale bar, 5 μm. **B)** Quantification of the duration of actin foci during fusion at stages 12/13 (circles) and stages 14/late 15 (triangles). A Student's t-test was used to statistically compare both samples and both timepoints. Control stage 12/13, 6.66±3.19, n=68. Control stage 14/late 15, 10.26±6.84, n=31. *robo1*$^{1/1}$ stage 12/13, 11.49±9.26, n=108. *robo1*$^{1/1}$ stage 14/late 15, 20.24±15.86, n=130. ***p<0.001, ****p<0.0001. **C)** Representative images of a single actin focus in a control and a *robo1*$^{1/1}$ embryo. Images were used to determine the intensity of actin at the focus. The dashed yellow line shows the region quantified. Phalloidin labels actin to visualize foci. Scale bar, 20 μm. **D)** The graph shows that *robo1*$^{1/1}$ forms foci with less actin than control embryos. The maximum values for each focus were aligned at position 0. The grey shade highlights the central region of the focus. **E)** Crosses indicate the average for each genotype. Comparison between the values highlighted in gray in D) using a Student's t-test. Control, 207.4±12.75, n=21 foci from 15 embryos. *robo1*$^{1/1}$, 188.3±16.12, n=17 foci from 13 embryos. ***p=0.0002.

downstream effectors of the Robo pathway regulate the actin cytoskeleton [241,250], we next investigated whether Robo1 regulates fusion through affecting actin focus dynamics. Since multinucleated myotubes are present in embryos lacking *robo1*, it was not surprising to detect the presence of actin foci in those embryos (Fig. 4.1.10A). The presence and duration of actin foci can be visualized by time-lapse imaging of embryos expressing *twist-Actin::GFP*, a fluorescent reporter that labels actin specifically in muscle cells and that allows for the observation of actin enrichment at the fusion site [50]. We performed time-lapse imaging on whole embryos from stage 12 through late stage 15, when fusion is occurring. In our analysis, the amount of time for which we observed the actin focus served as a proxy for the duration of fusion. We found that actin foci were present for significantly longer periods of time in *robo1*$^{1/1}$ embryos, almost twice as long as control actin foci (Fig. 4.1.10A,B). Moreover, we observed significant differences in the duration of fusion during early stages (stages 12/13) and later stages (stage 14/late 15) of fusion, in both control and mutant embryos (Fig. 4.1.10B). Actin foci in younger control embryos are present for an average of 6.6±3.2 versus 10.2±6.8 minutes in older control embryos. A similar trend was observed in *robo1*$^{1/1}$ embryos, where earlier fusion events take 11.5±9.3 minutes, and older events take 20.2±15.9 minutes, on average. While fusion duration is significantly increased in *robo1*$^{1/1}$ embryos during both developmental times, it is during stages 14 through late 15 (late fusion events) that the most striking differences are observed. We hypothesized that delays in fusion could result from defects in actin foci formation. These delays could lead to fewer fusion events and consequently to muscles with fewer nuclei and increased numbers of unfused myoblasts. To understand whether there were any structural alterations in the actin focus in *robo1* mutants, we used fixed imaging of embryos labelled with phalloidin and measured the pixel intensity of actin across each focus (Fig. 4.1.10C). We found that *robo1* mutant foci contained less actin than control foci (Fig. 4.1.10D,E), suggesting a role for Robo1 in the formation of the actin focus. Altogether, our data indicated that Robo1 is needed for the proper formation of the actin focus, where it regulates the duration of fusion events and consequently the number of fusion events that occur during muscle development.

Muscle-specific rescue of the *robo1* phenotypes (*)

Note about this section: In this section, we describe our attempts at rescuing the phenotypes caused by the lack of robo1 *by re-expressing it in the muscle in a* robo1

mutant background, which we thought had been successful. As we later found out, the genetic background in which these experiments were performed was not robo1$^{1/1}$*, but* robo1$^{1/+}$ *or* robo1$^{+/+}$ *combined with a lethal mutation in gene* y *(see section on Understanding the genetic background of the* robo1$^{1/1}$ *fly stocks). To understand how we identified the issues with the stocks, we are showing the data that was obtained with those stocks in a chronological way and labelled with an asterisk (*). The genotypes present in the images have been altered to reflect the verified genotypes after we discovered the issues in the stocks and sequenced them. Due to the nature of the issues we encountered, the interpretation of this data became more complicated and it will be discussed in the section Discussion.*

To further confirm the role of *robo1* in myonuclear positioning and myoblast fusion, we took advantage of the Gal4-UAS system to express myc-tagged Robo1 specifically in muscle cells using the muscle-specific driver *Mef2-GAL4*. Through immunofluorescence, we verified that overexpressing *robo1* in the muscle resulted in Robo1 expression at the attachment sites (Fig. 4.1.11A). Overexpressing *robo1* in *robo1* heterozygous muscle cells using *Mef2-Gal4* (*) resulted in nuclear positioning defects when compared with the control, although those defects were not as severe as those seen in the *robo1* mutants (Fig. 4.1.12A,B). Furthermore, we observed that overexpression using *Mef2-Gal4* in a *robo1*$^{1/+}$ background (*) resulted in significantly shorter muscles (Fig. 4.1.11B). Nevertheless, we found that expressing *robo1* with *Mef2-GAL4* allowed the heterozygous *robo1* embryos to hatch and occasionally pupate; in contrast, *robo1*$^{1/1}$ embryos were invariably embryonic lethal (Fig. 4.1.11C). Using Western Blot analysis, we quantified the amount of Robo1 being expressed and observed that with *Mef2-GAL4* it led to a 9.7-fold increase in Robo1 protein expression relative to controls (Fig. 4.1.11D). As levels of Robo1 have been shown to be critical for nervous system development [251–253], we speculated that these higher expression levels have a detrimental effect on muscle guidance and attachment to the correct tendon cells.

To further investigate the effects of Robo1 on myonuclear positioning, we examined the degree of defects using two additional muscle-specific drivers. *sns-GAL4* and *duf-GAL4* were used to drive the expression of the *UAS-robo1* construct in FCMs and FCs/myotubes, respectively, in a *robo1*$^{+/+}$ background. Although these two drivers are active in different muscle precursor cells, both ultimately result in increased levels of target protein (in this case, Robo1) in myotubes. Through Western Blot analysis, we observed lower levels of Robo1 expression compared to those

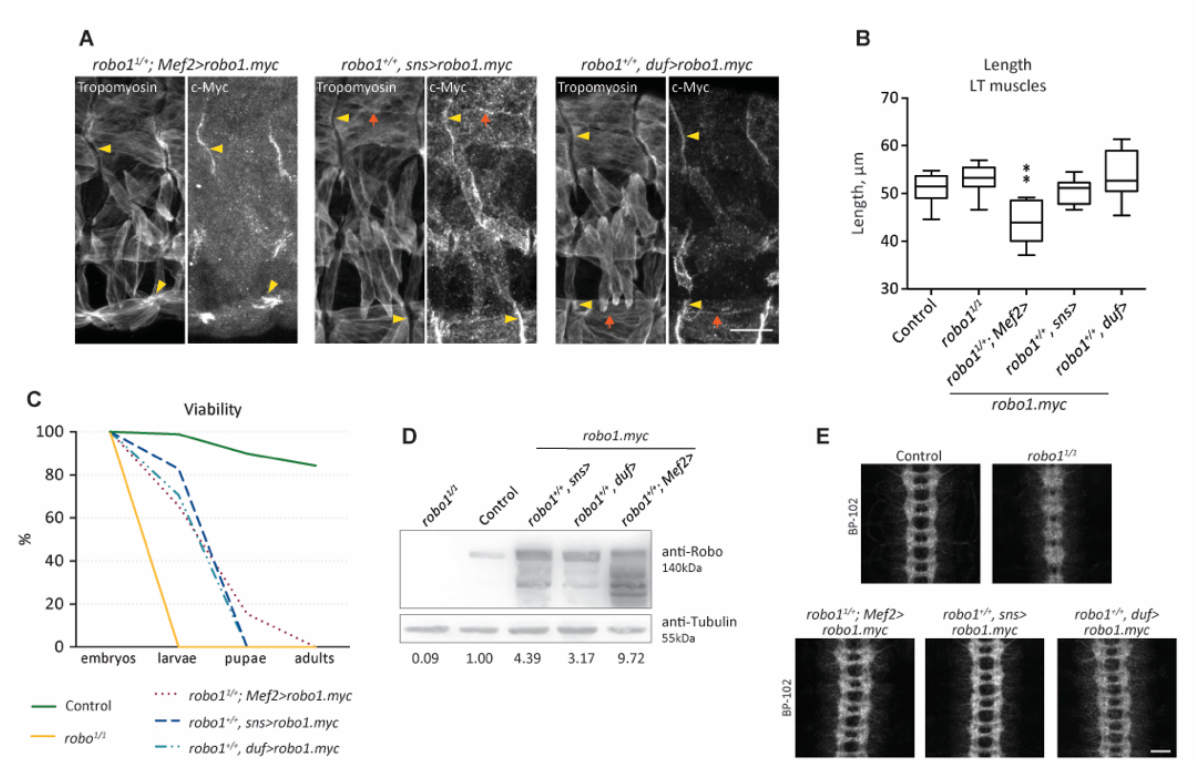


Figure 4.1.11 (*) - A) Representative images of embryos of the noted genotypes show the localization of myc-tagged Robo1 at attachment sites (yellow arrowheads) and at the muscle membranes (orange arrows). Scale bar, 20 µm. **B)** Quantification of the LT muscles length in *robo1* rescue embryos. Statistical analysis was done in comparison with the control using a Student's t-test. Control, 51.04±3.28 µm, n=10. *robo1*$^{1/1}$, 52.95±3.08 µm, n=10. *robo1*$^{1/+}$*; Mef2>robo.myc*, 44.18±4.41 µm, n=9, ** p=0.0012. *robo1*$^{+/+}$*, sns>robo.myc*, 50.34±2.62 µm, n=9. *robo1*$^{+/+}$*, duf>robo.myc,* 53.14±5.13 µm, n=11. **C)** Viability is shown as a percentage of the total number of embryos collected. Control, n=89. *robo1*$^{1/1}$, n=69. *robo1*$^{1/+}$*;Mef2>robo1.myc*, n=128. *robo1*$^{+/+}$*,sns>robo1.myc*, n=64. *robo1*$^{+/+}$*,duf>robo1.myc*, n=51. **D)** Western Blot showing increased expression of Robo1 with all drivers. Fold differences were obtained by comparing each genotype with the control. **E)** Representative images of stage 16 embryos stained for BP-102 to highlight the axons at the midline. Scale bar, 20 µm. The genotypes reflect the verified genotypes of these embryos after sequencing.

obtained using *Mef2-GAL4*. We detected a 4.4- and a 3.2-fold increase in Robo levels when using *sns-GAL4* and *duf-GAL4*, respectively, compared to control (Fig. 4.1.11D). With both drivers, we observed statistically significant defects in myonuclear spread compared to control (Fig. 4.1.12A,B). Additionally, these muscles have similar lengths compared to control and *robo1* mutants (Fig. 4.1.11B). We observed Robo1 expression at attachment sites, similar to overexpression with *Mef2-GAL4* (Fig. 4.1.11A). We also assessed viability when overexpressing *robo1* using the *sns-* and *duf-GAL4* drivers and observed viability past the embryonic stage (Fig. 4.1.11C). Our data showed that overexpression with all three drivers resulted in varying degrees of myonuclear positioning defects that seemed to be related with the levels of Robo1

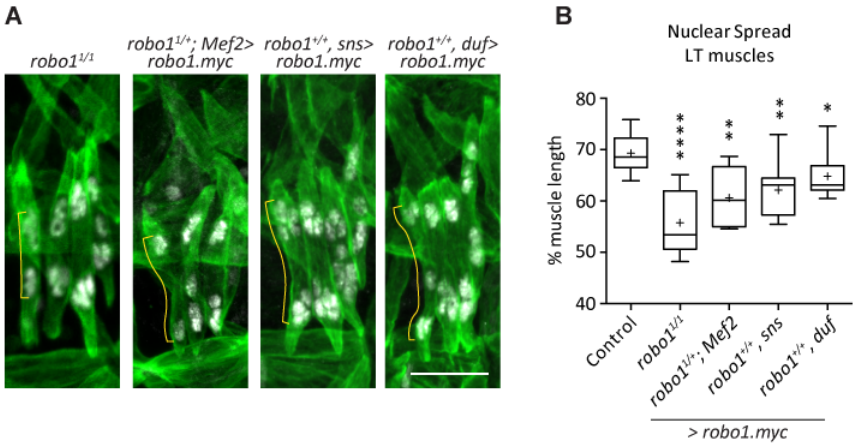


Figure 4.1.12 (*) - A) Representative images of stage 16 embryos of the noted genotypes. Tropomyosin, green. Nuclei, white. The yellow line represents the distance between myonuclear clusters (nuclear spread). Scale bar, 20μm. **B)** Quantification of nuclear spread as a percentage of the muscle length. Crosses indicate the average for each genotype. Statistical analysis was done in comparison with the control using a Student's t-test. Control, 69.36±3.65, n=10. *robo1*$^{1/1}$, 55.79±6.28, n=10; ****p<0.0001. *robo1*$^{1/+}$*;Mef2>robo1.myc*, 60.72±5.78, n=9, **p=0.0011. *robo1*$^{+/+}$*,sns>robo1.myc,* 62.20±5.32, n=9, **p=0.0030. *robo1*$^{+/+}$*, duf>robo1.myc* 64.82±4.03, n=11, *p=0.0143. The noted genotypes reflect the verified genotypes of these embryos after sequencing.

being expressed with each driver. These results suggested that excessive amounts of Robo1 can be detrimental and lead to defects in muscle guidance and myonuclear positioning.

Fusion events require two types of cells, the FCs and the FCMs. We next determined what cell type requires Robo1 activity for fusion to occur normally. To this end, we expressed *robo1* in a *robo1*$^{1/+}$ (*Mef2-Gal4*) or *robo1*$^{+/+}$ (*sns*- and *duf-Gal4*) (*) background using the three aforementioned muscle-cell Gal4 drivers: *Mef2-Gal4* is expressed in all muscle cells, *sns-Gal4* is expressed in FCMs, and *duf-Gal4* is expressed in FCs. We observed no increased presence of unfused with all drivers at stage 16 (Fig. 4.1.13A) and that these embryos resembled control embryos (Fig. 4.1.7A). We then counted the number of myonuclei in the LTs and confirmed that the nuclear number was significantly decreased with Mef2-Gal4 compared to the control, once again suggesting that the high levels of Robo1 affects the myoblast fusion events (Fig. 4.1.13B,C). However, it is interesting to notice that although we see no increased numbers of unfused myoblasts, we see decreased number of myonuclei in the LTs. Contrarily, *robo1* overexpression with *sns-Gal4* led to a significant increase in the number of nuclei in the LTs, while overexpression with *duf-Gal4* resulted in control-like number of nuclei. This suggests that increased levels of Robo1 in FCMs lead to more fusion events. Moreover, if Robo1 expression is higher in FCs, the number of fusion events in the LTs remains the same. One interesting observation

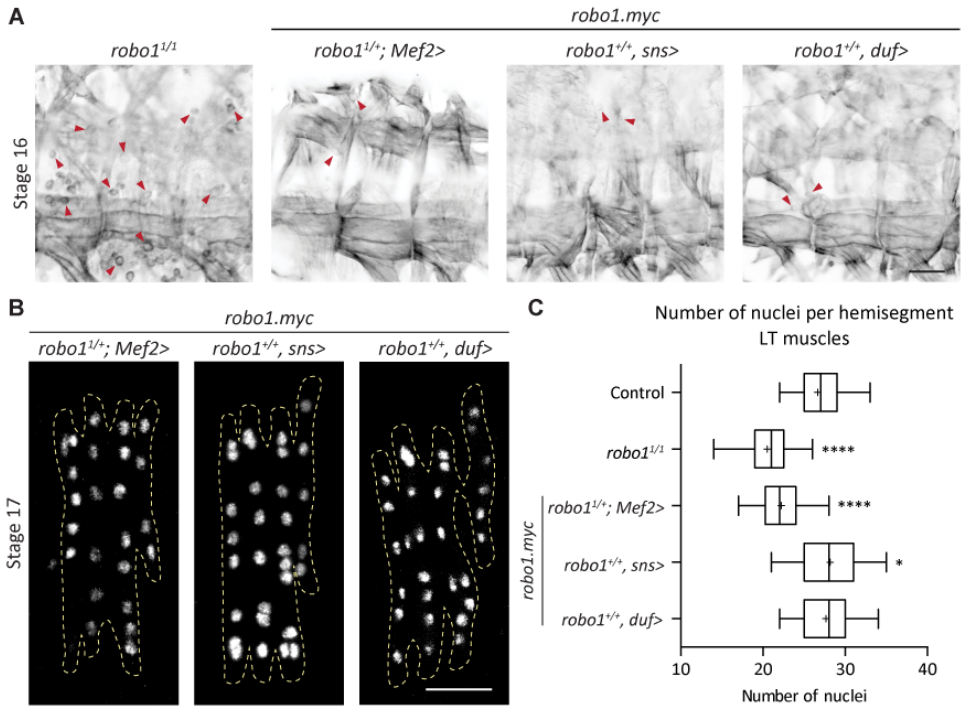


Figure 4.1.13 (*) - A) Representative images of the embryo interior of the noted genotypes. The red arrowheads indicate unfused myoblasts. Tropomyosin highlights the muscles. Scale bar, 20 μm. **B)** Representative images of a single hemisegment depicting the individual nuclei present in the LT muscles. The yellow dashed line outlines the four LT muscles in the hemisegment. Scale bar, 20 μm. **C)** Quantification of the number of nuclei in the LTs per hemisegment. Crosses indicate the average for each genotype. Statistical analysis was done in comparison with the control using a Student's t-test. Control, 26.64±2.60, n=45. *robo1*$^{1/1}$, 20.48±2.60, n=33, ****p<0.0001. *robo1*$^{1/+}$*;Mef2>robo1.myc*, 22.22±2.55, n=32, ****p=0.0001. *robo1*$^{+/+}$*,sns>robo1.myc*, 28.18±3.45, n=34, *p=0.0271. *robo1*$^{+/+}$*,duf>robo1.myc*, 27.64±3.20, n=39. The noted genotypes reflect the verified genotypes of these embryos after sequencing.

was that, similar to the myonuclear positioning analysis, rescue of the nuclear number was more successful when weaker drivers (i.e. *sns*- and *duf-GAL4*) were used. Altogether these data indicated that Robo1 plays a role in myoblast fusion, and that fusion events are sensitive to the levels of Robo1, with either an excess or a dearth of Robo1 in myoblasts or myotubes causing fusion defects.

Identifying the issues with the fly stocks carrying *robo1*$^{1/1}$

An additional phenotype that was observed during the above-mentioned experiments, was the wild-type organization of the CNS axons at the midline, which we considered as a rescue of the phenotype observed in *robo1*$^{1/1}$ embryos (*) (Fig. 4.1.11E). At the time, we assumed we were analyzing embryos part of a rescue experiment. Therefore,

this result was unexpected as the drivers used were thought to be muscle-specific, (i.e., no *robo1* would be expressed in the midline). A possible explanation for these results could be some residual expression of the construct driven by these drivers [254]. As we had shown above, our results suggested that levels of Robo1 seemed to play an important role for proper function.

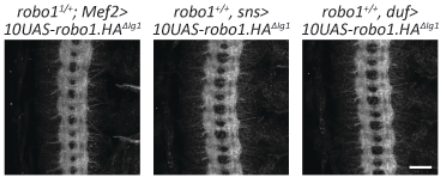


Figure 4.1.14 (*) – Representative images of embryos stained for BP-102 to highlight the axons at the midline. The genotypes noted reflect the verified genotypes of these embryos after sequencing. Scale bar, 20 μm.

To further confirm the Slit-independent roles of *robo1* in muscle development, we expressed a *robo1* construct lacking the Slit-binding domain (ΔIg1) in what we assumed was a *robo1*$^{1/1}$ background [255]. We observed that when we expressed this construct using the three muscle drivers, we obtained wild-type axons at the midline (Fig. 4.1.14). Since the axonal guidance is Slit-dependent, overexpressing the ΔIg1 construct should not be sufficient to rescue this phenotype, especially when using muscle-specific drivers. This suggested that our fly stocks may have lost the *robo1* mutation and/or other mutations have accumulated. Therefore, we decided to investigate the genetic background of the fly stocks that had been in use in this project.

Understanding the genetic background of the *robo1*^{1} fly stocks

Our first approach involved checking all the adult flies for the presence of the balancers (a combination of recessive deleterious mutations, inversion breakpoints and visible/fluorescent markers that prevent meiotic recombination and allow homozygous lethal or sterile mutations to stay in the population). We confirmed the presence of the correct balancers in the vast majority of the fly stocks tested and none of the fly stocks used in the experiments described above were affected by contamination with other flies or by the loss of the balancers.

We next did a series of complementation crosses (Table 4.1.1). This was an effective way of assessing the presence of the *robo1*^{1} mutation. We first confirmed that our *robo1*^{1} stock had both the published nervous system phenotype and the muscle phenotypes described earlier in this chapter, as well as embryonic lethality. Flies carrying *robo1*^{1} are 100% embryonic lethal; therefore, if the *robo1*^{1} mutation is homozygous, we should not see any adult flies without the balancer. In our particular case, the balancer carries *CyO* (curly wings), so if the flies in the parental generation

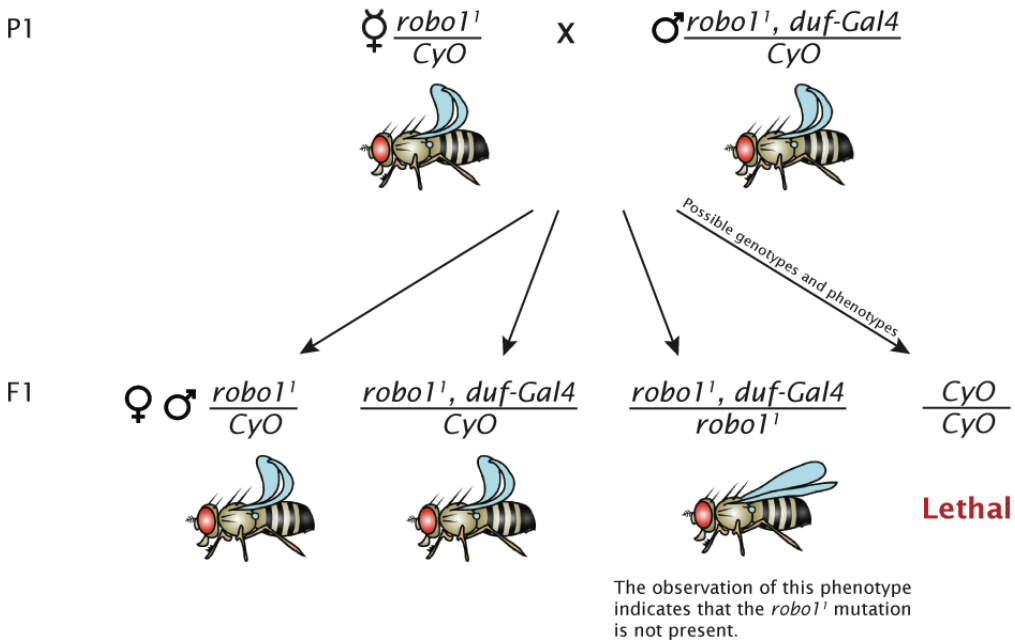


Figure 4.1.15 – Schematic representation of an example of a complementation cross to test for the presence of the *robo1¹* mutation. All flies carrying *CyO* present curly wings and those that do not carry *CyO* have straight wings. The F1 generation shows all possible outcomes from crossing the P1 generation.

carry *robo1¹* allele, all resulting adult flies should have curly and not straight wings (Fig. 4.1.15). From these test crosses, we confirmed that some of the stocks did not carry the *robo1¹* mutation, although the parental generation carried and maintained the balancer, which suggested the presence of a lethal mutation. To confirm our

Table 4.1.1 – Complementation crosses performed with *robo1¹* fly stocks.

Cross		Wings
robo1¹	*robo1¹;Mef2-Gal4*	curly
robo1¹	*robo1¹,sns-Gal4*	straight
robo1¹	*robo1¹,duf-Gal4*	straight
robo1¹	*robo1¹;UAS-robo1.myc*	straight
robo1¹	*robo1¹;10UAS-robo1.HA^{WT}*	straight
robo1¹	*robo1¹;10UAS-robo1.HA$^{\Delta Ig1}$*	straight

genetic results, we extracted DNA from adult flies and sequenced the stocks listed in Table 4.1.1. The sequencing results confirmed that two of the stocks carry the published *robo1¹* mutation, *robo1¹* and *robo1¹; Mef2-Gal4* (Fig. 4.1.16). These results confirmed that the stock which we used to characterize the mutant was correct and meant that our data in Figures 4.1.1-10 are valid. As discussed earlier, we confirmed

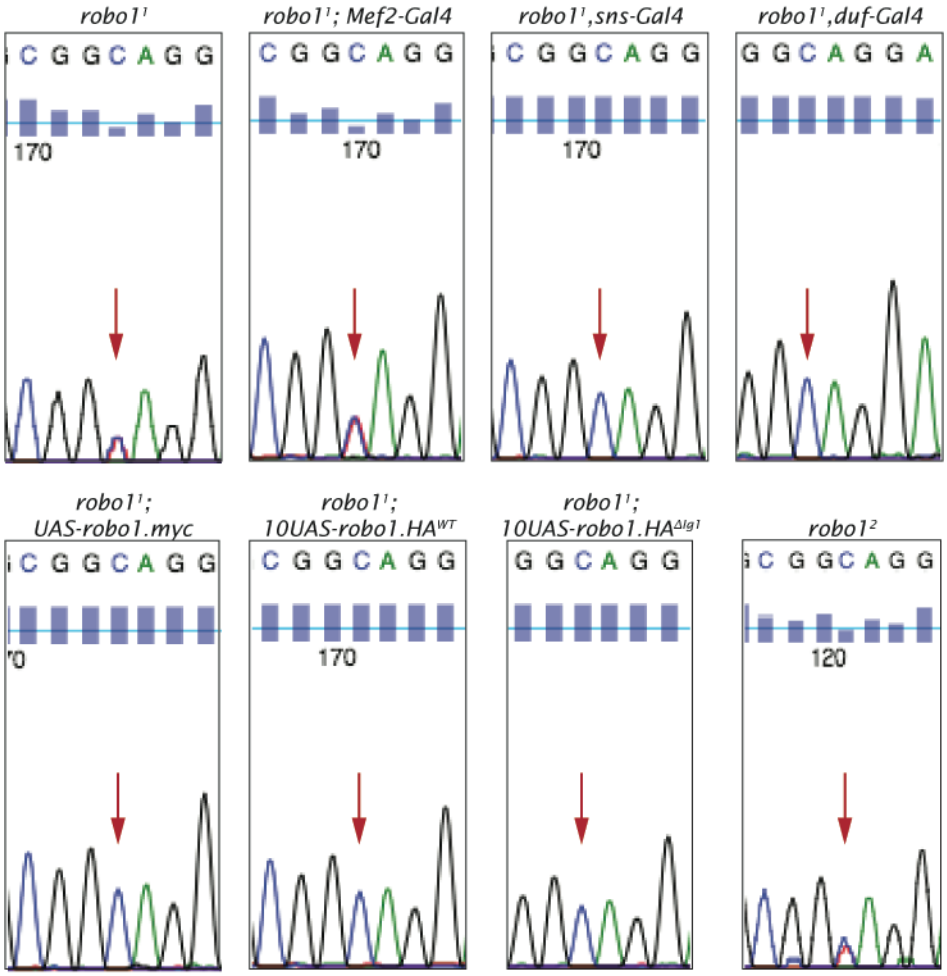


Figure 4.1.16 – Sequencing results of the noted genotypes. The red arrow indicates the nucleotide that is or should be altered.

that the rescue experiments (Figs. 4.1.11-14) were not rescue experiments, as the muscle specific *robo1* expression was done in a *robo1*^{1} heterozygous (*Mef2-Gal4*) or +/+ (*duf-* and *sns-Gal4*) background. Instead, these experiments need to be considered overexpression experiments. In addition to this, we also sequenced a different allele of *robo1* (*robo1*^{2}) that was used in our experiments. Although we observed more severe defects with allele *robo1*^{2}, the sequencing results indicated that these flies have the same mutation as *robo1*^{1} (Fig. 4.1.16). Thus, the molecular change in *robo1* is the same in these stocks. However, as they were maintained by the stock center and our lab as different stocks, these stocks may have accumulated different genetic changes in the background.

After we confirmed that the fly stock which we used to characterize the *robo1* mutant had the correct mutation, we hypothesized that an additional mutation in another gene could be present (referred to as gene *y*) leading to the lethality observed in homozygotes of our stocks. This would be particularly problematic if gene *y* generated the muscle phenotypes that we observed. To test this hypothesis, we

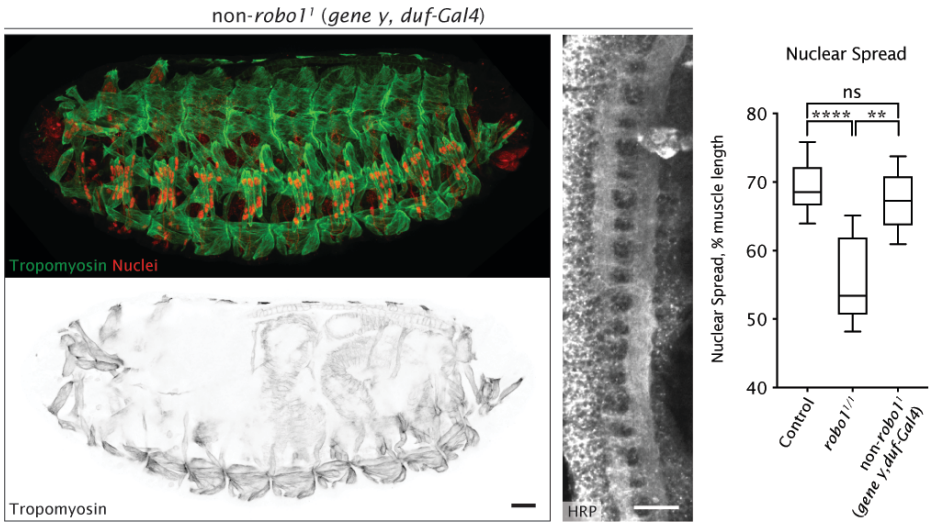


Figure 4.1.17 - Representative images of stage 16 embryonic muscles of the noted genotype and quantification of nuclear spread as a percentage of muscle length as follows (n equals number of embryos analyzed): control, 69.36, n=10; *robo1*^{1}, 55.79, n=10, ****p<0.0001; non-*robo1*^{1} (*gene y, duf-Gal4*), 67.27, n=5, **p=0.0032. ns (not significant) equal p>0.05. Tropomyosin, green. Nuclei, red. HRP, white. Scale bar, 20μm.

analyzed a stock with the following characteristics: 1) should have had the *robo1* mutation, but was found to be *robo1*^{1} negative, 2) maintained the balancer, suggesting that a lethal mutation was present, and 3) was a stock used in our previous experiments. We assessed the embryos for the excessive presence of unfused myoblasts and defects in myonuclear positioning (Fig. 4.1.17). Fortunately, we observed none of these phenotypes and the overall musculature appeared wild type. In addition, the midline axons seem to have no apparent defects, indicating that a mutation in gene *y* did not affect CNS development. Collectively, these data confirm that the mutation in gene *y* is not causing myoblast fusion or myonuclear positioning defects, and that the *robo1* mutation is, most likely, the cause of the new roles of *robo1* we described above. We are currently using verified stocks to do a rescue experiment by assessing the number of nuclei and myonuclear positioning in *robo1*$^{1/1}$ embryos where we reexpressed wildtype and ΔIg1 *robo1* using the driver *Mef2-Gal4*.

DISCUSSION

We used the *Drosophila* embryonic musculature to study the impact of muscle-tendon interactions on myonuclear positioning in muscle fibers. By focusing on one MTJ-related protein, Robo1, we found that this membrane receptor regulates myonuclear positioning in the developing fly musculature. This role for Robo1 is independent of the Kinesin-Dynein cortical pathway and represents a new mechanism for myonuclear positioning. Moreover, we found that this function of Robo1 appears to be independent of its ligand Slit. In addition, we defined a role for Robo1 in myoblast fusion, which is also Slit-independent. While fusion does occur in *robo1* mutant muscles, individual fusion events take longer than those in the control, particularly in the later stages of fusion. Concomitant with the increase in duration of fusion is the reduced level of actin at the fusion interface. Taken altogether, our work highlights the importance of myotendinous junction proteins in myonuclear positioning in *Drosophila* and reveals new additional roles for Robo1 during myogenesis.

Robo1 was first described as an essential repulsive guidance receptor during nervous system development, where it functions with its ligand Slit to control axon midline crossing (Kidd et al. 1998; Kidd et al. 1999). During mesodermal development, Robo is known to play two roles: the first in mesodermal cells as they migrate away from the midline where Slit is being expressed, and the second in growing muscle cells as they elongate towards Slit-expressing tendon cells to form MTJs [228,242,245]. Besides its role during MTJ formation, there are no reports of Robo1 being involved in other steps of embryonic muscle development. Since attachment of the muscle cell to the tendon via the MTJ occurs in *Drosophila* as myonuclei are being positioned, we hypothesized that proteins which are involved in the establishment of the MTJ may also be involved in myonuclear movement and positioning. Indeed, we show that the transmembrane receptor Robo1 is involved in myonuclear positioning. In the absence of *robo1*, stage 16 LT muscles have lengths similar to control muscles, suggesting that they are attaching to the appropriate tendon cells, and that the clusters of nuclei moved to a certain extent (compare with ens^{swo} , the strongest loss of function phenotype to date, Metzger et al. 2012). However, myonuclei in *robo1* mutant embryos were not able to move towards the muscle ends as much as in control embryos. This is true for both *robo1* alleles tested, for the transheterozygotes, and for the muscle-specific knockdown of *robo1* using RNAi; these data emphasize the importance of *robo1* in this process. At stage 17,

however, myonuclei were able to individualize and spread along the LT muscle to maximize their internuclear distance, indicating that *robo1* is not involved in this step of myonuclear positioning.

To investigate the mechanism of Robo1 activity in myonuclear positioning, we explored a well described pathway termed the cortical pulling pathway [168]. In this pathway, both microtubule motor proteins, Kinesin and Dynein, are necessary for proper nuclear positioning, by pulling the clusters of nuclei to the ends of the muscle using the microtubule network. Other proteins, such as Syd, Clip190, Glued, Pins/Raps have been linked to the cortical pathway [167–169]. A recent report also identified Aplip1, a regulator of Dynein and Kinesin, as localizing to the MTJ and acting through the cortical pulling pathway. Aplip1 regulates both Dynein localization at the muscle ends and the dynamic movements and position of myonuclei [170]. In our studies, we focused on the cortical pathway by exploring the effects of *robo1* on the networks of microtubules and on the localization of Dynein at the tip of the muscles. We did not detect any effects on the microtubule networks nor on Dynein localization in the *robo1* mutants. We also examined whether *robo1* genetically interacted with genes known to be involved in myonuclear positioning. Our failure to detect genetic interactions between *robo1* and *Dhc*, *Khc*, and *ens*, in addition to the lack of effects on the microtubules and Dynein localization, suggests the existence of an additional pathway regulating myonuclear positioning, where either Robo1 or Robo1-related proteins play a central role.

An interesting and unexpected observation was that the lack of *robo1* in embryos showed increased numbers of unfused myoblasts, which led us to investigate a possible role for *robo1* in myoblast fusion. Myoblast fusion can be divided into three steps: recognition and adhesion, actin focus formation, and fusion pore formation [154]. One way of assessing issues during fusion is by quantifying the appearance and duration of the actin foci [50,70]. Mutations in several genes, such as *kette*, *myoblast city*, *SCAR*, and *Arp2/3* confer severe fusion block phenotypes accompanied by enlarged F-actin foci, longer focus duration, and failure to resolve these structures and proceed with fusion [50,71]. While *robo1* mutants also exhibited abnormally long focus duration, they differed from these other mutants in that actin foci had a decreased amount of actin and foci eventually resolved, resulting in a less severe fusion phenotype. Examples of other mutants showing altered numbers of unfused myoblasts and reduced myonuclear numbers without having a severe fusion block, include *Muscle protein 20* and *Paxillin* [256]. While there is no evidence that Robo itself directly regulates actin dynamics, it was shown in other contexts that Robo

interacts with several signaling proteins, including netrin, several GAPs (GTPase activating proteins), and GEFs (Guanine Exchange Factors) that regulate the activity of RhoA, Rac1, and Cdc42, key regulators of actin cytoskeletal dynamics [257,258]. However, how Robo1 contributes to the regulation of the actin focus remains unclear. Exploring interactions with genes known to be essential for fusion, such as *loner,* a GEF, [71] or *duf,* an IG-domain recognition and adhesion receptor [43], will lead to a better understanding of the mechanism underlying Robo1's role in myoblast fusion.

When analyzing fusion events using time-lapse imaging approaches in control embryos, we found that actin foci remained present significantly longer in stage 14-15 embryos than in stage 12-13 embryos. These differences between stages are consistent with the proposed model of two-temporal phases of myoblast fusion. This model suggests that limited fusion occurs during stages 12-13, and that the majority of the fusion events happen in the remaining time (stages 14-15)[20]. *robo1*$^{1/1}$ embryos also showed this phasing difference between developmental stages, indicating that Robo1 does not contribute to this aspect of myoblast fusion. Nevertheless, in both phases, loss of *robo1* affects the duration of the actin foci, nearly doubling the time. Since myoblast fusion ceases towards the end of stage 15, all fusion events must happen within a specific time window (stages 12-15) [20]. Those FCMs that do not fuse within this time period remain unfused and ultimately are thought to die. Moreover, it has been observed that although several myoblasts can be in close proximity to the myotube while fusion is occurring [155], only one myoblast fuses at a time (Bothe and Baylies, unpublished observations). Considering these observations, one could assume that until a fusion event is finished, no other FCM can fuse with the same myotube. If this is true, the extended duration in the actin focus observed in embryos lacking *robo1* could explain the decreased nuclear number and the presence of unfused myoblasts at stage 16.

A common observation regarding the fusion and myonuclear positioning phenotypes seen in *robo1* mutant embryos is that these functions appear to be both independent of Slit. Slit-independent roles of the *robo* gene family have been identified in the directional guidance of interneuron migration to the cortex in mice [234], the *C. elegans* AVM mechanosensory neuron ventral guidance [235,259], and zebrafish axonal growth (Fricke et al. 2001). Additionally, it has been shown that Robo1 expression and localization is independent of its interaction with Slit in the *Drosophila* central nervous system [255]. To date, the reported functions of *robo* as a guidance receptor during *Drosophila* embryonic muscle development have been described as dependent on Slit expression, with Slit being required for muscle

precursors migration away from the midline and for myotubes elongating towards their tendon cells and forming the MTJ [228,230]. Our finding that Robo1 is acting independently of Slit during myoblast fusion and myonuclear positioning is novel. One possibility is that Robo1 homophilic interactions are responsible for the processes that we observe in our studies, similar to that reported for some aspects of axon guidance [260]. Robo receptors interact with Leucine-rich tendon-specific protein (LRT), a leucine-rich repeat (LRR) protein, during muscle elongation towards tendon cells [261]. Whether these two proteins interact during other aspects of muscle development, such as the ones highlighted here, remains to be discovered. Additionally, Slit-activated Robo forms a complex with N-cadherin, among other proteins, to modulate cell adhesion and transcription [262,263]. N-cadherin was reported to be negatively regulated by Loner and play a role during myoblast fusion [51]. Further experiments are required to understand whether N-cadherin and Loner interact with Robo during myoblast fusion or myonuclear positioning.

With the goal of further understanding the role of *robo1* in myonuclear positioning and myoblast fusion, we attempted to do rescue experiments using three muscle-specific drivers. However, as we later found out, the majority of our stocks did not carry the $robo1^{1}$ mutation. The results we obtained have to be interpreted in light of the verified genotypes. When we used *Mef2-Gal4* we were driving the expression of *robo1* in a *robo1* heterozygous background. For both *sns-* and *duf-Gal4*, we did robo1 overexpression (the genetic background was $robo1^{+/+}$). This background also carries another lethal mutation. Nevertheless, some conclusions can be drawn from those data. The expression of robo1 using these three drivers resulted in varying levels of Robo1 protein compared to the control. We measured the levels of Robo1 expressed with each driver and observed that the better results were obtained when lower levels of Robo1 were present. We observed nuclear positioning defects with the three drivers. However, the higher the expression of *robo1*, the worst the phenotype. This was particularly obvious when we used the strongest driver, *Mef2-GAL4*, where we observed significant nuclear positioning defects, and changes in the length of the myotubes, as well as orientation defects. Interestingly, when lower Robo levels were present, using *sns-* or *duf-GAL4*, the myonuclear positioning was more similar to control, yet still significant defects were observed. Additionally, the length of the muscles remained similar to both the control and the *robo1* mutant.

A similar trend was observed during the myoblast fusion studies. Overexpression using Mef2-Gal4 resulted in fewer myonuclei in the LTs, whereas *robo1* overexpression in the FCs led to similar number of nuclei compared to the

control. When *robo1* was overexpressed in the FCMs, we observed and increase in the number of myonuclei, which could indicate that Robo1 regulates the number of fusion events. Since Robo1 is involved in myotube guidance to the tendons, one hypothesis to interpret this data is that Robo1 in the FCMs guides them to myotubes [188]. Contrary to what was observed in *robo1*$^{1/1}$ embryos, it would be interesting to assess the duration of fusion in these embryos to see of each event take less time to occur. With both the weaker drivers, the Robo1 levels were still higher than in the control (4.4- and 3.2-fold increase with *sns*- and *duf-Gal4*, respectively). We found that the closer the levels of Robo1 to wild-type, the better the musculature and its characteristics. The notion that Robo1 expression levels are important dates back to the early 2000s, when it was observed that during midline crossing, Robo1 expression is tightly regulated, both spatially and temporally. Low levels of Robo1 at the cell membrane are required in the pre-crossing axons to inhibit repulsion by Slit; during and after midline crossing, Robo1 levels increase to ensure that the axons are repelled by Slit and prevent them from re-crossing the midline [251–253]. In light of these data, our results suggest that too much Robo1 within a cell can be detrimental for muscle development and that the amount of protein expressed must be regulated to achieve a muscle cell of a particular size and with the proper intracellular organization (i.e. myonuclear positioning). However, further studies are needed for a detailed understanding as to how Robo1 and its downstream effectors differentially function in FCs, FCMs, and myotubes.

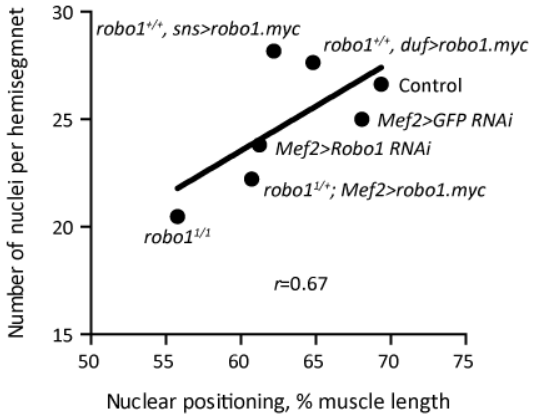


Figure 4.1.18 – Correlation between the number of nuclei and nuclear spread. Plot including genotypes where both nuclear number and positioning were assessed. The genotypes noted reflect the verified genotypes of these embryos after sequencing *r* corresponds to the Pearson correlation coefficient.

We have defined novel roles for Robo1 in myoblast fusion and myonuclear positioning. While Robo1 may be contributing to each process separately, it is tempting to speculate that there is a connection between both processes, that is, that the myonuclear number influences myonuclear positioning. To that end and regardless of the genetic background issues we experienced, we have found a correlation in our data set between these two muscle features. LT muscles with fewer nuclei show greater myonuclear positioning defects and vice-versa (Fig. 4.1.18). One caveat of this explanation is that *robo1* affects the

MTJ organization, which on its own could lead to positioning defects. Recently, it was reported that the CNM and EDMD-associated proteins needed for proper nuclear positioning are also required to maintain or relieve internuclear interactions [160]. How the number of nuclei and interactions between these nuclei regulate the position of the nuclei clusters remains an area for future study.

In conclusion, we demonstrated that muscle-tendon interactions influence aspects of muscle subcellular organization, such as myonuclear positioning. Additionally, we identified two novel roles for *robo1* in embryonic body wall muscle development. We found that Robo1 regulates myoblast fusion and myonuclear positioning in a Slit-independent fashion. Loss of *robo1* reduces the amount of actin in the actin focus and delays fusion. Our work leads to new directions worth exploring: What other aspects of muscle cell organization can be regulated by muscle-tendon interactions? Can other muscle-interacting cells regulate myonuclear positioning? What is the mechanism of action of Robo1 in myonuclear positioning and in myoblast fusion? If and how does nuclear number regulate nuclear positioning? Further experiments to answer these questions will lend insight into both muscle development and muscle disease.

FUTURE PERSPECTIVES

To better understand the roles of Robo1 during muscle development, there are a series of experiments that would complement and confirm what was described above. Ideally, we would be able to generate stocks that carry the *robo1*^{1} mutation as well as the muscle specific drivers to perform rescue experiments using the wild type *robo1* construct. From the data we presented, there is good indication to believe that we will obtain different levels of rescue, given the different levels of Robo1 expression each driver provides the muscles with. Moreover, to confirm the Slit-independence of Robo1 in these processes, we would rescue the phenotypes using the *robo1* construct lacking the Slit binding domain. The use of *robo1* constructs lacking cytoplasmic domains would also help to understand how Robo1 signaling affects muscle development.

As suggested in the Discussion, it would also be interesting to understand with what proteins Robo1 might be partnering to regulate myonuclear positioning and myoblast fusion. As a first step, Loner and N-cadherin are strong candidates as it has been reported that these proteins can interact with each other [51,262]. Robo1 can be part of a Slit-dependent multimolecular complex that inactivates N-cadherin [262] and Loner negatively regulates the presence of N-cadherin during myoblast fusion [51]. Both Robo1 and Loner interact with N-cadherin, so investigating the relationship between these three proteins can lead to understanding the mechanism behind Robo1 during myoblast fusion and myonuclear positioning.

Lastly, discovering what gene *y* is and the nature of its mutation would be of interest. Particularly, while gene *y* does not seem to affect muscle development, we cannot guarantee with the data available that the two mutations – gene *y* and *robo1*-- together could result in a muscle phenotype. A deficiency screening combined with sequencing could lead to the identification of this gene.

Part II

THE *DROSOPHILA* NINEIN HOMOLOGUE BSG25D COOPERATES WITH ENSCONSIN IN MYONUCLEAR POSITIONING

Jonathan N. Rosen[1], Mafalda Azevedo[1,2], David B. Soffar[1], Vitaly P. Boyko[1,3], Matthew B. Brendel[1,3], Victoria K. Schulman[1,4], and Mary K. Baylies[1,4]

[1]Program in Developmental Biology, Sloan Kettering Institute, Memorial Sloan Kettering Cancer Center, New York, NY
[2]Graduate Program in Areas of Basic and Applied Biology, Abel Salazar Biomedical Sciences Institute, University of Porto, Porto, Portugal
[3]Molecular Cytology Facility, Sloan Kettering Institute, Memorial Sloan Kettering Cancer Center, New York, NY
[4]Cell and Developmental Biology, Weill Cornell Graduate School of Medical Sciences, Cornell University, New York, NY

J. Cell Biol. 2019 Vol. 218 No. 2 524–540

Contribution to this work: Performed experiments and analyzed the data (myonuclear positioning and nuclei characteristics in larval muscles; tubulin analysis in larval muscles; larval locomotion; AFM in larval muscles [with the help of Matt Brendel]; colocalization analysis in embryos). Edited and revised the manuscript.

ABSTRACT

Skeletal muscle consists of multinucleated cells in which the myonuclei are evenly spaced throughout the cell. In *Drosophila*, this pattern is established in embryonic myotubes, where myonuclei move via microtubules (MTs) and the MT-associated protein Ensconsin (Ens)/MAP7, to achieve their distribution. Ens regulates multiple aspects of MT biology, but little is known about how Ens itself is regulated. We find that Ens physically interacts and colocalizes with Bsg25D, the *Drosophila* homologue of the centrosomal protein Ninein. Bsg25D loss enhances myonuclear positioning defects in embryos sensitized by partial Ens loss. Bsg25D overexpression causes severe positioning defects in immature myotubes and fully differentiated myofibers, where it forms ectopic MT organizing centers, disrupts perinuclear MT arrays, reduces muscle stiffness, and decreases larval crawling velocity. These studies define a novel relationship between Ens and Bsg25D. At endogenous levels, Bsg25D positively regulates Ens activity during myonuclear positioning, but excess Bsg25D disrupts Ens localization and MT organization, with disastrous consequences for myonuclear positioning and muscle function.

INTRODUCTION

In many cell types, nuclei occupy specific subcellular localizations that are functionally important [146]. In mammalian muscle, nuclei are positioned at the muscle cell periphery in a manner that maximizes internuclear distance. Myonuclear mispositioning is a feature of certain muscle diseases [148,208], and model organisms that are mutant for genes required to position myonuclei exhibit decreased muscle function [158,167,169,172,264]. These findings argue that correct nuclear positioning is essential for muscle function.

Skeletal muscle development and structure are highly conserved between the fruit fly *Drosophila melanogaster* and humans. In both humans and *Drosophila*, muscle cells are multinucleated and formed from the iterative fusion of muscle precursor cells, each of which contributes a nucleus to the growing myotube. After fusion, myonuclei in each *Drosophila* myotube are present as a single cluster. Subsequently, the myonuclei undergo coordinated movements that ultimately leave them evenly distributed along the length of the muscle cell. The first step of nuclear positioning occurs at stage 14 (10–11 h after egg laying [AEL]), when the myonuclei separate into two clearly defined groups along the myotube's long axis. Then, during stages 15 (11–13 h AEL) and 16 (13–16 h AEL), the two clusters of myonuclei migrate away from the myotube's center toward opposite muscle poles. During stage 17 (16–24 h AEL), the last stage of embryonic development, myonuclei spread out from the two clusters and fill in the myofiber evenly, such that the distance between myonuclei is maximized [158]. Finally, this even spacing is maintained, likely by active mechanisms, during the lifetime of the larval myofibers [172,200].

The regulation of myonuclear positioning is poorly understood. A key player in the process is Ensconsin (Ens)/MAP7, a microtubule (MT)-associated protein (MAP). Ens promotes Kinesin-based MT transport by relieving Kinesin from its autoinhibited conformation [265] or by recruiting Kinesin to MTs [183]. *ens* loss-of-function mutants exhibit a complete block in myonuclear separation and poleward cluster migration through stage 16; at this stage, control myonuclei reside in two clusters near opposite myotube poles, while ens mutant myonuclei are present as a single cluster [158]. Loss of Kinesin heavy chain (Khc) impairs myonuclear movement [158], as do mutations in the genes encoding the MT minus end–directed motor protein Dynein heavy chain and the motor protein adaptor Sunday driver [167–169]. Taken together, these findings demonstrate the centrality of MTs and associated proteins to myonuclear positioning.

Interestingly, *ens* is the only mutant isolated to date where myonuclear movement appears to be completely blocked. While maternal products may partially ameliorate the phenotypes of *Khc*, *Dhc*, and *syd* zygotic mutants, the uniqueness of the *ens* phenotype raises the possibility that Ens plays additional roles in myonuclear movement beyond its regulation of MT-based transport. Indeed, in other cell types, Ens has been shown to be a MT polymerizing factor [266]. How Ens promotes nuclear movement in muscle, and what other proteins regulate its critical activity, are outstanding questions in the field.

MT networks, which are essential for myonuclear positioning, undergo dramatic changes during muscle development. In mammalian cell culture, following myoblast fusion, centrosomes are lost and centrosomal proteins relocalize to alternative MT organizing centers (MTOCs) in the acentrosomal myotube, most prominently the myonuclear envelopes [267]. In *Drosophila*, MTs similarly reorganize during muscle development; starting in the embryonic myotube, most MTs run parallel to the cell's long axis, but by the third-instar stage of larval development, immunofluorescent staining for Tubulin clearly reveals that MT arrays also extend from myonuclear envelopes [158,172,200]. Only two genes, *pavarotti* and *RacGAP50C*, have been implicated in the regulation of muscle MT reorganization in the embryo [268]. Much more needs to be learned about how this transition occurs.

Proteins that regulate MT networks in other cell types are strong candidates for being factors in muscle MT organization and MT-dependent myonuclear positioning. One such factor is the MT minus end–binding protein Ninein, encoded by the gene *NIN*. Pioneering cell culture experiments showed that Ninein localizes to centrosomes [269] and noncentrosomal MTOCs [270] and that Ninein anchors MTs to MTOCs and promotes MT nucleation by docking γ-Tubulin [271–274]. More recently, cell culture studies and RNAi-based *in vivo* approaches have affirmed critical roles for Ninein in regulating MT organization in numerous cell types. Surprisingly, recently generated null *NIN* mutants in invertebrates are relatively normal: *Caenorhabditis elegans* mutants for the *NIN* orthologue *noca-1* are sterile with defects in the noncentrosomal MT arrays of the germline and epidermis but have grossly normal morphology and develop to adulthood [275]. Mutants for the *Drosophila NIN* orthologue *Bsg25D* are viable and fertile [276,277]. Loss of Ninein/NOCA-1 in *C. elegans* is partially compensated for by the MT minus end protein Patronin [275]; no redundant factors have been identified in *Drosophila*. Since *Bsg25D/Ninein* is conserved from invertebrates to humans, *Bsg25D* may have important functions not

readily detectable by single mutant analysis. How does Bsg25D function, and what proteins does it interact with in muscle?

In this work, we find that Bsg25D acts with Ens to regulate myonuclear positioning. Muscle-specific *Bsg25D* overexpression caused myonuclear positioning defects in embryonic myotubes, and overexpression of *Bsg25D* and *ens* reciprocally affected the speed and direction of myonuclear movement. In mature myofibers, overexpressed *Bsg25D* caused nuclear positioning phenotypes, MT defects, and reduced muscle stiffness and function. We conclude that Bsg25D, under wild-type conditions, binds to Ens and promotes its activity in myonuclear positioning, whereas when Bsg25D is expressed at high levels, it alters Ens localization and function, phenocopying ens mutants, and ultimately disrupts muscle MT networks and muscle function. Our results shed further light on the function of Ens in the process of nuclear movement and find a novel *in vivo* role for Bsg25D/Ninein, a poorly understood centrosomal protein, in myonuclear positioning.

MATERIALS AND METHODS

Drosophila genetics

Standard *Drosophila* genetics were performed at 25°C. The following stocks were used: *apterous$_{ME}$-NLS::dsRed* [50], *ens^{swo}* [158], *Df-ens$^{\Delta 3277}$* [183], *khc^{8}* [238], *dhc$^{4-19}$* [239], *plp^{5}* [278], *Dmef2-Gal4* [220], *rP298-Gal4* [279], *ubiquitin-Gal4[3xP3-GFP]* [280], *UAS-Ens-HA* [158], *UAS-2xEGFP* [281], *UAS-EB1-YFP* [282], and *patronin$^{\Delta 2}$* (gift from M. Gonzalez-Gaitan, University of Geneva, Geneva, Switzerland). *w^{1118}* (3605), *yw* (1495), *UAS-Rab7.GFP* (42706), *UASp-GFP.Golgi* (30902), *UAS-GFP.KDEL* (9899), *Df(2L)BSC693* (26545), *Df(3L)BSC441* (24945), *hs-FLP,hs-SceI* (25679), *γ-tub23C^{A6-2}* (5728), and *γ-tub23C^{A14-9}* (7041) were obtained from the Bloomington *Drosophila* Stock Center. P3-83 containing BAC clone CH321-49G22, referred to in the text as *BAC[Bsg25D+]*, was obtained from Genetivision. The following lines were developed for this work (details below): *Bsg25D^{null}*, *UAS-eos::Bsg25D*, and *UAS-ens::EGFP*. *ens^{swo}* and *Df-ens$^{\Delta 3277}$* homozygotes have the same nuclear positioning phenotype at stage 16 (data not shown). The *Df-ens$^{\Delta 3277}$* allele was used for genetic interaction experiments with Bsg25D overexpression (the three rightmost panels in Fig. 4.2.3A). All other experiments with *ens* mutants used the *ens^{swo}* allele.

Generation of mutant and transgenic *Drosophila* stocks

Bsg25D^{null} (referred to in this work as *Bsg25D$^{-/-}$*) flies were generated by accelerated homologous recombination without CRISPR/Cas9 [280]. Homology arms 5′ and 3′ of *Bsg25D* were PCR amplified and sequentially cloned into pTV^{Cherry} (gift from J.P. Vincent, Francis Crick Institute, London, UK). The following primers, containing the indicated restriction enzyme sites, were used: 5p homology arm: 5p forward NheI, 5′-GATCGC TAGCAGCCATTCGCCTCGCTCTTC-3′; 5p reverse KpnI, 5′-GATCGG TACCGCTGCCGTTCCAATCGATCG-3′; 3p homology arm: 3p forward BglII, 5′-GATCAG-ATCTGACAAACCTGAGGAGGGAGT-3′; 3p reverse AvrII, 5′-GATCCCTAGGCGTAGAAAGGGTAGAAATAT-3′.

The pTV^{Cherry}-Bsg25D donor cassette was then randomly integrated in *w^{1118}* flies by p-element transformation (Genetic Services, Inc.). Potential transgenic flies were screened for by mini-white expression, and a third chromosome transgenic line was

obtained. Following the published accelerated homologous recombination cross scheme [280], 14 putative mutant lines were recovered. One was validated as *Bsg25D*^{null} by PCR using primers designed to amplify genomic regions specific to either wild-type or mutant chromosomes, followed by sequencing. The *Bsg25D*$^{-/-}$ line used in this study had the mini w+ cassette inserted between bp334 in the Bsg25D 5′ UTR and bp5919 at the beginning of the Bsg25D 3′ UTR based on the published FLYBASE Bsg25D genomic sequence, leading to the removal of all protein coding sequences and, as a result, all protein isoforms (Fig. 4.2.2A). The following PCR primers were used for mutant verification: wild-type-specific *Bsg25D*: 1537 forward, 5′-ACAATACGGACGAGGACCAG-3′; 3907 reverse, 5′-TTCCTTTGC AGCCTTGAGTT-3′; mutant-specific *Bsg25D* pair 1: 7224 forward, 5′-GAGTTGCTGTTGCTGCAGAG-3′; 11081 reverse, 5′-TTGACCTCA GCGTCGTAGTG-3′; mutant-specific *Bsg25D* pair 2: 7326 forward, 5′-TGAAGATACCCCACCAAACC-3′; 10289 reverse, 5′-GCGCAC TCAGCAAAACATTA-3′. Mutant flies were confirmed by Western blotting for Bsg25D multiple times with biological replicates.

UAS-eos::Bsg25D (referred to in this paper as *UAS-Bsg25D*) flies were generated as follows: Eos was amplified from pME-eos (gift from D. Raible, University of Washington, Seattle, WA) using the following forward and reverse primers containing restriction sites for NotI and XhoI, respectively: F_NotI_eos_NotI, 5′-CAC CGCGGCCGCATGAGTGCGATTAAGCCAGACATG-3′; R_XhoI_eos_ no_stop_XhoI, 5′-CTCGAGTCGTCTGGCATTGTCAGGCAATCC-3′. The PCR product was cloned into pUAST. Next, *Bsg25D* was amplified from expressed sequence tag clone LD21844 (*Drosophila* Genome Resource Center [DGRC]), corresponding to transcript Bsg25D-PB, and cloned into pUAST-eos in frame with the N-terminal Eos. The following primers, both containing *KpnI* restriction sites, were used for PCR: F-CACC-KpnI-Bsg25D, 5′-CACCGG TACCATGGAGGTATCCGCCGATCCGTAC-3′; R-KpnI-stop-Bsg25D, 5′-GGTACCCTAAGGCATGCCAGGCAGTCCACC-3′. pUAS-eos:: Bsg25D was randomly integrated in *w*^{1118} flies by p-element transformation (Genetic Services, Inc.). Potential transgenic flies were selected by mini-white expression. The *eos::Bsg25D* line was used for all fly studies on overexpressed *Bsg25D*.

UAS-ens::EGFP flies were generated as follows. Full-length *ens* (LD09626; DGRC) was PCR-amplified using the following primers containing EcoRI and BamHI restriction sites, respectively: 5′-GAATTCATGGCGAGTCTTGGGGGCCAACAC-3′ and 5′-GGATCCCAGCAGCGATATATCTTTATTTTCGTG-3′. The PCR product was cloned into pUAST (DGRC) previously modified to contain a C-terminal EGFP tag. *pUAS-Ens::EGFP*

was randomly integrated in w^{1118} flies by p-element transformation (Best Gene, Inc.), and potential transgenic flies were screened for by mini-white expression.

Protein sequence analysis

Bsg25D protein sequence analysis was performed by InterProScan, which identifies domains by scanning protein sequences against predictive models provided by several different databases [283]. Alignment of Bsg25D to mouse Ninein was done using the Blastp algorithm (National Center for Biotechnology Information).

Viability assays

Viability assays were done at 25˚C essentially as previously described [169]. For comparison of GFP-and Bsg25D-overexpressing flies, embryos were bleached and selected at stage 16. For other viability assays, embryos were selected without bleaching under halocarbon oil at stage 5. In all cases, a minimum of 100 embryos were selected over multiple days. The number of hatched and unhatched embryos was counted, and all first-instar larvae were transferred to a vial with fresh food. The number of pupae and adults that eclosed was assessed. Viability is represented as a percentage of the initial number of embryos.

Fluorescent antibody staining

Embryos were prepared for staining as previously described [50]. Larvae were dissected and flat mounted in HL3.1 dissecting buffer and fixed for 20 min in formalin. Embryos and larvae were incubated in primary antibody overnight at 4˚C or for 1 h at room temperature at the following concentrations: rat anti-Tropomyosin (1:500; Abcam), rabbit anti-DsRed (1:400; Clontech), chicken anti-GFP (1:500; Abcam), mouse anti-α-Tubulin (1:500; Sigma), mouse anti-acetylated α-Tubulin (1:50; Santa Cruz Biotechnology), mouse anti-γ Tubulin clone GTU-88 (1:500; Sigma), guinea pig anti-Bsg25D ([284]; 1:400; gift from E. Lecuyer, Montreal Clinical Research Institute [IRCM], Montreal, Canada), rat anti-Ens (1:100; gift from P. Rorth, University of Copenhagen, Copenhagen, Denmark), rabbit anti-Plp (gift from J. Raff, University of Oxford, Oxford, UK), rabbit anti-Arl8 (1:100; Developmental Studies Hybridoma Bank), and mouse anti-SUMO-2 8A2 (1:50; Developmental Studies Hybridoma Bank).

Overexpressed *eos::Bsg25D* was detected either by Bsg25D antibody staining or by Eos signal. For both embryo and larva staining, Alexa Fluor 488-, Alexa Fluor 555-, and Alexa Fluor 647-conjugated secondary antibodies (Invitrogen) were applied 1:400 for 1 h at room temperature. Hoechst and Alexa Fluor-conjugated phalloidin (either Alexa Fluor 488 or Alexa Fluor 555; Life Technologies) were added with the secondary antibody at 1:400 and 1:200, respectively. Samples were mounted in ProLong Gold antifade reagent (Invitrogen).

Fixed sample imaging and analysis

Z-stacks of fixed samples were acquired using a Leica SP5 laser-scanning confocal microscope equipped with the LAS AF software using a 63x 1.4 NA HCX PL Apochromat oil objective and processed in Volocity (Perkin Elmer) or ImageJ (National Institutes of Health). For analysis of nuclear positioning at stage 16, the Line function in ImageJ was used to measure the distances from the dorsal-most nucleus to the dorsal myotube pole, the ventral-most nucleus to the ventral myotube pole, and the total myotube length. “Nuclear spread” was calculated by subtracting the first two values from the third and expressing the difference as a percentage of total myotube length. For statistical purposes, the mean of the four lateral transverse muscles in a hemisegment was considered one sample. Nuclear positioning data were collected from a maximum of four hemisegments (abdominal hemisegments 2–5) per embryo. Embryos were fixed over the course of multiple days and then pooled for staining and analysis. Myonuclear positioning in the ventral longitudinal (VL) 4 muscle of third-instar larvae was also assessed using the Line function in ImageJ. “Nearest neighbor” was defined as the distance between a nucleus and the nearest neighboring nucleus. “Largest gap” refers to the longest stretch of muscle fiber void of myonuclei, and internuclear distance refers to the distance between consecutive myonuclei along the longitudinal muscle axis. All three terms are presented as percentages of muscle length. Statistical analysis of nuclear positioning in larval muscles employed weighted averages to account for different numbers of myofibers analyzed for each larva. n refers to the total number of myofibers. MT density was calculated by measuring the intensity of Tubulin and Tropomyosin near the tips of the muscles, essentially as published [167]. For statistics, the average of Tubulin/Tropomyosin ratios from multiple cells in the same embryo was considered one sample. Student’s t tests were performed using Prism software or Excel. Analysis of Ens and Phalloidin signal

intensities in embryonic VL myotubes were performed in essentially the same fashion from single slices of confocal stacks.

Time-lapse imaging and analysis

Embryos to be subjected to time-lapse imaging of myonuclear movements were prepared as reported previously [167]. Embryos were bleached for 4 min, rinsed and mounted in halocarbon oil on a custom-made slide with an air-permeable membrane, and covered with a glass coverslip. Time-lapse series of myonuclear movements were acquired on a Zeiss LSM 700 equipped with the ZEN software and using a Plan-Apochromatic 20×/0.8 M27 objective with 1.7× optical zoom. Stacks were acquired every 3 min for 1 h at 25˚C. The line function in ImageJ was used to measure distance between clusters. To calculate Δ nuclear spread, the distance from the dorsal-most nucleus to the ventral-most nucleus in a cell at the beginning of the time-lapse series was subtracted from the same parameter at the end of the series. The difference was then divided by time elapsed to yield Δ nuclear spread, measured in micrometers per hour. Student's t tests and correlation analysis were performed using Prism software. F-tests were performed in Excel.

Embryos to be used for EB1-YFP analysis were prepared and mounted as above. Time-lapse series of EB1-YFP comets in the tips of stage 16 lateral transverse muscles were acquired on a Leica TCS SP8 confocal microscope at 25˚C using the HCX PL APO 63×/1.30 glycerol lens with 40× optical zoom using the Leica proprietary software. Comets were recorded from 19 cells (control) and 26 cells (*Bsg25D*$^{-/-}$). Z-stacks consisted of ~10 slices with a step size of 400 nm; stacks were acquired without intervals (i.e., nonstop) at a frame rate of ~23 frames per second for ~90 s. Time-lapse datasets were deconvolved by a blind deconvolution algorithm in Autoquant X3 software (Media Cybernetics). EB1-YFP comets were manually tracked in three dimensions using Imaris (Bitplane). For each EB1-YFP comet, the displacement distance between its position in the first and last frames of its run was exported and divided by the time elapsed to determine EB1-YFP comet speed. EB1-YFP speed was compared between groups by Student's t test.

Cell culture, coimmunoprecipitation, and Western blotting

For *Drosophila* S2 cell expression studies, pUAS-3xHA::Bsg25D was generated as follows. Full-length *Bsg25D* (LD21844; DGRC) was PCR amplified using the following primers: 5′-CACCATGGAGGTATCCGCGATCCGTAC-3′ and 5′-CTAAGGCATGCCAGGCAG TCCACC-3′. The amplicon was TOPO cloned into pENTR (Life Technologies) and then Gateway cloned using LR Clonase (Life Technologies) into pTHW (DGRC), which contains a UAS followed by an N-terminal 3xHA tag. The generation of pUAS-Ens::EGFP is described above (in Generation of mutant and transgenic *Drosophila* stocks), as the same plasmid was used for transforming flies and driving expression in S2 cells.

Experiments in S2 cells were performed to validate a physical interaction between Ens and Bsg25D detected in a yeast two-hybrid screen previously described [158]. S2 cells were cultured in Schneider's media plus 10% FBS using standard procedures. Protein expression was achieved by transfecting a plasmid expressing Gal4 from a constitutively active promoter (Ubiquitin-Gal4) along with pUAS-3xHA::Bsg25D and pUAS-Ens-EGFP or pUAS-3xHA::Bsg25D and pUAS-2xEGFP. Transfections used Effectene (QIAGEN). Cells were lysed 2 d after transfection in lysis buffer (150 mM NaCl, 2 mM MgOAc, 20 mM Tris, pH 7.5, 5% glycerol, 0.5% NP-40, 2 mM DTT, and one Complete Mini tab [Roche]). Following centrifugation, lysate supernatant was collected and protein concentration was determined by Bradford assay (Bio-Rad). 400 μg lysate was incubated with Protein G-Agarose beads overnight at 4˚C using rabbit anti-GFP (Torrey Pines Biolab) or rabbit anti-IgG (Santa Cruz Biotechnology) for mock immunoprecipitation controls. Following incubation, beads were washed four times with lysis buffer and boiled in 4× Laemmli buffer. Proteins released from beads and 40 μg (10%) inputs were then subjected to SDS-PAGE, transferred overnight to polyvinylidene difluoride membrane, and blotted with rat anti-HA (Roche), secondary stained at 1:5,000 with anti-rat HRP (Jackson ImmunoResearch), and detected with chemiluminescence (Denville Scientific). Membranes were then stripped according to standard practices and reblotted with mouse anti-GFP antibody (Roche) and HRP-conjugated anti-mouse secondary antibody (Jackson ImmunoResearch) and then developed. Coimmunoprecipitation between 3xHA::Bsg25D and Ens-GFP was demonstrated with multiple biological replicates.

To compare Bsg25D protein expression in control and $Bsg25D^{-/-}$ genotypes, w^{1118} and $Bsg25D^{-/-}$ third-instar larvae were dissected in HL3.1 relaxing buffer. The intestines of the larvae were removed, and the resultant pelts were lysed in lysis buffer (recipe above). Following Bradford determination of protein concentration (Bio-Rad), 80 μg lysate per genotype was loaded on a 7.5% SDS-PAGE protein gel. The gel was

transferred to nitrocellulose membrane overnight, blocked with 5% milk (for Bsg25D) or 5% BSA (for GAPDH) in TBS-Tween, and blotted overnight with guinea pig anti-Bsg25D antibody (1:1,000; gift from E. Lecuyer) or mouse anti-GAPDH primary antibody (1:10,000; Abcam). HRP-conjugated secondary antibodies against guinea pig (1:5,000; Jackson ImmunoResearch) or mouse (1:5,000; Jackson ImmunoResearch) were applied before development by chemiluminescence (Kindle Biosciences).

AFM

Larvae were dissected in HL3.1 dissecting buffer and fixed in formalin for 10 min before microscopy. Bright-field images of *Drosophila* larvae, for determination of location of stiffness measurements, were acquired using an inverted microscope (Axio Observer Z1; Zeiss) as the AFM base (LD Plan-Neofluar 20×/0.4 objective). An Asylum Research MFP-3D-BIO Atomic Force Microscope was used to collect force maps from the *Drosophila* larvae tissue. A CP CONT-PS-C (NanoAndMore.com) probe with a 6.1-μm polystyrene bead was used for all measurements. The Asylum Research GetReal calibration method was used for the determination of the spring constant (0.2 N/m). Each force map sampled a 20 × 20-μm to 40 × 40-μm region, depending on muscle width, in a 10 × 10-grid under fluid conditions (PBS). The trigger point was set to 50 nN with an approach velocity of 10 μm/s. The force-indentation curves were fit to the Hertz model for spherical tips using Asylum Research Software to determine the Young's modulus, with an assumed Poisson's ratio value of 0.45 for the sample [285]. For each genotype, at least three larvae were used; from each larva, at least 400 individual measurements, corresponding to four different muscles, were taken. Force maps of stiffness along with individual stiffness values for each measured point were then exported from Asylum Research Software for analysis. For statistics, the average of all the measurements from a single muscle was considered one sample.

Larval motility assays

Laval motility assays were performed essentially as previously described, either by using a charge-coupled device camera and Ethovision software (Noldus) to record third-instar larvae crawling and automatically calculate crawling speed [158] or by placing larvae at the center of an apple juice plate surrounded by zones defined by concentric circles and observing which zone they reached in 30 s of crawling at 25˚C

[286]. A minimum of 47 larvae per genotype were used. In all cases, data were acquired over multiple days. P values were calculated by Student's t test.

RESULTS

Bsg25D and Ens interact *in vitro* and colocalize in embryonic myotubes

We have previously shown that myonuclei in *ens* mutant embryos fail to separate into two clusters and migrate toward muscle poles [158]. To better understand the mechanisms underlying myonuclear positioning, we performed a yeast two-hybrid screen to identify proteins that interact with Ens. In addition to clones of *Khc*, which we have previously shown to genetically and physically interact with Ens [158], we recovered numerous clones corresponding to *Bsg25D*, the *Drosophila* homologue of vertebrate *Ninein* [276,277]. The sequence common to all recovered *Bsg25D* clones (nucleotides 1463–1,577/amino acids 487–526, using isoform Bsg25D-PB as a reference) falls entirely within the gene's fourth exon, which is present in all *Bsg25D* alternatively spliced transcripts; thus, the Ens-binding region is present in all Bsg25D isoforms (Fig. 4.2.1A). This region is found in the first of two spans of Bsg25D that contain numerous coiled coil domains. The Ens-binding region is nonoverlapping with the region of Bsg25D thought to be necessary for γ-Tubulin binding, based on alignment between Bsg25D and mouse Ninein, where the latter region was experimentally defined [274]. The Ens-binding region also does not overlap with the N-terminal Bsg25D region (amino acids 1–353) that has been shown to bind MTs *in vitro* [276]. The Ens–Bsg25D interaction was validated in S2 cells, where overexpressed Ens and full-length Bsg25D coimmunoprecipitated (Fig. 4.2.1A).

Next, we examined *Bsg25D* expression *in vivo*. *In situ* hybridization performed by the Berkeley *Drosophila* Genome Project showed *Bsg25D* transcripts in embryonic muscle [287–289]. By immunofluorescent antibody staining using an existing antibody against Bsg25D [284], we found that Bsg25D protein was present in discrete puncta in numerous cell types in the embryo. (The Bsg25D signal was absent from *Bsg25D* null mutants [Fig. 4.2.9A].) This punctate expression pattern was expected, as Bsg25D is known to localize to centrosomes in mononucleated cells [276,277]. Notably, it was most strongly expressed in primordial germ cells, as has been previously observed ([277]; Fig. 4.2.1B, red outlined box). Combined immunofluorescent labeling of Bsg25D and the muscle marker Tropomyosin showed

that from stage 14 to stage 16, the stages during which myonuclei split into two clusters and migrate toward muscle poles, Bsg25D was broadly but weakly expressed in the cytoplasm and strongly enriched in cytoplasmic puncta of myotubes (Fig. 4.2.1B). Analysis of orthogonal slices of Z-stacks confirmed the presence of Bsg25D puncta inside myotubes (Fig. 4.2.1C). At stage 16, there were between zero and eight Bsg25D puncta per myotube (mode = 1, mean = 2.1). Puncta were excluded from the nucleus but otherwise had no conspicuous localization. Single puncta were also visible in some unfused myoblasts. We used genetic reporters and antibody staining

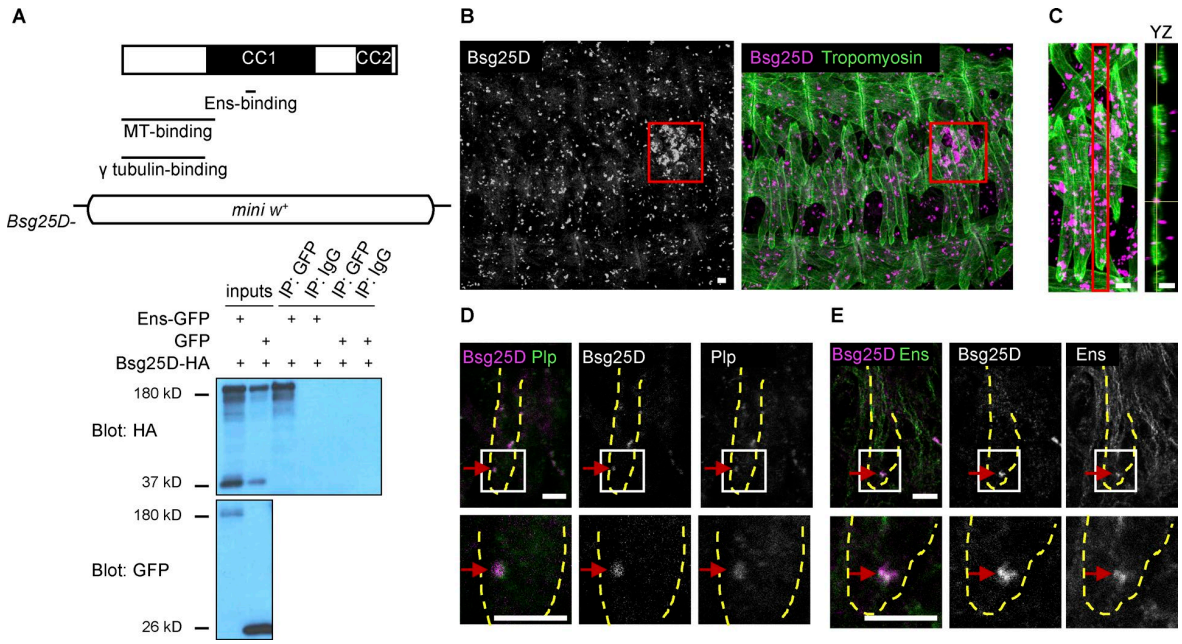


Figure 4.2.1- Bsg25D and Ens physically interact and colocalize in myotubes *in vivo*. **(A)** Top: Map of Bsg25D indicating coiled-coil (CC) domain-rich regions and regions that bind Ens (this work), MTs (Kowanda et al., 2016), and γ-Tubulin (predicted from alignment to mouse Ninein; Delgehyr et al., 2005). In *Bsg25D-*, the entire coding region has been removed and replaced by a mini-white (mini w+) reporter cassette. Bottom: Coimmunoprecipitation of overexpressed Ens-GFP and Bsg25D-HA from S2 cells. The largest Bsg25D-HA band is the main protein species, and smaller bands likely represent cleavage products. IP, immunoprecipitation. **(B)** Bsg25D expression in the stage 16 embryo. Left and right panels are the same image with and without Tropomyosin, a muscle marker. Left: Bsg25D, gray. Right: Bsg25D, magenta; Tropomyosin, green. Red box indicates primordial germ cells. **(C)** Left: Extended focus projection of one stage 16 hemisegment. Right: Orthogonal (YZ) section of indicated (red box) lateral transverse myotube. Crosshairs identify a Bsg25D+ punctum inside myotube. Bsg25D, magenta; Tropomyosin, green. **(D)** Immunofluorescent staining of stage 16 myotube for Bsg25D and Plp. Image is a single slice from a Z-stack. Bsg25D, magenta; Plp, green; colocalization, white (see red arrows). **(E)** Immunofluorescent staining of stage 16 myotube for Bsg25D and Ens. Image is a single slice from a Z-stack. In the merged image, Bsg25D, magenta; Ens, green; colocalization, white (highlighted by arrows). In D and E, images in bottom row are higher magnification views of boxed regions, and dashed lines outline lateral transverse muscles. In all images, scale bars = 5 μm.

to determine whether the Bsg25D puncta in myotubes reside in various organelles and subcellular structures. We did not observe Bsg25D colocalization with markers of Golgi apparatus, ER, or endosomes, though we did observe that 95% of Bsg25D puncta were in proximity to Arl8 (n = 60 myotube puncta), a protein that localizes to lysosomes ([290,291], 2006; Fig. 4.2.9B). Counter to our expectations [269,270,276,277], we also failed to detect colocalization between Bsg25D puncta and the MTOC component γ-Tubulin or the MT component α-Tubulin (Fig. 4.2.9B). Interestingly, however, all myotube Bsg25D puncta (n = 59) colocalized with the MTOC component Pericentrin-like protein (Plp), the sole *Drosophila* Pericentrin orthologue (Figs. 4.2.1D and 4.2.9C). This finding is consistent with physical interactions observed between their mammalian orthologues in cell culture [292].

Since we found that Bsg25D and Ens physically interact *in vitro*, we performed immunofluorescent antibody staining to determine whether they colocalize in embryonic myotubes. While the bulk of Ens protein localized to MTs, as expected for a MAP (Fig. 4.2.9D), there was also Ens protein present in Bsg25D puncta; thus, Ens and Bsg25D colocalize in cytoplasmic puncta in embryonic myotubes (Fig. 4.2.1E). Outside of these puncta, the broad, diffuse cytoplasmic Bsg25D signal was difficult to resolve, so it is possible that Bsg25D and Ens are both present in other parts of the cell as well. Since Bsg25D and Ens bind *in vitro* and colocalize in myotubes, we hypothesized that *Bsg25D* functions with *ens* during myonuclear positioning.

Loss of Bsg25D enhances ens myonuclear positioning defects

To determine whether Bsg25D functions in myonuclear positioning, we generated a null *Bsg25D* mutant. We used an accelerated homologous recombination approach [280] to remove the entire *Bsg25D* locus, including all predicted alternatively spliced transcripts (Fig. 4.2.1A and Materials and methods). Western blotting showed Bsg25D protein was absent from larval lysates (Fig. 4.2.2A and Materials and methods).

In agreement with recent reports [276,277], we found that *Bsg25D* homozygous null mutants (*Bsg2*5D$^{-/-}$) lacking maternal and zygotic *Bsg25D* were viable and fertile, with a modest decrease in the frequency of survival to adulthood relative to wild-type controls (70% vs. 96%; Fig. 4.2.10A). A standard larval motility assay revealed moderately impaired muscle function (Fig. 4.2.10B). Using a transgenic reporter that labels myonuclei in a specific set of muscles (i.e., the lateral transverse muscles; Richardson et al., 2007), we found that myonuclear positioning in stage 16

Bsg25D$^{-/-}$ myotubes was normal (Fig. 4.2.2B). Thus, Bsg25D is not essential for viability, fertility, or myonuclear positioning.

We next considered the possibility that *Bsg25D* plays a role in myonuclear positioning but that the pathway it affects is robust enough to withstand the loss of *Bsg25D* if the other components are present at wild-type levels. To investigate this possibility, we generated double mutants in which *Bsg25D* and candidate interactor genes were targeted. We found that *ens*$^{-/+}$ embryos lacking all maternal and zygotic *Bsg25D* had significantly more impaired myonuclear positioning than *ens*$^{-/+}$ embryos containing the normal complement of Bsg25D (Fig. 4.2.2,B–D): at stage 16, *Bsg25D*$^{-/-}$ *; ens*$^{-/+}$ myonuclear clusters traversed less of the distance toward the muscle poles. Further, in some myotubes, myonuclei are present as one cluster, resembling those found in *ens*$^{-/-}$ homozygotes [158]. Enhancement of myonuclear positioning defects was also observed when one copy of the null *Bsg25D* allele was replaced by a deficiency removing the gene (Fig. 4.2.2B–D), which argues that the enhancement effect was specific to the *Bsg25D* region. Moreover, we rescued the *Bsg25D*$^{-/-}$*;ens*$^{-/+}$ enhanced phenotype by reintroducing *Bsg25D*$^{+}$ from the large genomic Bacterial Artificial Chromosome (BAC) insertion CH321-49G22 (Fig. 4.2.2B–D). In addition, *Bsg25D*$^{-/-}$*;ens*$^{-/-}$ double mutants showed the *ens*$^{-/-}$ phenotype, which is the most severe clustering phenotype (Fig. 4.2.11A). We conclude that endogenous *Bsg25D* and *ens* likely affect a common pathway that moves myonuclei in embryonic myotubes.

Bsg25D and *ens* genetically interact in nonmuscle cells as well, as embryonic lethality occurred when Bsg25D and Ens were jointly removed in a specific genetic combination. Nearly 100% of embryos derived from *Bsg25D*$^{-/-}$*;ens*$^{-}$*/TM6* mothers and *Bsg25D*$^{-/-}$ fathers failed to hatch (Fig. 4.2.2E). However, embryos derived from the reciprocal cross survived well (Fig. 4.2.2E). *Bsg25D*$^{-/-}$*;ens*$^{-}$*/TM6* females crossed with wild-type males laid eggs that hatched, demonstrating that those females are fertile. We also observed widespread death when the third chromosome balancer *TM6* was replaced by a wild-type chromosome, indicating that the genetic interaction was not due to mutations on the balancer chromosome. The phenotype also persisted when one of the *Bsg25D* alleles was replaced with a deficiency completely uncovering *Bsg25D*. Furthermore, restoring *Bsg25D*$^{+}$ through a BAC transgene achieved nearly complete rescue (Fig. 4.2.2E, compare black and salmon-colored lines in graph). We conclude that *Bsg25D* and *ens* are jointly required to support normal embryonic

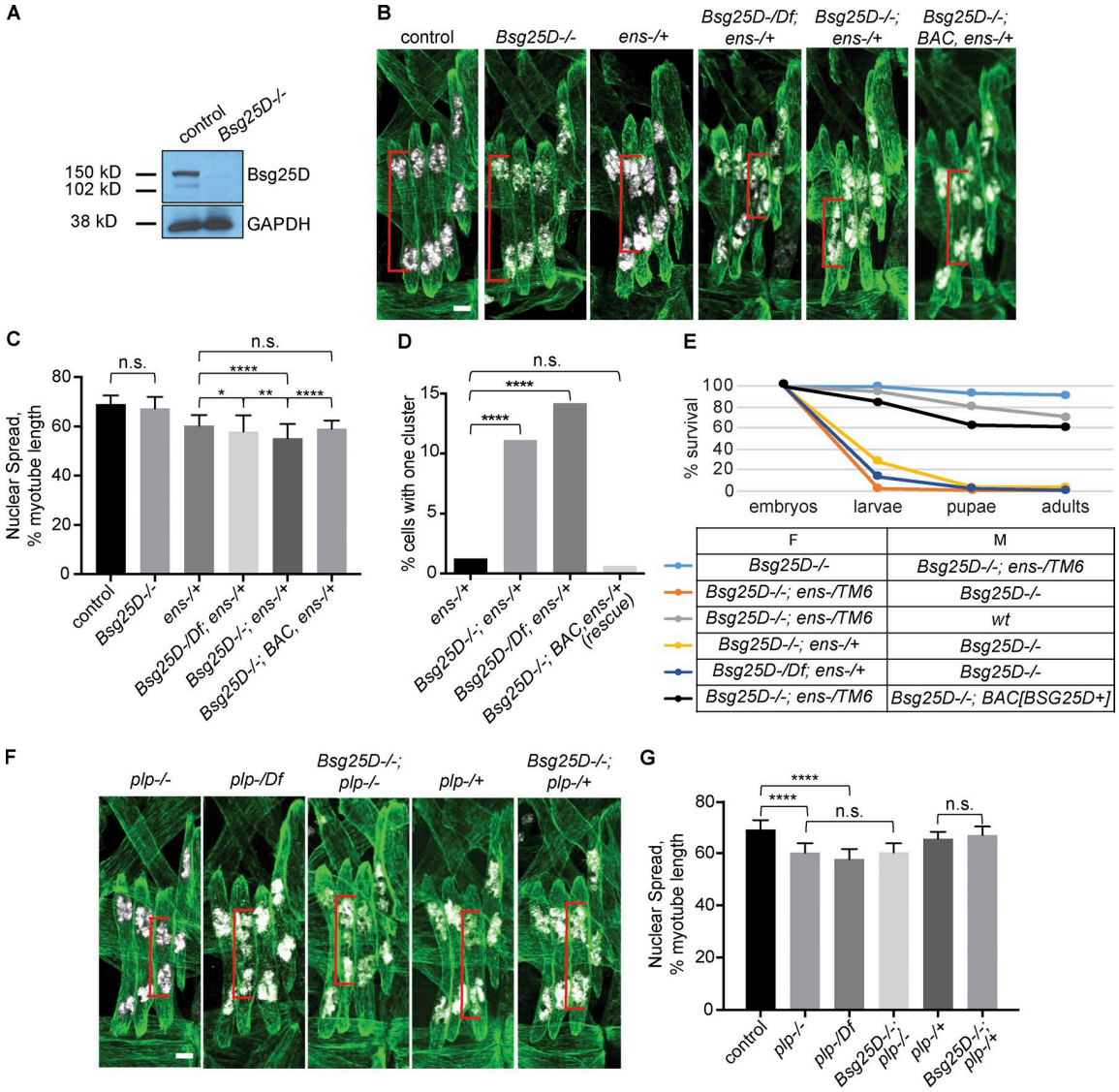


Figure 4.2.2 – *Bsg25D* genetically interacts with *ens*, but not *plp*. **(A)** Western blot showing loss of Bsg25D protein in *Bsg25D*$^{-/-}$ larval lysates. **(B)** Extended-focus projections of representative stage 16 hemisegments from indicated genotypes. **(C)** Bar graph showing mean nuclear spread and SD. For each genotype, *n* (number of hemisegments) is control, *n* = 39; *Bsg25D*$^{-/-}$, *n* = 61; *ens*$^{-/+}$, *n* = 46; *Bsg25D*$^{-}$*/Df;ens*$^{-/+}$, *n* = 43; *Bsg25D;ens*$^{-/+}$, *n* = 71; *Bsg25D*$^{-/-}$*;BAC, ens*$^{-/+}$, *n* = 44. P values were calculated by Student's t test. **(D)** Graph showing the percentage of myotubes that have a single nuclear cluster. P values were calculated by Fisher's exact test from contingency tables comparing *ens*$^{-/+}$ to each other genotype. *n* values (number of myotubes for each genotype) are *ens*$^{-/+}$, 239; *Bsg25D*$^{-/-}$*;ens*$^{-/+}$, 296; *Bsg25D*$^{-}$*/Df;ens*$^{-/+}$, 176; *Bsg25D*$^{-/-}$*;BAC, ens*$^{-/+}$ (rescue), 160. **(E)** Viability graph showing survival during development for individuals derived from indicated crosses. The following number of individuals were included for each genotype: *Bsg25D*$^{-/-}$×*Bsg25D*$^{-/-}$;ens^{-}/TM6, 140; *Bsg25D*$^{-/-}$*;ens*$^{-}$*/TM6*×*Bsg25D*$^{-/-}$, 153; *Bsg25D*$^{-/-}$*;ens*$^{-}$*/TM6*×wt, 140; *Bsg25D*$^{-/-}$*;ens*$^{-/+}$×*Bsg25D*$^{-/-}$, 113; *Bsg25D*$^{-}$*/Df;ens*$^{-/+}$×*Bsg25D*$^{-/-}$, 148; *Bsg25D*$^{-/-}$*;ens*$^{-}$*/TM6*×*Bsg25D-/-;BAC[Bsg25D+]*, 144. F, female; M, male. **(F)** Extended-focus projections of representative stage 16 hemisegments from indicated genotypes. **(G)** Bar graph showing mean nuclear spread and SD. For each genotype, number of hemisegments is *plp*$^{-/-}$, *n* = 47; *plp*$^{-}$*/Df*, *n* = 24; Bsg25D$^{-/-}$; plp$^{-/-}$, *n* = 39; plp$^{-/+}$, *n* = 34; *Bsg25D*$^{-/-}$*;plp*$^{-/+}$, *n* = 29. P values were calculated by Student's t test. The control data in G are the same as in C; for representative image, see first panel in B. *, P < 0.05; **, P < 0.01; ****, P < 0.0001. In all confocal images, red brackets indicate sample nuclear spread measurements. Tropomyosin, green; nuclei, white. Scale bars = 5 μm.

defects survive embryonic development [158], the observed lethality must be due to issues in nonmuscle cells.

To gain further insights to the role of *Bsg25D*, we tested for genetic interactions between *Bsg25D* and other genes involved in myonuclear positioning or MT biology. We did not detect interactions between *Bsg25D* and the genes encoding *Khc* and *Dhc* (which are essential for myonuclear positioning) or *patronin* and the γ-Tubulin homologue *γTub23C* (which interact with *Ninein/noca-1* in *C. elegans* [275]; Fig. 4.2.11B,C; and data not shown). We also tested *pericentrin-like protein* (*plp*) mutants. Interestingly, $plp^{-/-}$ mutants had myonuclear positioning defects; nuclear clusters usually split correctly but failed to move the normal distance toward the muscle poles by stage 16 (Fig. 4.2.2F,G). The same phenotype was observed when one allele of plp was replaced by a deficiency uncovering the gene (Fig. 4.2.2F,G). However, loss of *Bsg25D* did not further enhance myonuclear positioning defects in either *plp* homozygotes or heterozygotes (Fig. 4.2.2F,G); thus, although we observed colocalization between the two proteins in myotubes, we did not uncover a role for Bsg25D–Plp interactions in myonuclear positioning. Taken together, these results reveal dosage-sensitive genetic interactions only between *Bsg25D* and *ens*; these are not observed with other genes involved in MT biology or myonuclear positioning.

Muscle-specific overexpression of Bsg25D causes defects in embryonic myonuclear positioning by sequestering Ens

Having demonstrated that *Bsg25D* functions in myonuclear positioning, we next performed gain-of-function analysis with the Gal4/upstream activating sequence (UAS) system [218] using the muscle-specific *Dmef2* promoter to probe the activity of *Bsg25D* in muscle. Strikingly, in stage 16 myotubes overexpressing *Bsg25D*, myonuclei were present in a single cluster near the myotube center; in contrast, control myotubes at this stage had two nuclear clusters near opposite muscle poles (Fig. 4.2.3A). This suggests that overexpressed *Bsg25D* blocked myonuclear cluster separation (stage 14) and movement toward the muscle poles (stages 15 and 16).

That *Bsg25D* overexpression phenocopied loss of *ens* (Fig. 4.2.3A; [158]) led us to hypothesize that overexpressed Bsg25D inhibits or sequesters endogenous Ens

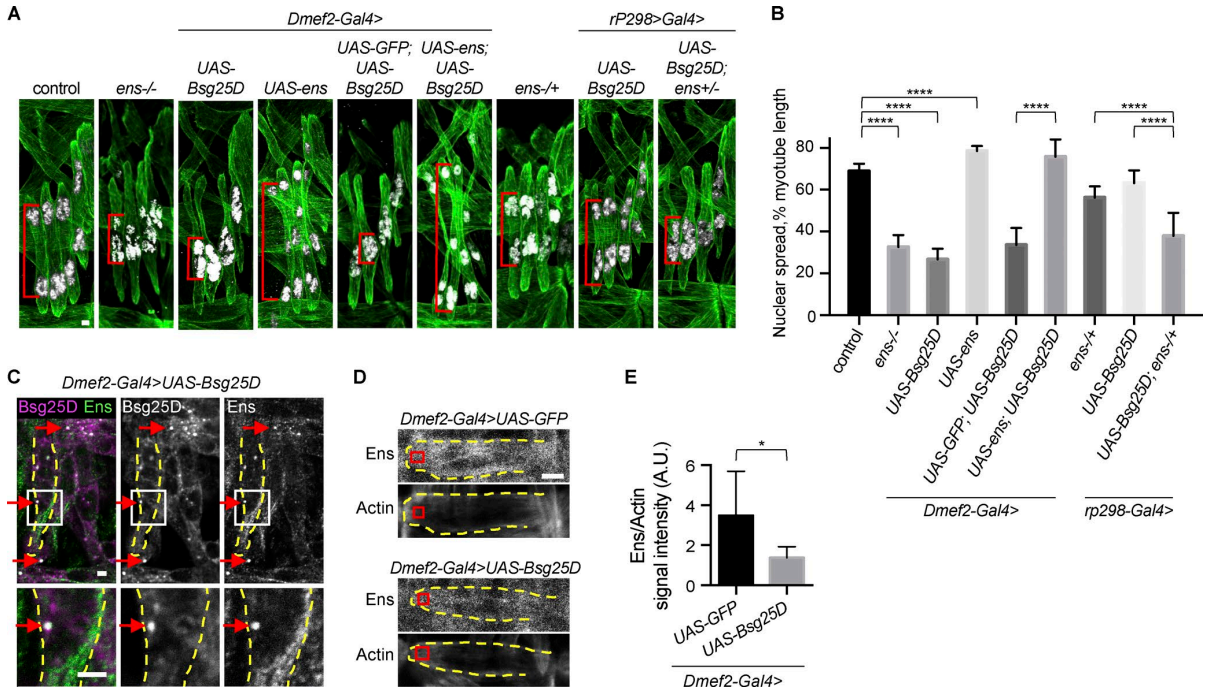


Figure 4.2.3 – Overexpressed *Bsg25D* causes nuclear positioning defects in embryonic myotubes by sequestering endogenous Ens. (A) Extended-focus projections of representative stage 16 hemisegments from indicated genotypes. Green, Tropomyosin; white, nuclei. Red brackets indicate sample nuclear spread measurements. **(B)** Bar graph showing mean nuclear spread and SD. For each genotype, the number of hemisegments is as follows: control, *n* = 22; *Dmef2-Gal4>UAS-Bsg25D*, *n* = 34; *Dmef2-Gal4>UAS-ens*, *n* = 47; *Dmef2-Gal4>UAS-GFP:UAS-Bsg25D*, *n* = 25; *Dmef2-Gal4>UAS-ens;UAS-Bsg25D*, *n* = 42; *ens*$^{-/+}$, *n* = 37; *rP298-Gal4>UAS-Bsg25D*, *n* = 33; *rP298-Gal4>UAS-Bsg25D;ens*$^{-/+}$, *n* = 37. Control data and the representative image are the same as in Fig. 2. ****, P < 0.0001. **(C)** Immunofluorescent antibody staining for Bsg25D and Ens in an embryo overexpressing Bsg25D. Arrows show examples of colocalization. Dashed yellow lines outline a lateral transverse myotube. In the merged image: magenta, Bsg25D; green, Ens; white, colocalization. Images in the bottom row are higher magnification views of boxed regions. **(D)** Representative images of stage 16 VL1 myotubes from indicated genotypes. Each image is a single slice from a confocal stack. Red boxes show where the signal intensity was quantified. **(E)** Graph showing Ens intensity, normalized to actin intensity. Number of myotubes is six for both genotypes, mean ± SD. *, P < 0.05. Scale bars = 2 μm (A and C) and 5 μm (D).

in myotubes. In support of this hypothesis, we found that Ens overexpression, but not overexpression of a control protein (GFP), could rescue Bsg25D-induced nuclear positioning defects. In fact, embryos overexpressing Bsg25D and Ens had even greater nuclear spread than control embryos (Fig. 4.2.3A,B). This finding led us to examine the effects of overexpressing Ens in otherwise wild-type embryos. We found that overexpressed Ens caused novel myonuclear positioning defects; nuclear spread was increased and nuclei were often present as individuals rather than as part of clusters (Fig. 4.2.3A,B). In sum, Ens overexpression and Bsg25D overexpression

confer reciprocal phenotypes, and Ens overexpression is epistatic to Bsg25D overexpression.

As further support of our hypothesis that overexpressed Bsg25D inhibits or sequesters endogenous Ens, we detected genetic interactions between overexpressed *Bsg25D* and endogenous *ens*. Both loss of one allele of *ens* and overexpression of *Bsg25D* with *rP298-Gal4*, a muscle-specific driver that produces a lower level of gene expression than *Dmef2-Gal4*, conferred reduced poleward movement of nuclear clusters (Fig. 4.2.3A,B). However, in $ens^{-/+}$ embryos expressing *rP298>Bsg25D*, a much stronger nuclear positioning phenotype occurred (Fig. 4.2.3A,B). This implies that Bsg25D affects the same pathway as loss of *ens*.

Finally, in support of our hypothesis, we found that overexpressed Bsg25D alters Ens localization. Like endogenous Bsg25D, overexpressed Bsg25D was present both broadly in the cytoplasm and in bright cytoplasmic puncta (Fig. 4.2.3C). Ens normally localizes to MTs (Fig. 4.2.9D), but in Bsg25D-overexpressing myotubes, Ens was strongly enriched at sites of Bsg25D accumulation in the cytoplasm (Fig. 4.2.3C). Outside of $Bsg25D^{+}$ puncta, Ens signal was lower in myotubes overexpressing Bsg25D than in controls overexpressing GFP (Fig. 4.2.3D,E). This argues that overexpression of Bsg25D reduces the amount of Ens on myotubes. Based on our genetic and imaging analyses, we conclude that overexpressed Bsg25D exerts its effect on myonuclear positioning by regulating Ens activity, at least in part by mislocalizing Ens.

Bsg25D and Ens levels regulate the dynamics of myonuclear positioning

We hypothesized that modulating Bsg25D and Ens levels affects nuclear positioning at stage 16 by disrupting the normal dynamics of myonuclear movement during stage 15, when nuclear clusters normally move toward muscle poles. To address this hypothesis, we performed time-lapse microscopy during stage 15, as done previously ([167]; Videos 1, 2, 3, 4, and 5). We measured the distance from the dorsal-most nucleus to the ventral-most nucleus (nuclear spread) at the beginning and end of the time-lapse series. We divided the difference between the final and initial nuclear spreads for each cell by the time elapsed and defined this quotient as Δ nuclear spread (Fig. 4.2.4A).

We observed that only 59% of control myotubes exhibited positive Δ nuclear spread over a 1-h period during stage 15. This was initially surprising, because we have previously seen that from stages 14 to 16, nuclear clusters move toward

myotube poles [158,167]. Our interpretation is that nuclear clusters move toward the muscle poles unevenly, with periods where the nuclear spread increases and periods where it decreases. Nuclear clusters all eventually arrive near the muscle poles because the net positive (poleward) movement is greater than negative (toward the center of the muscle) movement; however, during relatively short time-lapse recordings, the nuclear spread in individual cells can decrease quite dramatically.

The percentage of myotubes exhibiting positive versus negative Δ nuclear

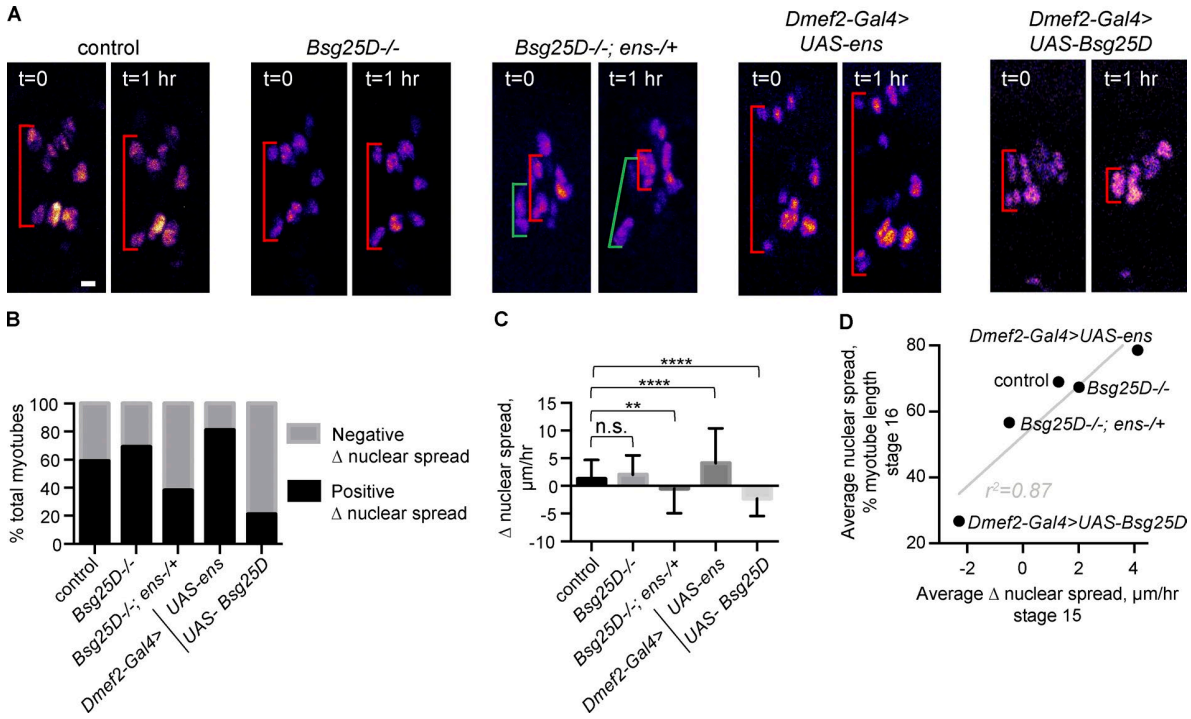


Figure 4.2.4 – Dynamics of myonuclear cluster separation are affected by levels of Bsg25D and Ens. (A) First and last frames from time-lapse series of myo- nuclear movement during stage 15 in indicated genotypes. Red brackets show change in nuclear spread over time. In *Bsg25D$^{-/-}$;ens$^{-/+}$* images, green and red brackets show adjacent myotubes undergoing opposite Δ nuclear spreads. All images are extended focus projections of Z-stacks. Nuclei are multicolored. Scale bar = 5 µm. **(B)** Graph showing percentages of myotubes undergoing positive versus negative Δ nuclear spread during stage 15. **(C)** Mean and SD of Δ nuclear spread during stage 15. For each genotype in B and C, the number of myotubes is as follows: control, *n* = 112; *Bsg25D$^{-/-}$*, *n* = 72; *Bsg25D$^{-/-}$;ens$^{-/+}$*, *n* = 86; *Dmef2- Gal4>UAS-ens*, *n* = 85; *Dmef2-Gal4>UAS-Bsg25D*, *n* = 62. P values were calculated by Student's t test. **, P < 0.01; ****, P < 0.0001. **(D)** Correlation between stage 15 mean Δ nuclear spread and stage 16 mean nuclear spread in fixed samples. Linear regression line is in gray; r^2 is the coefficient of determination.

spread varied with genotype (Fig. 4.2.4B). Embryos with muscle-specific Ens overexpression contained the highest percentage of myotubes with positive Δ nuclear spread (81%) and embryos with muscle-specific Bsg25D overexpression the lowest (21%). In Bsg25D-overexpressing embryos at stage 15, myonuclei were either present

in a single cluster or two slightly separated clusters. Negative Δ nuclear spread was due to loosely packed single clusters compacting or barely separated clusters coming back together (for example, Fig. 4.2.4A). Bsg25D-overexpressing cells exhibiting positive Δ nuclear spread had single nuclear clusters that appeared to separate slightly without dividing into two distinct clusters.

We detected a novel behavior in myonuclei from *Bsg25D*$^{-/-}$;*ens*$^{-/+}$ embryos. In some cells, two distinct nuclear clusters migrated a considerable distance toward each other and reformed one cluster. In this genotype, there was high variability in dynamic cluster behavior among myotubes; the SD of Δ nuclear spread was greater in *Bsg25D*$^{-/-}$;*ens*$^{-/+}$ cells than in controls (4.47 μm/h vs. 3.42 μm/h, P = 0.008; Fig. 4.2.4A).

For each genotype, we averaged Δ nuclear spread for each cell, including both negative and positive values (Fig. 4.2.4C). We found no statistically significant difference between control and *Bsg25D*$^{-/-}$ mutants. Control, *Bsg25D*$^{-/-}$, and Ens-overexpressing cells had a positive average Δ nuclear spread. *Bsg25D*$^{-/-}$;*ens*$^{-/+}$ and Bsg25D-overexpressing cells had a negative average Δ nuclear spread. Across genotypes, there was a strong correlation (r = 0.94) between average Δ nuclear spread at stage 15 and average nuclear spread in fixed embryos at stage 16 (Fig. 4.2.4D). Thus, the rate of nuclear spreading at stage 15 predicts and likely determines the degree of nuclear spread observed at stage 16.

Bsg25D overexpression causes defects in myonuclear positioning in fully differentiated larval muscle that are rescued by addition of Ens

Having characterized the effect of Bsg25D overexpression on embryonic myotubes, we next investigated Bsg25D overexpression in mature myofibers. Myofibers are established in the embryo at stage 17 and continue to grow and function during larval stages. We focused on the third-instar larval stage, a time point when the muscles are amenable to functional analysis and antibody staining [167]. Using the *Dmef2-Gal4* driver, which becomes active in embryonic muscle and persists through the larval stage, we overexpressed either Bsg25D or GFP (as a control) and measured larval motility as a readout of muscle function. Control larvae outperformed Bsg25D-overexpressing larvae (Fig. 4.2.5A), indicating that Bsg25D overexpression perturbs muscle function. Animals with muscle-specific overexpression of Bsg25D exhibited decreased survival to adulthood, with peak lethality occurring during the pupal stage

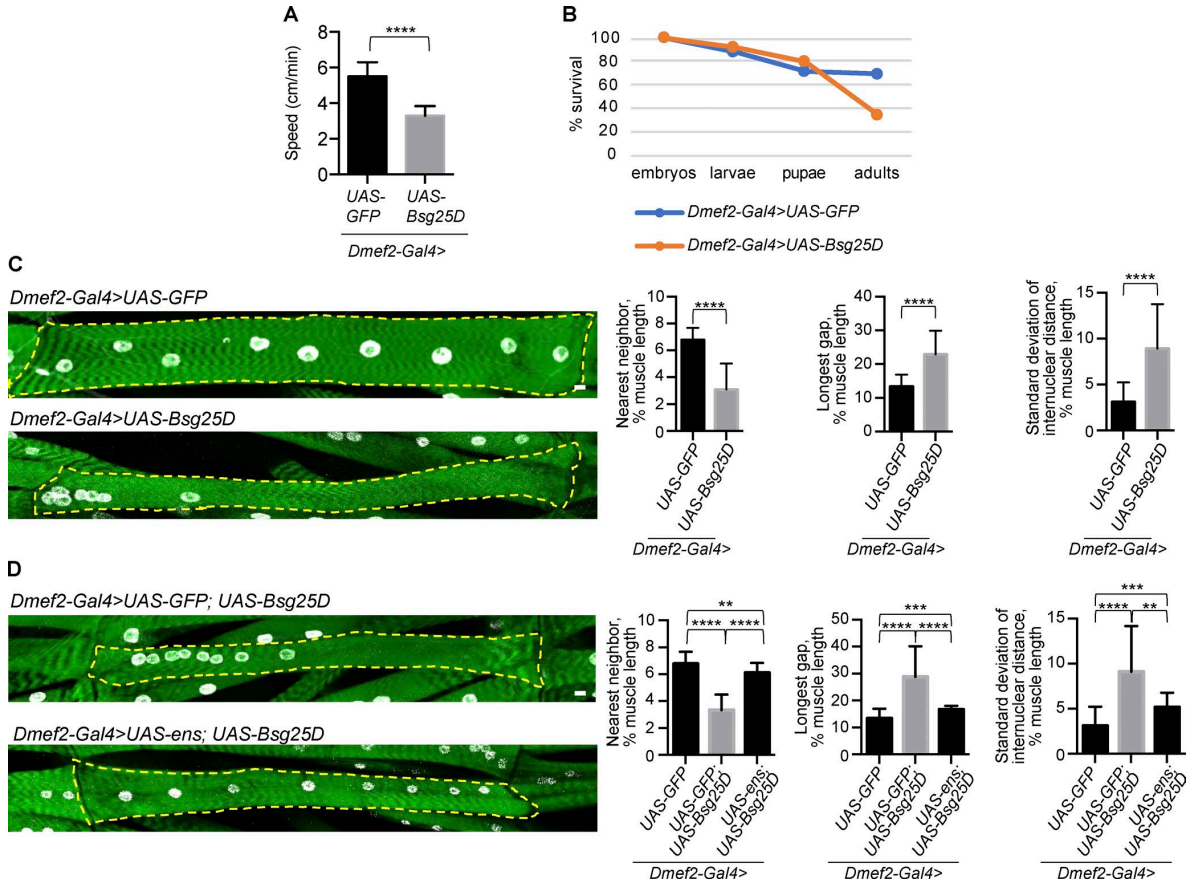


Figure 4.2.5 – Bsg25D overexpression induces nuclear positioning defects in larval myofibers that can be rescued by Ens. (A) Larval motility in larvae overexpressing either GFP (control) or Bsg25D in muscle. For *Dmef2-Gal4>UAS-GFP*, *n* = 30 larvae. For *Dmef2-Gal4>UAS-Bsg25D*, *n* = 12 larvae. P values were calculated by Student's t test. **(B)** Viability graph showing survival during development. *n* = 100 individuals for each genotype. **(C and D)** Representative extended focus projections of stained myofibers and nuclear positioning analyses. Green, phalloidin; white, nuclei. Dashed yellow line outlines individual myofibers. Scale bars = 10 μm. Graphs depict mean and SD for three methods for quantifying myonuclear positioning (see Materials and methods). For each genotype, the same images were analyzed with each method. For *Dmef2-Gal4>UAS-GFP*, *n* = 40 myofibers. For *Dmef2-Gal4>UAS-Bsg25D*, *n* = 45. For *Dmef2- Gal4>UAS-GFP;UAS-Bsg25D*, *n* = 23; *Dmef2-Gal4>UAS-ens;UAS-Bsg25D*, *n* = 19. *Dmef2-Gal4>UAS-GFP* data are the same in C and D. P values were calculated by Student's t test. **, P < 0.01; ***, P < 0.001; ****, P < 0.0001.

(Fig. 4.2.5B). Moreover, adult survivors were unable to fly, indicating that overexpressed Bsg25D also perturbs muscle function in adults (data not shown).

After assessing muscle function in Bsg25D-overexpressing larvae, we examined muscle structure. In control larvae with muscle-specific GFP expression, myonuclei were evenly spaced throughout muscle fibers, as expected (Fig. 4.2.5C). In larvae that had developed with sustained muscle-specific Bsg25D overexpression, however, myonuclei were frequently clustered together (Fig. 4.2.5C). This phenotype was highly penetrant and robustly quantifiable by three different analyses. First, the

average distance between each nucleus and its nearest neighbor was decreased. Second, the average longest stretch of myofiber devoid of myonuclei was increased. Third, the average SD of the distances between sequential nuclei (SD of internuclear distance) within a myofiber was increased, indicating irregular, uneven positioning of nuclei (Fig. 4.2.5C). Unlike stage 16 myotubes, where Bsg25D-induced myonuclear positioning defects were nearly uniform (i.e., one cluster of myonuclei near the myotube's center), larval muscle fibers overexpressing Bsg25D exhibited nuclear clusters that varied in both nuclear number and position within the fiber (Figs. 4.2.5C and S4 A). The total number of nuclei present per larval muscle was the same in Bsg25D-overexpressing and control larvae (Fig. 4.2.12B). As with other genotypes affecting myonuclear positioning [172], Bsg25D overexpression conferred a decrease in nuclear size (Fig. 4.2.12C).

Since Ens overexpression restored nuclear spread in Bsg25D-overexpressing embryonic myotubes (Fig. 4.2.3A,B), we hypothesized that "rescued" myotubes would develop into myofibers with normal myonuclear positioning. Indeed, when we overexpressed Ens along with Bsg25D starting in embryonic myotubes, the resulting larval myofibers had nearly normal nuclear positioning; in contrast, control myofibers expressing GFP with Bsg25D had severe nuclear positioning defects (Fig. 4.2.5D). These two genotypes had the same number of myonuclei per myofiber (Fig. 4.2.12D). From these experiments, we conclude that sustained Ens overexpression rescues nuclear positioning defects in Bsg25D-overexpressing mature muscles.

Overexpressed Bsg25D disrupts MT organization in myofibers

Since Bsg25D and Ens have been shown to regulate MT organization in other contexts [266,270,274,276,277,293], we hypothesized that Bsg25D–Ens interactions control myonuclear positioning by regulating the muscle MT network. However, we did not observe a difference in the density of the MT network in embryonic myotubes among control, *Bsg25D*$^{-/-}$, *Bsg25D*$^{-/-}$*;ens*$^{-/+}$, and *Bsg25D*-overexpressing genotypes (Fig. 4.2.6 A,B). Using time-lapse microscopy to follow genetically encoded EB1-YFP, a fluorescently tagged MT plus end–binding protein that tracks the growing ends of MTs, we observed that EB1-YFP "comets" moved with the same speed in control and *Bsg25D*$^{-/-}$ myotubes (control: 0.36 ± 0.12 μm/s, *Bsg25D*$^{-/-}$: 0.37 ± 0.11 μm/s; Videos 6 and 7 and Fig. 4.2.6C,D), indicating that MT polymerization rates were unaffected by complete loss of *Bsg25D*.

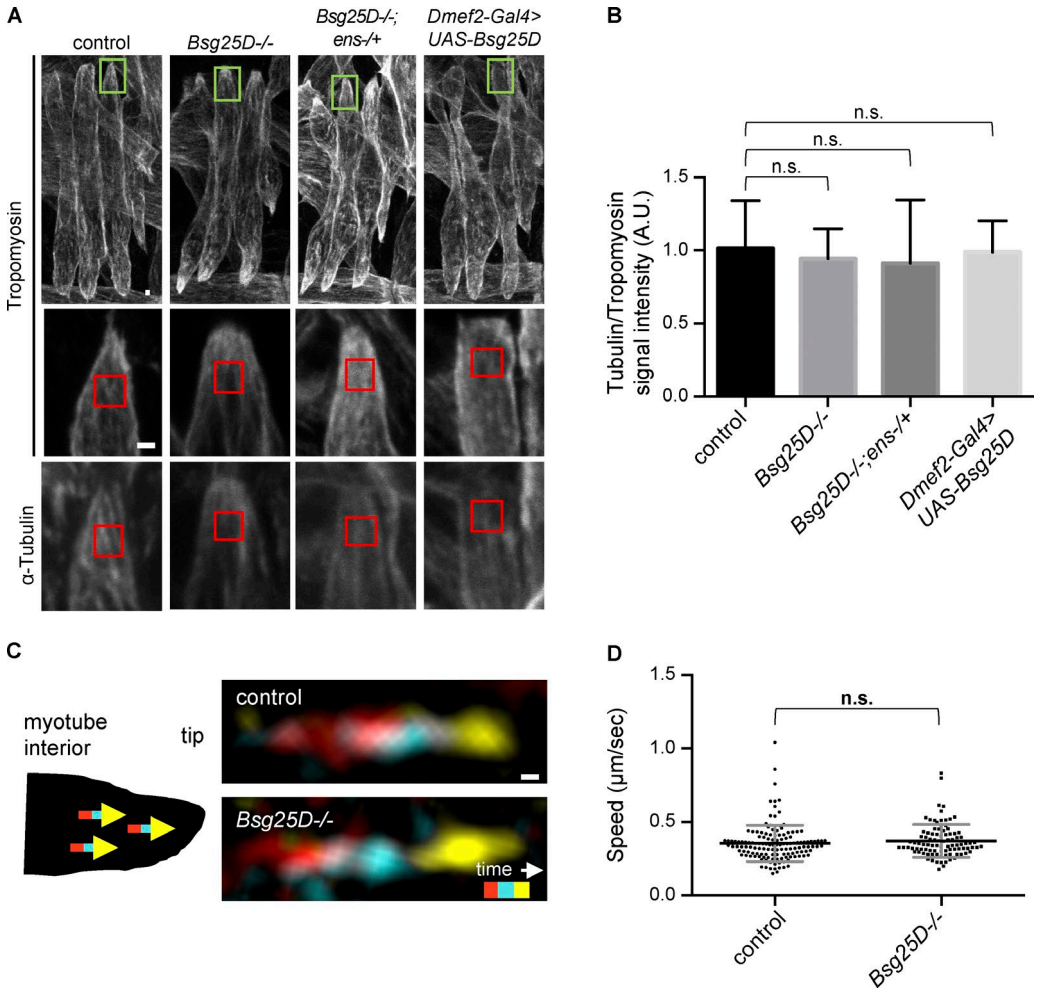


Figure 4.2.6 – MT density and dynamics are normal in *Bsg25D*$^{-/-}$ embryonic myotubes. **(A)** Representative extended-focus projections of Tropomyosin and α-Tubulin signal in stage 16 lateral transverse myotubes. Green boxes in the top row indicate muscle tips magnified in the second and third rows. Red boxes represent regions where signal intensity was quantified. Scale bar = 1 μm. **(B)** Bar graph showing the mean and SD of the ratio of Tubulin to Tropomyosin signal for indicated genotypes. The number of embryos for each genotype is as follows: control, *n* = 9; *Bsg25D*$^{-/-}$, *n* = 14; *Bsg25D*$^{-/-}$*;ens*$^{-/+}$, *n* = 11; *Dmef2-Gal4>UAS-Bsg25D*, *n* = 14. P values were calculated by Student's t test. The entire experiment was performed twice with similar results; images and graph are from one replicate. **(C)** Representative EB1-YFP comets for indicated genotypes. Schematic shows that comets run toward myotube tips. Images were generated by merging three frames from a time-lapse series, pseudocolored red (t1 = 0 s), cyan (t2 = 1.6 s), and yellow (t3 = 3.2 s). Scale bar = 0.1 μm. **(D)** Scatter plot showing mean speed ± SD (micrometers per second) of EB1-YFP comets. The number of EB1-YFP comets for each genotype is as follows: control, *n* = 140; *Bsg25D*$^{-/-}$, *n* = 94. P value was calculated by Student's t test.

Next, we examined the effect of Bsg25D levels on the mature MT organization of larval myofibers. Larval myofibers are advantageous for genetic analysis of MT organization because they are larger, more regularly shaped, and possess a more clearly organized MT network than myotubes. In control muscle fibers, as previously observed [158,172], there were two spatially defined populations of MTs: superficial

MTs that emanate from the nuclear envelope of each nucleus, and deeper MTs oriented parallel to the long axis of the fiber. While *Bsg25D* null mutants had normal myonuclear positioning (Fig. 4.2.12E,F) and MT organization (Fig. 4.2.7A), Bsg25D-overexpressing muscle fibers had severe defects in MT organization (Fig. 4.2.7A). Longitudinal MTs were present, but nuclear MT arrays were completely absent. Instead, MTs appeared to grow from Bsg25D-positive ectopic MTOCs in the cytoplasm, as determined by the colocalization of Bsg25D with the centers of star-shaped MT asters (Fig. 4.2.7B). Overexpressed Bsg25D also localized inside myonuclei (Fig. 4.2.7F), as has been seen with overexpressed human Ninein in cell culture. This cell culture localization was linked to posttranslational SUMO modification of Ninein [294], and we observed colocalization of the sole *Drosophila* SUMO protein, SUMO-2, and overexpressed Bsg25D in myonuclei, but not in Bsg25D-positive cytoplasmic puncta (Fig. 4.2.13). This is consistent with overexpressed nuclear Bsg25D being sumoylated and raises the possibility that sumoylation is necessary for overexpressed Bsg25D to localize to myonuclei.

Since we have shown that Bsg25D overexpression affects Ens localization in embryonic myotubes (Fig. 4.2.3C), we next determined how it affects Ens localization in mature myofibers. Immunofluorescent staining in control myofibers showed Ens broadly expressed with increased signal around myonuclei, consistent with Ens (a MAP) being present on MTs (Fig. 4.2.7C). This localization was not affected by loss of Bsg25D (Fig. 4.2.7C). However, in myofibers overexpressing Bsg25D, Ens was lost from nuclear peripheries and instead colocalized with Bsg25D puncta in the cytoplasm (Fig. 4.2.7C,D). However, Ens did not label the MTs emanating from Bsg25D puncta (Fig. 4.2.7B vs. D). Thus, when Bsg25D is overexpressed, Ens becomes mislocalized from MTs to cytoplasmic Bsg25D puncta.

To further investigate the Bsg25D-induced disruptions to the MT network in larval myofibers, we performed immunofluorescent antibody staining to detect MTs bearing an acetylation modification associated with MT stability. Control muscles exhibited acetylated MTs emanating from the nuclear envelope, as well as in the deeper longitudinal tracts (Fig. 4.2.7E). In Bsg25D-overexpressing myofibers, the antibody against acetylated MTs only weakly labeled longitudinal MTs (Fig. 4.2.7E). This indicates the longitudinal MTs in Bsg25D-overexpressing muscles were hypoacetylated relative to controls. (There was no acetylated tubulin signal around myonuclei, because there were no MTs there.) It was recently shown that MT acetylation in neuronal branches correlates with the subcellular localization of Ens [295], raising the possibility that overexpressed Bsg25D causes MT hypoacetylation

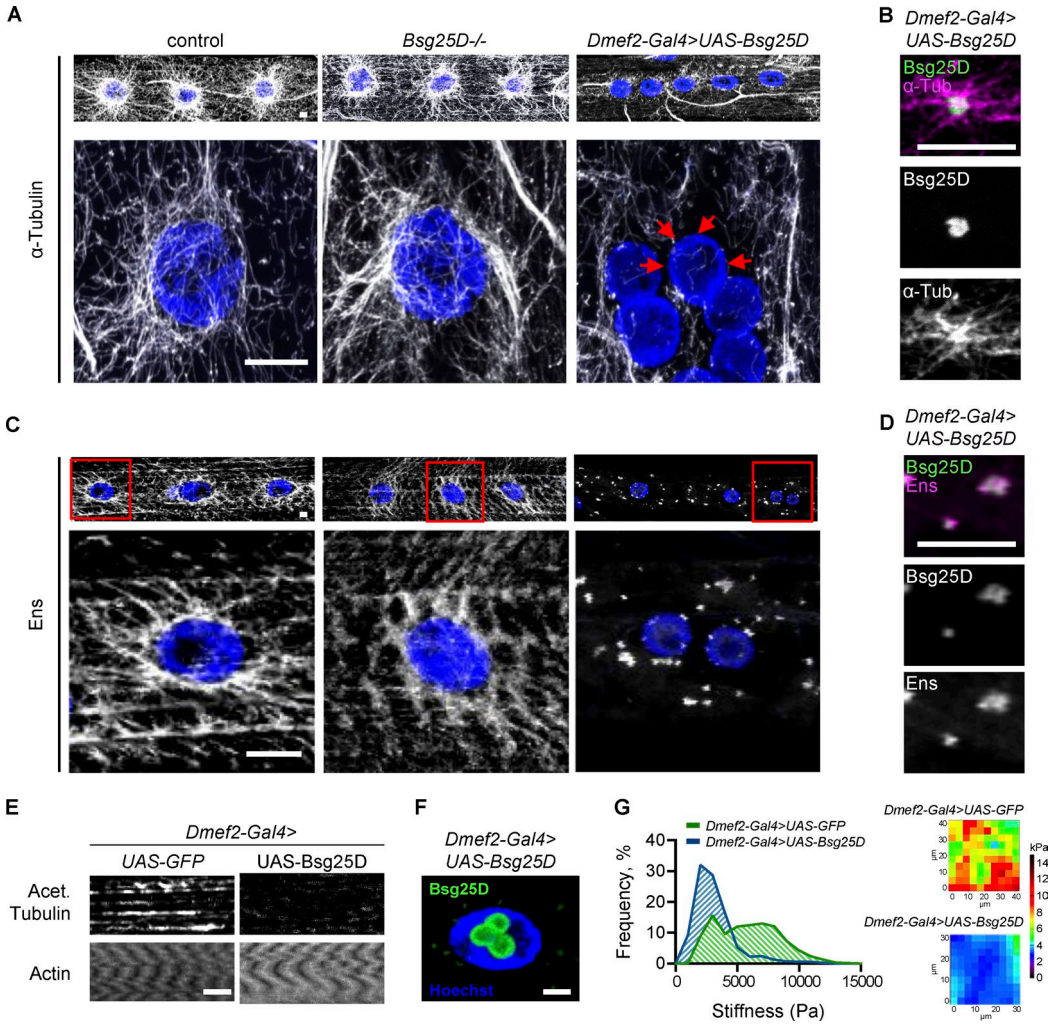


Figure 4.2.7 – *Bsg25D* overexpression perturbs normal MT organization and forms Ens-positive MTOCs in larval myofibers. (A) Top: α-Tubulin signal in extended-focus projections of larval myofibers. Bottom: Higher magnification images of nuclear MT arrays. Gray, α-Tubulin; blue, nuclei. Red arrows show myonuclear envelope without MTs. **(B)** Extended-focus projections of Bsg25D and α-Tubulin signal in a cytoplasmic Bsg25D punctum in *Dmef2-Gal4>UAS-Bsg25D* larval myofiber. Bsg25D, green; α-Tubulin, magenta; colocalization, white. **(C)** Top: Ens signal in extended-focus projections of larval myofibers of indicated genotypes. Bottom: Higher magnification images of nuclei delineated by red boxes. Gray, Ens; blue, nuclei. **(D)** Extended-focus projections of Bsg25D and Ens signal in a cytoplasmic Bsg25D punctum in *Dmef2-Gal4>UAS-Bsg25D* larval myofiber. Bsg25D, green; Ens, magenta; colocalization, white. **(E)** Staining of larval myofibers with phalloidin (labeling Actin) and an antibody against acetylated Tubulin. Images are single slices from Z-stacks, immediately below myonuclei. Staining for actin confirms the presence of intact myofibers. **(F)** Single slice through a *Dmef2-Gal4>UAS-Bsg25D* myofiber nucleus. Blue, Hoechst; green, Bsg25D. In all images, scale bars = 10 μm. In B, D, and F, Bsg25D localization is visualized by Eos, which fluorescently tags the N-terminus of overexpressed Bsg25D. **(G)** Left: Frequency histogram of all stiffness measurements from AFM for indicated genotypes. For *Dmef2-Gal4>UAS-GFP*, *n* = 21 myofibers. For *Dmef2-Gal4>UAS-Bsg25D*, *n* = 16 myofibers. In each genotype, multiple measurements were taken per myofiber; see materials and methods. P value was calculated by Student's *t* test: ****, P < 0.0001. Right: Examples of an AFM force map for each genotype.

by sequestering Ens away from MTs. Taken together, Bsg25D overexpression causes

defects in MT organization and posttranslational acetylation; the latter may be indicative of a loss of MT stability.

We next investigated whether Bsg25D overexpression affected the mechanical properties of myofibers by performing atomic force microscopy (AFM) to measure stiffness in control (GFP-overexpressing) and Bsg25D-overexpressing myofibers. We found a significant decrease in the stiffness of Bsg25D-overexpressing myofibers (*Dmef2-Gal4>UAS-GFP* mean ± SD = 5,895 ± 2,646 Pa, *Dmef2-Gal4>UAS-Bsg25D* mean ± SD = 3,167 ± 1,735 Pa, $P < 0.0001$; Fig. 4.2.7G), perhaps due to the changes in MT organization that we documented, although the role of MTs in regulating myofiber stiffness appears to be complex and variable between systems [296–298]. Alternatively, other cytoskeletal elements such as actin or myosin, which have been shown to be critical for generating stiffness in skeletal muscle [296], may have been disorganized or reduced in these muscles. Together, this series of experiments shows that overexpressed Bsg25D causes defects in the intracellular organization and mechanical properties of larval myofibers.

DISCUSSION

Bsg25D functions in myonuclear positioning

The *Bsg25D* null mutants we generated, like those in two recent reports, are viable and fertile [276,277]. Zheng et al. (2016) did not detect any mutant abnormalities, whereas Kowanda et al. (2016) observed a decrease in embryonic hatching and partially penetrant mitotic defects. Our null *Bsg25D* mutant has a lower rate of embryonic death than the mutant generated by Kowanda et al. (2016). The differences between the *Bsg25D* mutant phenotypes generated by different groups likely reflect the sensitivity of *Bsg25D* mutant phenotypes to genetic background. Because our null *Bsg25D* mutant did not have obvious defects, our analysis of *Bsg25D* required other approaches: generation of double mutants and gain-of-function analysis. Through these approaches, we uncovered a role for *Bsg25D* in myonuclear positioning, where it works with Ens. To our knowledge, Ninein null mice have not been reported; it will be interesting to observe what aspects of Ninein function are conserved in mammals.

Bsg25D and Ens regulate the dynamics of myonuclear movement

Our live imaging of stage 15 embryos yielded unexpected insights about the dynamics of myonuclear movement. We initially thought that nuclear clusters separated at stage 14 and then migrated toward their respective poles in a straightforward fashion. However, in all genotypes tested, we observed both myotubes where the nuclear spread increased during our window of observation and myotubes where nuclear spread decreased. These observations argue for a more complex model of myonuclear positioning in which the forces driving nuclear clusters toward muscle poles (for example, Bsg25D and Ens) are opposed by unknown forces driving clusters toward each other. Thus, the relative levels of these opposing forces during stages 14–16 determine myonuclear spread.

Overexpression of Bsg25D affects multiple aspects of muscle organization and function

Gain-of-function analysis revealed that overexpressed Bsg25D has potent activity in

embryonic myotubes and mature myofibers. In myotubes it perturbs myonuclear positioning; in myofibers it perturbs myonuclear positioning, MT organization, muscle stiffness, and muscle function. The severity of these phenotypes suggests it is critical for muscle cells to limit the amount of Bsg25D protein present. In overexpression experiments in the ovary, *Bsg25D* localization and activity is regulated by its 3′ UTR [276]; however, we found that *Bsg25D* overexpression constructs with or without 3′ UTR confer similar phenotypes in myotubes (data not shown), suggesting that the 3′ UTR is not critical to Bsg25D regulation in muscle. Developing muscle presumably employs other mechanisms to limit the levels of Bsg25D.

Unlike in myofibers, Bsg25D overexpression in embryonic myotubes confers no detectable MT defects. Consistent with these observations, overexpressed Bsg25D did not colocalize with α-Tubulin or γ-Tubulin (data not shown). It is unclear how myotubes resist the MT-altering effects of overexpressed Bsg25D that we observed in myofibers and others have observed in other systems [276,277,299]; perhaps myotubes lack an essential cofactor necessary for Bsg25D to induce ectopic MTOCs. In general, our data support that MTs in developing myotubes have different behaviors from MTs in myofibers and in other tissues.

While overexpressed Bsg25D does not perturb MTs in embryonic myotubes, does endogenous Bsg25D regulate MT organization? We failed to detect differences in MT density and polymerization rate between control and *Bsg25D*$^{-/-}$ myotubes; this is in contrast to the *C. elegans* larval epidermis, where *Bsg25D/Noca-1* mutants were found to have lower-than-normal MT polymerization rates by an EB1-based assay analogous to ours [275]. There are two caveats to our conclusion that *Bsg25D* does not function in MT regulation in *Drosophila* myotubes. First, we could not draw conclusions about the number of polymerizing MTs in each genotype because the EB1-YFP signal was weaker in mutant cells than control cells, making the number of traceable EB1-YFP comets an unreliable proxy for the number of polymerizing MTs. Second, it remains possible that MT phenotypes in *Bsg25D*$^{-/-}$ myotubes are masked by a redundantly acting factor. Though our negative data do not definitively rule out a role for endogenous Bsg25D in regulating MTs in muscle, the absence of clear MT phenotypes in Bsg25D$^{-/-}$ myotubes and myofibers leads us to favor the conclusion that Bsg25D functions in myonuclear positioning without playing a major role in MT regulation.

Ens and Bsg25D exhibit complex interactions

Our work reveals that Bsg25D and Ens work together in myonuclear positioning. It is not clear exactly where in the myotube they interact to promote myonuclear movement. In immunostained embryos, the most conspicuous Bsg25D signal in myotubes is in cytoplasmic puncta, which also stain positive for Ens. However, there is also a broad, low-level Bsg25D signal throughout the cytoplasm that our microscopy techniques cannot further resolve. Given that Ens coats MTs, it is plausible that Bsg25D interacts with Ens broadly on those structures. Indeed, studies have shown Bsg25D/Ninein interacting with the MT network as a cargo [300,301], and a Bsg25D fragment has been shown to directly bind MTs *in vitro* [276].

In both myotubes and myofibers, co-overexpression of Ens relieves the myonuclear clustering caused by overexpression of Bsg25D. The mechanisms by which Bsg25D and Ens function likely differ between these two developmental stages. In embryonic myotubes, Bsg25D overexpression phenocopies the ens mutant phenotype, so inhibition of Ens by high levels of Bsg25D is sufficient to explain the nuclear positioning defects. However, the nuclear positioning phenotypes in mature larval myofibers caused by long-term overexpression of Bsg25D are more severe than those caused by loss of Ens; thus, inhibition of Ens is not a sufficient explanation for the Bsg25D-induced defects. We propose that Bsg25D causes nuclear positioning defects in larval myofibers through the combined effect of multiple mechanisms, including inhibition of Ens, inhibition of other proteins involved in myonuclear positioning such as Dynein, and disruption of MT organization. Co-overexpressed Ens then suppresses at least some of these Bsg25D activities, restoring normal nuclear positioning.

The finding that embryos with reduced maternal/zygotic ens and a total absence of *Bsg25D* fail to survive to larval stages demonstrates that critical Bsg25D–Ens interactions occur outside of the muscle as well. Evidence from the literature raises the possibility that they interact in the female germline, as groups have separately reported overlapping localization patterns for Bsg25D and Ens proteins, with both found at the anterior pole of the developing oocyte during midoogenesis [183,276]. Moreover, misexpression of *Bsg25D* and loss of function of ens cause common phenotypes: reductions in Dynein and Gurken at the posterior pole and anterior-dorsal corner of the oocyte, respectively, and resulting embryos lacking dorsal appendages [183,276]. Thus, it may be the case that forced expression of

Bsg25D binds and disrupts endogenous Ens in the female germline as it does in muscle.

Centrosomal proteins participate in myonuclear movement

We find that in addition to Bsg25D, a second centrosomal protein, Plp (the *Drosophila* Pericentrin homologue), is involved in myonuclear positioning. The function of centrosomal proteins in muscle, which lacks centrosomes, has been unclear. Our work suggests that a general function of centrosomal proteins in muscle is to position myonuclei. This hypothesis is supported by the recent finding that the centrosomal protein PCM-1 is required for myonuclear positioning in C2C12 myotubes [302]. These findings underscore the conservation of mechanisms regulating nuclear movement and muscle organization. It is intriguing that although Bsg25D and Plp colocalize in myotubes, and each participates in myonuclear positioning, loss of *Bsg25D* does not enhance myonuclear positioning defects in plp mutants. It may be the case that the two proteins ultimately contribute to myonuclear positioning via separate pathways.

Model

We propose that endogenous Bsg25D positively regulates Ens in a manner dependent on their physical interaction (Fig. 4.2.8). The critical interaction could either be at Bsg25D–Ens cytoplasmic puncta or on Ens-coated MTs. Bsg25D could conceivably promote Ens activity by affecting its protein levels, subcellular localization, access to binding partners, or posttranslational modification, or by other means. In our model, embryos with the full complement of ens have enough Ens activity to withstand loss of the activator Bsg25D without showing diminished myonuclear movement. However, in embryos where Ens activity is limited by loss of one allele of *ens*, loss of Bsg25D further reduces Ens activity and perturbs myonuclear movement.

When Bsg25D is present at high concentrations in myotubes, it confers severe nuclear positioning phenotypes through its interactions with Ens (Fig. 4.2.8B). Overexpressed Bsg25D forms puncta that recruit endogenous Ens away from its normal localization on MTs, leading to a block in Ens-dependent myonuclear movement toward the muscle poles. In myofibers, these Bsg25D- and Ens-positive puncta serve as ectopic MTOCs. MTs are lost from the nuclear envelope, possibly because necessary factors are recruited to the ectopic MTOCs. Nuclei are

mispositioned, in part due to altered MT organization, and muscle function is decreased.

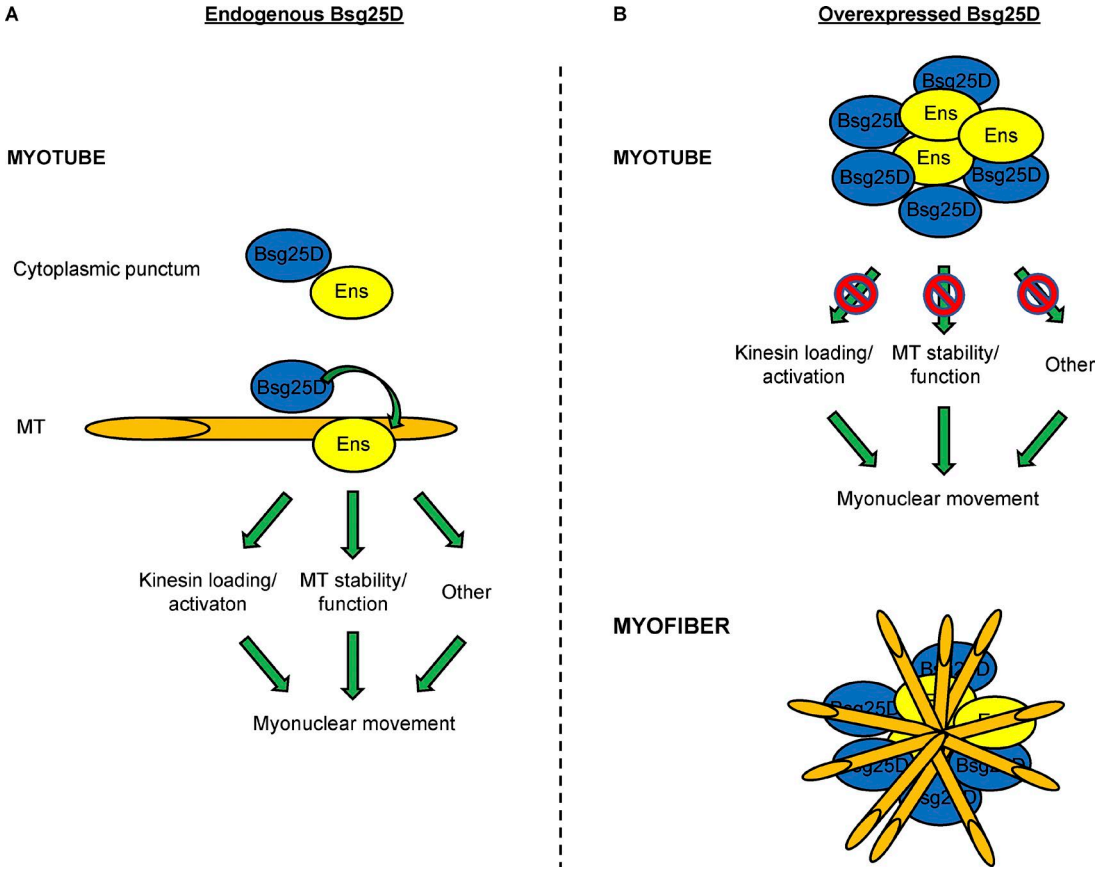


Figure 4.2.8 – Model of Bsg25D–Ens interactions. (A) Model of the Bsg25D–Ens interaction in wild-type myotubes. **(B)** Model of the Bsg25D–Ens interaction when Bsg25D is overexpressed. See Discussion for model details. Bsg25D, blue; Ens, yellow; MTs, orange.

Conclusion

We have identified *Drosophila* Bsg25D as a novel Ens interactor and shown that it functions with Ens in myonuclear positioning. We have found that overexpressed Bsg25D blocks myonuclear movements in embryonic myotubes and that sustained Bsg25D overexpression disrupts both myonuclear positioning and MT organization in mature larval myofibers; nuclear positioning defects in embryos and larvae are rescued by cooverexpression of Ens. Thus, Bsg25D–Ens interactions are critical for myonuclear positioning and muscle development. The human homologues of the two proteins have important functions that are illustrated by their association with disease; loss of Ninein causes Seckel syndrome [303], while high levels of MAP7 are associated with types of colon cancer and leukemia [304,305]. The use of model

systems to investigate how gain and loss of Ninein/Bsg25D and Ens/MAP7 affect cells *in vivo* will lend insights to human health.

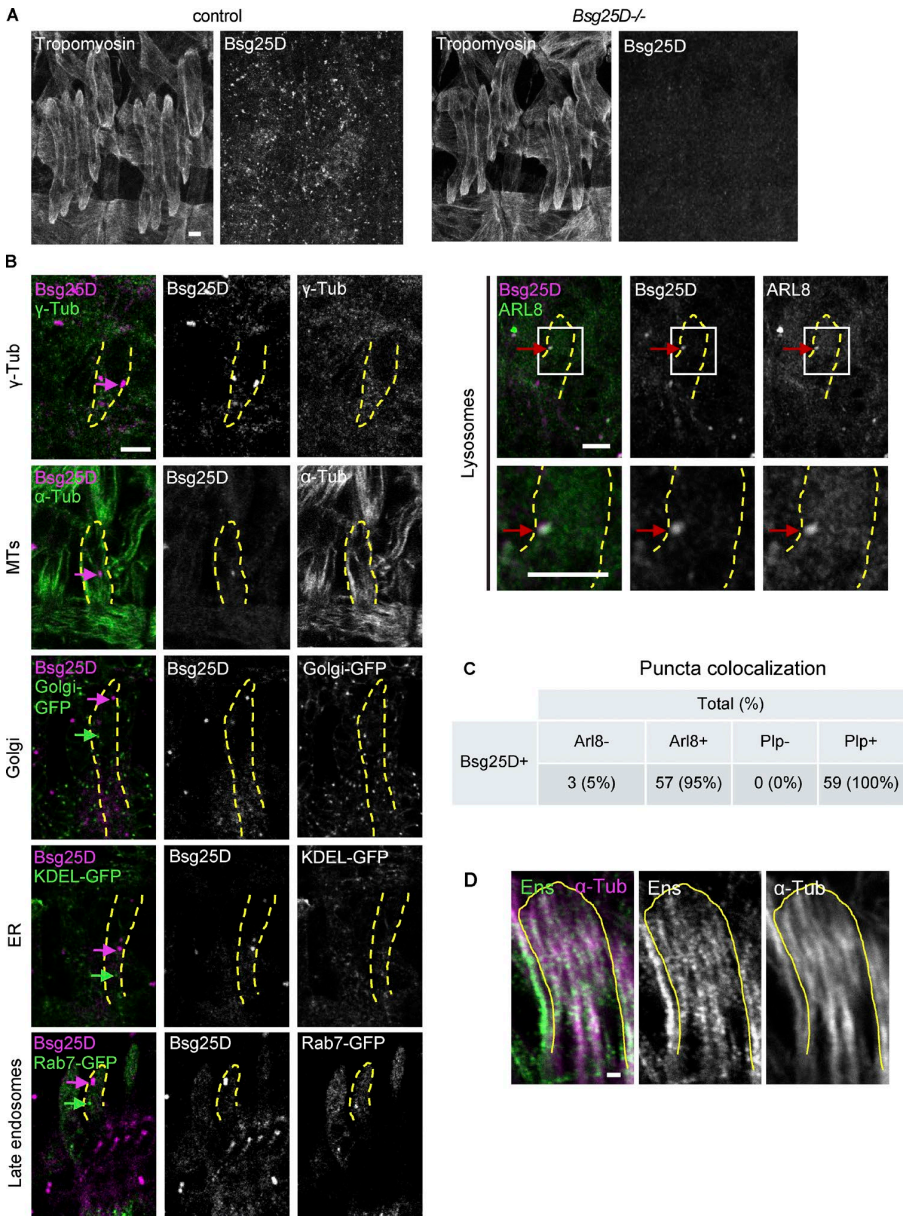


Figure 4.2.9 – Bsg25D puncta in developing myotubes localizes with Ens and the lysosome marker Arl8, but not with markers of other subcellular compartments. (A) Bsg25D antibody labels puncta in control, but not *Bsg25D*$^{-/-}$, embryos. Focused projections of stage 16 embryos stained for Tropomyo- sin and Bsg25D. Scale bar = 5 μm. **(B)** Bsg25D does not colocalize with γ-Tubulin (γ-Tub), MT, Golgi apparatus, ER, or endosome markers in myotubes, but does colocalize with a lysosome marker. Images of single slices from confocal stacks of stage 16 embryos stained for Bsg25D and various markers or organ- elle-GFP reporters. Yellow dashed lines indicate individual lateral transverse muscles, as determined by costaining for Tropomyosin (not depicted). Bsg25D, magenta; marker proteins, green. Magenta and green arrows point to puncta positive for Bsg25D or marker proteins, respectively. Scale bars = 5 μm. **(C)** Table of colocalization data of Bsg25D puncta with listed proteins. For each condition, *n* = 3 embryos. **(D)** Ens localization in control myotubes. Single slice from confocal stack of a stage 16 embryo stained for Ens and α-Tub. Ens, green; α-Tub, magenta; colocalization, white. Yellow line indicates a lateral transverse muscle, as determined by costaining with phalloidin (not depicted). Scale bar = 1 μm.

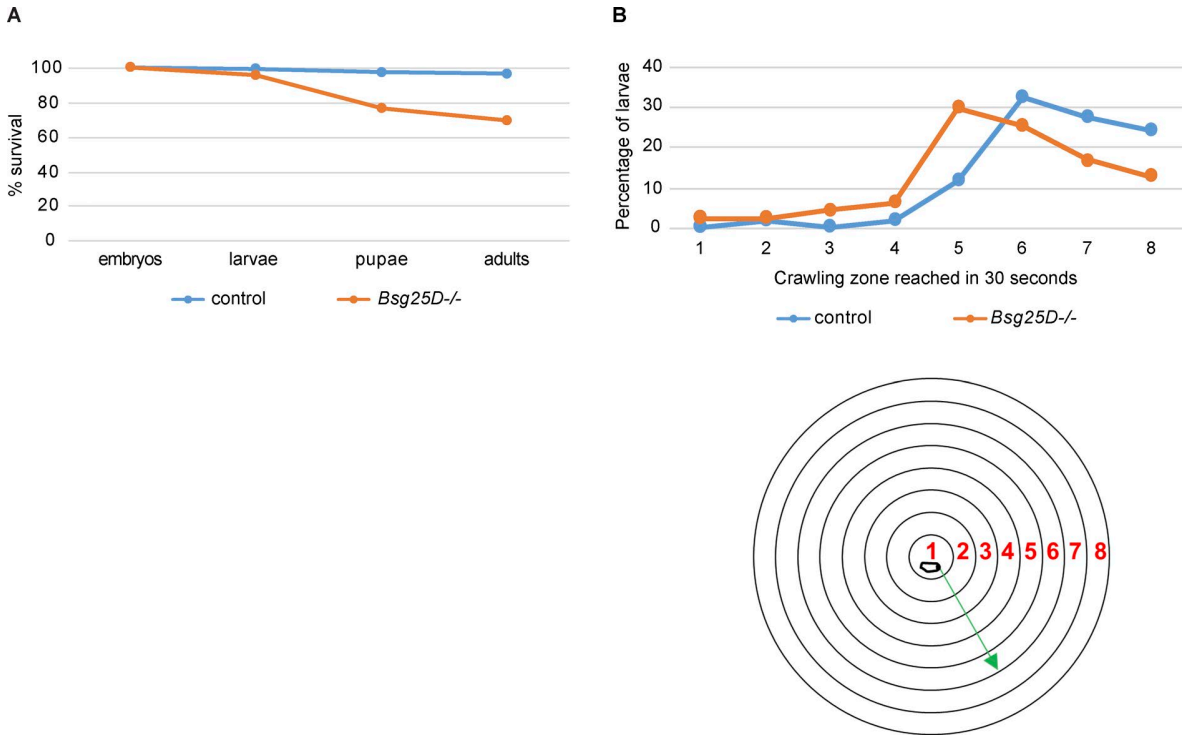


Figure 4.2.10 – *Bsg25D*$^{-/-}$ individuals have mild decreases in viability and motility. (A) Viability of control and *Bsg25D*$^{-/-}$ individuals during development. 96% of control embryos (*n* = 107) and 70% of *Bsg25D*$^{-/-}$ embryos (*n* = 119) survived to adulthood. **(B)** Motility of control *Bsg25D*$^{-/-}$ third-instar larvae. Top: Frequency histogram showing how far larvae of indicated genotypes could crawl in 30 s. Bottom: Diagram of experimental setup. The experimenter placed individual larvae in the center of an apple juice plate (crawling zone 1) and recorded what zone they reached in 30 s. For control and *Bsg25D*$^{-/-}$ larvae, the modes were zone 6 and zone 5, respectively. Control, *n* = 61 larvae; *Bsg25D*$^{-/-}$, *n* = 47 larvae.

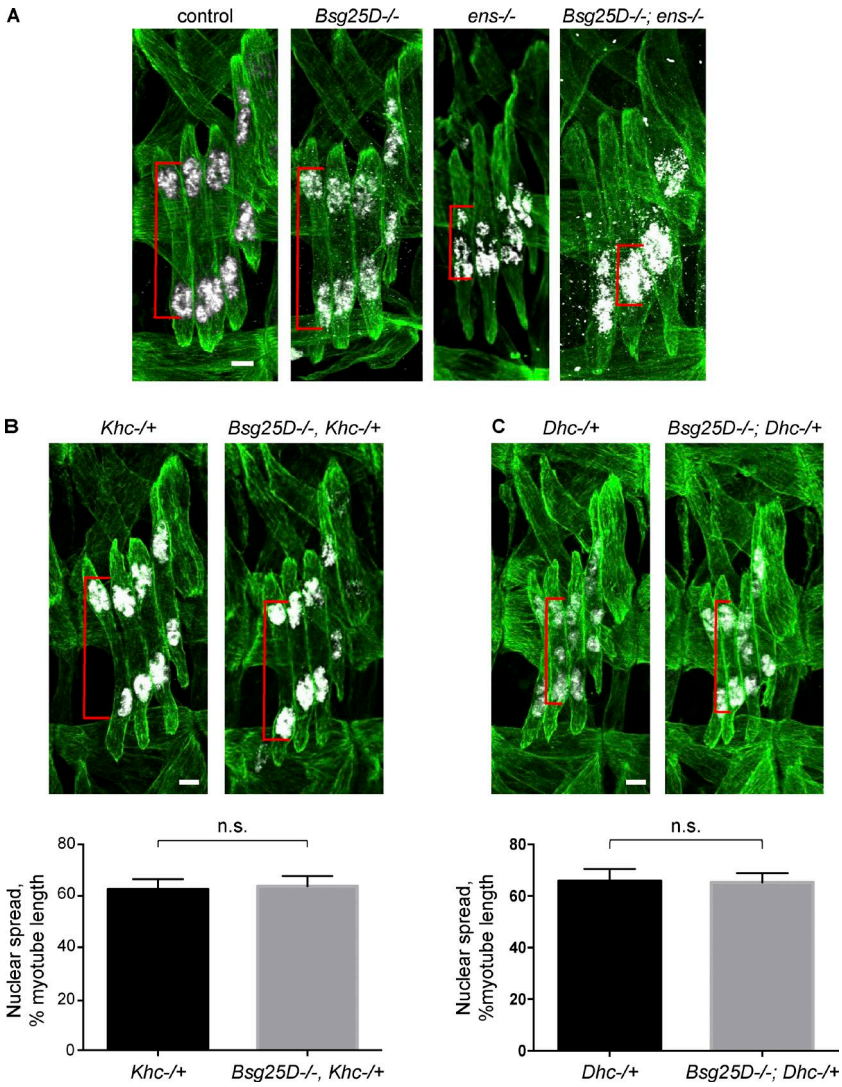


Figure 4.2.11 – *Bsg25D*$^{-/-}$ does not enhance the *ens*$^{-/-}$ phenotype and does not genetically interact with *Khc* or *Dhc* to regulate myonuclear positioning. (A) *Bsg25D*$^{-/-}$;*ens*$^{-/-}$ double mutants have myotubes with a single cluster of myonuclei, like *ens*$^{-/-}$ single mutants. Control and *Bsg25D*$^{-/-}$ images are reproduced from Fig. 2. The *ens*$^{-/-}$ image is reproduced from Fig. 3. Scale bar = 5 μm. **(B and C)** Bsg25D does not genetically interact with *Khc* or *Dhc* in myonuclear positioning. Top: extended focus projections of representative stage 16 hemisegments of indicated genotypes. Tropomyosin, green; nuclei, white. Scale bars = 5 μm. Note that myotubes with reduced *Dhc* are shorter, as has previously been shown (Folker et al., 2012). Bottom: Bar graphs showing mean nuclear spread and SD. For each genotype, the number of hemisegments is *Khc*$^{-/+}$, *n* = 31 and *Bsg25D*$^{-/-}$;*Khc*$^{-/+}$, *n* = 30 (A); *Dhc*$^{-/+}$, *n* = 45 and *Bsg25D*$^{-/-}$;*Dhc*$^{-/+}$, *n* = 43 (B). P values were calculated by Student's *t* test.

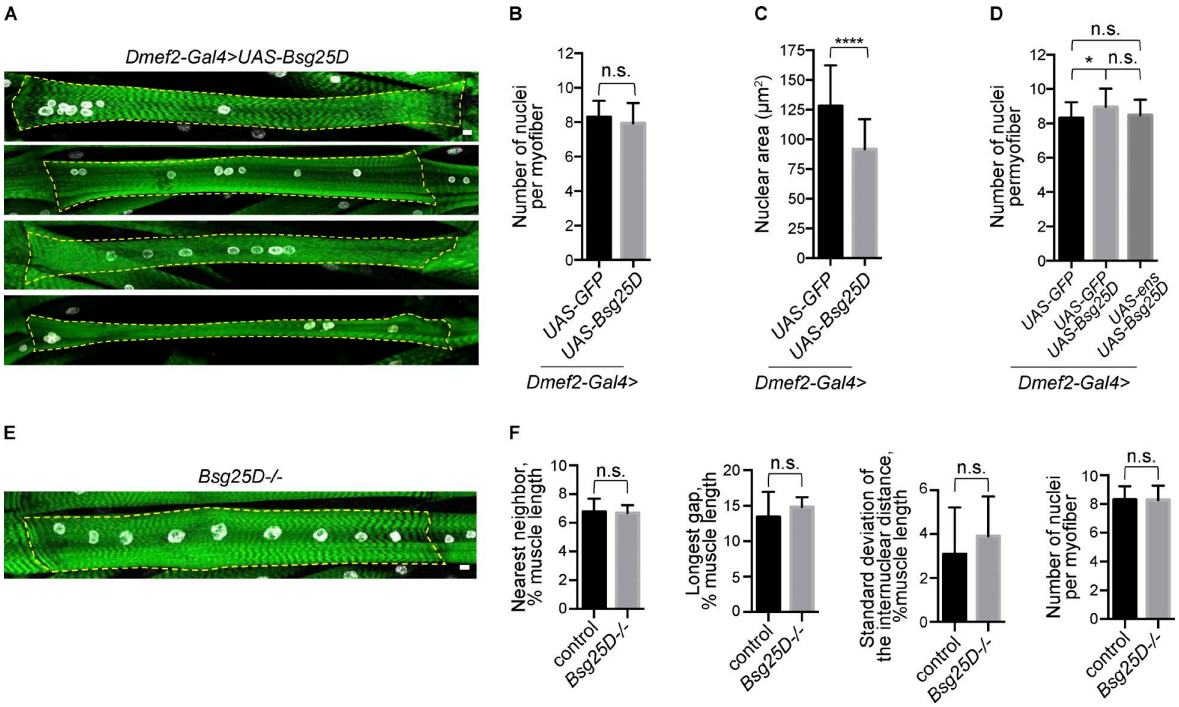


Figure 4.2.12 – Bsg25D overexpression induces myonuclear clusters of variable size and position and reduces nuclear size without affecting the number of nuclei per myofiber. **(A)** Four examples of Bsg25D-overexpressing myofibers with clustered myonuclei. Note that the cellular position of clusters, the number of myonuclei per cluster, the number of clusters per myofiber, and the location of the longest gap are variable. Phalloidin, green; nuclei, white. Scale bar = 10 μm. Yellow dashed line indicates myofiber edges. **(B)** Bsg25D overexpression does not affect the number of myonuclei per myofiber relative to GFP control. For each genotype, the number of myofibers is as follows: *Dmef2-Gal4>UAS-GFP*, *n* = 40; *Dmef2-Gal4>UAS-Bsg25D*, *n* = 45. **(C)** Mean nuclear area in larval myofibers of larvae expressing either GFP or Bsg25D in muscle. Measurements were done on extended focus projections of Z-stacks. For each genotype, the number of nuclei is as follows: *Dmef2-Gal4>UAS-GFP*, *n* = 82; *Dmef2-Gal4>UAS-Bsg25D*, *n* = 104. **(D)** Larva overexpressing either GFP or Ens with Bsg25D had the same number of nuclei per myofiber, allowing for straightforward comparisons of myonuclear positioning. For each genotype, the number of myofibers is as follows: *Dmef2-Gal4>UAS-GFP*, *n* = 40; *Dmef2-Gal4>UAS-GFP;UAS-Bsg25D*, *n* = 23; *Dmef2-Gal4>UAS-ens;UAS-Bsg25D*, *n* = 19. **(E and F)** *Bsg25D*$^{-/-}$ larvae have normal myonuclear positioning. **(E)** Extended-focus projection of representative *Bsg25D*$^{-/-}$ myofiber. Phalloidin, green; nuclei, white. Scale bar = 10 μm. Yellow dashed line indicates myofiber edges. **(F)** Quantification of myonuclear positioning and nuclear number in control and *Bsg25D*$^{-/-}$ myofibers. Control data are *Dmef2-Gal4>UAS-GFP* from Fig. 5. For all analyses, *n* = 40 myofibers for control and *n* = 17 myofibers for *Bsg25D*$^{-/-}$. P values were calculated by Student's *t* test. *, P < 0.05; ****, P < 0.0001.

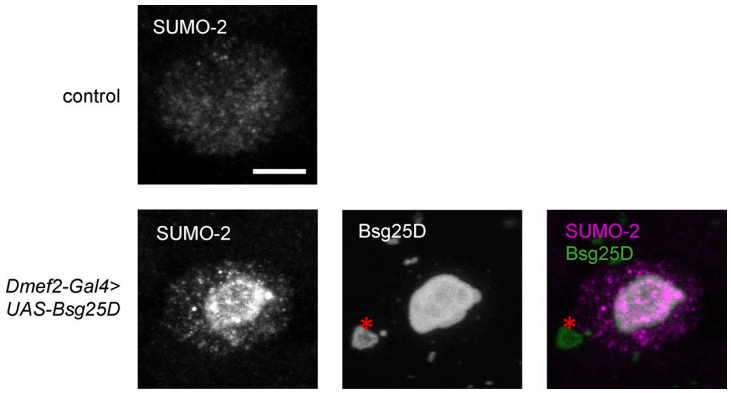
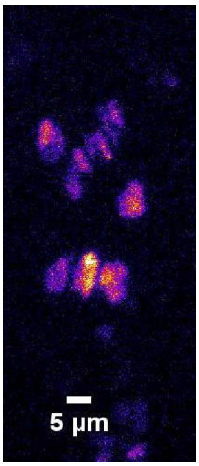
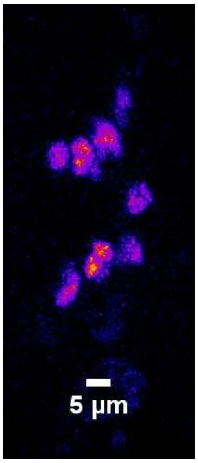


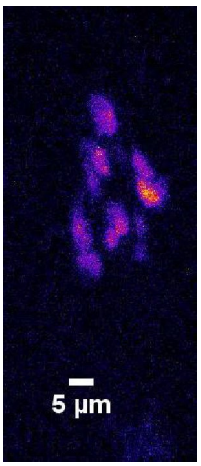
Figure 4.2.13 – Overexpressed Bsg25D colocalizes with SUMO-2 in myonuclei. In control myofibers, an antibody against SUMO-2 labels myonuclei in a punctate pattern. In myofibers overexpressing Bsg25D, SUMO-2 antibody labels the same structures and colocalizes with nuclear Bsg25D. Note that cytoplasmic Bsg25D does not colocalize with SUMO-2 (asterisks). Green, Eos::Bsg25D; magenta, SUMO2; colocalization, white. Scale bar = 5 μm.



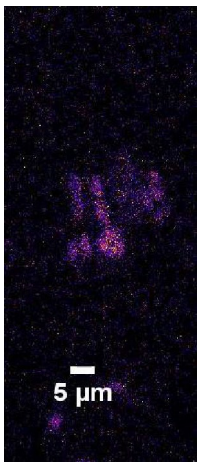
Video 1 – Nuclear movement in control LT myotubes. Nuclei are labeled and filmed as described in Materials and methods. Representative examples of each listed genotype are included.



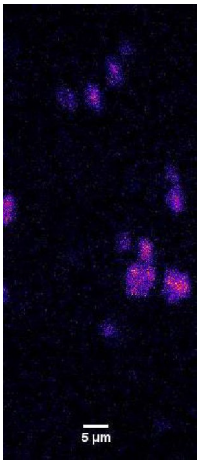
Video 2 – Nuclear movement in *Bsg25D*$^{-/-}$ LT myotubes. Nuclei are labeled and filmed as described in Materials and methods. Representative examples of each listed genotype are included.



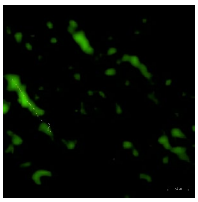
Video 3 – Nuclear movement in*Bsg25D*$^{-/-}$;*ens*$^{-/+}$ LT myotubes. Nuclei are labeled and filmed as described in Materials and methods. Representative examples of each listed genotype are included.



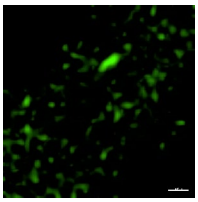
Video 4 – Nuclear movement in *Dmef2-GAL4> UAS-Bsg25D* LT myotubes. Nuclei are labeled and filmed as described in Materials and methods. Representative examples of each listed genotype are included.



Video 5 – Nuclear movement in *Dmef2-GAL4> UAS-ens* LT myotubes. Nuclei are labeled and filmed as described in Materials and methods. Representative examples of each listed genotype are included.



Video 6 – EB1-YFP in control myotubes. Representative EB1-YFP videos for the listed genotypes. See Materials



Video 7 – EB1-YFP in *Bsg25D*$^{-/-}$ myotubes. Representative EB1-YFP videos for the listed genotypes. See Materials and methods for details.

Part III

ADDITIONAL UNPUBLISHED RESULTS

Part III of this Thesis describes different pieces of data that were not included in either Part I or Part II of the Chapter 4 – Results. All data included here are unpublished data acquired during the doctoral studies and most represent preliminary data since the sample size is insufficient to draw significant conclusions. These offer interesting starting points for future graduate students or postdoctoral fellows.

Derailed

One of the features that *Drosophila* muscle development shares with vertebrates is the establishment of muscle-tendon interactions in an interface called myotendinous junctions. The receptor Tyr kinase *derailed* (*drl*) was identified as a regulator of this process in fly muscle [306]. Derailed is a membrane receptor that binds Wnt proteins and loss of *drl* often resulted in misguidance of LTs [306].

Previous data from the lab using muscle-specific overexpression of *drl* showed missing/disrupted Ventral Oblique muscles, as well as occasional extra or missing LT muscles. Additionally, Src42A and Src64B are required for muscle attachment, and overexpression of Src causes defects in integrin-mediated adhesion at muscle attachment sites. Since we were interested in understanding the effects of the muscle-tendon interactions in myonuclear positioning, we investigated *drl* as a potential candidate.

We analyzed three different alleles of *drl* and observed significant defects with all, particularly R343 and Red2 (Fig. 4.3.1). For alleles R343 and Red2, nuclear spread analysis was done based on the negative space visible by reduced Tropomyosin expression, rather than by using a nuclear marker. Although, relatively easy to identify these negative signal areas, the final result might slightly differ from that obtained when using a nuclear marker. In addition to the nuclear spread defects, we also observed the attachment defects previously described [306]. Approximately 60% of $drl^{P3.765}$ embryos showed extra LT(s) in at least one of the hemisegments analyzed. Since these mutant alleles are not embryonic lethal, we were able to assess

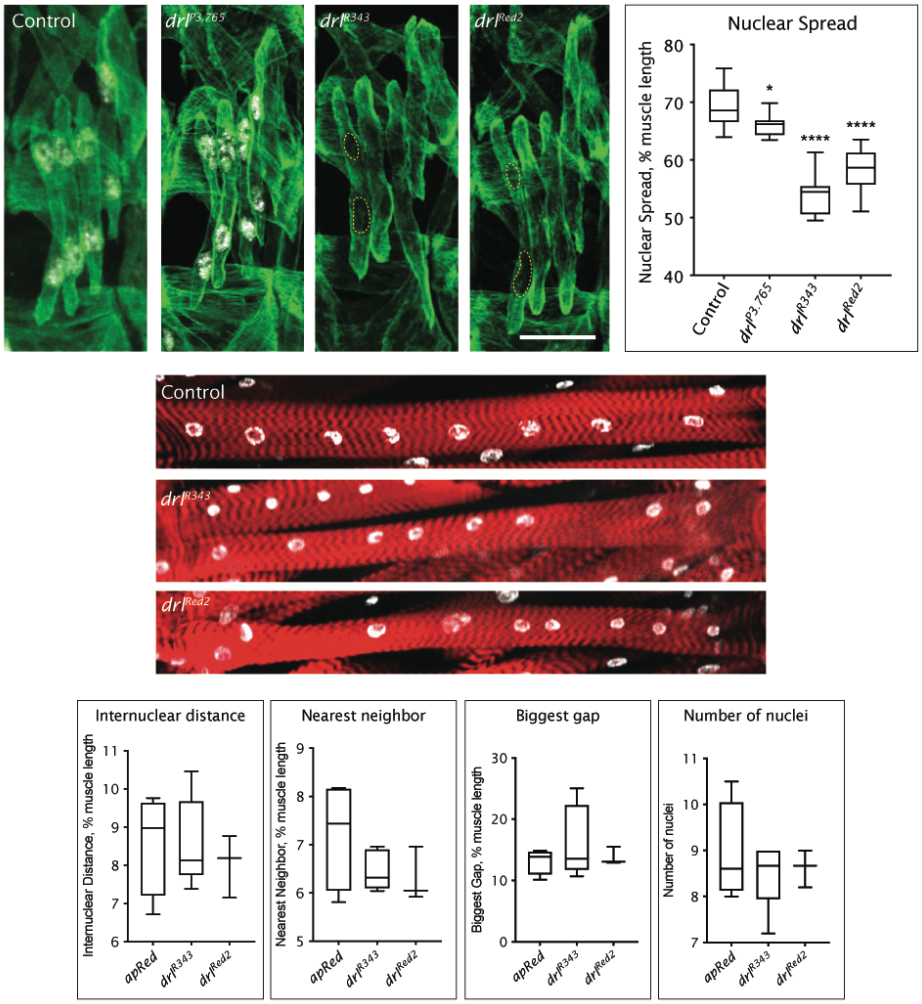


Figure 4.3.1 – **Top panel:** representative images of stage 16 embryonic muscles of the noted genotypes and quantification of nuclear spread as a percentage of muscle length as follows (n equals number of embryos analyzed): control, 69.36, n=10; *drl*$^{P3.765}$, 65.96, n=10, *p=0.0174; *drl*^{R343}, 53.98, n=10, ****p<0.0001; *drl*^{Red2}, 58.38, n=10, ****p<0.0001. Yellow dashed circles represent the position where the clusters of nuclei are. Tropomyosin, green. Nuclei, white. Scale bar, 20μm. **Middle panel**: representative images of third instar VL4 larval muscles of the noted genotypes. Actin, red. Nuclei, white. **Bottom panel:** quantification of internuclear distance, nearest neighbor, and biggest gap as a percentage of muscle length, and number of nuclei as follows (n equals number of larvae analyzed): Internuclear distance: control, 8.608, n=4; *drl*^{R343}, 8.594, n=5; *drl*^{Red2}, 8.040, n=3. Nearest neighbor: control, 7.215, n=4; *drl*^{R343}, 6.464, n=5; *drl*^{Red2}, 6.310, n=3. Biggest gap: control, 13.19, n=4; *drl*^{R343}, 16.34, n=5; *drl*^{Red2}, 13.84, n=3. Number of nuclei: control, 8.928, n=4; *drl*^{R343}, 8.508, n=5; *drl*^{Red2}, 8.623, n=3.

myonuclear positioning in third instar larvae by measuring internuclear distance, nearest neighbor and biggest gap (Figure 4.3.1 Middle and Bottom panels). Lack of *drl* in myofibers does not seem to affect myonuclear positioning or the number of nuclei.

Collectively, these data seem to indicate that Derailed plays a role in myonuclear positioning during embryonic development, but not in developed muscles. Since a good number of embryos was used in the nuclear spread

quantification (10 embryos per genotypes,), this set of data does not qualify as preliminary. It would be interesting to quantify embryos carrying a nuclear marker, such as *apRed*, in order to better estimate the nuclear positioning defects. Muscle-specific knockdown, rescue experiments and genetic interaction studies will further confirm the extent to which Derailed regulates myonuclear positioning.

Inflated

One of the main components of stable myotendinous junctions are the integrins. In *Drosophila*, this specialized interface that connects muscles to tendons, there are two types of integrins: αPS1βPS integrin is produced by the mature tendon cell and αPS2βPS integrin secreted by the muscle cell[184,188]. Due to the importance of these proteins in the maintenance of the MTJ and muscle, we studied one of the components of integrins. Inflated (*if*) is one of 5 fly integrin α subunits (αPS2). It can associate with an integrin β subunit, becoming a receptor for extracellular matrix proteins. It is

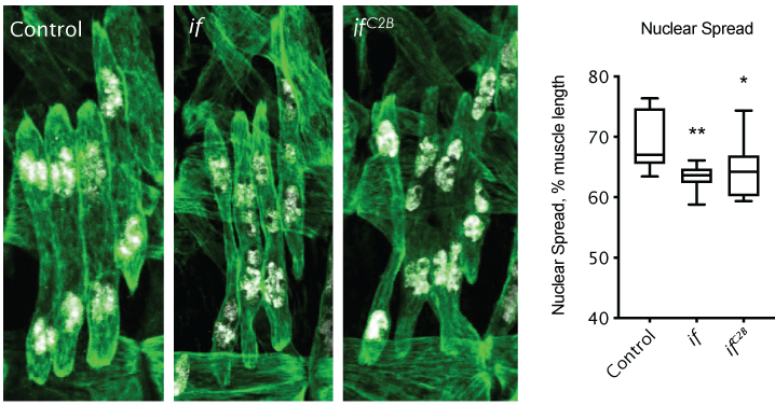


Figure 4.3.2 - Representative images of stage 16 embryonic muscles of the noted genotypes and quantification of nuclear spread as a percentage of muscle length as follows (n equals number of embryos analyzed): control, 69.19, n=10; *if*, 63.30, n=9, **p=0.0038; if^{C2B}, 64.44, n=10, *p=0.0411. Tropomyosin, green. Nuclei, white.

required in numerous tissues for cell migration and adhesion between cell layers [307]. With integrin being essential for muscle attachment to tendon, we selected partial loss-of-function alleles that did not resulted in embryos with severe attachment defects in order to effectively assess myonuclear positioning. Both alleles tested displayed decreased nuclear spread without significant muscle detachment as described in the literature (Fig. 4.3.2) [307]. These data suggested that *inflated* seems to regulate myonuclear positioning via the MTJ and further studies need to be performed to understand the mechanism behind this.

Kon-tiki

Kon-tiki (*kon*) is a transmembrane receptor protein present at the myotube tips, that acts via Dgrip to regulate myotube targeting in a subset of myotubes and interacts with integrins during embryonic myogenesis [308,309]. It plays a muscle-autonomous role, promoting muscle migration to form a stable myotendinous junction [308].

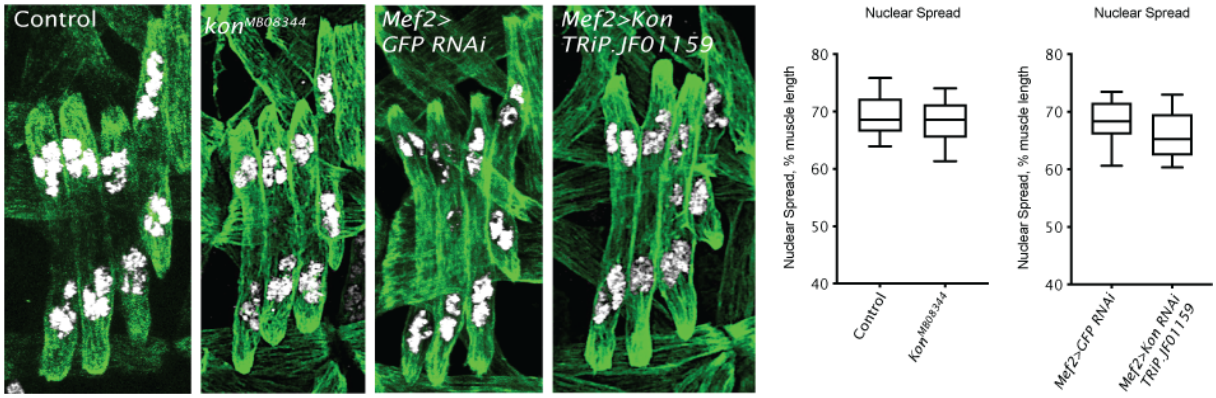


Figure 4.3.3– Representative images of stage 16 embryonic muscles of the noted genotypes and quantification of nuclear spread as a percentage of muscle length as follows (n equals number of embryos analyzed): control, 69.36, n=10; *kon*^{MB08344}, 68.34, n=10; *Mef2-Gal4>GFP RNAi*, 68.41, n=10; *Mef2-Gal4>Kon TRiP.JF01159,* 65.87, n=5. Tropomyosin, green. Nuclei, white.

As one of our main goals was to assess the effect of MTJ manipulation on myonuclear positioning, we analyzed a *kon* mutant and muscle-specific *kon* knockdown (Figure 4.3.3). We observed no significant defects in myonuclear positioning in the LT muscles of these embryos. One possible explanation for the lack of defects observed could be the low expression of Kon in the LT tips. These results are part of our screening for genes involved in MTJ with myonuclear positioning defects and due to the lack of the phenotype we did not perform further experiments with these stocks.

Note about the data shown above in this section: Data including robo1, derailed, inflated *and* kon-tiki *are part of a screening performed to identify MTJ proteins that affected myonuclear positioning. From this screen, Robo1 displayed the most severe nuclear positioning defects without significant muscle detachment, hence why it was the focus of our studies. Nevertheless, both derailed and inflated are good candidates for further studies to understand the role of the muscle-tendon interactions in myonuclear positioning.*

Kugelkern

The nucleus is delimited by the nuclear envelope (NE), a double lipid bilayer that separates the nucleoplasm from the cytoplasm. The NE consists of several proteins and complexes present at the inner or outer nuclear membrane (INM and ONM, respectively). The nuclear lamina intimately associates with the INM and consists primarily of lamins and lamin-associated proteins, that are crucial in shaping and maintaining nuclear shape integrity. Defects in lamins are often associated with various disease, called laminopathies, that affect several tissues including the muscle [310,311]. Kugelkern/*kuk* localizes to the INM, where it colocalizes with lamins, and

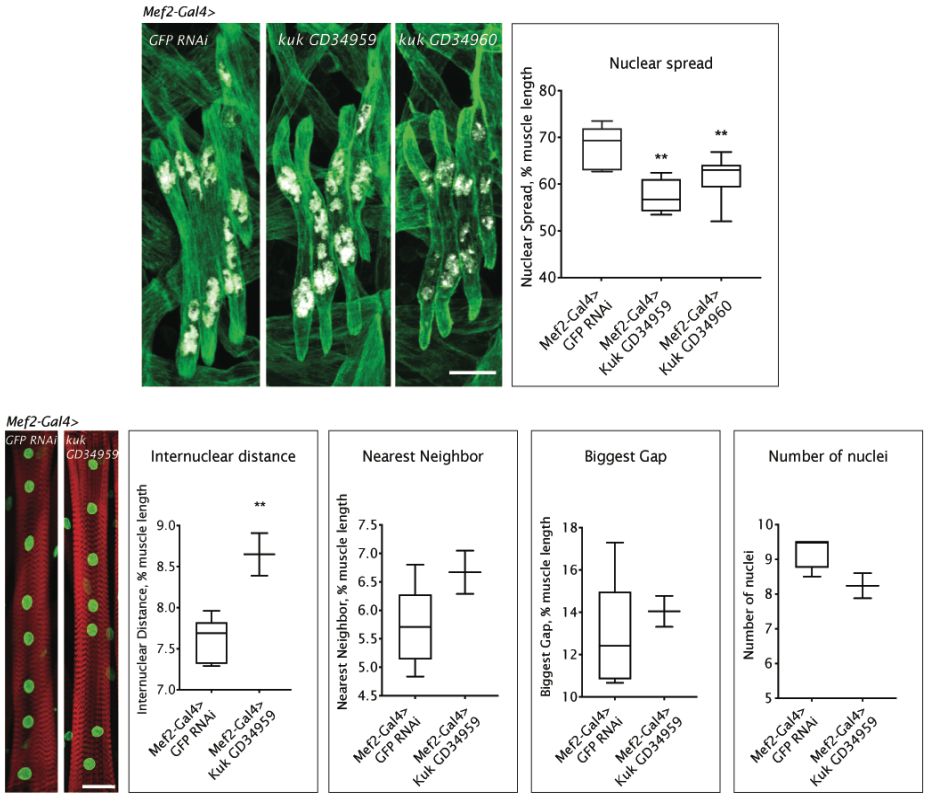


Figure 4.3.4 - **Top panel:** representative images of stage 16 embryonic muscles of the noted genotypes and quantification of nuclear spread as a percentage of muscle length as follows (n equals number of embryos analyzed): Mef2-Gal4>GFP RNAi, 68.07, n=7; Mef2-Gal4>kuk GD34959, 57.36, n=4, **p=0.0027; Mef2-Gal4>kuk GD34960, 61.62, n=10, **p=0.0077. Tropomyosin, green. Nuclei, white. Scale bar, 10μm. **Bottom panel:** representative images of third instar VL4 larval muscles of the noted genotypes and quantification of internuclear distance, nearest neighbor, and biggest gap as a percentage of muscle length, and number of nuclei as follows (n equals number of larvae analyzed): Internuclear distance: Mef2-Gal4>GFP RNAi, 7.594, n=5; Mef2-Gal4>kuk GD34959, 8.650, n=2, **p=0.0082. Nearest neighbor: Mef2-Gal4>GFP RNAi, 5.708, n=5; Mef2-Gal4>kuk GD34959, 6.670, n=2. Biggest gap: Mef2-Gal4>GFP RNAi, 12.81, n=5; Mef2-Gal4>kuk GD34959, 14.05, n=2. Number of nuclei: Mef2-Gal4>GFP RNAi, 9.20, n=5; Mef2-Gal4>kuk GD34959, 8.24, n=2. Actin, red. Lamin Dm0, green. Scale bar, 5μm.

contributes to the regulation of nuclear size, shape and position, in *Drosophila* blastoderm nuclei during cellularization [312,313]. We hypothesized that *kuk* could be involved in regulating nuclear shape and position in the *Drosophila* muscle. To test this hypothesis, we reduced the expression of *kuk* using two RNAi (GD34959 and GD34960) and the muscle-specific driver *Mef2-Gal4* in embryos and larvae; this allowed us to determine the effects of reduced *kuk* in developing and mature muscles.

Muscle-specific reduction of *kuk* in stage 16 embryos (developing myotubes) using both RNAi constructs led to defects in myonuclear positioning (Fig. 4.3.4). When compared to the control (GFP RNAi), the % nuclear spread decreased from 68 to 57 and 61 (Figure 4.3.4 Top panel). For the mature muscle analysis, we used third instar larvae VL4 muscles to assess nuclear positioning by measuring internuclear distance, nearest neighbor and biggest gap. We observed a significant increase in the internuclear distance, suggesting that *kuk* is also required for myonuclear positioning in the mature muscle. However, we saw no differences in the nearest neighbor and the biggest gap measurements. Additionally, we counted the number of nuclei per VL4 muscle and saw no significant differences compared to the control. Moreover, we qualitatively evaluated nuclear shape and observed no differences when compared to the control larval myonuclei, suggesting that *kuk* does not play a role in shaping nuclei in the *Drosophila* mature muscle.

It is worth noting that, although these are preliminary data due to the reduced sample size (for kuk GD34959 only 4 embryos and 2 larvae were analyzed), kuk seems to affect nuclear positioning in a muscle-specific manner in more than one stage of development and should be further investigated. Analysis using mutants and genetic interaction studies may help clarify the role and mechanisms of Kugelkern during myonuclear positioning.

Myosin heavy chain

The sarcomere is the basic contractile unit of cardiac and skeletal muscle and its main components are actin (thin filament) and myosin (thick filament). According to the sliding filament theory, individual sarcomere shortening and contraction occurs when force is generated by myosin binding to actin, creating cross-bridges and allowing them to slide past one another [314]. Sarcomeres are organized into myofibrils. Coordinated contraction of all sarcomeres along the myofibrils allow the whole muscle to contract and generate force. It is interesting to observe that the

mechanisms and molecular players regulating muscle contraction are conserved amongst many species, including *Drosophila melanogaster* [225].

During embryonic muscle development, the position of the clusters of nuclei is regulated by several proteins (see chapter 1 part II). Once clusters of nuclei have moved to their proper locations in the cell, the clusters break down into individual nuclei that spread along the muscle. However, the mechanisms that drive this step of myonuclear positioning are unknown.

We tested the hypothesis that sarcomeric contraction is involved in myonuclear dispersion. We used the *Mhc* (myosin heavy chain) mutant Mhc^{1}, which prevents contraction, and assessed myonuclear positioning in stage 16 and stage 17 embryos (Fig. 4.3.5). We observed that at stage 16 in $Mhc^{1/1}$ homozygous mutant embryos, the clusters of nuclei appeared to have the proper localization within the muscles when compared with the heterozygous $Mhc^{1/+}$ counterpart, although no quantification of nuclear spread was done at this stage. More interestingly, $Mhc^{1/1}$ embryos at stage 17 show dispersion of the myonuclei along the muscle cell. The muscle structure seems to be perturbed, which could be explained by the lack of Mhc in addition to the fixation and labelling processing. To confirm the lack of contraction in Mhc^{1} embryos, we performed time lapse microscopy and observed that embryos lacking Mhc do not contract yet have dispersed myonuclei. These results indicate that contraction is not required for myonuclear dispersion and further studies are needed to understand the mechanisms behind this step of myonuclear positioning.

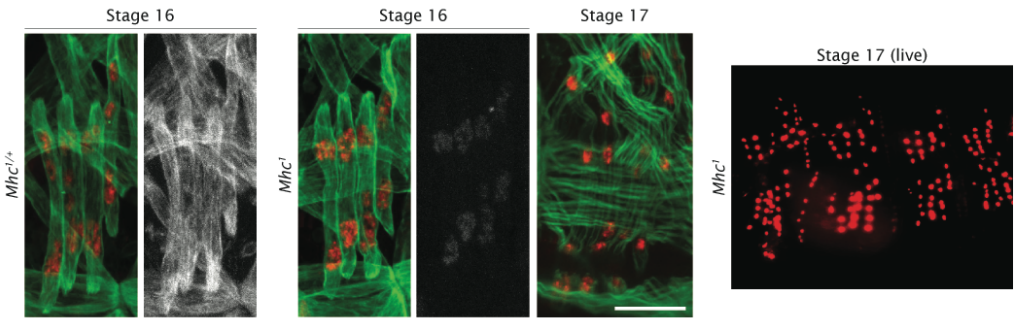


Figure 4.3.5 – Left panel: Representative images of $Mhc^{1/+}$ LT muscles. The expression of MHC is visible in gray. **Middle panel:** Representative images of fixed Mhc^{1} LT muscles at stage 16 and stage 17. The lack of MHC is visible for stage 16 (compare with the left panel). In stage 17, actin is shown in green. **Right panel:** Still image from a time lapse movie showing the dispersed myonuclei in the LT muscles. Tropomyosin, green. Nuclei, red. MHC, gray. Scale bar, 20μm.

Klp61F

During muscle development, the microtubule cytoskeletal networks experience a drastic remodulation. The microtubules nucleating from a centrosomal microtubule organizing center (MTOC) start nucleating from the nuclear envelope, forming astral MTs. In Drosophila, it is yet unknown when this process occurs. Third instar larvae show the presence of astral MTs and these structures seems to be important for maintaining the distance between nuclei, according to a recent *in silico* study [200]. Additionally, in Bsg25D overexpression larval muscles display severe nuclear positioning defects and lack the presence of astral MTs [162]. Since astral MTs seems to be important in mature muscle, we hypothesized that they could also be necessary to drive myonuclear dispersion during embryogenesis. To explore this hypothesis, we analyze Klp61F, a kinesin-5 homologue and a tetrameric motor protein that crosslinks adjacent microtubules to slide them apart or constrain them. Klp61F is essential the bipolar spindle assembly in S2 cell division, contributes for the metaphase spindle length, and in non-mitotic cells it is required for the transport pf secretory proteins from the Golgi to the cell surface [315,316]. Not knowing when the cytoskeletal rearrangements occur, our hypothesis compared the astral MTs separating nuclei to the mitotic spindle during mitosis. We considered that Klp61F could be necessary to: 1) muscle development to slide MTs allowing the (clusters of) nuclei to spread; 2) the formation of the MT asters; and 3) maintenance of the astral MTs length. We assessed myonuclear positioning at stage 16 in three individual alleles of *Klp61F* (06345, 07012 and urc-1) (Figure 4.3.6). One of the alleles, *Klp61F*^{06345}, showed very promising results as there were significant myonuclear positioning defects. Since the phenotype was somewhat similar to that of *ens*^{swo} [158], we next investigated the hypothesis that

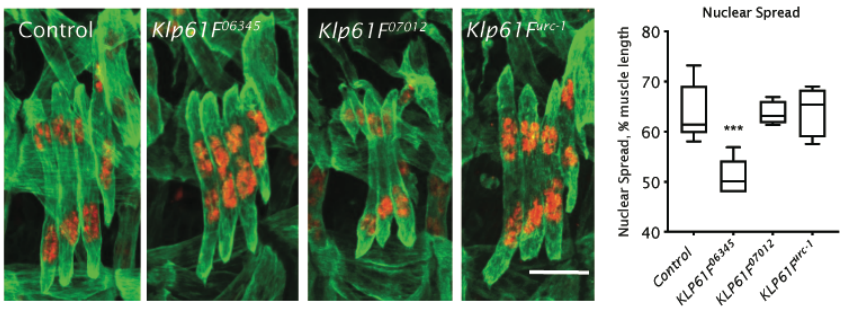


Figure 4.3.6 – Representative images of stage 16 embryonic muscles of the noted genotypes and quantification of nuclear spread as a percentage of muscle length as follows (n equals number of embryos analyzed): control, 63.70, n=6; *Klp61F*^{06345}, 51.01, n=6, *p=0.0010; *Klp61F*^{07012}, 63.64, n=4; *Klp61F*$^{urc-1}$, 64.00, n=5. Tropomyosin, green. Nuclei, red.

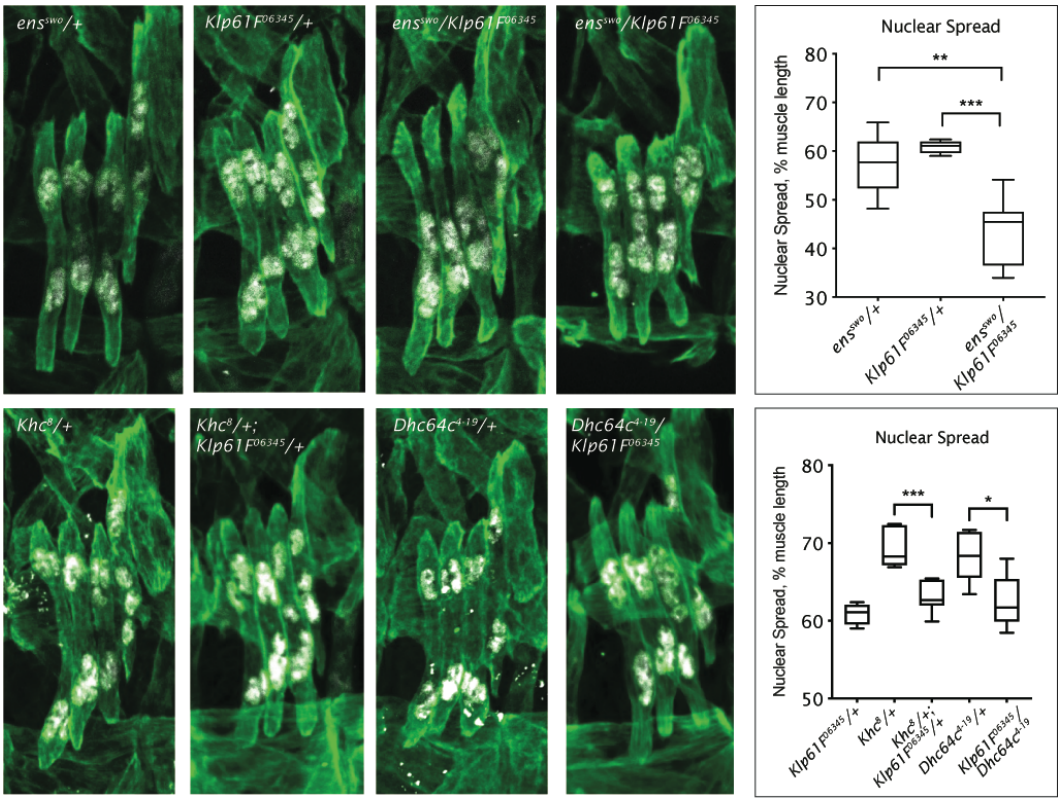


Figure 4.3.7 – Top panel: Representative images of stage 16 embryonic muscles of the noted genotypes and quantification of nuclear spread as a percentage of muscle length as follows (n equals number of embryos analyzed): *ens^{swo}/+*, 57.28, n=5; *Klp61F^{06345}/+*, 60.90, n=4; *ens^{swo}/Klp61F^{06345}*, 43.89, n=8; **p=0.0048; ***p=0.0007. Tropomyosin, green. Nuclei, white. **Bottom panel:** Representative images of stage 16 embryonic muscles of the noted genotypes and quantification of nuclear spread as a percentage of muscle length as follows (n equals number of embryos analyzed): *Klp61F^{06345}/+*, 60.90, n=4; *Khc^{8}/+*, 69.22, n=6; **p=0.0048; *Khc^{8}/+;Klp61F^{06345}/+*, 63.09, n=6; **p=0.0048; Dhc64c$^{4-19}$/+, 68.22, n=6; *Klp61F^{06345}/Dhc64c$^{4-19}$*, 62.45, n=5;*p=0.0218; ***p=0.0009. Tropomyosin, green. Nuclei, white.

Klp61F could be regulating myonuclear positioning by interacting with Ensconsin by performing genetic interaction tests (Figure 4.3.7 Top panel). Interestingly, embryos carrying one copy of *ens^{swo}* and one copy of *Klp61F^{06345}* had significantly worse nuclear spread defects than those carrying only one copy of each mutation. These data indicate that *Klp61F* and *ensconsin* genetically interact with each other to regulate myonuclear positioning. Additionally, tested the genetic interaction of *Klp61F* with two other proteins previously described in the lab, Khc and Dhc (Figure 4.3.7 Bottom panel). Since we only obtained significant differences between the *Khc* or *Dhc* with *Klp61F*, we concluded that *Klp61F* does not genetically interact with either *Khc* or *Dhc*. Although the data with allele *Klp61F^{06345}* was very promising, particularly after we identified a genetic interaction with *enconsin*, neither of the other alleles nor the muscle-specific knockdown using *Klp61F* RNAi (Figure 4.3.8 Top panel) resulted in a similar phenotype. To understand whether what we were observing was due to the

mutation in *Klp61F* or not, we performed two different experiments: we used transheterozygotes and two different deficiencies (a deficiency is a large deletion that includes several genes, often used in complementation tests) (Figure 4.3.8 Middle and bottom panel). The nuclear spread defects visible in the homozygous mutant *Klp61F*^{06345} were no longer visible when we used deficiencies that entirely removed the gene *Klp61F*, which suggested that the phenotype we observed could be due to an additional mutation the fly stock accumulated. This would also imply that the genetic interaction with *ensconsin* could be due to a different genetic mutation rather than the one on *Klp61F*. Even though we do not know if there is an additional mutation

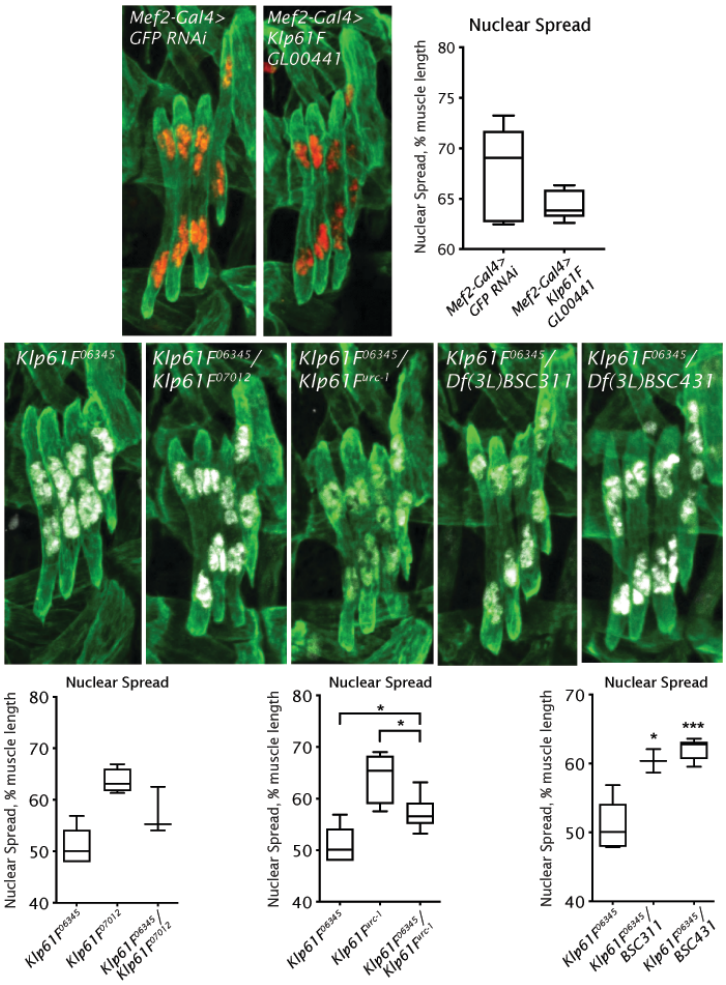


Figure 4.3.8 – Top panel: Representative images of stage 16 embryonic muscles of the noted genotypes and quantification of nuclear spread as a percentage of muscle length as follows (n equals number of embryos analyzed): *Mef2-Gal4>GFP RNAi*, 62.46, n=7; *Mef2-Gal4>Klp61F GL00441,* 60.90, n=6. Tropomyosin, green. Nuclei, red. **Middle panel:** Representative images of stage 16 embryonic muscles of the noted genotypes. Tropomyosin, green. Nuclei, white. **Bottom panel:** quantification of nuclear spread of the genotypes in the middle panel as a percentage of muscle length as follows (n equals number of embryos analyzed): *Klp61F*^{06345}, 51.01, n=6; *Klp61F*^{07012}, 63.64, n=4; *Klp61F*^{06345}*/Klp61F*^{07012}, 57.31, n=3. *Klp61F*$^{urc-1}$, 64.00, n=5; *Klp61F*^{06345}*/Klp61F*$^{urc-1}$, 57.19, n=6; *p>0.05. *Klp61F*^{06345}*/Df(3L)BSC311,* 60.36, n=2, *p=0.0161. *Klp61F*^{06345}*/Df(3L)BSC431,* 62.08, n=5, ***p=0.0001.

and if yes, in what gene, it could be very interesting to sequence the third chromosome or do a deficiency screening to discover what is genetically interacting with *ensconsin*.

Chapter 4 – Results
Part III

Chapter 5
Final Remarks

SUMMARY OF FINDINGS

In Chapter 4 Part I of this Thesis, we were interested in understanding the impact of muscle-tendon interactions on myonuclear positioning. We studied Robo1, a membrane receptor involved in the formation of the myotendinous junction. Our data revealed two novel roles of Robo1 during *Drosophila* myogenesis. We showed that loss of *robo1* leads to increased numbers of unfused myoblasts, myoblast fusion events that last longer and display actin foci with lower levels of actin, myotubes with fewer mispositioned myonuclei. These novel roles of Robo1 appear to be independent of its signaling molecule, Slit. We investigated the participation of Robo1 in the cortical pulling pathway described in previous studies and found that Robo1 involvement in myonuclear positioning seems to be independent of this pathway. Moreover, we demonstrated that the levels of Robo1 expression are important for proper muscle development. We observed that either lack or excess of Robo1 resulted in nuclear number changes and severe myonuclear positioning defects. Additionally, we described the measures we took to deal with a genetic setback and the data we gathered to confirm our findings. This work allowed us to identify a dual role for Robo1 in muscle development and to conclude that muscle-tendon interactions regulate aspects of muscle intracellular organization, such as myonuclear positioning.

In Chapter 4 Part II, we wanted to better understand the mechanisms that regulate myonuclear positioning. Ensconsin had been previously described as a regulator as this process, however little was known about how Ens promoted nuclear movement. We identified Bsg25D as a partner of Ensconsin to regulate the position on myonuclei in developing and mature myotubes. Misexpression of both *Bsg25D* and *ens* caused changes in the speed and direction of myonuclear movement in myotubes. In mature muscle cells, *Bsg25D* overexpression resulted myonuclear positioning defects, disruption of the microtubule cytoskeleton network, as well as a decrease in the overall muscle stiffness and reduced muscle function. Additionally, we demonstrated that the levels of Bsg25D have to be fine-tuned for correct muscle development and function. We showed the relevance of genetic interaction studies to discover new mechanisms and key players that regulate muscle development and myonuclear positioning, in particular. This work identified a novel regulator of myonuclear positioning and contributed to the understanding of how Ens functions to regulate the process of myonuclear movement.

Chapter 5 – Final Remarks

In Chapter 4 Part III, we showed preliminary data and demonstrated the potential of pursuing the analyses of some of the genes studied. Data obtained from looking at other MTJ genes revealed significant myonuclear positioning defects strengthening our conclusion that muscle-tendon interactions regulate the position of myonuclei during *Drosophila* myogenesis. Further knowledge on this subject is required and *derailed* and *inflated*, in particular, are good candidates to advance the knowledge on the impact of muscle-tendon interactions in aspects of intracellular organization, such as myonuclear positioning.

CONCLUSIONS

In this Thesis we have presented the work developed to achieve our main goals: 1) analyze the input of tendon cells in myonuclear movement and positioning by manipulating the MTJ to determine how tendons influence myonuclear positioning and lead to a fine tuning of muscle architecture; and 2) determine the impact of myonuclear positioning on cytoskeletal organization and muscle structure and function by analyzing mutants with myonuclear positioning defects and assessing larval muscle organization and locomotion. Our work has allowed us to expand the knowledge on muscle development in *Drosophila*, particularly in regard to the importance of muscle interactions with other cell types (i.e. tendons) for myonuclear positioning and mechanisms that regulate this process intracellularly. Additionally, it allowed us to identify a dual role for the same protein in two processes of myogenesis: myoblast fusion and myonuclear positioning. We identified a new regulator of Ensconsin, an essential player in myonuclear positioning, and expanded the knowledge on the relationship between myonuclear positioning and muscle function. Moreover, in both studies we concluded that levels of expression play an important role in the regulation of proper muscle development.

The major limitation we encountered during these studies occurred when we identified genetic issues in most of the stocks we were using in Part I of Chapter 4. Fortunately, we were able to identify the issue and confirm the validity of the majority of our data and, therefore, our conclusions remained valid.

Collectively, the data presented in this Thesis opens new avenues into studying the pathways these proteins are involved in and ask a multitude of questions related with muscle development such as: how do muscles control the number of fusion events during development? If and how does nuclear number regulate nuclear positioning? How do nuclear clusters maintain their cohesion during cluster spread? What other aspects of muscle cell organization can be regulated by muscle-tendon interactions? Can other muscle-interacting cells regulate myonuclear positioning? When do the rearrangements of the microtubule network occur during fly myogenesis?

Future studies to identify key players and mechanisms in myoblast fusion and myonuclear positioning will shed further insight into muscle development and function, as well as provide knowledge to better understand muscle dysfunction and disease.

BIBLIOGRAPHY

[1] A.M. Michelson, S.M. Abmayr, M. Bate, A.M. Arias, T. Maniatis, Expression of a MyoD family member prefigures muscle pattern in Drosophila embryos., Genes Dev. 4 (1990) 2086–2097.

[2] S.M. Abmayr, C.A. Keller, Drosophila myogenesis and insights into the role of nautilus., Curr. Top. Dev. Biol. 38 (1998) 35–80.

[3] K.C. Dobi, V.K. Schulman, M.K. Baylies, Specification of the somatic musculature in Drosophila., Wiley Interdiscip. Rev. Dev. Biol. 4 (2015) 357–375. doi:10.1002/wdev.182.

[4] M. V. Taylor, Comparison of Muscle Development in Drosophila and Vertebrates, in: Muscle Dev. Drosoph., 2007. doi:10.1007/0-387-32963-3_14.

[5] N. Azpiazu, P.A. Lawrence, J.P. Vincent, M. Frasch, Segmentation and specification of the Drosophila mesoderm., Genes Dev. 10 (1996) 3183–3194.

[6] M. Frasch, Induction of visceral and cardiac mesoderm by ectodermal Dpp in the early Drosophila embryo., Nature. 374 (1995) 464–467. doi:10.1038/374464a0.

[7] K. Staehling-Hampton, F.M. Hoffmann, M.K. Baylies, E. Rushtont, M. Bate, Dpp induces mesodermal gene expression in Drosophila, Nature. (1994). doi:10.1038/372783a0.

[8] M.K. Baylies, M. Bate, M.R. Gomez, Myogenesis: A view from Drosophila, Cell. 93 (1998) 921–927. doi:10.1016/S0092-8674(00)81198-8.

[9] A. Carmena, M. Bate, F. Jimenez, Lethal of scute, a proneural gene, participates in the specification of muscle progenitors during Drosophila embryogenesis., Genes Dev. 9 (1995) 2373–2383.

[10] A. Carmena, B. Murugasu-Oei, D. Menon, F. Jimenez, W. Chia, Inscuteable and numb mediate asymmetric muscle progenitor cell divisions during Drosophila myogenesis., Genes Dev. 12 (1998) 304–315.

[11] S. Fuerstenberg, E. Giniger, Multiple roles for notch in Drosophila myogenesis., Dev. Biol. 201 (1998) 66–77. doi:10.1006/dbio.1998.8944.

[12] A. Carmena, S. Gisselbrecht, J. Harrison, F. Jiménez, A.M. Michelson, Combinatorial signaling codes for the progressive determination of cell fates in the Drosophila embryonic mesoderm, Genes Dev. (1998). doi:10.1101/gad.12.24.3910.

[13] M. Ruiz Gomez, M. Bate, Segregation of myogenic lineages in Drosophila requires numb., Development. 124 (1997) 4857–4866.

[14] K.C. Dobi, M.S. Halfon, M.K. Baylies, Whole-genome analysis of muscle founder cells implicates the chromatin regulator Sin3A in muscle identity, Cell Rep. (2014). doi:10.1016/j.celrep.2014.07.005.

[15] M.J. Boyle, C.A. Berg, Control in time and space: Tramtrack69 cooperates with notch and ecdysone to repress ectopic fate and shape changes during Drosophila egg chamber maturation, Development. (2009). doi:10.1242/dev.042770.

[16] L. Bataille, H. Boukhatmi, J.-L. Frendo, A. Vincent, Dynamics of transcriptional (re)-programming of syncytial nuclei in developing muscles., BMC Biol. 15 (2017) 48. doi:10.1186/s12915-017-0386-2.

[17] C. Bourgouin, S.E. Lundgren, J.B. Thomas, apterous is a drosophila LIM domain gene required for the development of a subset of embryonic muscles, Neuron. (1992). doi:10.1016/0896-6273(92)90192-G.

[18] C. Dohrmann, N. Azpiazu, M. Frasch, A new Drosophila homeo box gene is expressed in mesodermal precursor cells of distinct muscles during embryogenesis, Genes Dev. (1990). doi:10.1101/gad.4.12a.2098.

[19] T. Jagla, F. Bellard, Y. Lutz, G. Dretzen, M. Bellard, K. Jagla, Ladybird determines cell fate decisions during diversification of Drosophila somatic muscles, Development. (1998).

[20] K. Beckett, M.K. Baylies, 3D analysis of founder cell and fusion competent myoblast arrangements outlines a new model of myoblast fusion, Dev. Biol. (2007). doi:10.1016/j.ydbio.2007.06.024.

[21] B.E. Richardson, K. Beckett, M.K. Baylies, Live imaging of Drosophila myoblast fusion, Methods Mol. Biol. (2008). doi:10.1007/978-1-59745-250-2_15.

[22] M. Peckham, J.E. Molloy, J.C. Sparrow, D.C. White, Physiological properties of the dorsal

longitudinal flight muscle and the tergal depressor of the trochanter muscle of Drosophila melanogaster., J. Muscle Res. Cell Motil. 11 (1990) 203–215.
[23] A. Ghazi, S. Anant, K. VijayRaghavan, Apterous mediates development of direct flight muscles autonomously and indirect flight muscles through epidermal cues, Development. (2000).
[24] V. Sudarsan, S. Anant, P. Guptan, K. Vijayraghavan, H. Skaer, Myoblast Diversification and Ectodermal Signaling in Drosophila, Dev. Cell. (2001). doi:10.1016/S1534-5807(01)00089-2.
[25] H. Deng, S.C. Hughes, J.B. Bell, A.J. Simmonds, Alternative requirements for vestigial, scalloped, and Dmef2 during muscle differentiation in drosophila melanogaster, Mol. Biol. Cell. (2009). doi:10.1091/mbc.E08-03-0288.
[26] C. Schönbauer, J. Distler, N. Jährling, M. Radolf, H.U. Dodt, M. Frasch, F. Schnorrer, Spalt mediates an evolutionarily conserved switch to fibrillar muscle fate in insects, Nature. (2011). doi:10.1038/nature10559.
[27] T. Maqbool, C. Soler, T. Jagla, M. Daczewska, N. Lodha, S. Palliyil, K. VijayRaghavan, K. Jagla, Shaping leg muscles in Drosophila: Role of landybird, a conserved regulator of appendicular myogenesis, PLoS One. (2006). doi:10.1371/journal.pone.0000122.
[28] S. Roy, K. VijayRaghavan, Muscle pattern diversification in Drosophila: The story of imaginal myogenesis, BioEssays. (1999). doi:10.1002/(SICI)1521-1878(199906)21:6<486::AID-BIES5>3.0.CO;2-M.
[29] A.E. Munsterberg, J. Kitajewski, D.A. Bumcrot, A.P. McMahon, A.B. Lassar, Combinatorial signaling by Sonic hedgehog and Wnt family members induces myogenic bHLH gene expression in the somite., Genes Dev. 9 (1995) 2911–2922.
[30] R.J. Bryson-Richardson, P.D. Currie, The genetics of vertebrate myogenesis, Nat. Rev. Genet. (2008). doi:10.1038/nrg2369.
[31] D. Duprez, C. Fournier-Thibault, N. Le Douarin, Sonic Hedgehog induces proliferation of committed skeletal muscle cells in the chick limb., Development. 125 (1998) 495–505.
[32] F. Relaix, D. Rocancourt, A. Mansouri, M. Buckingham, A Pax3/Pax7-dependent population of skeletal muscle progenitor cells., Nature. 435 (2005) 948–953. doi:10.1038/nature03594.
[33] T. Sato, D. Rocancourt, L. Marques, S. Thorsteinsdottir, M. Buckingham, A Pax3/Dmrt2/Myf5 regulatory cascade functions at the onset of myogenesis., PLoS Genet. 6 (2010) e1000897. doi:10.1371/journal.pgen.1000897.
[34] M. Maroto, R. Reshef, A.E. Münsterberg, S. Koester, M. Goulding, A.B. Lassar, Ectopic Pax-3 activates MyoD and Myf-5 expression in embryonic mesoderm and neural tissue, Cell. (1997). doi:10.1016/S0092-8674(00)80190-7.
[35] M.A. Rudnicki, P.N. Schnegelsberg, R.H. Stead, T. Braun, H.H. Arnold, R. Jaenisch, MyoD or Myf-5 is required for the formation of skeletal muscle., Cell. 75 (1993) 1351–1359.
[36] P. Hasty, A. Bradley, J.H. Morris, D.G. Edmondson, J.M. Venuti, E.N. Olson, W.H. Klein, Muscle deficiency and neonatal death in mice with a targeted mutation in the myogenin gene., Nature. 364 (1993) 501–506. doi:10.1038/364501a0.
[37] L. Kassar-Duchossoy, B. Gayraud-Morel, D. Gomes, D. Rocancourt, M. Buckingham, V. Shinin, S. Tajbakhsh, Mrf4 determines skeletal muscle identity in Myf5:Myod double-mutant mice., Nature. 431 (2004) 466–471. doi:10.1038/nature02876.
[38] E. Dodou, S.-M. Xu, B.L. Black, mef2c is activated directly by myogenic basic helix-loop-helix proteins during skeletal muscle development in vivo., Mech. Dev. 120 (2003) 1021–1032.
[39] J.D. Molkentin, B.L. Black, J.F. Martin, E.N. Olson, Cooperative activation of muscle gene expression by MEF2 and myogenic bHLH proteins., Cell. 83 (1995) 1125–1136.
[40] B. Lilly, S. Galewsky, A.B. Firulli, R.A. Schulz, E.N. Olson, D-MEF2: A MADS box transcription factor expressed in differentiating mesoderm and muscle cell lineages during Drosophila embryogenesis, Proc. Natl. Acad. Sci. U. S. A. (1994). doi:10.1073/pnas.91.12.5662.
[41] A.J. Harris, M.J. Duxson, R.B. Fitzsimons, F. Rieger, Myonuclear birthdates distinguish the origins of primary and secondary myotubes in embryonic mammalian skeletal muscles, Development. (1989).
[42] K. Rochlin, S. Yu, S. Roy, M.K. Baylies, Myoblast fusion: when it takes more to make one., Dev. Biol. 341 (2010) 66–83. doi:10.1016/j.ydbio.2009.10.024.

[43] M. Ruiz-Gómez, N. Coutts, A. Price, M. V. Taylor, M. Bate, Drosophila dumbfounded: A myoblast attractant essential for fusion, Cell. (2000). doi:10.1016/S0092-8674(00)00024-6.
[44] M. Strünkelnberg, B. Bonengel, L.M. Moda, A. Hertenstein, H. Gert de Couet, R.G.P. Ramos, K.F. Fischbach, Rst and its paralogue kirre act redundantly during embryonic muscle development in Drosophila, Development. (2001).
[45] R.D. Artero, I. Castanon, M.K. Baylies, The immunoglobulin-like protein hibris functions as a dose-dependent regulator of myoblast fusion and is differentially controlled by Ras and Notch signaling, Development. (2001).
[46] B.A. Bour, M. Chakravarti, J.M. West, S.M. Abmayr, Drosophila SNS, a member of the immunoglobulin superfamily that is essential for myoblast fusion, Genes Dev. (2000). doi:10.1101/gad.14.12.1498.
[47] C. Shelton, K.S. Kocherlakota, S. Zhuang, S.M. Abmayr, The immunoglobulin superfamily member Hbs functions redundantly with Sns in interactions between founder and fusion-competent myoblasts, Development. (2009). doi:10.1242/dev.026302.
[48] S. Bao, K.F. Fischbach, V. Corbin, R.L. Cagan, Preferential adhesion maintains separation of ommatidia in the Drosophila eye, Dev. Biol. (2010). doi:10.1016/j.ydbio.2010.06.013.
[49] R.G.P. Ramos, G.L. Igloi, B. Lichte, U. Baumann, D. Maier, T. Schneider, J.H. Brandstatter, A. Frohlich, K.F. Fischbach, The irregular chiasm C-roughest locus of Drosophila, which affects axonal projections and programmed cell death, encodes a novel immunoglobulin-like protein, Genes Dev. (1993). doi:10.1101/gad.7.12b.2533.
[50] B.E. Richardson, K. Beckett, S.J. Nowak, M.K. Baylies, SCAR/WAVE and Arp2/3 are crucial for cytoskeletal remodeling at the site of myoblast fusion, Development. 134 (2007) 4357–4367. doi:10.1242/dev.010678.
[51] C. Dottermusch-Heidel, V. Groth, L. Beck, S.-F. Onel, The Arf-GEF Schizo/Loner regulates N-cadherin to induce fusion competence of Drosophila myoblasts., Dev. Biol. 368 (2012) 18–27. doi:10.1016/j.ydbio.2012.04.031.
[52] J. Hamp, A. Lower, C. Dottermusch-Heidel, L. Beck, B. Moussian, M. Flotenmeyer, S.-F. Onel, Drosophila Kette coordinates myoblast junction dissolution and the ratio of Scar-to-WASp during myoblast fusion., J. Cell Sci. 129 (2016) 3426–3436. doi:10.1242/jcs.175638.
[53] S.F. Onel, M.B. Rust, R. Jacob, R. Renkawitz-Pohl, Tethering membrane fusion: common and different players in myoblasts and at the synapse., J. Neurogenet. 28 (2014) 302–315. doi:10.3109/01677063.2014.936014.
[54] C.A. Charlton, W.A. Mohler, G.L. Radice, R.O. Hynes, H.M. Blau, Fusion competence of myoblasts rendered genetically null for N-cadherin in culture., J. Cell Biol. 138 (1997) 331–336.
[55] K.L. Sens, S. Zhang, P. Jin, R. Duan, G. Zhang, F. Luo, L. Parachini, E.H. Chen, An invasive podosome-like structure promotes fusion pore formation during myoblast fusion, J. Cell Biol. 191 (2010) 1013 LP – 1027. http://jcb.rupress.org/content/191/5/1013.abstract.
[56] J.H. Kim, Y. Ren, W.P. Ng, S. Li, S. Son, Y.-S. Kee, S. Zhang, G. Zhang, D.A. Fletcher, D.N. Robinson, E.H. Chen, Mechanical tension drives cell membrane fusion., Dev. Cell. 32 (2015) 561–573. doi:10.1016/j.devcel.2015.01.005.
[57] B.R. Kaipa, H. Shao, G. Schäfer, T. Trinkewitz, V. Groth, J. Liu, L. Beck, S. Bogdan, S.M. Abmayr, S.F. Önel, Dock mediates Scar- and WASp-dependent actin polymerization through interaction with cell adhesion molecules in founder cells and fusion-competent myoblasts, J. Cell Sci. (2013). doi:10.1242/jcs.113860.
[58] K.S. Kocherlakota, J.-M. Wu, J. McDermott, S.M. Abmayr, Analysis of the cell adhesion molecule sticks-and-stones reveals multiple redundant functional domains, protein-interaction motifs and phosphorylated tyrosines that direct myoblast fusion in Drosophila melanogaster, Genetics. 178 (2008) 1371–1383. doi:10.1534/genetics.107.083808.
[59] S. Kim, K. Shilagardi, S. Zhang, S.N. Hong, K.L. Sens, J. Bo, G.A. Gonzalez, E.H. Chen, A Critical Function for the Actin Cytoskeleton in Targeted Exocytosis of Prefusion Vesicles during Myoblast Fusion, Dev. Cell. (2007). doi:10.1016/j.devcel.2007.02.019.
[60] S.D. Menon, Z. Osman, K. Chenchill, W. Chia, A positive feedback loop between dumbfounded and rolling pebbles leads to myotube enlargement in Drosophila, J. Cell

Biol. (2005). doi:10.1083/jcb.200501126.
[61] E.H. Chen, E.N. Olson, Antisocial, an Intracellular Adaptor Protein, Is Required for Myoblast Fusion in Drosophila, Dev. Cell. (2001). doi:10.1016/S1534-5807(01)00084-3.
[62] A. Rau, D. Buttgereit, A. Holz, R. Fetter, S.K. Doberstein, A. Paululat, N. Staudt, J. Skeath, A.M. Michelson, R. Renkawitz-Pohl, Rolling pebbles (rols) is required in Drosophila muscle precursors for recruitment of myoblasts for fusion, Development. (2001).
[63] S. Haralalka, C. Shelton, H.N. Cartwright, E. Katzfey, E. Janzen, S.M. Abmayr, Asymmetric Mbc, active Rac1 and F-actin foci in the fusioncompetent myoblasts during myoblast fusion in Drosophila, Development. (2011). doi:10.1242/dev.057653.
[64] Y. Zhang, D. Featherstone, W. Davis, E. Rushton, K. Broadie, Drosophila D-titin is required for myoblast fusion and skeletal muscle striation., J. Cell Sci. 113 (Pt 1 (2000) 3103–3115.
[65] S. Bulchand, S.D. Menon, S.E. George, W. Chia, The intracellular domain of dumbfounded affects myoblast fusion efficiency and interacts with rolling pebbles and loner, PLoS One. (2010). doi:10.1371/journal.pone.0009374.
[66] S.K. Doberstein, R.D. Fetter, A.Y. Mehta, C.S. Goodman, Genetic analysis of myoblast fusion: Blown fuse is required for progression beyond the prefusion complex, J. Cell Biol. (1997). doi:10.1083/jcb.136.6.1249.
[67] P. Jin, R. Duan, F. Luo, G. Zhang, S.N. Hong, E.H. Chen, Competition between blown fuse and WASP for WIP binding regulates the dynamics of WASP-dependent actin polymerization in vivo, Dev. Cell. (2011). doi:10.1016/j.devcel.2011.04.007.
[68] L. Balagopalan, M.-H. Chen, E.R. Geisbrecht, S.M. Abmayr, The CDM Superfamily Protein MBC Directs Myoblast Fusion through a Mechanism That Requires Phosphatidylinositol 3,4,5-Triphosphate Binding but Is Independent of Direct Interaction with DCrk, Mol. Cell. Biol. (2006). doi:10.1128/mcb.00016-06.
[69] B.J. Galletta, X.P. Niu, M.R.S. Erickson, S.M. Abmayr, Identification of a Drosophila homologue to vertebrate Crk by interaction with MBC, Gene. (1999). doi:10.1016/S0378-1119(99)00010-4.
[70] S. Deng, I. Bothe, M.K. Baylies, The Formin Diaphanous Regulates Myoblast Fusion through Actin Polymerization and Arp2/3 Regulation, PLoS Genet. 11 (2015) 1–29. doi:10.1371/journal.pgen.1005381.
[71] E.H. Chen, B.A. Pryce, J.A. Tzeng, G.A. Gonzalez, E.N. Olson, Control of myoblast fusion by a guanine nucleotide exchange factor, loner, and its effector ARF6, Cell. 114 (2003) 751–762. doi:10.1016/S0092-8674(03)00720-7.
[72] M.R.S. Erickson, B.J. Galletta, S.M. Abmayr, Drosophila myoblast city encodes a conserved protein that is essential for myoblast fusion, dorsal closure, and cytoskeletal organization, J. Cell Biol. (1997). doi:10.1083/jcb.138.3.589.
[73] I. Bothe, S. Deng, M. Baylies, PI(4,5)P2 regulates myoblast fusion through Arp2/3 regulator localization at the fusion site., Development. 141 (2014) 2289–2301. doi:10.1242/dev.100743.
[74] S. Hakeda-Suzuki, J. Ng, J. Tzu, G. Dietzl, Y. Sun, M. Harms, T. Nardine, L. Luo, B.J. Dickson, Rac function and regulation during Drosophila development, Nature. (2002). doi:10.1038/416438a.
[75] B. Estrada, A.D. Maeland, S.S. Gisselbrecht, J.W. Bloor, N.H. Brown, A.M. Michelson, The MARVEL domain protein, Singles Bar, is required for progression past the pre-fusion complex stage of myoblast fusion, Dev. Biol. (2007). doi:10.1016/j.ydbio.2007.04.045.
[76] R. Massarwa, S. Carmon, B.Z. Shilo, E.D. Schejter, WIP/WASp-Based Actin-Polymerization Machinery Is Essential for Myoblast Fusion in Drosophila, Dev. Cell. 12 (2007) 557–569. doi:10.1016/j.devcel.2007.01.016.
[77] G. Schäfer, S. Weber, A. Holz, S. Bogdan, S. Schumacher, A. Müller, R. Renkawitz-Pohl, S.F. Önel, The Wiskott-Aldrich syndrome protein (WASP) is essential for myoblast fusion in Drosophila, Dev. Biol. (2007). doi:10.1016/j.ydbio.2007.01.015.
[78] K. Brinkmann, M. Winterhoff, S.F. Önel, J. Schultz, J. Faix, S. Bogdan, WHAMY is a novel actin polymerase promoting myoblast fusion, macrophage cell motility and sensory organ development in Drosophila, J. Cell Sci. (2016). doi:10.1242/jcs.179325.
[79] N. Dyer, E. Rebollo, P. Domínguez, N. Elkhatib, P. Chavrier, L. Daviet, C. González, M. González-Gaitán, Spermatocyte cytokinesis requires rapid membrane addition mediated by ARF6 on central spindle recycling endosomes, Development. (2007).

doi:10.1242/dev.010983.
[80] S. Eden, R. Rohatgi, A. V. Podtelejnikov, M. Mann, M.W. Kirschner, Mechanism of regulation of WAVE1-induced actin nucleation by Rac1 and Nck, Nature. (2002). doi:10.1038/nature00859.
[81] Z. Chen, D. Borek, S.B. Padrick, T.S. Gomez, Z. Metlagel, A.M. Ismail, J. Umetani, D.D. Billadeau, Z. Otwinowski, M.K. Rosen, Structure and control of the actin regulatory WAVE complex, Nature. (2010). doi:10.1038/nature09623.
[82] B. Gildor, R. Massarwa, B.Z. Shilo, E.D. Schejter, The SCAR and WASp nucleation-promoting factors act sequentially to mediate Drosophila myoblast fusion, EMBO Rep. (2009). doi:10.1038/embor.2009.129.
[83] S. Deng, I. Bothe, M. Baylies, Diaphanous regulates SCAR complex localization during Drosophila myoblast fusion., Fly (Austin). 10 (2016) 178–186. doi:10.1080/19336934.2016.1195938.
[84] E.R. Geisbrecht, S. Haralalka, S.K. Swanson, L. Florens, M.P. Washburn, S.M. Abmayr, Drosophila ELMO/CED-12 interacts with Myoblast city to direct myoblast fusion and ommatidial organization, Dev. Biol. (2008). doi:10.1016/j.ydbio.2007.11.022.
[85] N. Ramesh, R. Geha, Recent advances in the biology of WASP and WIP, Immunol. Res. (2009). doi:10.1007/s12026-008-8086-1.
[86] S. Haralalka, C. Shelton, H.N. Cartwright, F. Guo, R. Trimble, R.P. Kumar, S.M. Abmayr, Live imaging provides new insights on dynamic F-actin filopodia and differential endocytosis during myoblast fusion in Drosophila., PLoS One. 9 (2014) e114126. doi:10.1371/journal.pone.0114126.
[87] W.A. Mohler, G. Shemer, J.J. Del Campo, C. Valansi, E. Opoku-Serebuoh, V. Scranton, N. Assaf, J.G. White, B. Podbilewicz, The type 1 membrane protein EFF-1 is essential for developmental cell fusion, Dev. Cell. (2002). doi:10.1016/S1534-5807(02)00129-6.
[88] A. Sapir, O. Avinoam, B. Podbilewicz, L. V. Chernomordik, Viral and Developmental Cell Fusion Mechanisms: Conservation and Divergence, Dev. Cell. (2008). doi:10.1016/j.devcel.2007.12.008.
[89] S.F. Önel, R. Renkawitz-Pohl, FuRMAS: Triggering myoblast fusion in Drosophila, Dev. Dyn. (2009). doi:10.1002/dvdy.21961.
[90] V.K. Schulman, K.C. Dobi, M.K. Baylies, Morphogenesis of the somatic musculature in Drosophila melanogaster, Wiley Interdiscip. Rev. Dev. Biol. 4 (2015) 313–334. doi:10.1002/wdev.180.
[91] E.D. Schejter, Myoblast fusion: Experimental systems and cellular mechanisms, Semin. Cell Dev. Biol. (2016). doi:10.1016/j.semcdb.2016.07.016.
[92] N. Dhanyasi, D. Segal, E. Shimoni, V. Shinder, B.Z. Shilo, K. VijayRaghavan, E.D. Schejter, Surface apposition and multiple cell contacts promote myoblast fusion in Drosophila flight muscles, J. Cell Biol. (2015). doi:10.1083/jcb.201503005.
[93] J. Fernandes, M. Bate, K. Vijayraghavan, Development of the indirect flight muscles of Drosophila, Development. (1991).
[94] R.D. Gunage, H. Reichert, K. VijayRaghavan, Identification of a new stem cell population that generates Drosophila flight muscles, Elife. (2014). doi:10.7554/eLife.03126.
[95] R. Aradhya, M. Zmojdzian, J.P. da Ponte, K. Jagla, Muscle niche-driven Insulin-Notch-Myc cascade reactivates dormant adult muscle precursors in drosophila, Elife. (2015). doi:10.7554/eLife.08497.
[96] B. Gildor, E.D. Schejter, B.Z. Shilo, Bidirectional Notch activation represses fusion competence in swarming adult Drosophila myoblasts, Dev. (2012). doi:10.1242/dev.077495.
[97] P. Mukherjee, B. Gildor, B.Z. Shilo, K. Vijayraghavan, E.D. Schejter, The actin nucleator WASp is required for myoblast fusion during adult Drosophila myogenesis, Development. (2011). doi:10.1242/dev.055012.
[98] T.M. Brunetti, B.J. Fremin, R.M. Cripps, Identification of singles bar as a direct transcriptional target of Drosophila Myocyte enhancer factor-2 and a regulator of adult myoblast fusion, Dev. Biol. (2015). doi:10.1016/j.ydbio.2015.02.026.
[99] D. Segal, N. Dhanyasi, E.D. Schejter, B.-Z. Shilo, Adhesion and Fusion of Muscle Cells Are Promoted by Filopodia., Dev. Cell. 38 (2016) 291–304. doi:10.1016/j.devcel.2016.07.010.
[100] A.R. Demonbreun, B.H. Biersmith, E.M. McNally, Membrane fusion in muscle development and repair., Semin. Cell Dev. Biol. 45 (2015) 48–56.

doi:10.1016/j.semcdb.2015.10.026.
[101] G.D. Rosen, J.R. Sanes, R. LaChance, J.M. Cunningham, J. Roman, D.C. Dean, Roles for the integrin VLA-4 and its counter receptor VCAM-1 in myogenesis, Cell. (1992). doi:10.1016/0092-8674(92)90633-N.
[102] V. Horsley, K.M. Jansen, S.T. Mills, G.K. Pavlath, IL-4 acts as a myoblast recruitment factor during mammalian muscle growth, Cell. (2003). doi:10.1016/S0092-8674(03)00319-2.
[103] G.T. Powell, G.J. Wright, Jamb and jamc are essential for vertebrate myocyte fusion., PLoS Biol. 9 (2011) e1001216. doi:10.1371/journal.pbio.1001216.
[104] C. Sedwick, Jamb and jamc muscle in on myoblast fusion., PLoS Biol. 9 (2011) e1001217. doi:10.1371/journal.pbio.1001217.
[105] R.L. Sohn, P. Huang, G. Kawahara, M. Mitchell, J. Guyon, R. Kalluri, L.M. Kunkel, E. Gussoni, A role for nephrin, a renal protein, in vertebrate skeletal muscle cell fusion, Proc. Natl. Acad. Sci. U. S. A. (2009). doi:10.1073/pnas.0904398106.
[106] B.P. Srinivas, J. Woo, W.Y. Leong, S. Roy, A conserved molecular pathway mediates myoblast fusion in insects and vertebrates, Nat. Genet. (2007). doi:10.1038/ng2055.
[107] A. Hollnagel, C. Grund, W.W. Franke, H.-H. Arnold, The Cell Adhesion Molecule M-Cadherin Is Not Essential for Muscle Development and Regeneration, Mol. Cell. Biol. (2002). doi:10.1128/mcb.22.13.4760-4770.2002.
[108] G.L. Radice, H. Rayburn, H. Matsunami, K.A. Knudsen, M. Takeichi, R.O. Hynes, Developmental defects in mouse embryos lacking N-cadherin, Dev. Biol. (1997). doi:10.1006/dbio.1996.8443.
[109] M. Schwander, M. Leu, M. Stumm, O.M. Dorchies, U.T. Ruegg, J. Schittny, U. Müller, β1 integrins regulate myoblast fusion and sarcomere assembly, Dev. Cell. (2003). doi:10.1016/S1534-5807(03)00118-7.
[110] A.E. Hochreiter-Hufford, C.S. Lee, J.M. Kinchen, J.D. Sokolowski, S. Arandjelovic, J.A. Call, A.L. Klibanov, Z. Yan, J.W. Mandell, K.S. Ravichandran, Phosphatidylserine receptor BAI1 and apoptotic cells as new promoters of myoblast fusion, Nature. (2013). doi:10.1038/nature12135.
[111] N. Hamoud, V. Tran, L.P. Croteau, A. Kania, J.F. Côté, G-protein coupled receptor BAI3 promotes myoblast fusion in vertebrates, Proc. Natl. Acad. Sci. U. S. A. (2014). doi:10.1073/pnas.1313886111.
[112] M. Laurin, N. Fradet, A. Blangy, A. Hall, K. Vuori, J.F. Côté, The atypical Rac activator Dock180 (Dock1) regulates myoblast fusion in vivo, Proc. Natl. Acad. Sci. U. S. A. (2008). doi:10.1073/pnas.0805546105.
[113] A. Zolkiewska, Disintegrin-like/cysteine-rich region of ADAM 12 is an active cell adhesion domain, Exp. Cell Res. (1999). doi:10.1006/excr.1999.4632.
[114] M.F. Galliano, C. Huet, J. Frygelius, A. Polgren, U.M. Wewer, E. Engvall, Binding of ADAM12, a marker of skeletal muscle regeneration, to the muscle-specific actin-binding protein, α-actinin-2, is required for myoblast fusion, J. Biol. Chem. (2000). doi:10.1074/jbc.275.18.13933.
[115] F. Galbiati, D. Volonté, J.A. Engelman, P.E. Scherer, M.P. Lisanti, Targeted Down-regulation of Caveolin-3 Is Sufficient to Inhibit Myotube Formation in Differentiating C2C12 Myoblasts, J. Biol. Chem. (1999). doi:10.1074/jbc.274.42.30315.
[116] D. Volonte, A.J. Peoples, F. Galbiati, Modulation of myoblast fusion by caveolin-3 in dystrophic skeletal muscle cells: Implications for Duchenne muscular dystrophy and Limb-girdle muscular dystrophy-1C, Mol. Biol. Cell. (2003). doi:10.1091/mbc.E03-03-0161.
[117] E. Vasyutina, B. Martarelli, C. Brakebusch, H. Wende, C. Birchmeier, The small G-proteins Rac1 and Cdc42 are essential for myoblast fusion in the mouse, Proc. Natl. Acad. Sci. U. S. A. (2009). doi:10.1073/pnas.0902501106.
[118] D. Baas, S. Caussanel-Boude, A. Guiraud, F. Calhabeu, E. Delaune, F. Pilot, E. Chopin, I. Machuca-Gayet, A. Vernay, S. Bertrand, J.F. Rual, P. Jurdic, D.E. Hill, M. Vidal, L. Schaeffer, E. Goillot, CKIP-1 regulates mammalian and zebrafish myoblast fusion, J. Cell Sci. (2012). doi:10.1242/jcs.101048.
[119] C.A. Moore, C.A. Parkin, Y. Bidet, P.W. Ingham, A role for the Myoblast city homologues Dock1 and Dock5 and the adaptor proteins Crk and Crk-like in zebrafish myoblast fusion, Development. (2007). doi:10.1242/dev.001214.
[120] K.R. Doherty, A.R. Demonbreun, G.Q. Wallace, A. Cave, A.D. Posey, K. Heretis, P. Pytel,

E.M. McNally, The endocytic recycling protein EHD2 interacts with myoferlin to regulate myoblast fusion, J. Biol. Chem. (2008). doi:10.1074/jbc.M802306200.
[121] P. Bi, A. Ramirez-Martinez, H. Li, J. Cannavino, J.R. McAnally, J.M. Shelton, E. Sanchez-Ortiz, R. Bassel-Duby, E.N. Olson, Control of muscle formation by the fusogenic micropeptide myomixer., Science. 356 (2017) 323–327. doi:10.1126/science.aam9361.
[122] M.E. Quinn, Q. Goh, M. Kurosaka, D.G. Gamage, M.J. Petrany, V. Prasad, D.P. Millay, Myomerger induces fusion of non-fusogenic cells and is required for skeletal muscle development., Nat. Commun. 8 (2017) 15665. doi:10.1038/ncomms15665.
[123] Q. Zhang, A.A. Vashisht, J. O'Rourke, S.Y. Corbel, R. Moran, A. Romero, L. Miraglia, J. Zhang, E. Durrant, C. Schmedt, S.C. Sampath, S.C. Sampath, The microprotein Minion controls cell fusion and muscle formation, Nat. Commun. (2017). doi:10.1038/ncomms15664.
[124] S. Charrasse, F. Comunale, Y. Grumbach, F. Poulat, A. Blangy, C. Gauthier-Rouvière, RhoA GTPase regulates M-cadherin activity and myoblast fusion, Mol. Biol. Cell. (2006). doi:10.1091/mbc.E05-04-0284.
[125] C.A. Griffin, K.A. Kafadar, G.K. Pavlath, MOR23 Promotes Muscle Regeneration and Regulates Cell Adhesion and Migration, Dev. Cell. (2009). doi:10.1016/j.devcel.2009.09.004.
[126] K.R. Doherty, A. Cave, D.B. Davis, A.J. Delmonte, A. Posey, J.U. Early, M. Hadhazy, E.M. McNally, Normal myoblast fusion requires myoferlin, Development. (2005). doi:10.1242/dev.02155.
[127] A. Landemaine, P.-Y. Rescan, J.-C. Gabillard, Myomaker mediates fusion of fast myocytes in zebrafish embryos., Biochem. Biophys. Res. Commun. 451 (2014) 480–484. doi:10.1016/j.bbrc.2014.07.093.
[128] W. Luo, E. Li, Q. Nie, X. Zhang, Myomaker, Regulated by MYOD, MYOG and miR-140-3p, Promotes Chicken Myoblast Fusion., Int. J. Mol. Sci. 16 (2015) 26186–26201. doi:10.3390/ijms161125946.
[129] D.P. Millay, J.R. O'Rourke, L.B. Sutherland, S. Bezprozvannaya, J.M. Shelton, R. Bassel-Duby, E.N. Olson, Myomaker is a membrane activator of myoblast fusion and muscle formation., Nature. 499 (2013) 301–305. doi:10.1038/nature12343.
[130] W. Zhang, S. Roy, Myomaker is required for the fusion of fast-twitch myocytes in the zebrafish embryo., Dev. Biol. 423 (2017) 24–33. doi:10.1016/j.ydbio.2017.01.019.
[131] Y. Gruenbaum-Cohen, I. Harel, K.B. Umansky, E. Tzahor, S.B. Snapper, B.Z. Shilo, E.D. Schejter, The actin regulator N-WASp is required for muscle-cell fusion in mice, Proc. Natl. Acad. Sci. U. S. A. (2012). doi:10.1073/pnas.1116065109.
[132] D. Sieiro, N. Véron, C. Marcelle, The chicken embryo as an efficient model to test the function of muscle fusion genes in amniotes, PLoS One. (2017). doi:10.1371/journal.pone.0177681.
[133] S.Y. Park, Y. Yun, J.S. Lim, M.J. Kim, S.Y. Kim, J.E. Kim, I.S. Kim, Stabilin-2 modulates the efficiency of myoblast fusion during myogenic differentiation and muscle regeneration, Nat. Commun. (2016). doi:10.1038/ncomms10871.
[134] F.J. Conti, S.J. Monkley, M.R. Wood, D.R. Critchley, U. Müller, Talin 1 and 2 are required for myoblast fusion, sarcomere assembly and the maintenance of myotendinous junctions, Development. (2009). doi:10.1242/dev.035857.
[135] S.J. Nowak, P.C. Nahirney, A.K. Hadjantonakis, M.K. Baylies, Nap1-mediated actin remodeling is essential for mammalian myoblast fusion, J. Cell Sci. (2009). doi:10.1242/jcs.047597.
[136] R. Duan, P.J. Gallagher, Dependence of myoblast fusion on a cortical actin wall and nonmuscle myosin IIA, Dev. Biol. (2009). doi:10.1016/j.ydbio.2008.10.035.
[137] D.P. Millay, L.B. Sutherland, R. Bassel-Duby, E.N. Olson, Myomaker is essential for muscle regeneration., Genes Dev. 28 (2014) 1641–1646. doi:10.1101/gad.247205.114.
[138] S.A. Di Gioia, S. Connors, N. Matsunami, J. Cannavino, M.F. Rose, N.M. Gilette, P. Artoni, N.L. De Macena Sobreira, W.M. Chan, B.D. Webb, C.D. Robson, L. Cheng, C. Van Ryzin, A. Ramirez-Martinez, P. Mohassel, M. Leppert, M.B. Scholand, C. Grunseich, C.R. Ferreira, T. Hartman, I.M. Hayes, T. Morgan, D.M. Markie, M. Fagiolini, A. Swift, P.S. Chines, C.E. Speck-Martins, F.S. Collins, E.W. Jabs, C.G. Bönnemann, E.N. Olson, J.C. Carey, S.P. Robertson, I. Manoli, E.C. Engle, C. V. Andrews, B.J. Barry, D.G. Hunter, S.E.

Mackinnon, S. Shaaban, M. Erazo, T. Frempong, K. Hao, T.P. Naidich, J.C. Rucker, Z. Zhang, B.B. Biesecker, L.L. Bonnycastle, C.C. Brewer, B.P. Brooks, J.A. Butman, W.W. Chien, K. Farrell, E.J. FitzGibbon, A.L. Gropman, E.B. Hutchinson, M.S. Jain, K.A. King, T.J. Lehky, J. Lee, D.K. Liberton, N. Narisu, S.M. Paul, N. Sadeghi, J. Snow, B. Solomon, A. Summers, C. Toro, A. Thurm, C.K. Zalewski, A defect in myoblast fusion underlies Carey-Fineman-Ziter syndrome, Nat. Commun. (2017). doi:10.1038/ncomms16077.

[139] Q. Zhang, A.A. Vashisht, J. O'Rourke, S.Y. Corbel, R. Moran, A. Romero, L. Miraglia, J. Zhang, E. Durrant, C. Schmedt, S.C. Sampath, S.C. Sampath, The microprotein Minion controls cell fusion and muscle formation., Nat. Commun. 8 (2017) 15664. doi:10.1038/ncomms15664.

[140] P. Seale, L.A. Sabourin, A. Girgis-Gabardo, A. Mansouri, P. Gruss, M.A. Rudnicki, Pax7 is required for the specification of myogenic satellite cells, Cell. (2000). doi:10.1016/S0092-8674(00)00066-0.

[141] H. Yin, F. Price, M.A. Rudnicki, Satellite cells and the muscle stem cell niche, Physiol. Rev. (2013). doi:10.1152/physrev.00043.2011.

[142] J.G. Tidball, Inflammatory cell response to acute muscle injury, Med. Sci. Sports Exerc. (1995). doi:10.1249/00005768-199507000-00011.

[143] J. Rantanen, T. Hurme, R. Lukka, J. Heino, H. Kalimo, Satellite cell proliferation and the expression of myogenin and desmin in regenerating skeletal muscle: evidence for two different populations of satellite cells., Lab. Invest. 72 (1995) 341–347.

[144] M.D. Grounds, Z. Yablonka-Reuveni, Molecular and cell biology of skeletal muscle regeneration., Mol. Cell Biol. Hum. Dis. Ser. 3 (1993) 210–256. doi:10.1007/978-94-011-1528-5_9.

[145] F.J. Calero-Cuenca, C.S. Janota, E.R. Gomes, Dealing with the nucleus during cell migration, Curr. Opin. Cell Biol. 50 (2018) 35–41. doi:10.1016/j.ceb.2018.01.014.

[146] G.G. Gundersen, H.J. Worman, Nuclear positioning, Cell. 152 (2013) 1376–1389. doi:10.1016/j.cell.2013.02.031.

[147] V. Dubowitz, C.A. Sewry, Definition of pathological changes seen in muscle biopsies, in: Muscle Biopsy, 2007. doi:10.1016/b978-1-4160-2593-1.50009-7.

[148] E.S. Folker, M.K. Baylies, Nuclear positioning in muscle development and disease, Front. Physiol. 4 DEC (2013) 1–10. doi:10.3389/fphys.2013.00363.

[149] A.J. Spiro, G.M. Shy, N.K. Gonatas, Myotubular Myopathy: Persistence of Fetal Muscle in an Adolescent Boy, Arch. Neurol. (1966). doi:10.1001/archneur.1966.00470070005001.

[150] C.A. Sewry, S.C. Brown, E. Mercuri, G. Bonne, L. Feng, G. Camici, G.E. Morris, F. Muntoni, Skeletal muscle pathology in autosomal dominant Emery-Dreifuss muscular dystrophy with lamin A/C mutations, Neuropathol. Appl. Neurobiol. (2001). doi:10.1046/j.0305-1846.2001.00323.x.

[151] D.S. Osorio, E.R. Gomes, The contemporary nucleus: A trip down memory lane, Biol. Cell. 105 (2013) 430–441. doi:doi:10.1111/boc.201300009.

[152] Y.L. Lee, B. Burke, LINC complexes and nuclear positioning, Semin. Cell Dev. Biol. 82 (2018) 67–76. doi:10.1016/j.semcdb.2017.11.008.

[153] D.A. Starr, KASH and SUN proteins, Curr. Biol. (2011). doi:10.1016/j.cub.2011.04.022.

[154] S. Deng, M. Azevedo, M. Baylies, Acting on identity: Myoblast fusion and the formation of the syncytial muscle fiber, Semin. Cell Dev. Biol. 72 (2017) 45–55. doi:10.1016/j.semcdb.2017.10.033.

[155] S.M. Abmayr, G.K. Pavlath, Myoblast fusion: lessons from flies and mice, Development. 139 (2012) 641–656. doi:10.1242/dev.068353.

[156] J.H. Kim, P. Jin, R. Duan, E.H. Chen, Mechanisms of myoblast fusion during muscle development, Curr. Opin. Genet. Dev. 32 (2015) 162–170. doi:10.1016/j.gde.2015.03.006.

[157] B. Cadot, V. Gache, E.R. Gomes, Moving and positioning the nucleus in skeletal muscle-one step at a time, Nucleus. 6 (2015) 373–381. doi:10.1080/19491034.2015.1090073.

[158] T. Metzger, V. Gache, M. Xu, B. Cadot, E.S. Folker, B.E. Richardson, E.R. Gomes, M.K. Baylies, MAP and kinesin-dependent nuclear positioning is required for skeletal muscle function, Nature. 484 (2012) 120–124. doi:10.1038/nature10914.

[159] W. Roman, E.R. Gomes, Nuclear positioning in skeletal muscle, Semin. Cell Dev. Biol. 82 (2018) 51–56. doi:10.1016/j.semcdb.2017.11.005.

[160] M.A. Collins, T.R. Mandigo, J.M. Camuglia, G.A. Vazquez, A.J. Anderson, C.H. Hudson,

J.L. Hanron, E.S. Folker, Emery–Dreifuss muscular dystrophy–linked genes and centronuclear myopathy–linked genes regulate myonuclear movement by distinct mechanisms, Mol. Biol. Cell. 28 (2017) 2303–2317. doi:10.1091/mbc.E16-10-0721.
[161] T.R. Mandigo, B.D. Turcich, A.J. Anderson, M.R. Hussey, E.S. Folker, Drosophila emerins control LINC complex localization and transcription to regulate myonuclear position , J. Cell Sci. (2019) jcs.235580. doi:10.1242/jcs.235580.
[162] J.N. Rosen, M. Azevedo, D.B. Soffar, V.P. Boyko, M.B. Brendel, V.K. Schulman, M.K. Baylies, The Drosophila Ninein homologue Bsg25D cooperates with Ensconsin in myonuclear positioning, J. Cell Biol. 218 (2019) 524–540. doi:10.1083/jcb.201808176.
[163] B. Cadot, V. Gache, E. Vasyutina, S. Falcone, C. Birchmeier, E.R. Gomes, Nuclear movement during myotube formation is microtubule and dynein dependent and is regulated by Cdc42, Par6 and Par3, EMBO Rep. 13 (2012) 741–749. doi:10.1038/embor.2012.89.
[164] W.E. Clark, An experimental study of the regeneration of mammalian striped muscle, J. Anat. 80 (1946) 24-36.4. https://www.ncbi.nlm.nih.gov/pubmed/17104987.
[165] S.B.P. Chargé, M.A. Rudnicki, Cellular and Molecular Regulation of Muscle Regeneration, Physiol. Rev. (2004). doi:10.1152/physrev.00019.2003.
[166] D. Chaturvedi, H. Reichert, R.D. Gunage, K. VijayRaghavan, Identification and functional characterization of muscle satellite cells in Drosophila, Elife. 6 (2017) 1–25. doi:10.7554/eLife.30107.
[167] E.S. Folker, V.K. Schulman, M.K. Baylies, Muscle length and myonuclear position are independently regulated by distinct Dynein pathways, Development. 139 (2012) 3827–3837. doi:10.1242/dev.079178.
[168] E.S. Folker, V.K. Schulman, M.K. Baylies, Translocating myonuclei have distinct leading and lagging edges that require Kinesin and Dynein., Development. 141 (2014) 355–66. doi:10.1242/dev.095612.
[169] V.K. Schulman, E.S. Folker, J.N. Rosen, M.K. Baylies, Syd/JIP3 and JNK Signaling Are Required for Myonuclear Positioning and Muscle Function, PLoS Genet. 10 (2014). doi:10.1371/journal.pgen.1004880.
[170] A.L. Auld, S.A. Roberts, C.B. Murphy, J.M. Camuglia, E.S. Folker, Aplip1, the Drosophila homolog of JIP1, regulates myonuclear positioning and muscle stability., J. Cell Sci. 131 (2018). doi:10.1242/jcs.205807.
[171] J.M. Camuglia, T.R. Mandigo, R. Moschella, J. Mark, C.H. Hudson, D. Sheen, E.S. Folker, An RNAi based screen in Drosophila larvae identifies fascin as a regulator of myoblast fusion and myotendinous junction structure, Skelet. Muscle. 8 (2018) 1–13. doi:10.1186/s13395-018-0159-9.
[172] H. Elhanany-Tamir, Y. V. Yu, M. Shnayder, A. Jain, M. Welte, T. Volk, Organelle positioning in muscles requires cooperation between two KASH proteins and microtubules, J. Cell Biol. 198 (2012) 833–846. doi:10.1083/jcb.201204102.
[173] M. Perillo, E.S. Folker, Specialized positioning of myonuclei near cell-cell junctions, Front. Physiol. 9 (2018) 1–10. doi:10.3389/fphys.2018.01531.
[174] A.L. Auld, E.S. Folker, Nucleus-dependent sarcomere assembly is mediated by the LINC complex, Mol. Biol. Cell. 27 (2016) 2351–2359. doi:10.1091/mbc.e16-01-0021.
[175] P. Meinke, E. Mattioli, F. Haque, S. Antoku, M. Columbaro, K.R. Straatman, H.J. Worman, G.G. Gundersen, G. Lattanzi, M. Wehnert, S. Shackleton, Muscular Dystrophy-Associated SUN1 and SUN2 Variants Disrupt Nuclear-Cytoskeletal Connections and Myonuclear Organization, PLoS Genet. 10 (2014). doi:10.1371/journal.pgen.1004605.
[176] A. Reuveny, M. Shnayder, D. Lorber, S. Wang, T. Volk, Ma2/d promotes myonuclear positioning and association with the sarcoplasmic reticulum, Development. 145 (2018) dev159558. doi:10.1242/dev.159558.
[177] A. Janin, V. Gache, Nesprins and lamins in health and diseases of cardiac and skeletal muscles, Front. Physiol. 9 (2018) 1–12. doi:10.3389/fphys.2018.01277.
[178] S. Wang, A. Reuveny, T. Volk, Nesprin provides elastic properties to muscle nuclei by cooperating with spectraplakin and EB1, J. Cell Biol. 209 (2015) 529–538. doi:10.1083/jcb.201408098.
[179] A.J. Koch, J.M. Holaska, Emerin in health and disease, Semin. Cell Dev. Biol. (2014). doi:10.1016/j.semcdb.2013.12.008.
[180] K.L. Tan, N.A. Haelterman, C.S. Kwartler, E.S. Regalado, P.T. Lee, S. Nagarkar-Jaiswal, D.C. Guo, L. Duraine, M.F. Wangler, M.J. Bamshad, D.A. Nickerson, G. Lin, D.M. Milewicz,

H.J. Bellen, Ari-1 Regulates Myonuclear Organization Together with Parkin and Is Associated with Aortic Aneurysms, Dev. Cell. 45 (2018) 226-244.e8. doi:10.1016/j.devcel.2018.03.020.
[181] M. Balakrishnan, M.K. Baylies, Myonuclear Positioning and Aneurysms Are LINC'd by Ariande, Dev. Cell. 45 (2018) 149–150. doi:10.1016/j.devcel.2018.04.004.
[182] M. Métivier, B.Y. Monroy, E. Gallaud, R. Caous, A. Pascal, L. Richard-Parpaillon, A. Guichet, K.M. Ori-McKenney, R. Giet, Dual control of Kinesin-1 recruitment to microtubules by Ensconsin in Drosophila neuroblasts and oocytes, Dev. 146 (2019) 1–12. doi:10.1242/dev.171579.
[183] H.H. Sung, I.A. Telley, P. Papadaki, A. Ephrussi, T. Surrey, P. Rørth, Drosophila Ensconsin Promotes Productive Recruitment of Kinesin-1 to Microtubules, Dev. Cell. 15 (2008) 866–876. doi:10.1016/j.devcel.2008.10.006.
[184] R. Schweitzer, E. Zelzer, T. Volk, Connecting muscles to tendons: tendons and musculoskeletal development in flies and vertebrates, Development. 137 (2010) 3347–3347. doi:10.1242/dev.057885.
[185] A.R. Gillies, R.L. Lieber, Structure and function of the skeletal muscle extracellular matrix, Muscle Nerve. 44 (2012) 318–331. doi:10.1002/mus.22094.Structure.
[186] C.F. Bentzinger, Y.X. Wang, N.A. Dumont, M.A. Rudnicki, Cellular dynamics in the muscle satellite cell niche, EMBO Rep. 14 (2013) 1062–1072. doi:10.1038/embor.2013.182.
[187] S. Thomopoulos, V. Birman, G.M. Genin, Structural interfaces and attachments in biology, Struct. Interfaces Attach. Biol. 9781461433 (2013) 1–386. doi:10.1007/978-1-4614-3317-0.
[188] M. Valdivia, F. Vega-Macaya, P. Olguín, Mechanical Control of Myotendinous Junction Formation and Tendon Differentiation during Development, Front. Cell Dev. Biol. 5 (2017) 1–8. doi:10.3389/fcell.2017.00026.
[189] M.H. Wilson, E.L.F. Holzbaur, Opposing microtubule motors drive robust nuclear dynamics in developing muscle cells, J. Cell Sci. 125 (2012) 4158 LP – 4169. doi:10.1242/jcs.108688.
[190] M.H. Wilson, E.L.F. Holzbaur, Nesprins anchor kinesin-1 motors to the nucleus to drive nuclear distribution in muscle cells, Development. 142 (2015) 218 LP – 228. doi:10.1242/dev.114769.
[191] V. Gache, E.R. Gomes, B. Cadot, Microtubule motors involved in nuclear movement during skeletal muscle differentiation, Mol. Biol. Cell. 28 (2017) 865–874. doi:10.1091/mbc.e16-06-0405.
[192] E. Bugnard, K.J.M. Zaal, E. Ralston, Reorganization of microtubule nucleation during muscle differentiation, Cell Motil. Cytoskeleton. 60 (2005) 1–13. doi:10.1002/cm.20042.
[193] P. Gimpel, Y.L. Lee, R.M. Sobota, A. Calvi, V. Koullourou, R. Patel, K. Mamchaoui, F. Nédélec, S. Shackleton, J. Schmoranzer, B. Burke, B. Cadot, E.R. Gomes, Nesprin-1α-Dependent Microtubule Nucleation from the Nuclear Envelope via Akap450 Is Necessary for Nuclear Positioning in Muscle Cells, Curr. Biol. 27 (2017) 2999-3009.e9. doi:10.1016/j.cub.2017.08.031.
[194] M.H. Wilson, E.L.F. Holzbaur, Nesprins anchor kinesin-1 motors to the nucleus to drive nuclear distribution in muscle cells, J. Cell Sci. 128 (2015) e1–e1. doi:10.1242/jcs.167718.
[195] R. Piccirillo, F. Demontis, N. Perrimon, A.L. Goldberg, Mechanisms of muscle growth and atrophy in mammals and Drosophila, Dev. Dyn. 243 (2014) 201–215. doi:10.1002/dvdy.24036.
[196] S.E. Windner, A. Manhart, A. Brown, A. Mogilner, M.K. Baylies, Nuclear Scaling Is Coordinated among Individual Nuclei in Multinucleated Muscle Fibers, Dev. Cell. 49 (2019) 48-62.e3. doi:10.1016/j.devcel.2019.02.020.
[197] H. Kohsaka, S. Okusawa, Y. Itakura, A. Fushiki, A. Nose, Development of larval motor circuits in Drosophila, Dev. Growth Differ. 54 (2012) 408–419. doi:10.1111/j.1440-169X.2012.01347.x.
[198] F. Demontis, N. Perrimon, Integration of Insulin receptor/Foxo signaling and dMyc activity during muscle growth regulates body size in Drosophila, Development. 136 (2009) 983–993. doi:10.1242/dev.027466.
[199] S. Wang, T. Volk, Composite biopolymer scaffolds shape muscle nucleus: Insights and

perspectives from Drosophila, Bioarchitecture. 5 (2015) 35–43. doi:10.1080/19490992.2015.1106061.
[200] A. Manhart, S. Windner, M. Baylies, A. Mogilner, Mechanical positioning of multiple nuclei in muscle cells, PLoS Comput. Biol. 14 (2018) 1–25. doi:10.1371/journal.pcbi.1006208.
[201] H. De Forges, A. Bouissou, F. Perez, Interplay between microtubule dynamics and intracellular organization, Int. J. Biochem. Cell Biol. 44 (2012) 266–274. doi:10.1016/j.biocel.2011.11.009.
[202] S. Falcone, W. Roman, K. Hnia, V. Gache, N. Didier, J. Laine, F. Aurade, I. Marty, I. Nishino, N. Charlet-Berguerand, N.B. Romero, G. Marazzi, D. Sassoon, J. Laporte, E.R. Gomes, N-WASP is required for Amphiphysin-2/BIN1-dependent nuclear positioning and triad organization in skeletal muscle and is involved in the pathophysiology of centronuclear myopathy, EMBO Mol. Med. 6 (2014) 1455–1475. doi:10.15252/emmm.201404436.
[203] W. Roman, J.P. Martins, F.A. Carvalho, R. Voituriez, J.V.G. Abella, N.C. Santos, B. Cadot, M. Way, E.R. Gomes, Myofibril contraction and crosslinking drive nuclear movement to the periphery of skeletal muscle, Nat. Cell Biol. 19 (2017) 1189–1201. doi:10.1038/ncb3605.
[204] W. Roman, J.P. Martins, E.R. Gomes, Local Arrangement of Fibronectin by Myofibroblasts Governs Peripheral Nuclear Positioning in Muscle Cells, Dev. Cell. 46 (2018) 102-111.e6. doi:10.1016/j.devcel.2018.05.031.
[205] J.C. Bruusgaard, K. Liestøl, M. Ekmark, K. Kollstad, K. Gundersen, Number and spatial distribution of nuclei in the muscle fibres of normal mice studied in vivo, J. Physiol. 551 (2003) 467–478. doi:10.1113/jphysiol.2003.045328.
[206] O. Casar-Borota, J. Jacobsson, R. Libelius, C.H. Oldfors, E. Malfatti, N.B. Romero, A. Oldfors, A novel dynamin-2 gene mutation associated with a late-onset centronuclear myopathy with necklace fibres, Neuromuscul. Disord. 25 (2015) 345–348. doi:10.1016/j.nmd.2015.01.001.
[207] Z. Chen, Z. Ren, W. Mei, Q. Ma, Y. Shi, Y. Zhang, S. Li, L. Xiang, J. Zhang, A novel SYNE1 gene mutation in a Chinese family of Emery-Dreifuss muscular dystrophy-like, BMC Med. Genet. 18 (2017) 4–9. doi:10.1186/s12881-017-0424-5.
[208] N.B. Romero, Centronuclear myopathies: a widening concept., Neuromuscul. Disord. 20 (2010) 223–228. doi:10.1016/j.nmd.2010.01.014.
[209] V.K. Schulman, E.S. Folker, M.K. Baylies, A method for reversible drug delivery to internal tissues of Drosophila embryos, Fly (Austin). 7 (2013) 37–41. doi:10.4161/fly.25438.
[210] M. Fujioka, R.J. Wessells, Z. Han, J. Liu, K. Fitzgerald, G.L. Yusibova, M. Zamora, P. Ruiz-Lozano, R. Bodmer, J.B. Jaynes, Embryonic even skipped-dependent muscle and heart cell fates are required for normal adult activity, heart function, and lifespan., Circ. Res. 97 (2005) 1108–1114. doi:10.1161/01.RES.0000191546.08532.B2.
[211] S. Knirr, M. Frasch, Molecular integration of inductive and mesoderm-intrinsic inputs governs even-skipped enhancer activity in a subset of pericardial and dorsal muscle progenitors., Dev. Biol. 238 (2001) 13–26. doi:10.1006/dbio.2001.0397.
[212] M. Landgraf, S. Thor, Development of Drosophila motoneurons: specification and morphology., Semin. Cell Dev. Biol. 17 (2006) 3–11. doi:10.1016/j.semcdb.2005.11.007.
[213] M. Frasch, T. Hoey, C. Rushlow, H. Doyle, M. Levine, Characterization and localization of the even-skipped protein of Drosophila., EMBO J. (1987). doi:10.1002/j.1460-2075.1987.tb04817.x.
[214] J.A. Williams, J.B. Bell, S.B. Carroll, Control of Drosophila wing and haltere development by the nuclear vestigial gene product, Genes Dev. (1991). doi:10.1101/gad.5.12b.2481.
[215] J.A. Kaltschmidt, C.M. Davidson, N.H. Brown, A.H. Brand, Rotation and asymmetry of the mitotic spindle direct asymmetric cell division in the developing central nervous system., Nat. Cell Biol. 2 (2000) 7–12. doi:10.1038/71323.
[216] J. Haseloff, E.L. Dormand, A.H. Brand, Live imaging with green fluorescent protein., Methods Mol. Biol. 122 (1999) 241–259. doi:10.1385/1-59259-722-x:241.
[217] J.R. Brent, K.M. Werner, B.D. McCabe, Drosophila larval NMJ dissection., J. Vis. Exp. (2009). doi:10.3791/1107.
[218] A.H. Brand, N. Perrimon, Targeted gene expression as a means of altering cell fates and generating dominant phenotypes., Development. 118 (1993) 401–15.

doi:10.1101/lm.1331809.
[219] M.K. Baylies, M. Bate, twist: A myogenic switch in Drosophila, Science (80-.). (1996). doi:10.1126/science.272.5267.1481.
[220] G. Ranganayakulu, D. a Elliott, R.P. Harvey, E.N. Olson, Divergent roles for NK-2 class homeobox genes in cardiogenesis in flies and mice., Development. 125 (1998) 3037–3048.
[221] Y.Q. Zhang, A.M. Bailey, H.J.G. Matthies, R.B. Renden, M.A. Smith, S.D. Speese, G.M. Rubin, K. Broadie, Drosophila fragile x-related gene regulates the MAP1B homolog Futsch to control synaptic structure and function, Cell. (2001). doi:10.1016/S0092-8674(01)00589-X.
[222] S. Ritzenthaler, E. Suzuki, A. Chiba, Postsynaptic filopodia in muscle cells interact with innervating motoneuron axons, Nat. Neurosci. (2000). doi:10.1038/79833.
[223] D. Dutta, J.W. Bloor, M. Ruiz-Gomez, K. VijayRaghavan, D.P. Kiehart, Real-time imaging of morphogenetic movements in Drosophila using Gal4-UAS-driven expression of GFP fused to the actin-binding domain of moesin, Genesis. (2002). doi:10.1002/gene.10113.
[224] F. Schnorrer, C. Schönbauer, C.C.H. Langer, G. Dietzl, M. Novatchkova, K. Schernhuber, M. Fellner, A. Azaryan, M. Radolf, A. Stark, K. Keleman, B.J. Dickson, Systematic genetic analysis of muscle morphogenesis and function in Drosophila, Nature. (2010). doi:10.1038/nature08799.
[225] S.B. Lemke, F. Schnorrer, Mechanical forces during muscle development, Mech. Dev. 144 (2017) 92–101. doi:10.1016/j.mod.2016.11.003.
[226] J.A. Campos-Ortega, V. Hartenstein, The Embryonic Development of Drosophila melanogaster, 2nd ed., Springer Berlin Heidelberg, Berlin, Heidelberg, 1997. doi:10.1007/978-3-662-22489-2.
[227] M. Azevedo, V.K. Schulman, E. Folker, M. Balakrishnan, M. Baylies, The Nuclear Envelope, 1411 (2016) 291–312. doi:10.1007/978-1-4939-3530-7.
[228] S.G. Kramer, T. Kidd, J.H. Simpson, C.S. Goodman, Switching repulsion to attraction: Changing responses to slit during transition in mesoderm migration, Science (80-.). 292 (2001) 737–740. doi:10.1126/science.1058766.
[229] M. Seeger, G. Tear, D. Ferres-Marco, C.S. Goodman, Mutations affecting growth cone guidance in drosophila: Genes necessary for guidance toward or away from the midline, Neuron. 10 (1993) 409–426. doi:10.1016/0896-6273(93)90330-T.
[230] T. Kidd, K.S. Bland, C.S. Goodman, Slit Is the Midline Repellent for the Robo Receptor in Drosophila, Cell. 96 (1999) 785–794. doi:10.1016/S0092-8674(00)80589-9.
[231] J.A. Zallen, B.A. Yi, C.I. Bargmann, The conserved immunoglobulin superfamily member SAX-3/robo directs multiple aspects of axon guidance in C. elegans, Cell. 92 (1998) 217–227. doi:10.1016/S0092-8674(00)80916-2.
[232] T. Kidd, K. Brose, K.J. Mitchell, R.D. Fetter, M. Tessier-Lavigne, C.S. Goodman, G. Tear, Roundabout controls axon crossing of the CNS midline and defines a novel subfamily of evolutionarily conserved guidance receptors, Cell. 92 (1998) 205–215. doi:10.1016/S0092-8674(00)80915-0.
[233] J.H. Simpson, T. Kidd, K.S. Bland, C.S. Goodman, Short-range and long-range guidance by Slit and its robo receptors: Robo and Robo2 play distinct roles in midline guidance, Neuron. 28 (2000) 753–766. doi:10.1016/S0896-6273(00)00151-3.
[234] O. Marin, Directional guidance of interneuron migration to the cerebral cortex relies on subcortical Slit1/2-independent repulsion and cortical attraction, Development. 130 (2003) 1889–1901. doi:10.1242/dev.00417.
[235] J.A. Zallen, S.A. Kirch, C.I. Bargmann, Genes required for axon pathfinding and extension in the C. elegans nerve ring., Development. 126 (1999) 3679–92. http://www.ncbi.nlm.nih.gov/pubmed/10409513.
[236] C. Fricke, J.S. Lee, S. Geiger-Rudolph, F. Bonhoeffer, C.B. Chien, astray, a Zebrafish roundabout homolog required for retinal axon guidance, Science (80-.). (2001). doi:10.1126/science.1059496.
[237] P.K. Shah, M.R. Tanner, I. Kovacevic, A. Rankin, T.E. Marshall, N. Noblett, N.N. Tran, T. Roenspies, J. Hung, Z. Chen, C. Slatculescu, T.J. Perkins, Z. Bao, A. Colavita, PCP and SAX-3/Robo Pathways Cooperate to Regulate Convergent Extension-Based Nerve Cord Assembly in C. elegans, Dev. Cell. 41 (2017) 195-203.e3. doi:https://doi.org/10.1016/j.devcel.2017.03.024.

[238] K.M. Brendza, D.J. Rese, S.P. Gilbert, W.M. Saxton, Lethal kinesin mutations reveal amino acids important for ATPase activation and structural coupling, J. Biol. Chem. 274 (1999) 31506–31514. doi:10.1074/jbc.274.44.31506.
[239] J. Gepner, M.G. Li, S. Ludmann, C. Kortas, K. Boylan, S.J.P. Iyadurai, M. McGrail, T.S. Hays, Cytoplasmic dynein function is essential in Drosophila melanogaster, Genetics. 142 (1996) 865–878.
[240] I.B.N. Clark, V. Muha, A. Klingseisen, M. Leptin, H.-A.J. Muller, Fibroblast growth factor signalling controls successive cell behaviours during mesoderm layer formation in Drosophila, Development. 138 (2011) 2705–2715. doi:10.1242/dev.060277.
[241] G.J. Bashaw, T. Kidd, D. Murray, T. Pawson, C.S. Goodman, Repulsive Axon Guidance: Abelson and Enabled Play Opposing Roles Downstream of the Roundabout Receptor, Cell. 101 (2000) 703–715. doi:10.1016/S0092-8674(00)80883-1.
[242] E. Ordan, T. Volk, A non-signaling role of Robo2 in tendons is essential for Slit processing and muscle patterning, Development. 142 (2015) 3512–3518. doi:10.1242/dev.128157.
[243] F. Schnorrer, B.J. Dickson, Muscle building mechanisms of myotube guidance and attachment site selection, Dev. Cell. 7 (2004) 9–20. doi:10.1016/j.devcel.2004.06.010.
[244] T.R.F. Wright, The phenogenetics of the embryonic mutant lethal myospheroid, in Drosophila melanogaster, J. Exp. Zool. 143 (1960) 77–99. doi:doi:10.1002/jez.1401430107.
[245] E. Ordan, M. Brankatschk, B. Dickson, F. Schnorrer, T. Volk, Slit cleavage is essential for producing an active, stable, non-diffusible short-range signal that guides muscle migration, Development. 142 (2015) 1431–1436. doi:10.1242/dev.119131.
[246] K.M. Bhat, I. Gaziova, S. Krishnan, Regulation of Axon Guidance by Slit and Netrin Signaling in the Drosophila Ventral Nerve Cord, Genetics. 176 (2007) 2235 LP – 2246. http://www.genetics.org/content/176/4/2235.abstract.
[247] K.M. Bhat, Post-guidance signaling by extracellular matrix-associated Slit/Slit-N maintains fasciculation and position of axon tracts in the nerve cord, PLOS Genet. 13 (2017) e1007094. https://doi.org/10.1371/journal.pgen.1007094.
[248] B.E. Richardson, S.J. Nowak, M.K. Baylies, Myoblast fusion in fly and vertebrates: new genes, new processes and new perspectives., Traffic. 9 (2008) 1050–1059. doi:10.1111/j.1600-0854.2008.00756.x.
[249] S. Berger, G. Schafer, D.A. Kesper, A. Holz, T. Eriksson, R.H. Palmer, L. Beck, C. Klambt, R. Renkawitz-Pohl, S.-F. Onel, WASP and SCAR have distinct roles in activating the Arp2/3 complex during myoblast fusion, J. Cell Sci. 121 (2008) 1303–1313. doi:10.1242/jcs.022269.
[250] A. Hsouna, Y.-S. Kim, M.F.A. VanBerkum, Abelson tyrosine kinase is required to transduce midline repulsive cues, J. Neurobiol. 57 (2003) 15–30. doi:10.1002/neu.10232.
[251] Y. Zou, E. Stoeckli, H. Chen, M. Tessier-Lavigne, Squeezing axons out of the gray matter: A role for Slit and Semaphorin proteins from midline and ventral spinal cord, Cell. 102 (2000) 363–375. doi:10.1016/S0092-8674(00)00041-6.
[252] H. Long, C. Sabatier, L. Ma, A. Plump, W. Yuan, D.M. Ornitz, A. Tamada, F. Murakami, C.S. Goodman, M. Tessier-Lavigne, Conserved roles for Slit and Robo proteins in midline commissural axon guidance, Neuron. 42 (2004) 213–223. doi:10.1016/S0896-6273(04)00179-5.
[253] T. Yang, H. Huang, Q. Shao, S. Yee, T. Majumder, G. Liu, miR-92 Suppresses Robo1 Translation to Modulate Slit Sensitivity in Commissural Axon Guidance, Cell Rep. 24 (2018) 2694-2708.e6. doi:10.1016/j.celrep.2018.08.021.
[254] M.P. Zappia, M. V Frolov, E2F function in muscle growth is necessary and sufficient for viability in Drosophila, Nat. Commun. 7 (2016) 10509. doi:10.1038/ncomms10509.
[255] H.E. Brown, M.C. Reichert, T.A. Evans, Slit Binding via the Ig1 Domain Is Essential for Midline Repulsion by *Drosophila* Robo1 but Dispensable for Receptor Expression, Localization, and Regulation *in Vivo*, G3: Genes|Genomes|Genetics. 5 (2015) 2429–2439. doi:10.1534/g3.115.022327.
[256] L. Bataillé, I. Delon, J.P. Da Ponte, N.H. Brown, K. Jagla, `Downstream of identity genes: Muscle-type-specific regulation of the fusion process, Dev. Cell. 19 (2010) 317–328. doi:10.1016/j.devcel.2010.07.008.
[257] A.R. Ypsilanti, A. Chedotal, Cell Adhesion Molecules, 2014. doi:10.1007/978-1-4614-

8090-7.
[258] P. Friedl, R. Mayor, Tuning Collective Cell Migration by Cell–Cell Junction Regulation, Cold Spring Harb. Perspect. Biol. 9 (2017) a029199. doi:10.1101/cshperspect.a029199.
[259] J.C. Hao, T.W. Yu, K. Fujisawa, J.G. Culotti, K. Gengyo-Ando, S. Mitani, G. Moulder, R. Barstead, M. Tessier-Lavigne, C.I. Bargmann, C. elegans Slit Acts in Midline, Dorsal-Ventral, and Anterior-Posterior Guidance via the SAX-3/Robo Receptor, Neuron. 32 (2001) 25–38. doi:https://doi.org/10.1016/S0896-6273(01)00448-2.
[260] B. Hivert, Z. Liu, C.Y. Chuang, P. Doherty, V. Sundaresan, Robo1 and Robo2 are homophilic binding molecules that promote axonal growth, Mol. Cell. Neurosci. 21 (2002) 534–545. doi:10.1006/mcne.2002.1193.
[261] B. Wayburn, T. Volk, LRT, a tendon-specific leucine-rich repeat protein, promotes muscle-tendon targeting through its interaction with Robo, Development. 136 (2009) 3607 LP – 3615. http://dev.biologists.org/content/136/21/3607.abstract.
[262] J. Rhee, T. Buchan, L. Zukerberg, J. Lilien, J. Balsamo, Cables links Robo-bound Abl kinase to N-cadherin-bound β-catenin to mediate Slit-induced modulation of adhesion and transcription, Nat. Cell Biol. 9 (2007) 883–892. doi:10.1038/ncb1614.
[263] J. Rhee, N.S. Mahfooz, C. Arregui, J. Lilien, J. Balsamo, M.F.A. VanBerkum, Activation of the repulsive receptor roundabout inhibits N-cadherin-mediated cell adhesion, Nat. Cell Biol. 4 (2002) 798–805. doi:10.1038/ncb858.
[264] J. Zhang, A. Felder, Y. Liu, L.T. Guo, S. Lange, N.D. Dalton, Y. Gu, K.L. Peterson, A.P. Mizisin, G.D. Shelton, R.L. Lieber, J. Chen, Nesprin 1 is critical for nuclear positioning and anchorage, Hum. Mol. Genet. (2009). doi:10.1093/hmg/ddp499.
[265] K. Barlan, W. Lu, V.I. Gelfand, The microtubule-binding protein ensconsin is an essential cofactor of kinesin-1, Curr. Biol. 23 (2013) 317–322. doi:10.1016/j.cub.2013.01.008.
[266] E. Gallaud, R. Caous, A. Pascal, F. Bazile, J.P. Gagné, S. Huet, G.G. Poirier, D. Chrétien, L. Richard-Parpaillon, R. Giet, Ensconsin/map7 promotes microtubule growth and centrosome separation in Drosophila neural stem cells, J. Cell Biol. 204 (2014) 1111–1121. doi:10.1083/jcb.201311094.
[267] A.M. Tassin, B. Maro, M. Bornens, Fate of microtubule-organizing centers during myogenesis in vitro, J. Cell Biol. (1985). doi:10.1083/jcb.100.1.35.
[268] C.M. Guerin, S.G. Kramer, Cytoskeletal remodeling during myotube assembly and guidance: Coordinating the actin and microtubule networks, Commun. Integr. Biol. 2 (2009) 452–457. doi:10.4161/cib.2.5.9158.
[269] V. Bouckson-Castaing, M. Moudjou, D.J.P. Ferguson, S. Mucklow, Y. Belkaid, G. Milon, P.R. Crocker, Molecular characterisation of ninein, a new coiled-coil protein of the centrosome, J. Cell Sci. (1996).
[270] M.M. Mogensen, A. Malik, M. Piel, V. Boukson-Castaing, M. Bornens, Microtubule minus-end anchorage at Centrosomal and non-centrosomal sites: The role of ninein, J. Cell Sci. (2000).
[271] M. Abal, M. Piel, V. Bouckson-Castaing, M. Mogensen, J.B. Sibarita, M. Bornens, Microtubule release from the centrosome in migrating cells, J. Cell Biol. (2002). doi:10.1083/jcb.200207076.
[272] H. Shinohara, N. Sakayori, M. Takahashi, N. Osumi, Ninein is essential for the maintenance of the cortical progenitor character by anchoring the centrosome to microtubules, Biol. Open. 2 (2013) 739–749. doi:10.1242/bio.20135231.
[273] M. Casenghi, F.A. Barr, E.A. Nigg, Phosphorylation of Nlp by Plk1 negatively regulates its dynein-dynactin-dependent targeting to the centrosome, J. Cell Sci. (2005). doi:10.1242/jcs.02622.
[274] N. Delgehyr, J. Sillibourne, M. Bornens, Microtubule nucleation and anchoring at the centrosome are independent processes linked by ninein function, J. Cell Sci. (2005). doi:10.1242/jcs.02302.
[275] S. Wang, D. Wu, S. Quintin, R.A. Green, D.K. Cheerambathur, S.D. Ochoa, A. Desai, K. Oegema, NOCA-1 functions with γ-tubulin and in parallel to Patronin to assemble non-centrosomal microtubule arrays in C. elegans, Elife. (2015). doi:10.7554/eLife.08649.
[276] M. Kowanda, J. Bergalet, M. Wieczorek, G. Brouhard, É. Léuyer, P. Lasko, Loss of function of the Drosophila Ninein-related centrosomal protein Bsg25D causes mitotic defects and impairs embryonic development, Biol. Open. (2016). doi:10.1242/bio.019638.
[277] Y. Zheng, V. Mennella, S. Marks, J. Wildonger, E. Elnagdi, D. Agard, T.L. Megraw, The Seckel syndrome and centrosomal protein Ninein localizes asymmetrically to stem cell

centrosomes but is not required for normal development, behavior, or DNA damage response in Drosophila, Mol. Biol. Cell. (2016). doi:10.1091/mbc.E15-09-0655.
[278] M. Martinez-Campos, R. Basto, J. Baker, M. Kernan, J.W. Raff, The Drosophila pericentrin-like protein is essential for cilia/flagella function, but appears to be dispensable for mitosis, J. Cell Biol. (2004). doi:10.1083/jcb.200402130.
[279] S.D. Menon, W. Chia, Drosophila Rolling pebbles: A Multidomain Protein Required for Myoblast Fusion that Recruits D-Titin in Response to the Myoblast Attractant Dumbfounded, Dev. Cell. (2001). doi:10.1016/S1534-5807(01)00075-2.
[280] L.A. Baena-Lopez, C. Alexandre, A. Mitchell, L. Pasakarnis, J.P. Vincent, Accelerated homologous recombination and subsequent genome modification in Drosophila, Dev. (2013). doi:10.1242/dev.100933.
[281] M.S. Halfon, S. Gisselbrecht, J. Lu, B. Estrada, H. Keshishian, A.M. Michelson, New fluorescent protein reporters for use with the Drosophila Gal4 expression system and for vital detection of balancer chromosomes, Genesis. (2002). doi:10.1002/gene.10136.
[282] N.A. Bulgakova, I. Grigoriev, A.S. Yap, A. Akhmanova, N.H. Brown, Dynamic microtubules produce an asymmetric E-cadherin-Bazooka complex to maintain segment boundaries, J. Cell Biol. (2013). doi:10.1083/jcb.201211159.
[283] P. Jones, D. Binns, H.Y. Chang, M. Fraser, W. Li, C. McAnulla, H. McWilliam, J. Maslen, A. Mitchell, G. Nuka, S. Pesseat, A.F. Quinn, A. Sangrador-Vegas, M. Scheremetjew, S.Y. Yong, R. Lopez, S. Hunter, InterProScan 5: Genome-scale protein function classification, Bioinformatics. (2014). doi:10.1093/bioinformatics/btu031.
[284] C. Iampietro, J. Bergalet, X. Wang, N.A.L. Cody, A. Chin, F.A. Lefebvre, M. Douziech, H.M. Krause, E. Lécuyer, Developmentally regulated elimination of damaged nuclei involves a Chk2-dependent mechanism of mRNA nuclear retention, Dev. Cell. 29 (2014) 468–481. doi:10.1016/j.devcel.2014.03.025.
[285] E.J. Chen, J. Novakofski, W. Kenneth Jenkins, W.D. O'Brien, Young's modulus measurements of soft tissues with application to elasticity imaging, IEEE Trans. Ultrason. Ferroelectr. Freq. Control. (1996). doi:10.1109/58.484478.
[286] I. Fernandes, F. Schöck, The nebulin repeat protein Lasp regulates I-band architecture and filament spacing in myofibrils, J. Cell Biol. (2014). doi:10.1083/jcb.201401094.
[287] P. Tomancak, A. Beaton, R. Weiszmann, E. Kwan, S.Q. Shu, S.E. Lewis, S. Richards, M. Ashburner, V. Hartenstein, S.E. Celniker, G.M. Rubin, Systematic determination of patterns of gene expression during Drosophila embryogenesis., Genome Biol. (2002). doi:10.1186/gb-2002-3-12-research0088.
[288] P. Tomancak, B.P. Berman, A. Beaton, R. Weiszmann, E. Kwan, V. Hartenstein, S.E. Celniker, G.M. Rubin, Global analysis of patterns of gene expression during Drosophila embryogenesis, Genome Biol. (2007). doi:10.1186/gb-2007-8-7-r145.
[289] A.S. Hammonds, C.A. Bristow, W.W. Fisher, R. Weiszmann, S. Wu, V. Hartenstein, M. Kellis, B. Yu, E. Frise, S.E. Celniker, Spatial expression of transcription factors in Drosophila embryonic organ development, Genome Biol. (2013). doi:10.1186/gb-2013-14-12-r140.
[290] R.D. Bagshaw, J.W. Callahan, D.J. Mahuran, The Arf-family protein, Arl8b, is involved in the spatial distribution of lysosomes, Biochem. Biophys. Res. Commun. (2006). doi:10.1016/j.bbrc.2006.03.221.
[291] I. Hofmann, S. Munro, An N-terminally acetylated Arf-like GTPase is localised to lysosomes and affects their motility, J. Cell Sci. (2006). doi:10.1242/jcs.02958.
[292] C.T. Chen, H. Hehnly, Q. Yu, D. Farkas, G. Zheng, S.D. Redick, H.F. Hung, R. Samtani, A. Jurczyk, S. Akbarian, C. Wise, A. Jackson, M. Bober, Y. Guo, C. Lo, S. Doxsey, A Unique Set of Centrosome Proteins Requires Pericentrin for Spindle-Pole Localization and Spindle Orientation, Curr. Biol. (2014). doi:10.1016/j.cub.2014.08.029.
[293] S. Srivatsa, S. Parthasarathy, Z. Molnár, V. Tarabykin, Sip1 downstream effector ninein controls neocortical axonal growth, ipsilateral branching, and microtubule growth and stability, Neuron. 85 (2015) 998–1012. doi:10.1016/j.neuron.2015.01.018.
[294] T.S. Cheng, L.K. Chang, S.L. Howng, P.J. Lu, C.I. Lee, Y.R. Hong, SUMO-1 modification of centrosomal protein hNinein promotes hNinein nuclear localization, Life Sci. 78 (2006) 1114–1120. doi:10.1016/j.lfs.2005.06.021.
[295] S.R. Tymanskyj, B. Yang, A. Falnikar, A.C. Lepore, L. Ma, MAP7 regulates axon collateral branch development in dorsal root ganglion neurons, J. Neurosci. (2017).

doi:10.1523/JNEUROSCI.3260-16.2017.
[296] A.M. Collinsworth, S. Zhang, W.E. Kraus, G.A. Truskey, Apparent elastic modulus and hysteresis of skeletal muscle cells throughout differentiation, Am. J. Physiol. - Cell Physiol. (2002). doi:10.1152/ajpcell.00502.2001.
[297] S. Nishimura, S. Nagai, M. Katoh, H. Yamashita, Y. Saeki, J.I. Okada, T. Hisada, R. Nagai, S. Sugiura, Microtubules modulate the stiffness of cardiomyocytes against shear stress, Circ. Res. (2006). doi:10.1161/01.RES.0000197785.51819.e8.
[298] J.P. Kerr, P. Robison, G. Shi, A.I. Bogush, A.M. Kempema, J.K. Hexum, N. Becerra, D.A. Harki, S.S. Martin, R. Raiteri, B.L. Prosser, C.W. Ward, Detyrosinated microtubules modulate mechanotransduction in heart and skeletal muscle, Nat. Commun. (2015). doi:10.1038/ncomms9526.
[299] E.E. Stillwell, J. Zhou, H.C. Joshi, Human ninein is a centrosomal autoantigen recognized by CREST patient sera and plays a regulatory role in microtubule nucleation, Cell Cycle. (2004). doi:10.4161/cc.3.7.947.
[300] A. Dammermann, A. Merdes, Assembly of centrosomal proteins and microtubule organization depends on PCM-1, J. Cell Biol. (2002). doi:10.1083/jcb.200204023.
[301] D.K. Moss, G. Bellett, J.M. Carter, M. Liovic, J. Keynton, A.R. Prescott, E.B. Lane, M.M. Mogensen, Ninein is released from the centrosome and moves bi-directionally along microtubules, J. Cell Sci. (2007). doi:10.1242/jcs.010322.
[302] A. Espigat-Georger, V. Dyachuk, C. Chemin, L. Emorine, A. Merdes, Nuclear alignment in myotubes requires centrosome proteins recruited by nesprin-1, J. Cell Sci. 129 (2016) 4227–4237. doi:10.1242/jcs.191767.
[303] A. Dauber, S.H. LaFranchi, Z. Maliga, J.C. Lui, J.E. Moon, C. McDeed, K. Henke, J. Zonana, G.A. Kingman, T.H. Pers, J. Baron, R.G. Rosenfeld, J.N. Hirschhorn, M.P. Harris, V. Hwa, Novel microcephalic primordial dwarfism disorder associated with variants in the centrosomal protein ninein, J. Clin. Endocrinol. Metab. (2012). doi:10.1210/jc.2012-2150.
[304] C. Blum, A. Graham, M. Yousefzadeh, J. Shrout, K. Benjamin, M. Krishna, R. Hoda, R. Hoda, D.J. Cole, E. Garrett-Mayer, C. Reed, M. Wallace, M. Mitas, The expression ratio of Map7/B2M is prognostic for survival in patients with stage II colon cancer, Int. J. Oncol. (2008). doi:10.3892/ijo_00000043.
[305] L. Fu, H. Fu, L. Zhou, K. Xu, Y. Pang, K. Hu, J. Wang, L. Tian, Y. Liu, J. Wang, H. Jing, W. Huang, X. Ke, J. Shi, High expression of MAP7 predicts adverse prognosis in young patients with cytogenetically normal acute myeloid leukemia, Sci. Rep. (2016). doi:10.1038/srep34546.
[306] C. a Callahan, J.L. Bonkovsky, a L. Scully, J.B. Thomas, derailed is required for muscle attachment site selection in Drosophila., Development. 122 (1996) 2761–2767.
[307] D. Devenport, T.A. Bunch, J.W. Bloor, D.L. Brower, N.H. Brown, Mutations in the Drosophila alphaPS2 integrin subunit uncover new features of adhesion site assembly, Dev. Biol. 308 (2007) 294—308. doi:10.1016/j.ydbio.2007.02.046.
[308] F. Schnorrer, I. Kalchhauser, B.J. Dickson, The Transmembrane Protein Kon-tiki Couples to Dgrip to Mediate Myotube Targeting in Drosophila, Dev. Cell. 12 (2007) 751–766. doi:10.1016/j.devcel.2007.02.017.
[309] J.J. Perez-Moreno, M. Bischoff, M.D. Martin-Bermudo, B. Estrada, The conserved transmembrane proteoglycan Perdido/Kon-tiki is essential for myofibrillogenesis and sarcomeric structure in Drosophila, J. Cell Sci. 127 (2014) 3162–3173. doi:10.1242/jcs.150425.
[310] A. Dobrzynska, S. Gonzalo, C. Shanahan, P. Askjaer, The nuclear lamina in health and disease, Nucleus. 7 (2016) 233–248. doi:10.1080/19491034.2016.1183848.
[311] S.R. Schulze, B. Curio-Penny, S. Speese, G. Dialynas, D.E. Cryderman, C.W. McDonough, D. Nalbant, M. Petersen, V. Budnik, P.K. Geyer, L.L. Wallrath, A comparative study of Drosophila and human A-type lamins, PLoS One. 4 (2009). doi:10.1371/journal.pone.0007564.
[312] A. Brandt, F. Papagiannouli, N. Wagner, M. Wilsch-Bräuninger, M. Braun, E.E. Furlong, S. Loserth, C. Wenzl, F. Pilot, N. Vogt, T. Lecuit, G. Krohne, J. Großhans, Developmental control of nuclear size and shape by kugelkern and kurzkern, Curr. Biol. 16 (2006) 543–552. doi:10.1016/j.cub.2006.01.051.
[313] S. Melcer, Y. Gruenbaum, Nuclear morphology: When round kernels do the Charleston, Curr. Biol. (2006). doi:10.1016/j.cub.2006.02.032.

[314] P.J. Mansfield, D.A. Neumann, Chapter 3 - Structure and Function of Skeletal Muscle, in: P.J. Mansfield, D.A.B.T.-E. of K. for the P.T.A. (Third E. Neumann (Eds.), Mosby, St. Louis (MO), 2019: pp. 34–49. doi:https://doi.org/10.1016/B978-0-323-54498-6.00003-5.
[315] M.T. Valentine, P.M. Fordyce, S.M. Block, Eg5 steps it up!, Cell Div. 1 (2006) 1–8. doi:10.1186/1747-1028-1-31.
[316] M.M.S. Heck, A. Pereira, P. Pesavento, Y. Yannoni, A.C. Spradling, L.S.B. Goldstein, The kinesin-like protein KLP61F is essential for mitosis in Drosophila, J. Cell Biol. (1993). doi:10.1083/jcb.123.3.665.

Bibliography

Seminars in Cell & Developmental Biology xxx (2017) xxx–xxx

Contents lists available at ScienceDirect

Seminars in Cell & Developmental Biology

journal homepage: www.elsevier.com/locate/semcdb

Review

Acting on identity: Myoblast fusion and the formation of the syncytial muscle fiber

Su Deng[a], Mafalda Azevedo[a,b], Mary Baylies[a,*]

[a] Program in Developmental Biology, Sloan Kettering Institute, New York, NY 10065, United States
[b] Graduate Program in Basic and Applied Biology (GABBA), Institute of Biomedical Sciences Abel Salazar, University of Porto, Porto, Portugal

ARTICLE INFO

Article history:
Received 15 August 2017
Received in revised form 25 October 2017
Accepted 30 October 2017
Available online xxx

Keywords:
Drosophila
Muscle development
Membrane fusion
Actin cytoskeleton

ABSTRACT

The study of *Drosophila* muscle development dates back to the middle of the last century. Since that time, *Drosophila* has proved to be an ideal system for studying muscle development, differentiation, function, and disease. As in humans, *Drosophila* muscle forms via a series of conserved steps, starting with muscle specification, myoblast fusion, attachment to tendon cells, interactions with motorneurons, and sarcomere and myofibril formation. The genes and mechanisms required for these processes share striking similarities to those found in humans. The highly tractable genetic system and imaging approaches available in *Drosophila* allow for an efficient interrogation of muscle biology and for application of what we learn to other systems. In this article, we review our current understanding of muscle development in *Drosophila*, with a focus on myoblast fusion, the process responsible for the generation of syncytial muscle cells. We also compare and contrast those genes required for fusion in *Drosophila* and vertebrates.
© 2017 Published by Elsevier Ltd.

Contents

1. Introduction 00
2. Preparing for fusion: specification of muscle cells 00
   2.1. Muscle specification in the *Drosophila* embryo forms the larval muscles 00
   2.2. Muscle specification in the *Drosophila* pupa forms the adult muscles 00
   2.3. Muscle specification in vertebrates 00
3. Making larval muscle: myoblast fusion in the *Drosophila* embryo 00
   3.1. Recognition and adhesion 00
   3.2. Actin rearrangements at the fusion site 00
   3.3. Fusion pore formation 00
4. Making adult muscle: myoblast fusion in the *Drosophila* pupa 00
5. Making muscle in vertebrates: myoblast fusion 00
6. Conclusion 00
   Acknowledgements 00
   References 00

1. Introduction

From *Drosophila* to human, skeletal muscles develop and mature through similar steps: cells of the mesoderm are first specified to be skeletal muscle cells, which then undergo cell–cell fusion to add mass to these cells. After fusion is completed, sarcomeres assemble to provide contractile force, and the muscle cell builds connections with its surrounding tissues, such as tendons and motor neurons. Many of the genes that are critical for these steps are conserved across species. This also holds true for *nautilus*, which is the fly ortholog of vertebrate MYOD and a key regulator of myogenic differentiation in *Drosophila* (Michelson et al. [137]; reviewed by (Abmayr and Keller, [138])). As discussed below, Nautilus interacts with other transcription and chromatin regulators, and determines muscle identity, morphology, and size (reviewed in Dobi et al. [1]).

During *Drosophila*'s life cycle, two periods of myoblast fusion occur to form the larval muscle system and adult muscle system, respectively (Fig. 1). The larval body wall muscles form during the embryonic stage. These muscles have been intensively studied as they represent muscle at its simplest: a single muscle fiber forms

* Corresponding author.
E-mail address: m-baylies@ski.mskcc.org (M. Baylies).

https://doi.org/10.1016/j.semcdb.2017.10.033
1084-9521/© 2017 Published by Elsevier Ltd.

Please cite this article in press as: S. Deng, et al., Acting on identity: Myoblast fusion and the formation of the syncytial muscle fiber, Semin Cell Dev Biol (2017), https://doi.org/10.1016/j.semcdb.2017.10.033

a single muscle. The adult muscle system forms during the pupal stage of development. In contrast to the larva, each single adult muscle is composed of multiple muscle fibers and thus more closely resembles the muscle organization found in vertebrate skeletal muscle (reviewed by Dobi et al. [1]; Taylor [2]. This pertains in particular to the indirect flight muscles, the largest and best-studied muscle set of the adult fly. In this review, we first give a brief overview of muscle specification (Fig. 2) and then focus on a discussion of the current studies in myoblast fusion both in *Drosophila* (Fig. 3, Table 1) and vertebrates (Table 2).

2. Preparing for fusion: specification of muscle cells

2.1. *Muscle specification in the* Drosophila *embryo forms the larval muscles*

The body wall or skeletal muscles are derived from somatic (*Drosophila*) or paraxial (mammals) mesoderm, respectively. In *Drosophila*, the allocation of somatic mesoderm depends on the communication between the mesoderm and the ectoderm [49–51], as well as the combination of transcription factors that are expressed in the mesoderm (reviewed in Baylies [52]; Dobi et al [1]. After the allocation of the somatic mesoderm, the bHLH protein Lethal of Scute (L'sc) is expressed in clusters of promuscle cells (Fig. 2A), under the control of the Receptor Tyrosine Kinase (RTK) pathway [53]. In each cluster, a combination of the Notch and RTK-Ras signaling pathway activities restricts the expression of L'sc to one cell—the muscle progenitor cell (Fig. 2B, C) [53–55]. Each progenitor cell then undergoes an asymmetric division to form either two founder cells (FC) or a single FC and an adult muscle progenitor (AMP) (Fig. 2D) [56,57]. The cytoplasmic membrane-associated protein Numb plays a critical role in determining muscle fate. Numb antagonizes Notch-mediated lateral inhibition and allows the expression of muscle identity proteins in the muscle progenitor cells [57]. Different combinations of identity transcription factors expressed in each muscle progenitor, such as Slouch, Eve, Krüppel, Apterous, and the MyoD ortholog, Nautilus, in conjunction with chromatin regulators such as Sin3a [58] determine the different cell identities of each FC, and hence, the final muscle pattern (Fig. 2E, [1]. After L'sc is restricted to the progenitor cell, the remaining cells in the promuscle cell cluster adopt a fusion competent myoblast (FCM) fate. The specification of FCMs is controlled by Notch-mediated lateral inhibition as well as by the transcription factors Lame duck and Tramtrack [59].

Completion of FC and FCM specification allows for fusion between the two cell types, generating syncytial muscle cells (Figs. 2 E and 3). Throughout the period of fusion, the transcriptional profiles in both FCs and FCMs are dynamically regulated [60–63]. With the completion of each round of fusion, the fused FCM nuclei undergo progressive reprogramming, such that FCM-specific genes are suppressed, and the transcriptional pattern of the FC nucleus is adopted. The nucleus from the FC retains the expression of identity transcription factors after fusion. Additional experimental evidence suggests that the nucleus from the FC remains transcriptionally different from other nuclei in the same muscle fiber [60]. Fusion events between FCs and FCMs are completed at late stage 15 (~13.5 h AEL) [64,65]. Myotubes derived from myoblast fusion differentiate into fully striated, functional larval muscles (Fig. 1A, C). These muscles grow without additional fusion events throughout the larval stage.

2.2. *Muscle specification in the* Drosophila *pupa forms the adult muscles*

Compared to the larval muscle, less is known about the specification process of adult *Drosophila* muscles. The prominent muscle groups in the adult *Drosophila* include the Direct Flight Muscles (DFM), the Indirect Flight Muscles (IFM), the jump muscles, the abdominal muscles, and the leg muscles. Based on morphology and gene expression, these adult somatic muscles can be divided into two types: tubular and fibrillar muscles. The *Drosophila* abdominal, jump, leg and direct flight muscles are tubular muscles with aligned myofibrils that rely on glycolytic metabolism, while the Indirect Flight Muscles (IFMs) are fibrillar muscles with distinct, unaligned myofibrils (Fig. 1D) and are primarily oxidative [66]. The IFMs are composed of 7 pairs of dorsal-ventral muscles (DVMs) and 6 pairs of dorsal longitudinal muscles (DLMs) (Fig. 1B). DVMs and DLMs have different orientation and attachment sites, and are generated from fusion between myoblasts and templates with different origins (reviewed in Dobi et al. [1]. The specification of DFMs requires the homeodomain transcription factors Cut and Apterous [67]. The specification of IFMs depends on the transcriptional regulators Vestigial [68] and Scalloped [69]. In addition, Spalt major in the IFMs directs the fibrillar muscle fate [70]. Readers are directed to reviews on the specification of adult muscle for more detail [1,71,72].

2.3. *Muscle specification in vertebrates*

Similar to *Drosophila*, the specification of muscle progenitor cells in vertebrates also requires a combination of signals from adjacent tissues (reviewed in Munsterberg et al., [139]; Bryson-Richardson and Currie [73]. Extracellular signals induce the expression of Paired Box (Pax) 3 and Pax7 in the somites [74]. Pax genes have dual roles: they enhance the proliferation of muscle precursor cells [75], and they activate the expression of MyoD and Myf5, two

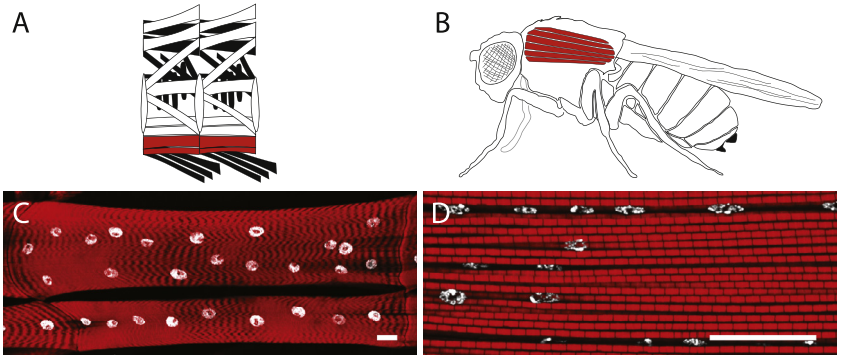


Fig 1. Larval and adult *Drosophila* muscles. A) Schematic representation of the larval muscles. The Ventral Longitudinal (VL) muscles 3 (top) and 4 (bottom) are highlighted in red. B) Schematic representation of the adult muscles. The Dorsal Longitudinal Muscles (DLMs) that compose the major portion of the Indirect Flight Muscles are highlighted in red. C) Representative image of the 3rd instar larval VL muscles 3 and 4. D) Representative image of the DLMs where it is possible to observe multiple myofibrils and nuclei. C and D) Actin labeling in sarcomere, red; Nuclei, white. Scale bars, 25 μm.

Please cite this article in press as: S. Deng, et al., Acting on identity: Myoblast fusion and the formation of the syncytial muscle fiber, Semin Cell Dev Biol (2017), https://doi.org/10.1016/j.semcdb.2017.10.033

members of the myogenic regulatory factor (MRF) family [76,77], reviewed in Bryson-Richardson and Currie [73]. MRFs are a family of four transcription factors: MyoD, Myf5, myogenin, and MRF4. MRFs activate the expression of genes required for muscle differentiation. MyoD and Myf5 are the first MRFs expressed in muscles and function redundantly to trigger myoblast specification [78]. Myogenin functions after muscle progenitor formation and regulates terminal differentiation of committed myoblasts [79] but can also function upstream of MyoD to direct the specification of some myogenic cells [80]. In addition to MRFs, other transcription factors are required for muscle differentiation, such as the Myocyte enhancer factor 2 (Mef2), which plays a conserved role in muscle cell differentiation from *Drosophila* to human [81–83]. After the specification of myogenic cells, two waves of myogenesis take place to form the final vertebrate muscle pattern. The first wave generates primary myofibers. The primary fibers function similarly to FCs in *Drosophila*, and determine the shape and identity of muscles (slow or fast). The second wave generates secondary myofibers that align alongside the primary myofibers and adds mass to the muscles [84]. The formation of both types of myofibers requires fusion of myoblasts. *In vitro* experiments suggest that the fusion process occurs in two periods: the first involves the fusion of individual myoblasts to form the nascent myotubes; the second period involves fusion between the myotube and additional myoblasts (reviewed in Rochlin et al. [85].

3. Making larval muscle: myoblast fusion in the *Drosophila* embryo

3.1. Recognition and adhesion

Myoblast fusion begins with cell–cell recognition and adhesion (Fig. 3A, Table 1). In *Drosophila*, recognition and adhesion between the FC and FCMs are mediated by cell-specific immunoglobulin super family (IgSF) members. The IgSF members expressed in the FC are Dumbfounded (Duf) and Roughest (Rst) [9]. Duf and Rst are transmembrane proteins that function redundantly to mediate recognition and adhesion [19]. In the FCMs, Sticks and Stones (Sns) and Hibris (Hbs) are the counterparts of Duf and Rst [10,20]. Hbs can partially compensate for Sns function, but its activity is less efficient than Sns [86]. Expression of Rst is also detected in a subset of FCMs; however, its function in the FCM is unclear [19]. The interaction between Duf-Sns and Rst-Hbs is required for cell recognition and adhesion. Ectopic expression of Duf induces myoblast aggregation and adhesion, but is insufficient to trigger fusion [9]. The interaction between Duf/Rst-Sns/Hbs is also required in other developmental events such axon guidance and eye development [87,88], and this "cassette" of transmembrane proteins is referred to as an "adhesion module" in these contexts. If the FC/myotube and FCMs are not in direct contact before adhesion, cell migration is required to bring the two types of cells into close proximity [3,85]. An intriguing recent development in the understanding of fusion-related adhesion is the identification of N-cadherin as a contributor to myoblast fusion in the *Drosophila* embryo. N-cadherin is a member of the cadherin family of adhesion proteins. N-cadherin is present, but not restricted at the fusion site [12]. One possible function of N-cadherin is to mediate cell adhesion through the formation of cellular junction-like structures at the fusion site [89]. For membrane fusion to proceed, however, N-cadherin needs to be removed from the fusion site [89]. Kette and Schizo/Loner, upstream regulators of Arp2/3-mediated actin rearrangements (see Actin rearrangement section below), are reported to facilitate removal of N-cadherin [89,12,90]. Notably, N-cadherin loss of function does not result in fusion defects in the *Drosophila* embryo [91,12], suggesting potential redundant functions with other members of the cadherin family.

3.2. Actin rearrangements at the fusion site

After the cells adhere to one another, signals from these transmembrane recognition and adhesion molecules cause the actin cytoskeleton in both the FC and FCM to undergo remodeling, resulting in a filamentous-actin (F-actin)-based focus structure in the FCM and a thin sheath of F-actin on the opposing inner membrane in the FC (Fig. 2B). The actin focus in the FCM mediates the formation of invasive finger-like membrane protrusions [92]. This actin structure in the FCM is thought to provide the necessary force to push the lipid bilayers of the cells into close proximity. In response to the mechanical forces generated by the invasive protrusions from the FCM, non-muscle Myosin II (MyoII) is recruited to the fusion site in the FC/myotube. The accumulation of MyoII generates cortical tension, facilitates cell membrane juxtaposition, and promotes fusion pore formation (see below) [14].

A major regulator of the actin focus during myoblast fusion is Arp2/3. Arp2/3 is a multi-subunit protein complex that binds to actin filaments and polymerizes new actin filaments at a 70° angle from the pre-existing actin filament. Arp2/3 is activated by the nucleation-promoting factors (NPFs), Wiskott-Aldrich Syndrome protein (WASp) and SCAR (also known as WAVE). Signal transduction from the membrane to these actin cytoskeleton regulators is partially mediated by the activity of Crk, as well as Dreadlock (Dock), the *Drosophila* homolog of Nck. Both Dock and Crk are adapter proteins with *src* homology 2 (SH2)/SH3 domains. Dock can interact with all four IgSF transmembrane proteins that have

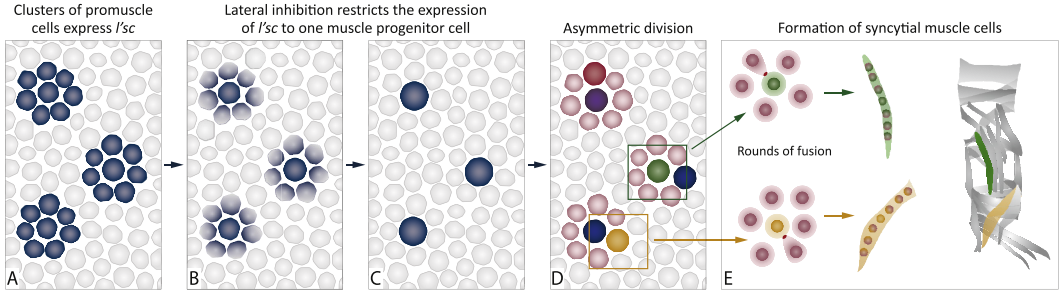


Fig. 2. Specification, Fusion and Differentiation of Muscle Cells. A) Expression of L'sc occurs in clusters of mesodermal cells with competency to become muscle progenitor cells. B and C) The activity of the Notch and RTK-Ras pathways restricts the expression of L'sc to a single muscle progenitor cell of a particular identity. D) The remaining cells from the initial cluster of promuscle cells become FCMs (pink). The muscle progenitor cells undergo asymmetric division to form either two founder cells (red and purple) or one founder cell (green or yellow) and an adult muscle progenitor (blue). E) Founder cells shown in panel 2D express different identity genes and undergo several rounds of fusion (actin foci, red) to form syncytial muscle cells with different characteristics. The green founder cell expresses *apterous* and forms muscle LT1 and the yellow founder cell expresses *nautilus* to form muscle VA1 (modified from [1]). The myotubes maturate by attaching to tendon cells and developing sarcomeres (not shown). The final position of these muscles is highlighted in the hemisegment schematic on the right.

Please cite this article in press as: S. Deng, et al., Acting on identity: Myoblast fusion and the formation of the syncytial muscle fiber, Semin Cell Dev Biol (2017), https://doi.org/10.1016/j.semcdb.2017.10.033

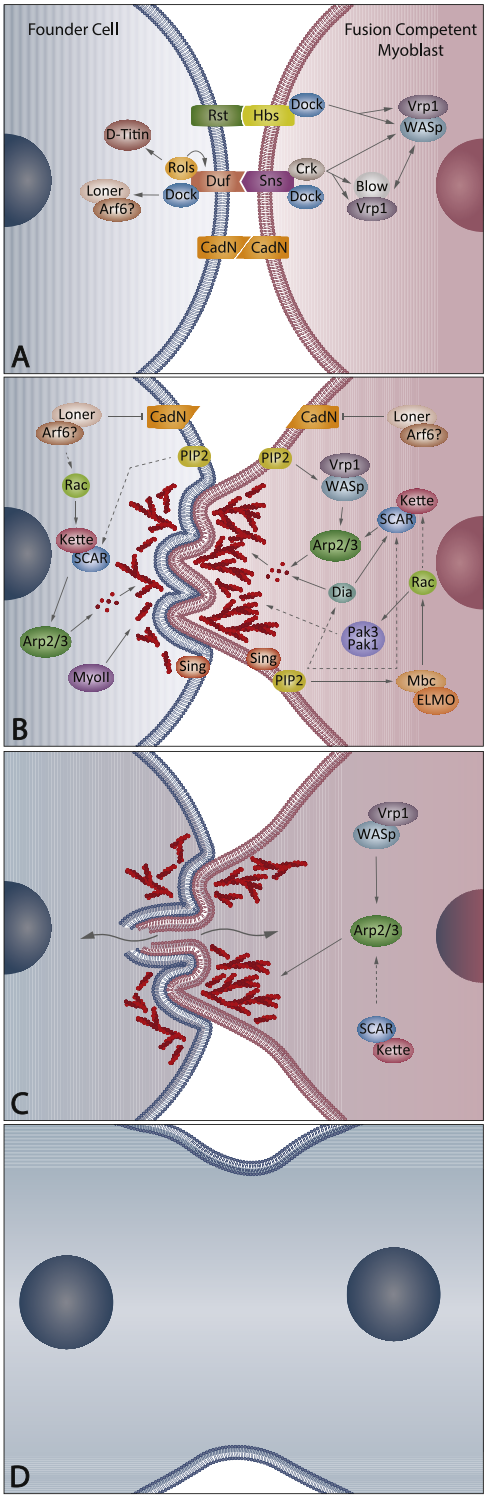


Fig. 3. Schematic representation of myoblast fusion. In the *Drosophila* embryo, fusion of an individual founder cell (FC) with multiple fusion competent myoblasts (FCMs) gives rise to a single multinucleated muscle cell; the number of FCM fusion events determines the number of nuclei in the mature muscle cell. A) Recognition and Adhesion: FC and FCM express different membrane proteins that allow the two cells to recognize and adhere to each other. When in contact, each cell initiates the fusion process by recruiting several proteins to the fusion site. B) Actin Focus Formation: Through the activity of the fusion machinery on both the FC and the FCM, actin (red) monomers are assembled into filaments and form a dense F-actin focus on the FCM side and a thin layer on the FC side. The FCM actin focus invades the FC with multiple finger-like protrusions. N-cadherin is removed from the membrane to allow for the next steps of fusion. C) Pore Formation. The formation of a fusion pore in the membrane occurs, allowing for the exchange of cytoplasm between both cells. The repression of the FCM transcriptional profile begins (FCM pink nucleus turns blue). D) Post Fusion. After one fusion event, the resulting cell has one additional nucleus that has the transcriptional profile of the FC (blue nuclei). At this moment, the cell either prepares for another round of fusion or stops fusing with FCMs.

SH2 or SH3 domains, but it only genetically interacts with Duf, Sns, and Hbs [93]. In addition, rescue experiments using a series of *sns* deletions and site-directed mutations suggest that Sns functions through interacting with a complex array of proteins [94]. In the FCMs, the Dock SH3 domain biochemically and genetically interacts with WASp, as well as the WASp regulator, Verprolin 1 (Vrp1, also known as Solitary (Sltr) and D-Wip) [93]. In both the FC and FCMs, Dock biochemically and genetically interacts with the Arp2/3 NPF SCAR. Through a similar mechanism as Dock, Crk biochemically interacts with Sns. In a FCM, Crk physically interacts with the WASp regulatory proteins Vrp1 and Blow [95]. Thus, the adaptor proteins Dock and Crk function as links that relay signals from the membrane to the actin cytoskeleton.

In the FC, another adaptor protein that links activity at the membrane to the actin cytoskeleton is Rolling pebbles (Rols, also known as Antisocial (Ants)/Rols). Rols is recruited to the fusion site by Duf. In a positive feedback loop, Rols replenishes Duf at the membrane, and thus enables additional rounds of fusion [96]. Rols interacts with two proteins that regulate the actin cytoskeleton organization: Myoblast city (Mbc) [17,18] and D-titin [97]. Mbc is the *Drosophila* homolog of the mammalian protein DOCK1, which mediates actin rearrangements by acting as a guanine nucleotide exchange factor (GEF) for the small GTPase Rac. However, recent data suggest that the downstream target of Rols is not Mbc: rescue experiments suggest that the activity of Mbc is not required in the FC for the initial fusion event [98]. Another actin cytoskeletal protein that can bind to Rols is D-titin [97]. D-titin is recruited to the fusion site by Rols and mediates myoblast fusion in a mechanism that remains unclear. D-titin is also involved in maintaining myotube morphology [97]; Zhang et al., 2000.

While Mbc appears not to be required by the FCs initially, Schizo/Loner, another GEF that regulates actin rearrangements, is required in FCs to mediate fusion. Schizo/Loner is recruited to the fusion site by Duf and Rst [99]. Domain analysis suggests that the function of Schizo/Loner is to recruit and activate the small GTPase dARF6 at the fusion site. Schizo/Loner and dARF6 control the membrane localization of Rac [11]. However, *arf6* maternal/zygotic null mutants do not have a myoblast fusion defect [100], and the fusion phenotype in a dominant negative *dARF6* background is not as severe as that in the *schizo/loner* mutant. Together these data suggest that the downstream target of Schizo/Loner is another GTPase or that there is redundancy with other dARF family members such as dARF1 [11].

Once activated, the small GTPase Rac regulates the function of SCAR and is critically important in both FCs and FCMs to mediate fusion. The activity of SCAR is controlled by the pentameric WRC complex (the WAVE/SCAR regulatory complex). The WRC is composed of Kette/Nap1, Sra1, Abi, Hspc300, and SCAR itself [101]. Rac activity is essential for the localization of the WRC to the fusion site, as well as activation of SCAR via the release of the SCAR VCA domain from an inhibited state [102,103]. As part of the WRC, Kette is also essential for myoblast fusion as it controls the localization and stability of SCAR [3]. It has not been reported whether loss of function in the other WRC components, Sra1, Abi and Hspc300, lead to a fusion phenotype. This may be due to a lack of appropriate mutant alleles, as well as a maternal supply of protein/mRNA in the embryo that masks the role of these proteins during the time period in which fusion takes place. Nevertheless, overexpression of WRC components in muscle cells results in fusion block and suggests a potential role of other WRC components during fusion [104].

Please cite this article in press as: S. Deng, et al., Acting on identity: Myoblast fusion and the formation of the syncytial muscle fiber, Semin Cell Dev Biol (2017), https://doi.org/10.1016/j.semcdb.2017.10.033

In the FC, SCAR activates its downstream target Arp2/3, and rearranges the actin cytoskeleton into a thin sheath along the fusion site [92]. In the FCM, SCAR activity is also regulated by Rac. However, Rac localization and activation is regulated through Mbc [98]. Mbc is recruited to the fusion site by the phospholipid PI(4,5)P2 (PIP2). When PIP2 activity is sequestered via overexpression of the pleckstrin homology domain of phospholipase C-gamma ($PH^{plcgamma}$), Mbc is concentrated in the cytoplasm instead of at the fusion site, leading to mislocalization of active Rac [15]. Mbc interacts with ELMO using its SH3 domain and forms the Mbc/ELMO complex. The GEF activity of Mbc/ELMO is tightly regulated during myoblast fusion, and it controls the level of active Rac. Both overexpression and loss of function of Mbc/ELMO cause defects in myoblast fusion, which are reminiscent of constitutively active Rac and Rac mutants, respectively [105]. When activated by Mbc/ELMO, Rac, in turn, binds to the WRC and regulates Arp2/3 activity at the fusion site.

In addition to SCAR, the other NPF, WASp, also regulates Arp2/3 at the fusion site. Unlike SCAR, which functions both in FCs and FCMs, WASp activity is only required in the FCM [5]. The activity of WASp is regulated by Blown Fuse (Blow) and Vrp1. The WASp-homology-1 (WH1) domain in WASp can bind to the WASp-binding domain (WBD) in Vrp1 [106]. The interaction between WASp and Vrp1 is required to stabilize and localize WASp at the fusion site [5]. This interaction is disrupted when Blow competes with WASp for Vrp1 WBD binding [5]. Thus, after cell recognition and adhesion, a signal is transduced from the membrane via the adaptor protein Crk, which recruits Blow and Vrp1 to the fusion site. At the fusion site, the WASp-Vrp1 complex promotes actin polymerization by regulating Arp2/3 activity. Blow suppresses WASp activity by competing with WASp for Vrp1 binding and by dissociating the WASp-Vrp1 complex. Since the binding affinity between Blow-Vrp1 is lower than WASp-Vrp1, dissociated WASp interacts with Vrp1 again and promotes another round of branched actin polymerization [5]. It has been reported that in FCs, the function of WASp and SCAR is redundant, as overexpression of WASp in the FCs can partially restore fusion in *kette* mutant background [89]. FCM-specific reduction of the WASp level in a *kette* mutant background rescues fusion defects. It has been proposed that a particular ratio of active WASp and SCAR needs to be maintained for fusion to occur [89].

Recent studies have indicated that in addition to the branched actin network generated by Arp2/3, the linear actin filament nucleated by Diaphanous (Dia) also plays a role during myoblast fusion [8,107]. Dia is a member of the formin family of actin polymerization proteins. Dia is enriched at the actin focus during the formation of *Drosophila* somatic musculature and dorsal pharyngeal musculature. Dia loss of function blocks myoblast fusion [8]. Interestingly, overexpression of active Dia also leads to fusion defects [8,107], suggesting that the activity of Dia is highly regulated. Notably, in addition to Dia, the WASp family member WHAMY can also promote the assembly of linear actin filament. It has been reported that WHAMY synergizes with WASp during myoblast fusion [23]. Altogether, these data suggest that a balance between linear and branched actin filament is required at the fusion site for fusion to occur.

3.3. Fusion pore formation

A critical step in cell fusion is the formation of fusion pores that allow for cytoplasmic continuity between the fusing cells (Fig. 3C). Studies from virus-cell fusion and *C. elegans* epithelial cell fusion have identified fusogens that mediate fusion pore formation [108]; reviewed in Sapir et al. [109]. A fusogen is a transmembrane protein that localizes to the fusion site and its presence is essential and sufficient to trigger membrane fusion [109]. Despite the identification of many gene products that are required for myoblast fusion in both *Drosophila* and vertebrates, no fusogen has been identified in these systems to date. Therefore, the mechanism that brings the membranes in close proximity to allow pore formation during myoblast membrane fusion remains a critical, open question.

It has been proposed that the actin cytoskeleton plays a crucial role in forcing the juxtaposition of the FC/FCM cell membranes, leading to the formation and expansion of fusion pores (reviewed by Onel and Renkawitz-Pohl, Schejter, Schulman et al., [110–112]. During *Drosophila* embryonic myoblast fusion, the F-actin focus in the FCM forms podosome-like structures at the fusion site, which provide an invasive force on the apposing FC and pushes the cell membranes of the FCM and FC into closer proximity. The F-actin focus later evolves into a single-channel fusion pore on the membrane of the fusing cells [92]. Studies aimed at investigating the function of actin regulators during pore formation have been performed. In these studies, the exchange of fluorescent proteins between the FCM and the FC were measured as a reporter of cytoplasmic continuity in various fusion mutant backgrounds. From these experiments, it has been proposed that SCAR-regulated actin remodeling is required for the initiation of fusion pore formation [103]. The function of WASp and its regulators is required for the formation of invasive structures [5,95,92]. Therefore it is believed that WASp-regulated actin remodeling is required for pore formation [5,95,92] and expansion [103]. Notably, the actin focus resolves prior to fusion, suggesting that actin and other proteins located at the fusion site need to be removed, allowing fusion to occur. Thus far, the removal of proteins associated with the actin cytoskeleton at the fusion site has not been well studied. One potential protein involved in this process is Schizo/Loner, which has been reported to remove N-cadherin from the fusion site to permit fusion [12]. In addition, the transmembrane protein *singles bar* (*sing*) is required during myoblast fusion. *sing* mutant embryos display a cell fusion block with accumulation of vesicles at the fusion site, suggesting a potential role of Sing in vesicle trafficking during fusion [113].

Other studies suggest alternative models of fusion pore formation [114,4,110]. Electron microscopy images have shown the presence of prefusion complexes at the fusion site. These prefusion complexes contain electron-dense, paired vesicles at the apposed plasma membranes. It has been suggested that these paired vesicles resolve into membrane plaques. Subsequently, the juxtaposed plasma membranes vesiculate and form sacs that enclose the extracellular space. Multiple fusion pores are observed in these situations [4]. Similar membrane structures and multiple fusion pores at the fusion site have also been reported during myoblast fusion which leads to the formation of the *Drosophila* adult flight muscle [114]. These data emphasize the requirement for the delivery and the clearing of vesicles at the fusion site as critical for membrane breakdown [4]. These data also suggest that instead of one fusion pore, multiple pores are formed to facilitate fusion. It is still unclear whether these differences of fusion pore number arise from different fixation methods, context or other variables (reviewed in Schejter [111]).

4. Making adult muscle: myoblast fusion in the *Drosophila* pupa

The *Drosophila* adult muscles form during metamorphosis in the pupal stages. During the first few hours of metamorphosis, most of the *Drosophila* larval body wall muscles are destroyed through histolysis, but a few muscles, such as the Dorsal Oblique (DO1-3) muscles, escape degradation and serve as templates for some adult muscles, notably the Dorsal Longitudinal Flight muscles [115]. The growth of adult muscles is achieved through hundreds of cell–cell

Please cite this article in press as: S. Deng, et al., Acting on identity: Myoblast fusion and the formation of the syncytial muscle fiber, Semin Cell Dev Biol (2017), https://doi.org/10.1016/j.semcdb.2017.10.033

Table 1
List of gene products required in *Drosophila* myoblast fusion.

Protein	Localization	Function	Reference(s)
Arp2/3	Cytoplasm	Actin polymerization	[3]
Blown Fuse (Blow)	Cytoplasm	Regulation of WASp activity	[4], [5]
Crk	Cytoplasm	Adaptor protein	[6,7]
Diaphanous (Dia)	Cytoplasm	Actin polymerization	[8]
Dumbfounded (Duf)	FC – Membrane	Recognition and Adhesion	[9]
Hibris (Hbs)	FCM – Membrane	Recognition and Adhesion	[10]
Kette	Cytoplasm	SCAR activation	[3]
Schizo/Loner	Cytoplasm	Rac localization and N-cadherin removal	[11], [12]
Myoblast City (Mbc)	Cytoplasm	Regulation of Rac activity	[13]
Myosin II (Myo II)	FC – Cytoplasm	Cortical tension generation on the FC/myotube	[14]
N-cadherin	Membrane	Adhesion	[12]
PI(4,5)P2	Membrane	Actin cytoskeleton remodeling	[15]
Rac	Cytoplasm	SCAR activation	[16]
Rolling pebbles (Rols)	Cytoplasm	Adaptor protein involved with Duf recycling	[17], [18]
Rst	FC – Membrane	Recognition and Adhesion	[19]
SCAR	Cytoplasm	Arp2/3 activation	[3]
Singles Bar (Sing)	Membrane	Vesicle trafficking	[113]
Sticks and Stones (Sns)	FCM – Membrane	Recognition and Adhesion	[20]
Verprolin1 (Vrp1)	Cytoplasm	Regulation WASp activity	[21], [5]
WASp	Cytoplasm	Arp2/3 activation	[22]
WHAMY	Cytoplasm	Actin polymerization	[23]

fusion events, in which a pool of myoblasts fuse with either template myotubes or muscle precursor cells [115].

The pathways that regulate myoblast fusion to form the *Drosophila* adult muscles are not fully understood. Based on our current knowledge, the mechanisms that regulate myoblast fusion during adult myogenesis are similar to those that regulate embryonic myogenesis. Fusion occurs between the adult muscle progenitors (AMPs) and myoblasts that migrate from the imaginal discs to form the adult abdominal muscles, the leg muscles, and the DVMs. The DLMs are formed through fusion between myoblasts and the muscle templates that are preserved during histolysis [115]. The AMPs associated with the wing imaginal disc go through two phases of amplification during adult muscle development. The initial phase is a symmetrical division which is regulated by Notch signaling and leads to increased AMP numbers. The second phase is an asymmetrical division that is regulated by Notch and Wnt signaling and results in AMP self-renewal and the generation of myoblast progeny required for the later fusion events [116]. It has been proposed that during muscle injury, the AMPs could function similarly to satellite cells, whose progeny fuse with myotubes to repair muscles [116]. A recent study has shown that dIlp6 signals from a muscle niche can activate dormant AMPs through the Insulin-Notch-dMyc cascade [117].

Similar to embryonic myoblast fusion, the transmembrane proteins Duf, Rst, Sns, and Hbs are required to mediate cell recognition and adhesion [118]. After adhesion, the fusing myoblast flattens on the myotube, such that the cell membranes are in tight apposition [114]. Actin accumulates primarily at the myoblast side of the fusion site, after receiving signals from the cell membrane, and forms a focus-like structure. As with embryonic myogenesis, actin rearrangements during adult myogenesis require the function of Arp2/3, as well as the actin nucleation-promoting factors (NPFs) WASp and SCAR. Loss of function studies revealed that WASp is required for fusion pore initiation. [119]. Similar to embryonic myoblast fusion, the MARVEL domain protein Sing is expressed in adult muscles, and its activity is required for adult myoblast fusion [120].

Despite these similarities, however, there are differences between *Drosophila* embryonic and adult myogenesis. In embryos, FCMs and FCs are positioned relatively close to one another prior to fusion. The FCMs in contact with FCs/myotubes are responsible for the early fusion events. The FCMs that are located more internally migrate prior to making contact and fusing with the FCs/myotubes [64,65]. During adult myogenesis, myoblasts often need to migrate long distances from the imaginal discs to the muscle template/myotubes. More importantly, during migration, these myoblasts maintain a semi-differentiated state via the Notch signaling pathway. Each myoblast expresses the Notch ligand Delta and represses the differentiation of its neighboring cells. Notch signaling decays when myoblasts reach the vicinity of the myotubes, and this allows for the terminal differentiation of the myoblasts and the expression of FCM markers such as Sns [118].

During adult muscle formation, the adhesion between myoblasts and myotubes also requires filopodia that emanate from the myotube surface. The filopodia are actin-based structures that bring the myoblasts and myotubes into close proximity. The formation and maintenance of filopodia requires the activity of Enabled and IRSp53 [121]. The requirement for these two proteins during embryonic myoblast fusion has not been reported. In addition, reducing WASp and SCAR activity simultaneously in embryos abolishes actin focus formation [15]. However, double knockdown of WASp and SCAR during adult muscle formation results in enlarged actin foci, suggesting novel roles of the NPFs during *Drosophila* adult myoblast fusion [119].

5. Making muscle in vertebrates: myoblast fusion

Compared to *Drosophila*, the vertebrate muscle is a more complex system, both in terms of its structure and the regulatory mechanisms required during development. Over the past few decades, researchers have identified numerous genes that are required for myoblast fusion in vertebrates (reviewed in Rochlin et al. [85]; Demonbreun et al. [122]. Nevertheless, how these different proteins coordinate fusion remains unclear. The morphological steps that are required for myoblast fusion and many of the genes necessary for the process are conserved between *Drosophila* and vertebrates. Therefore, we review recent updates in vertebrate fusion-related genes based on their localization and which steps they are involved in during fusion (Table 2).

Similar to the process of *Drosophila* myoblast fusion, the myotube-myoblast fusion during muscle development in vertebrates is also asymmetric and requires recognition molecules located on the cell membrane. One pair of membrane proteins required for fusion is Integrin vLA-4 and its receptor VCAM-1. Integrin vLA-4 is expressed in myotubes and VCAM-1 in myoblasts.

Please cite this article in press as: S. Deng, et al., Acting on identity: Myoblast fusion and the formation of the syncytial muscle fiber, Semin Cell Dev Biol (2017), https://doi.org/10.1016/j.semcdb.2017.10.033

Table 2
List of gene products required for vertebrate myoblast fusion.

Protein	Location and function	Animal model	Reference(s)
Adam12	Membrane Mediates myoblast adhesion Interaction with the actin-binding protein α-actinin-2 promotes myoblast fusion	Mouse	[24,142]
BAI1	Membrane Mediates recognition of phosphatidylserine on apoptotic cells Regulates myoblast fusion through Dock1/Rac1 pathway	Mouse	[25]
BAI3	Membrane Interacts with the scaffold protein ELMO to regulate myoblast fusion, possibly through the ELMO/DOCK/Rac1 pathway	Chicken	[26]
Caveolin-3	Membrane Involved in myoblast fusion (unclear role) Contradictory fusion phenotypes in different experimental models	Mouse	[27,143]
Cdc42	Cytoplasm Required for actin rearrangement at the fusion site	Mouse	[136]
CKIP-1	Cytoplasm Regulates myoblast fusion by interacting with both phosphoinositides on the membrane and Arp2/3 subunit	Mouse Zebrafish	[29]
Crk Crkl	Cytoplasm Adaptor proteins Crk/Crkl genetically interact with DOCK1/DOCK5 to regulate myoblast fusion	Zebrafish	[30]
DOCK1	Cytoplasm Required for myoblast fusion by activating Rac1	Zebrafish Mouse	[31,30]
DOCK5	Cytoplasm Functions redundantly with DOCK1 Also involved in post-fusion myofiber development	Zebrafish Mouse	[31,30]
EHD2	Membrane and cytoplasm Regulates myoblast fusion by mediating endocytic recycling of membrane proteins, such as Myoferlin	Mouse	[32]
Gm7325 Myomixer Minion	Membrane Interacts with Myomaker to induce fusion	Mouse	[33,34]; Zhang et al., 2017
Myomerger	Functions in cell recognition (proposed)		
JAM-B JAM-C	Membrane Both physically interact to mediate fusion Facilitate myocytes recognition and adhesion (proposed)	Zebrafish	[35]
Kirrel	Membrane Required for fast muscle precursor fusion	Zebrafish	[36]
M-cadherin	Membrane Mediates myoblast adhesion Promotes fusion by activating the Rac1 pathway	Mouse	[37]
MOR23	Membrane Regulates cell adhesion during myoblast fusion	Mouse	[38]
Myoferlin	Membrane Regulates myoblast fusion through unclear mechanism, potentially by acting as a scaffold protein that links fusion proteins with the membrane	Mouse	[39]
Myomaker	Membrane Muscle-specific protein that induces fusion during muscle development and repair Mediate cell recognition (proposed)	Mouse Zebrafish Chicken	[40–42,140]
N-WASp	Cytoplasm Required in both fusing partners	Mouse	[43]
Rac1	Cytoplasm Required for proper recruiting of Arp2/3 to the contact site Regulates actin remodeling during fusion Unlike in *Drosophila*, constitutively active Rac1 in zebrafish leads to myoblasts hyperfusion	Mouse Zebrafish Chicken	[44,36,28]
Stab2	Membrane Involved in the phosphatidylserine-dependent fusion of myoblasts during muscle development and regeneration	Mouse	[45]
Talin 1/2	Cytoplasm Regulates myoblast fusion, potentially by mediating the interaction between integrins and cytoskeleton	Mouse	[46]
VLA4 VCAM1	Membrane VLA-4 and its counter receptor VCAM-1 are involved in secondary myogenesis	Mouse	[47]
β-1 integrin	Membrane Involved with membrane breakdown during myoblast fusion	Mouse	[48]

Please cite this article in press as: S. Deng, et al., Acting on identity: Myoblast fusion and the formation of the syncytial muscle fiber, Semin Cell Dev Biol (2017), https://doi.org/10.1016/j.semcdb.2017.10.033

Interactions between vLA-4 and VCAM-1 are required for the alignment of the secondary myofiber with the primary myofiber, as well as for the second phase of muscle cell fusion [47]. In addition to vLA-4 and VCAM-1, the transcription factor NFAT2C also mediates cell recognition by regulating the expression of IL-4. IL-4 is a cytokine that functions as a secreted myoblast recruitment factor [123]. Another pair of membrane proteins required for fusion is the immunoglobin superfamily proteins Jamb and Jamc. In zebrafish, Jamb and Jamc are expressed in fast-muscle myoblasts. The physical interaction between Jamb and Jamc is required for myoblast fusion during the formation of fast-twitch muscles. Loss of function of either protein severely impairs myoblast fusion [35,124]. In addition, it has been shown that Nephrin, an ortholog of the *Drosophila* transmembrane protein Sns, localizes on myoblasts and mediates cell recognition [125]. In zebrafish, Kirrel, an ortholog of Nephrin, is localized to membranes of myoblasts and is required for fusion [36]. After recognition, adhesion molecules such as M-cadherin [126], N-cadherin [127], and integrin family members [48] mediate the adhesion and alignment of the myoblasts. It has been reported that the G-protein coupled receptors BAI1 and BAI3 also play a role during fusion, through signal transduction from the membrane to the cytoskeleton via the Dock1/Rac1 pathway [26,25].

Unlike in *Drosophila,* an actin focus structure has not been reported during vertebrate myoblast fusion. Nevertheless, actin cytoskeletal rearrangements play a critical role in vertebrate muscle formation. Similar to *Drosophila mbc* mutants, *Dock1*-null mice embryos exhibit severely impaired myoblast fusion and skeletal muscle content is reduced [31]. Dock1 is the mammalian ortholog of Mbc, and it functions as a GEF protein that activates Rac GTPase. In a conditional *Rac1* knockout mouse model, the recruitment of Arp2/3 and F-actin to the cell-contact site is reduced, resulting in impaired myoblast migration and fusion [28]. Experiments using C2C12 mouse myoblast cell culture suggest that Nap1, the mammalian ortholog of Kette and the downstream target of Rac1, is also required for regulating WAVE dependent actin remodeling during myoblast fusion [128]. Moreover, a recent study reported the requirement of the non-muscle myosin IIA (NM-MHC-IIA) during myoblast fusion. NM-MHC-IIA is involved in the formation of the cortical actin wall in the FC/myotube in the rat L6 myoblast cell culture, providing structural and mechanical support to facilitate membrane alignment and fusion pore formation [129]. Together, these data suggest a conserved role of actin during muscle development.

It has been a major challenge to identify muscle-specific genes that ensure that fusion occurs only between myoblasts rather than other cell types. The first such gene found in vertebrates is Myomaker/Tmem8c. Myomaker is a transmembrane protein that is specifically expressed in the muscles during muscle development and regeneration [40–42,130,140]. In humans, reduced Myomaker function is linked to Carey-Fineman-Ziter syndrome [131], a congenital myopathy. Myomaker is required for fusion and is localized to the adhesion site. Expressing Myomaker in fibroblasts is sufficient to induce fusion between fibroblasts and myoblasts, but it is not sufficient to induce fibroblast–fibroblast fusion [42]. These reports suggest that additional proteins on the myoblasts are required to interact with Myomaker to induce fusion.

Recently, Gm7325, the potential counterpart of Myomaker, has been identified by three different labs, and was given the name Myomixer [33], Myomerger [34] and Minion Zhang et al., 2017. Gm7325 is an 84 amino acid microprotein with a similar expression pattern to Myomaker. The function of Gm7325 is required for Myomaker-induced fusion, as simultaneous expression of Myomaker and Gm7325 induces fusion between non-muscle cells [33,34]; Zhang et al., 2017. The mechanism by which Myomaker and Gm7325 regulates fusion is not well understood. A physical interaction between Myomaker and Gm7325 has been reported [33], but remains controversial [34,140]. In Gm7325- and Myomaker-deficient myoblasts, cell fusion is blocked at different fusion stages. Based on whether the cell membranes align in the deficient myoblasts, it has been proposed that Myomaker is necessary for cell recognition, while Gm7325 is required for downstream events such as actin cytoskeleton remodeling Zhang et al., 2017.

Cell fusion in vertebrates is required not only during early embryonic myogenesis, but also during muscle regeneration after damage. As with *Drosophila* adult muscle progenitors (AMPs), a pool of myoblasts remains undifferentiated during vertebrate myogenesis. These myoblasts are satellite cells that associate with myofibers. Satellite cells contribute to post-natal muscle growth, as well as to muscle repair. The specification of satellite cells is critically dependent on Pax7, as no satellite cells are found in *Pax7* mutant mice [132]. With intact muscles, satellite cells are mitotically quiescent and express Pax7 and Myf5, but not Myogenin or MyoD (reviewed in Yin et al. [141]). Upon muscle injury, myofiber necrosis triggers inflammatory responses, which induce satellite cells to proliferate [133]. After proliferation, the majority of satellite cells differentiate and start to express MyoD and myogenin [134]. These cells later fuse with damaged myofibers or fuse with each other to generate new muscle fibers [135]. Thus far, the process of satellite cell fusion is mechanistically similar to myoblast fusion during primary and secondary myofiber formation.

6. Conclusion

Myoblast fusion in organisms ranging from the fly to human occurs through conserved steps: cell recognition, membrane apposition, actin rearrangement, pore formation, and cytoplasmic continuity. The investigation of myoblast fusion in *Drosophila* continues to provide valuable insights to vertebrate muscle development. However, there are many questions that remain unanswered: How do muscles control the number of fusion events during development and during repair? How do the nuclei added to a myotube adopt the program of the growing myotube? How are movement and transcriptional diversity among the added myonuclei controlled? And when considering the mechanisms of fusion, how are the ratios of linear and branched actin filaments controlled at the actin focus? What are the actin depolymerization factors that resolve the actin focus after fusion pore formation? What causes pore formation between the engaged cells? The knowledge gained from answering these questions in model systems such as *Drosophila* will illuminate how the key steps of fusion are controlled and how the syncytial muscle cell develops and is maintained.

Acknowledgements

We thank the members of the Baylies lab for helpful discussions, Iliona Wolfowicz for the fly drawing in Fig. 1, and our funding agencies SFRH/BD/52041/2012 to MA, NIH [GM078318, AR108981] to MKB, and National Cancer Institute [P30 CA 008748] core grant to MSKCC.

References

[1] K.C. Dobi, V.K. Schulman, M.K. Baylies, Specification of the somatic musculature in Drosophila, Wiley Interdiscip. Rev. Dev. Biol. 4 (2015) 357–375.
[2] M.V. Taylor, Comparison of muscle development, in: H. Sink (Ed.), Drosophila and Vertebrates Muscle Development in Drosophila, Springer New York, New York NY, 2006, pp. 169–203.
[3] B.E. Richardson, K. Beckett, S.J. Nowak, M.K. Baylies, SCAR/WAVE and Arp2/3 are crucial for cytoskeletal remodeling at the site of myoblast fusion, Development 134 (2007) 4357–4367.

Please cite this article in press as: S. Deng, et al., Acting on identity: Myoblast fusion and the formation of the syncytial muscle fiber, Semin Cell Dev Biol (2017), https://doi.org/10.1016/j.semcdb.2017.10.033

[4] S.K. Doberstein, R.D. Fetter, A.Y. Mehta, C.S. Goodman, Genetic analysis of myoblast fusion: blown fuse is required for progression beyond the prefusion complex, J. Cell Biol. 136 (1997) 1249–1261.
[5] P. Jin, R. Duan, F. Luo, G. Zhang, S.N. Hong, E.H. Chen, Competition between Blown fuse and WASP for WIP binding regulates the dynamics of WASP-dependent actin polymerization in vivo, Dev. Cell 20 (2011) 623–638.
[6] L. Balagopalan, M.-H. Chen, E.R. Geisbrecht, S.M. Abmayr, The CDM superfamily protein MBC directs myoblast fusion through a mechanism that requires phosphatidylinositol 3,4,5-triphosphate binding but is independent of direct interaction with DCrk, Mol. Cell. Biol. 26 (2006) 9442–9455.
[7] B.J. Galletta, X.P. Niu, M.R. Erickson, S.M. Abmayr, Identification of a Drosophila homologue to vertebrate Crk by interaction with MBC, Gene 228 (1999) 243–252.
[8] S. Deng, I. Bothe, M.K. Baylies, The formin diaphanous regulates myoblast fusion through actin polymerization and arp2/3 regulation, PLoS Genet. 11 (2015) e1005381.
[9] M. Ruiz Gomez, N. Coutts, A. Price, M.V. Taylor, M. Bate, Drosophila dumbfounded: a myoblast attractant essential for fusion, Cell 102 (2000) 189–198.
[10] R.D. Artero, I. Castanon, M.K. Baylies, The immunoglobulin-like protein Hibris functions as a dose-dependent regulator of myoblast fusion and is differentially controlled by Ras and Notch signaling, Development 128 (2001) 4251–4264.
[11] E.H. Chen, B.A. Pryce, J.A. Tzeng, G.A. Gonzalez, E.N. Olson, Control of myoblast fusion by a guanine nucleotide exchange factor, loner, and its effector ARF6, Cell 114 (2003) 751–762.
[12] C. Dottermusch-Heidel, V. Groth, L. Beck, S.-F. Onel, The Arf-GEF Schizo/Loner regulates N-cadherin to induce fusion competence of Drosophila myoblasts, Dev. Biol. 368 (2012) 18–27.
[13] M.R. Erickson, B.J. Galletta, S.M. Abmayr, Drosophila myoblast city encodes a conserved protein that is essential for myoblast fusion, dorsal closure, and cytoskeletal organization, J. Cell Biol. 138 (1997) 589–603.
[14] J.H. Kim, Y. Ren, W.P. Ng, S. Li, S. Son, Y.-S. Kee, S. Zhang, G. Zhang, D.A. Fletcher, D.N. Robinson, et al., Mechanical tension drives cell membrane fusion, Dev. Cell 32 (2015) 561–573.
[15] I. Bothe, S. Deng, M. Baylies, PI(4,5)P2 regulates myoblast fusion through Arp2/3 regulator localization at the fusion site, Development 141 (2014) 2289–2301.
[16] S. Hakeda-Suzuki, J. Ng, J. Tzu, G. Dietzl, Y. Sun, M. Harms, T. Nardine, L. Luo, B.J. Dickson, Rac function and regulation during Drosophila development, Nature 416 (2002) 438–442.
[17] E.H. Chen, E.N. Olson, Antisocial, an intracellular adaptor protein, is required for myoblast fusion in Drosophila, Dev. Cell 1 (2001) 705–715.
[18] A. Rau, D. Buttgereit, A. Holz, R. Fetter, S.K. Doberstein, A. Paululat, N. Staudt, J. Skeath, A.M. Michelson, R. Renkawitz-Pohl, rolling pebbles (rols) is required in Drosophila muscle precursors for recruitment of myoblasts for fusion, Development 128 (2001) 5061–5073.
[19] M. Strünkelnberg, B. Bonengel, L.M. Moda, A. Hertenstein, H.G. de Couet, R.G. Ramos, K.F. Fischbach, rst and its paralogue kirre act redundantly during embryonic muscle development in Drosophila, Development 128 (2001) 4229–4239.
[20] B.A. Bour, M. Chakravarti, J.M. West, S.M. Abmayr, Drosophila SNS, a member of the immunoglobulin superfamily that is essential for myoblast fusion, Genes Dev. 14 (2000) 1498–1511.
[21] R. Massarwa, S. Carmon, B.-Z. Shilo, E.D. Schejter, WIP/WASp-based actin-polymerization machinery is essential for myoblast fusion in Drosophila, Dev. Cell 12 (2007) 557–569.
[22] G. Schäfer, S. Weber, A. Holz, S. Bogdan, S. Schumacher, A. Müller, R. Renkawitz-Pohl, S.-F. Onel, The Wiskott-Aldrich syndrome protein (WASP) is essential for myoblast fusion in Drosophila, Dev. Biol. 304 (2007) 664–674.
[23] K. Brinkmann, M. Winterhoff, S.-F. Onel, J. Schultz, J. Faix, S. Bogdan, WHAMY is a novel actin polymerase promoting myoblast fusion, macrophage cell motility and sensory organ development in Drosophila, J. Cell. Sci. 129 (2016) 604–620.
[24] M.F. Galliano, C. Huet, J. Frygelius, A. Polgren, U.M. Wewer, E. Engvall, Binding of ADAM12, a marker of skeletal muscle regeneration, to the muscle-specific actin-binding protein, alpha −actinin-2, is required for myoblast fusion, J. Biol. Chem. 275 (2000) 13933–13939.
[25] A.E. Hochreiter-Hufford, C.S. Lee, J.M. Kinchen, J.D. Sokolowski, S. Arandjelovic, J.A. Call, A.L. Klibanov, Z. Yan, J.W. Mandell, K.S. Ravichandran, Phosphatidylserine receptor BAI1 and apoptotic cells as new promoters of myoblast fusion, Nature 497 (2013) 263–267.
[26] N. Hamoud, V. Tran, L.-P. Croteau, A. Kania, J.-F. Côté, G-protein coupled receptor BAI3 promotes myoblast fusion in vertebrates, Proc. Natl. Acad. Sci. U.S.A. 111 (2014) 3745–3750.
[27] F. Galbiati, D. Volonte, J.A. Engelman, P.E. Scherer, M.P. Lisanti, Targeted down-regulation of caveolin-3 is sufficient to inhibit myotube formation in differentiating C2C12 myoblasts. Transient activation of p38 mitogen-activated protein kinase is required for induction of caveolin-3 expression and subsequent myotube formation, J. Biol. Chem. 274 (1999) 30315–30321.
[28] E. Vasyutina, B. Martarelli, C. Brakebusch, H. Wende, C. Birchmeier, The small G-proteins Rac1 and Cdc42 are essential for myoblast fusion in the mouse, Proc. Natl. Acad. Sci. U. S. A. 106 (2009) 8935–8940.
[29] D. Baas, S. Caussanel-Boude, A. Guiraud, F. Calhabeu, E. Delaune, F. Pilot, E. Chopin, I. Machuca-Gayet, A. Vernay, S. Bertrand, et al., CKIP-1 regulates mammalian and zebrafish myoblast fusion, J. Cell. Sci. 125 (2012) 3790–3800.
[30] C.A. Moore, C.A. Parkin, Y. Bidet, P.W. Ingham, A role for the Myoblast city homologues Dock1 and Dock5 and the adaptor proteins Crk and Crk-like in zebrafish myoblast fusion, Development 134 (2007) 3145–3153.
[31] M. Laurin, N. Fradet, A. Blangy, A. Hall, K. Vuori, J.-F. Côté, The atypical Rac activator Dock180 (Dock1) regulates myoblast fusion in vivo, Proc. Natl. Acad. Sci. U.S.A. 105 (2008) 15446–15451.
[32] K.R. Doherty, A.R. Demonbreun, G.Q. Wallace, A. Cave, A.D. Posey, K. Heretis, P. Pytel, E.M. McNally, The endocytic recycling protein EHD2 interacts with myoferlin to regulate myoblast fusion, J. Biol. Chem. 283 (2008) 20252–20260.
[33] P. Bi, A. Ramirez-Martinez, H. Li, J. Cannavino, J.R. McAnally, J.M. Shelton, E. Sánchez-Ortiz, R. Bassel-Duby, E.N. Olson, Control of muscle formation by the fusogenic micropeptide myomixer, Science 356 (2017) 323–327.
[34] M.E. Quinn, Q. Goh, M. Kurosaka, D.G. Gamage, M.J. Petrany, V. Prasad, D.P. Millay, Myomerger induces fusion of non-fusogenic cells and is required for skeletal muscle development, Nat. Commun. 8 (2017) 15665.
[35] G.T. Powell, G.J. Wright, Jamb and jamc are essential for vertebrate myocyte fusion, PLoS Biol. 9 (2011) e1001216.
[36] B.P. Srinivas, J. Woo, W.Y. Leong, S. Roy, A conserved molecular pathway mediates myoblast fusion in insects and vertebrates, Nat. Genet. 39 (2007) 781–786.
[37] S. Charrasse, F. Comunale, Y. Grumbach, F. Poulat, A. Blangy, C. Gauthier-Rouvière, RhoA GTPase regulates M-cadherin activity and myoblast fusion, Mol. Biol. Cell 17 (2006) 749–759.
[38] C.A. Griffin, K.A. Kafadar, G.K. Pavlath, MOR23 promotes muscle regeneration and regulates cell adhesion and migration, Dev. Cell 17 (2009) 649–661.
[39] K.R. Doherty, A. Cave, D.B. Davis, A.J. Delmonte, A. Posey, J.U. Earley, M. Hadhazy, E.M. McNally, Normal myoblast fusion requires myoferlin, Development 132 (2005) 5565–5575.
[40] A. Landemaine, P.-Y. Rescan, J.-C. Gabillard, Myomaker mediates fusion of fast myocytes in zebrafish embryos, Biochem. Biophys. Res. Commun. 451 (2014) 480–484.
[41] W. Luo, E. Li, Q. Nie, X. Zhang, Myomaker, regulated by MYOD, MYOG and miR-140-3p, promotes chicken myoblast fusion, Int. J. Mol. Sci. 16 (2015) 26186–26201.
[42] D.P. Millay, J.R. O'Rourke, L.B. Sutherland, S. Bezprozvannaya, J.M. Shelton, R. Bassel-Duby, E.N. Olson, Myomaker is a membrane activator of myoblast fusion and muscle formation, Nature 499 (2013) 301–305.
[43] Y. Gruenbaum-Cohen, I. Harel, K.-B. Umansky, E. Tzahor, S.B. Snapper, B.-Z. Shilo, E.D. Schejter, The actin regulator N-WASp is required for muscle-cell fusion in mice, Proc. Natl. Acad. Sci. U.S.A. 109 (2012) 11211–11216.
[44] D. Sieiro, N. Véron, C. Marcelle, The chicken embryo as an efficient model to test the function of muscle fusion genes in amniotes, PLoS One 12 (2017) e0177681.
[45] S.-Y. Park, Y. Yun, J.-S. Lim, M.-J. Kim, S.-Y. Kim, J.-E. Kim, I.-S. Kim, Stabilin-2 modulates the efficiency of myoblast fusion during myogenic differentiation and muscle regeneration, Nat. Commun. 7 (2016) 10871.
[46] F.J. Conti, S.J. Monkley, M.R. Wood, D.R. Critchley, U. Müller, Talin 1 and 2 are required for myoblast fusion, sarcomere assembly and the maintenance of myotendinous junctions, Development 136 (2009) 3597–3606.
[47] G.D. Rosen, J.R. Sanes, R. LaChance, J.M. Cunningham, J. Roman, D.C. Dean, Roles for the integrin VLA-4 and its counter receptor VCAM-1 in myogenesis, Cell 69 (1992) 1107–1119.
[48] M. Schwander, M. Leu, M. Stumm, O.M. Dorchies, U.T. Ruegg, J. Schittny, U. Müller, Beta1 integrins regulate myoblast fusion and sarcomere assembly, Dev. Cell 4 (2003) 673–685.
[49] N. Azpiazu, P.A. Lawrence, J.P. Vincent, M. Frasch, Segmentation and specification of the Drosophila mesoderm, Genes Dev. 10 (1996) 3183–3194.
[50] M. Frasch, Induction of visceral and cardiac mesoderm by ectodermal Dpp in the early Drosophila embryo, Nature 374 (1995) 464–467.
[51] K. Staehling-Hampton, F.M. Hoffmann, M.K. Baylies, E. Rushton, M. Bate, dpp induces mesodermal gene expression in Drosophila, Nature 372 (1994) 783–786.
[52] M.K. Baylies, M. Bate, M. Ruiz Gomez, Myogenesis: a view from Drosophila, Cell 93 (1998) 921–927.
[53] A. Carmena, M. Bate, F. Jiménez, Lethal of scute, a proneural gene, participates in the specification of muscle progenitors during Drosophila embryogenesis, Genes Dev. 9 (1995) 2373–2383.
[54] A. Carmena, B. Murugasu-Oei, D. Menon, F. Jiménez, W. Chia, Inscuteable and numb mediate asymmetric muscle progenitor cell divisions during Drosophila myogenesis, Genes Dev. 12 (1998) 304–315.
[55] S. Fuerstenberg, E. Giniger, Multiple roles for notch in Drosophila myogenesis, Dev. Biol. 201 (1998) 66–77.
[56] A. Carmena, S. Gisselbrecht, J. Harrison, F. Jiménez, A.M. Michelson, Combinatorial signaling codes for the progressive determination of cell fates in the Drosophila embryonic mesoderm, Genes Dev. 12 (1998) 3910–3922.
[57] M. Ruiz Gomez, M. Bate, Segregation of myogenic lineages in Drosophila requires numb, Development 124 (1997) 4857–4866.
[58] K.C. Dobi, M.S. Halfon, M.K. Baylies, Whole-genome analysis of muscle founder cells implicates the chromatin regulator Sin3A in muscle identity, Cell Rep. 8 (2014) 858–870.
[59] M.J. Boyle, C.A. Berg, Control in time and space: tramtrack69 cooperates with Notch and Ecdysone to repress ectopic fate and shape changes during Drosophila egg chamber maturation, Development 136 (2009) 4187–4197.

Please cite this article in press as: S. Deng, et al., Acting on identity: Myoblast fusion and the formation of the syncytial muscle fiber, Semin Cell Dev Biol (2017), https://doi.org/10.1016/j.semcdb.2017.10.033

[60] L. Bataillé, H. Boukhatmi, J.-L. Frendo, A. Vincent, Dynamics of transcriptional (re)-programming of syncytial nuclei in developing muscles, BMC Biol. 15 (2017) 48.
[61] C. Bourgouin, S.E. Lundgren, J.B. Thomas, Apterous is a Drosophila LIM domain gene required for the development of a subset of embryonic muscles, Neuron 9 (1992) 549–561.
[62] C. Dohrmann, N. Azpiazu, M. Frasch, A new Drosophila homeo box gene is expressed in mesodermal precursor cells of distinct muscles during embryogenesis, Genes Dev. 4 (1990) 2098–2111.
[63] T. Jagla, F. Bellard, Y. Lutz, G. Dretzen, M. Bellard, K. Jagla, ladybird determines cell fate decisions during diversification of Drosophila somatic muscles, Development 125 (1998) 3699–3708.
[64] K. Beckett, M.K. Baylies, 3D analysis of founder cell and fusion competent myoblast arrangements outlines a new model of myoblast fusion, Dev. Biol. 309 (2007) 113–125.
[65] B.E. Richardson, K. Beckett, M.K. Baylies, Live imaging of Drosophila myoblast fusion, Methods Mol. Biol. 475 (2008) 263–274.
[66] M. Peckham, J.E. Molloy, J.C. Sparrow, D.C. White, Physiological properties of the dorsal longitudinal flight muscle and the tergal depressor of the trochanter muscle of Drosophila melanogaster, J. Muscle Res. Cell. Motil. 11 (1990) 203–215.
[67] A. Ghazi, S. Anant, K. Vijayraghavan, Apterous mediates development of direct flight muscles autonomously and indirect flight muscles through epidermal cues, Development 127 (2000) 5309–5318.
[68] V. Sudarsan, S. Anant, P. Guptan, K. Vijayraghavan, H. Skaer, Myoblast diversification and ectodermal signaling in Drosophila, Dev. Cell 1 (2001) 829–839.
[69] H. Deng, S.C. Hughes, J.B. Bell, A.J. Simmonds, Alternative requirements for Vestigial, Scalloped, and Dmef2 during muscle differentiation in Drosophila melanogaster, Mol. Biol. Cell 20 (2009) 256–269.
[70] C. Schönbauer, J. Distler, N. Jährling, M. Radolf, H.-U. Dodt, M. Frasch, F. Schnorrer, Spalt mediates an evolutionarily conserved switch to fibrillar muscle fate in insects, Nature 479 (2011) 406–409.
[71] T. Maqbool, C. Soler, T. Jagla, M. Daczewska, N. Lodha, S. Palliyil, K. Vijayraghavan, K. Jagla, Shaping leg muscles in Drosophila: role of ladybird, a conserved regulator of appendicular myogenesis, PLoS One 1 (2006) e122.
[72] S. Roy, K. Vijayraghavan, Muscle pattern diversification in Drosophila: the story of imaginal myogenesis, Bioessays 21 (1999) 486–498.
[73] R.J. Bryson-Richardson, P.D. Currie, The genetics of vertebrate myogenesis, Nat. Rev. Genet. 9 (2008) 632–646.
[74] D. Duprez, C. Fournier-Thibault, N. Le Douarin, Sonic Hedgehog induces proliferation of committed skeletal muscle cells in the chick limb, Development 125 (1998) 495–505.
[75] F. Relaix, D. Rocancourt, A. Mansouri, M. Buckingham, A Pax3/Pax7-dependent population of skeletal muscle progenitor cells, Nature 435 (2005) 948–953.
[76] M. Maroto, R. Reshef, A.E. Münsterberg, S. Koester, M. Goulding, A.B. Lassar, Ectopic Pax-3 activates MyoD and Myf-5 expression in embryonic mesoderm and neural tissue, Cell 89 (1997) 139–148.
[77] T. Sato, D. Rocancourt, L. Marques, S. Thorsteinsdóttir, M. Buckingham, A Pax3/Dmrt2/Myf5 regulatory cascade functions at the onset of myogenesis, PLoS Genet. 6 (2010) e1000897.
[78] M.A. Rudnicki, P.N. Schnegelsberg, R.H. Stead, T. Braun, H.H. Arnold, R. Jaenisch, MyoD or Myf-5 is required for the formation of skeletal muscle, Cell 75 (1993) 1351–1359.
[79] P. Hasty, A. Bradley, J.H. Morris, D.G. Edmondson, J.M. Venuti, E.N. Olson, W.H. Klein, Muscle deficiency and neonatal death in mice with a targeted mutation in the myogenin gene, Nature 364 (1993) 501–506.
[80] L. Kassar-Duchossoy, B. Gayraud-Morel, D. Gomès, D. Rocancourt, M. Buckingham, V. Shinin, S. Tajbakhsh, Mrf4 determines skeletal muscle identity in Myf5:Myod double-mutant mice, Nature 431 (2004) 466–471.
[81] E. Dodou, S.-M. Xu, B.L. Black, mef2c is activated directly by myogenic basic helix-loop-helix proteins during skeletal muscle development in vivo, Mech. Dev. 120 (2003) 1021–1032.
[82] B. Lilly, S. Galewsky, A.B. Firulli, R.A. Schulz, E.N. Olson, D-MEF2: a MADS box transcription factor expressed in differentiating mesoderm and muscle cell lineages during Drosophila embryogenesis, Proc. Natl. Acad. Sci. U.S.A. 91 (1994) 5662–5666.
[83] J.D. Molkentin, B.L. Black, J.F. Martin, E.N. Olson, Cooperative activation of muscle gene expression by MEF2 and myogenic bHLH proteins, Cell 83 (1995) 1125–1136.
[84] A.J. Harris, M.J. Duxson, R.B. Fitzsimons, F. Rieger, Myonuclear birthdates distinguish the origins of primary and secondary myotubes in embryonic mammalian skeletal muscles, Development 107 (1989) 771–784.
[85] K. Rochlin, S. Yu, S. Roy, M.K. Baylies, Myoblast fusion: when it takes more to make one, Dev. Biol. 341 (2010) 66–83.
[86] C. Shelton, K.S. Kocherlakota, S. Zhuang, S.M. Abmayr, The immunoglobulin superfamily member Hbs functions redundantly with Sns in interactions between founder and fusion-competent myoblasts, Development 136 (2009) 1159–1168.
[87] S. Bao, K.-F. Fischbach, V. Corbin, R.L. Cagan, Preferential adhesion maintains separation of ommatidia in the Drosophila eye, Dev. Biol. 344 (2010) 948–956.
[88] R.G. Ramos, G.L. Igloi, B. Lichte, U. Baumann, D. Maier, T. Schneider, J.H. Brandstätter, A. Fröhlich, K.F. Fischbach, The irregular chiasm C-roughest locus of Drosophila, which affects axonal projections and programmed cell death, encodes a novel immunoglobulin-like protein, Genes Dev. 7 (1993) 2533–2547.
[89] J. Hamp, A. Löwer, C. Dottermusch-Heidel, L. Beck, B. Moussian, M. Flötenmeyer, S.-F. Onel, Drosophila Kette coordinates myoblast junction dissolution and the ratio of Scar-to-WASp during myoblast fusion, J. Cell. Sci. 129 (2016) 3426–3436.
[90] S.-F. Onel, M.B. Rust, R. Jacob, R. Renkawitz-Pohl, Tethering membrane fusion: common and different players in myoblasts and at the synapse, J. Neurogenet. 28 (2014) 302–315.
[91] C.A. Charlton, W.A. Mohler, G.L. Radice, R.O. Hynes, H.M. Blau, Fusion competence of myoblasts rendered genetically null for N-cadherin in culture, J. Cell Biol. 138 (1997) 331–336.
[92] K.L. Sens, S. Zhang, P. Jin, R. Duan, G. Zhang, F. Luo, L. Parachini, E.H. Chen, An invasive podosome-like structure promotes fusion pore formation during myoblast fusion, J. Cell Biol. 191 (2010) 1013–1027.
[93] B.R. Kaipa, H. Shao, G. Schäfer, T. Trinkewitz, V. Groth, J. Liu, L. Beck, S. Bogdan, S.M. Abmayr, S.-F. Onel, Dock mediates Scar- and WASp-dependent actin polymerization through interaction with cell adhesion molecules in founder cells and fusion-competent myoblasts, J. Cell. Sci. 126 (2013) 360–372.
[94] K.S. Kocherlakota, J.-M. Wu, J. McDermott, S.M. Abmayr, Analysis of the cell adhesion molecule sticks-and-stones reveals multiple redundant functional domains, protein-interaction motifs and phosphorylated tyrosines that direct myoblast fusion in Drosophila melanogaster, Genetics 178 (2008) 1371–1383.
[95] S. Kim, K. Shilagardi, S. Zhang, S.N. Hong, K.L. Sens, J. Bo, G.A. Gonzalez, E.H. Chen, A critical function for the actin cytoskeleton in targeted exocytosis of prefusion vesicles during myoblast fusion, Dev. Cell 12 (2007) 571–586.
[96] S.D. Menon, Z. Osman, K. Chenchill, W. Chia, A positive feedback loop between Dumbfounded and Rolling pebbles leads to myotube enlargement in Drosophila, J. Cell Biol. 169 (2005) 909–920.
[97] S.D. Menon, W. Chia, Drosophila rolling pebbles: a multidomain protein required for myoblast fusion that recruits D-Titin in response to the myoblast attractant Dumbfounded, Dev. Cell 1 (2001) 691–703.
[98] S. Haralalka, C. Shelton, H.N. Cartwright, E. Katzfey, E. Janzen, S.M. Abmayr, Asymmetric Mbc, active Rac1 and F-actin foci in the fusion-competent myoblasts during myoblast fusion in Drosophila, Development 138 (2011) 1551–1562.
[99] S. Bulchand, S.D. Menon, S.E. George, W. Chia, The intracellular domain of Dumbfounded affects myoblast fusion efficiency and interacts with Rolling pebbles and Loner, PLoS One 5 (2010) e9374.
[100] N. Dyer, E. Rebollo, P. Domínguez, N. Elkhatib, P. Chavrier, L. Daviet, C. González, M. González-Gaitán, Spermatocyte cytokinesis requires rapid membrane addition mediated by ARF6 on central spindle recycling endosomes, Development 134 (2007) 4437–4447.
[101] S. Eden, R. Rohatgi, A.V. Podtelejnikov, M. Mann, M.W. Kirschner, Mechanism of regulation of WAVE1-induced actin nucleation by Rac1 and Nck, Nature 418 (2002) 790–793.
[102] Z. Chen, D. Borek, S.B. Padrick, T.S. Gomez, Z. Metlagel, A.M. Ismail, J. Umetani, D.D. Billadeau, Z. Otwinowski, M.K. Rosen, Structure and control of the actin regulatory WAVE complex, Nature 468 (2010) 533–538.
[103] B. Gildor, R. Massarwa, B.-Z. Shilo, E.D. Schejter, The SCAR and WASp nucleation-promoting factors act sequentially to mediate Drosophila myoblast fusion, EMBO Rep. 10 (2009) 1043–1050.
[104] S. Deng, I. Bothe, M. Baylies, Diaphanous regulates SCAR complex localization during Drosophila myoblast fusion, Fly (Austin) 10 (2016) 178–186.
[105] E.R. Geisbrecht, S. Haralalka, S.K. Swanson, L. Florens, M.P. Washburn, S.M. Abmayr, Drosophila ELMO/CED-12 interacts with Myoblast city to direct myoblast fusion and ommatidial organization, Dev. Biol. 314 (2008) 137–149.
[106] N. Ramesh, R. Geha, Recent advances in the biology of WASP and WIP, Immunol. Res. 44 (2009) 99–111.
[107] S. Haralalka, C. Shelton, H.N. Cartwright, F. Guo, R. Trimble, R.P. Kumar, S.M. Abmayr, Live imaging provides new insights on dynamic F-actin filopodia and differential endocytosis during myoblast fusion in Drosophila, PLoS One 9 (2014) e114126.
[108] W.A. Mohler, G. Shemer, J.J. del Campo, C. Valansi, E. Opoku-Serebuoh, V. Scranton, N. Assaf, J.G. White, B. Podbilewicz, The type I membrane protein EFF-1 is essential for developmental cell fusion, Dev. Cell 2 (2002) 355–362.
[109] A. Sapir, O. Avinoam, B. Podbilewicz, L.V. Chernomordik, Viral and developmental cell fusion mechanisms: conservation and divergence, Dev. Cell 14 (2008) 11–21.
[110] S.-F. Onel, R. Renkawitz-Pohl, FuRMAS: triggering myoblast fusion in Drosophila, Dev. Dyn. 238 (2009) 1513–1525.
[111] E.D. Schejter, Myoblast fusion: experimental systems and cellular mechanisms, Semin. Cell Dev. Biol. 60 (2016) 112–120.
[112] V.K. Schulman, K.C. Dobi, M.K. Baylies, Morphogenesis of the somatic musculature in Drosophila melanogaster, Wiley Interdiscip Rev Dev Biol 4 (2015) 313–334.
[113] B. Estrada, A.D. Maeland, S.S. Gisselbrecht, J.W. Bloor, N.H. Brown, A.M. Michelson, The MARVEL domain protein, Singles Bar, is required for progression past the pre-fusion complex stage of myoblast fusion, Dev. Biol. 307 (2007) 328–339.

Please cite this article in press as: S. Deng, et al., Acting on identity: Myoblast fusion and the formation of the syncytial muscle fiber, Semin Cell Dev Biol (2017), https://doi.org/10.1016/j.semcdb.2017.10.033

[114] N. Dhanyasi, D. Segal, E. Shimoni, V. Shinder, B.-Z. Shilo, K. Vijayraghavan, E.D. Schejter, Surface apposition and multiple cell contacts promote myoblast fusion in Drosophila flight muscles, J. Cell Biol. 211 (2015) 191–203.
[115] J. Fernandes, M. Bate, K. Vijayraghavan, Development of the indirect flight muscles of Drosophila, Development 113 (1991) 67–77.
[116] R.D. Gunage, H. Reichert, K. Vijayraghavan, Identification of a new stem cell population that generates Drosophila flight muscles, Elife 3 (2014) 180.
[117] R. Aradhya, M. Zmojdzian, J.P. Da Ponte, K. Jagla, Muscle niche-driven insulin-notch-myc cascade reactivates dormant adult muscle precursors in drosophila, Elife 4 (2015) 2609.
[118] B. Gildor, E.D. Schejter, B.-Z. Shilo, Bidirectional Notch activation represses fusion competence in swarming adult Drosophila myoblasts, Development 139 (2012) 4040–4050.
[119] P. Mukherjee, B. Gildor, B.-Z. Shilo, K. Vijayraghavan, E.D. Schejter, The actin nucleator WASp is required for myoblast fusion during adult Drosophila myogenesis, Development 138 (2011) 2347–2357.
[120] T.M. Brunetti, B.J. Fremin, R.M. Cripps, Identification of singles bar as a direct transcriptional target of Drosophila Myocyte enhancer factor-2 and a regulator of adult myoblast fusion, Dev. Biol. 401 (2015) 299–309.
[121] D. Segal, N. Dhanyasi, E.D. Schejter, B.-Z. Shilo, Adhesion and fusion of muscle cells are promoted by filopodia, Dev. Cell 38 (2016) 291–304.
[122] A.R. Demonbreun, B.H. Biersmith, E.M. McNally, Membrane fusion in muscle development and repair, Semin. Cell Dev. Biol. 45 (2015) 48–56.
[123] V. Horsley, K.M. Jansen, S.T. Mills, G.K. Pavlath, IL-4 acts as a myoblast recruitment factor during mammalian muscle growth, Cell 113 (2003) 483–494.
[124] C. Sedwick, Jamb and jamc muscle in on myoblast fusion, PLoS Biol. 9 (2011) e1001217.
[125] R.L. Sohn, P. Huang, G. Kawahara, M. Mitchell, J. Guyon, R. Kalluri, L.M. Kunkel, E. Gussoni, A role for nephrin, a renal protein, in vertebrate skeletal muscle cell fusion, Proc. Natl. Acad. Sci. U.S.A. 106 (2009) 9274–9279.
[126] A. Hollnagel, C. Grund, W.W. Franke, H.-H. Arnold, The cell adhesion molecule M-cadherin is not essential for muscle development and regeneration, Mol. Cell. Biol. 22 (2002) 4760–4770.
[127] G.L. Radice, H. Rayburn, H. Matsunami, K.A. Knudsen, M. Takeichi, R.O. Hynes, Developmental defects in mouse embryos lacking N-cadherin, Dev. Biol. 181 (1997) 64–78.
[128] S.J. Nowak, P.C. Nahirney, A.-K. Hadjantonakis, M.K. Baylies, Nap1-mediated actin remodeling is essential for mammalian myoblast fusion, J. Cell. Sci. 122 (2009) 3282–3293.
[129] R. Duan, P.J. Gallagher, Dependence of myoblast fusion on a cortical actin wall and nonmuscle myosin IIA, Dev. Biol. 325 (2009) 374–385.
[130] D.P. Millay, L.B. Sutherland, R. Bassel-Duby, E.N. Olson, Myomaker is essential for muscle regeneration, Genes Dev. 28 (2014) 1641–1646.
[131] S.A. Di Gioia, S. Connors, N. Matsunami, J. Cannavino, M.F. Rose, N.M. Gilette, P. Artoni, N.L. de Macena Sobreira, W.-M. Chan, B.D. Webb, et al., A defect in myoblast fusion underlies Carey-Fineman-Ziter syndrome, Nat. Commun. 8 (2017) 16077.
[132] P. Seale, L.A. Sabourin, A. Girgis-Gabardo, A. Mansouri, P. Gruss, M.A. Rudnicki, Pax7 is required for the specification of myogenic satellite cells, Cell 102 (2000) 777–786.
[133] J.G. Tidball, Inflammatory cell response to acute muscle injury, Med. Sci. Sports Exerc. 27 (1995) 1022–1032.
[134] J. Rantanen, T. Hurme, R. Lukka, J. Heino, H. Kalimo, Satellite cell proliferation and the expression of myogenin and desmin in regenerating skeletal muscle: evidence for two different populations of satellite cells, Lab. Invest. 72 (1995) 341–347.
[135] M.D. Grounds, Z. Yablonka-Reuveni, Molecular and cell biology of skeletal muscle regeneration, Mol. Cell Biol. Hum. Dis. Ser. 3 (1993) 210–256.
[136] E. Vasyutina, B. Martarelli, C. Brakebusch, H. Wende, C. Birchmeier, The small G-proteins Rac1 and Cdc42 are essential for myoblast fusion in the mouse, Proc. Natl. Acad. Sci. U. S. A. 106 (2009) 8935–8940.
[137] A.M. Michelson, S.M. Abmayr, M. Bate, A.M. Arias, T. Maniatis, Expression of a MyoD family member prefigures muscle pattern in Drosophila embryos, Genes Dev. 4 (1990) 2086–2097.
[138] S.M. Abmayr, C.A. Keller, Drosophila myogenesis and insights into the role of nautilus, Curr. Top. Dev. Biol. 38 (1998) 35–80.
[139] A.E. Münsterberg, J. Kitajewski, D.A. Bumcrot, A.P. McMahon, A.B. Lassar, Combinatorial signaling by Sonic hedgehog and Wnt family members induces myogenic bHLH gene expression in the somite, Genes Dev. 9 (1995) 2911–2922.
[140] W. Zhang, S. Roy, Myomaker is required for the fusion of fast-twitch myocytes in the zebrafish embryo, Dev. Biol. 423 (2017) 24–33.
[141] H. Yin, F. Price, M.A. Rudnicki, Satellite cells and the muscle stem cell niche, Physiol. Rev. 93 (2013) 23–67.
[142] A. Zolkiewska, Disintegrin-like/cysteine-rich region of ADAM 12 is an active cell adhesion domain, Exp. Cell Res 252 (1999) 423–431.
[143] D. Volonte, A.J. Peoples, F. Galbiati, Modulation of myoblast fusion by caveolin-3 in dystrophic skeletal muscle cells: implications for Duchenne muscular dystrophy and limb-girdle muscular dystrophy-1C, Mol. Biol. Cell 14 (2003) 4075–4088.

Please cite this article in press as: S. Deng, et al., Acting on identity: Myoblast fusion and the formation of the syncytial muscle fiber, Semin Cell Dev Biol (2017), https://doi.org/10.1016/j.semcdb.2017.10.033

Chapter 19

Imaging Approaches to Investigate Myonuclear Positioning in *Drosophila*

Mafalda Azevedo, Victoria K. Schulman, Eric Folker, Mridula Balakrishnan, and Mary Baylies

Abstract

In the skeletal muscle, nuclei are positioned at the periphery of each myofiber and are evenly distributed along its length. Improper positioning of myonuclei has been correlated with muscle disease and decreased muscle function. Several mechanisms required for regulating nuclear position have been identified using the fruit fly, *Drosophila melanogaster*. The conservation of the myofiber between the fly and vertebrates, the availability of advanced genetic tools, and the ability to visualize dynamic processes using fluorescent proteins in vivo makes the fly an excellent system to study myonuclear positioning. This chapter describes time-lapse and fixed imaging methodologies using both the *Drosophila* embryo and the larva to investigate mechanisms of myonuclear positioning.

Key words *Drosophila*, Muscle, Nuclear movement, Embryo, Larvae

1 Introduction

The skeletal muscle provides an important system in which to study mechanisms of myonuclear positioning. Myofibers, the cellular units of the skeletal muscle, are multinucleated and position their myonuclei to reside above the sarcomeres at the cell periphery and along the length of the fiber to maximize internuclear distance. Moreover, mispositioned myonuclei correlate with muscle disease [1], and recent data suggest that mispositioned myonuclei may cause muscle weakness [2–4], illustrating the functional importance of proper positioning.

To identify the cellular mechanisms of myonuclear movement in vivo, we have utilized the musculature of *Drosophila* embryos and larvae [2–6]. *Drosophila* muscles share the conserved myofiber structure found in vertebrates: *Drosophila* myofibers are multinucleated, maintain particular sizes and shapes, attach to particular tendon cells, become innervated by specific motoneurons, build sarcomeres, and are essential for locomotion (reviewed in [7, 8]).

Sue Shackleton et al. (eds.), *The Nuclear Envelope: Methods and Protocols*, Methods in Molecular Biology, vol. 1411,
DOI 10.1007/978-1-4939-3530-7_19, © Springer Science+Business Media New York 2016

The *Drosophila* system also offers unparalleled genetic approaches to manipulate genes of interest within the whole organism or specifically within muscle tissue. In addition to their powerful genetics, *Drosophila* embryos are also amenable to drug treatments commonly used to manipulate cell biological processes in culture, providing additional opportunities to probe the cellular machinery responsible for myonuclear movement [6]. Lastly *Drosophila* embryos are amenable to time-lapse microscopy without perturbing development such that cell biological processes, including myonuclear dynamics, can be assessed [5].

There are 30 individual muscles per abdominal hemisegment of the *Drosophila* embryo (Fig. 1). Formation of these individual body wall myofibers depends on the specification and fusion of two myoblast cell types: founder cells (FCs) and fusion-competent myoblasts (FCMs). Each FC contains the information necessary to direct the formation of a specific muscle. FCs can be identified by the expression of identity genes, such as the transcriptional regulators *even-skipped* and *apterous* [9–11]. The combination of identity genes and chromatin regulators expressed by a particular FC regulates the final morphology of the specific muscle. In contrast, FCMs are more naïve cells. Upon fusion to an FC, FCMs become reprogrammed to the specific developmental program of the FC, as evidenced by the observation that each newly incorporated FCM nucleus begins to express the same combination of identity genes as the FC [7]. Myoblast fusion is an iterative process; depending on the particular muscle, body wall muscles in *Drosophila* embryos contain between 2 and 25 myonuclei. As myoblast fusion concludes, the polarized

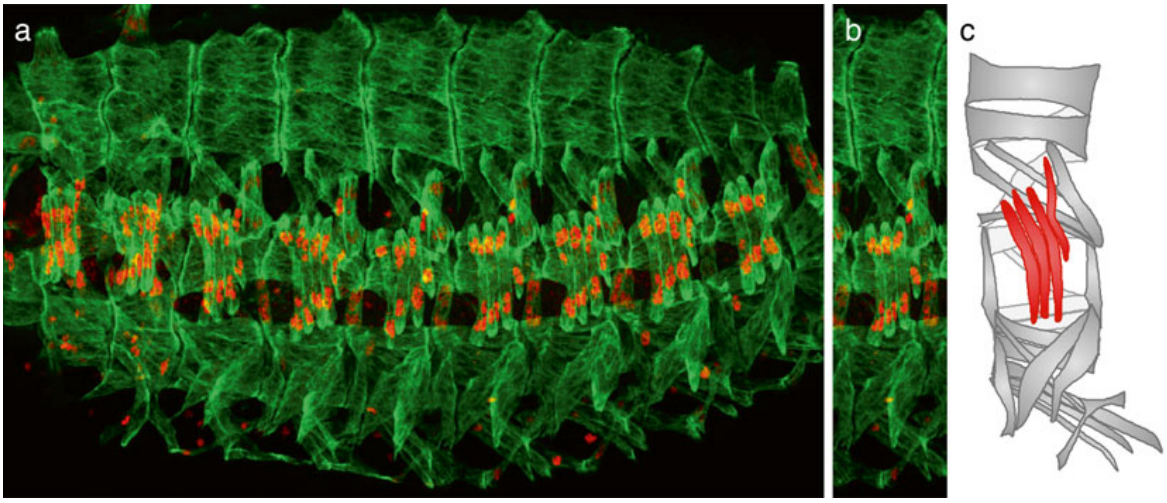


Fig. 1 The *Drosophila* embryonic musculature. The *Drosophila* embryo is divided in hemisegments, each containing 30 muscles. (**A**) Stage 16 embryo showing the musculature in green (Tropomyosin) and the nuclei of the lateral transverse (LT) muscles in red (DsRed). (**B**) Image of a single hemisegment. (**C**) Schematic representation of all the muscles present in one hemisegment; the LT muscles are highlighted in *red*. For additional detail *see* Dobi et al. [7]

syncytial myotube extends processes toward specific tendon cells and forms stable myotendinous junctions. Specific motoneurons innervate each muscle, leading to coordinated contraction at the final stage of embryogenesis [8, 12].

Although mispositioned nuclei are observed in all muscles when certain genes are disrupted, myonuclear positioning has been best characterized in the lateral transverse (LT) muscles of the developing embryo. We have shown that LT myonuclei undergo not one but a series of movements to maximize internuclear distance in vivo (Fig. 2; [2–5]). Post-fusion (stage 14), the myonuclei are located in a single group within the myotube. Over the course of development, these nuclei segregate into smaller groups that follow characteristic migration patterns (stages 15, 16) before evenly distributing throughout the myofiber at the end of embryonic stage 17 [2, 8]. During larval development, in which the muscles grow up to 40-fold [13], the myonuclei in the individual muscles maintain regular spacing along the muscle fiber. These myonuclei are positioned above the sarcomeres along the periphery of the muscle fiber (Fig. 3; [2]).

To date, there are several mechanisms required for the different movements of myonuclei in *Drosophila*. These mechanisms require microtubules; microtubule-associated proteins, such as ensconsin; the microtubule motor proteins, kinesin and dynein; and motor protein adaptors, such as kinesin light chain, dynein light chain, p150/Glued, cytoplasmic linker protein-190 (CLIP190), sunday driver (Syd or JNK-interacting protein 3 (JIP3)), and JNK signaling [2–5]. We refer the reader to Schulman et al. [8] in which we discuss our current thinking about the different mechanisms at work during each stage of myonuclear movement. To identify these mechanisms, we have developed various techniques to define and quantify myonuclear position in *Drosophila* [2–5]. This chapter describes these methodologies in both fixed and live *Drosophila* embryonic and larval preparations.

2 Materials

2.1 Imaging of Fixed Embryonic Muscles

2.1.1 Embryo Collection and Fixation (Fig. 4)

1. Embryo laying pot: 100 ml plastic beaker punched with holes to allow air exchange and prevent condensation. To make holes use a hot syringe needle with gauge (Sub-Q 26G5/8).
2. Embryo collection plates (apple juice plates): Microwave 1500 ml of ddH_2O, 50 g of granulated sugar, and 45 g of agar until a homogeneous solution is formed. Add 500 ml of cold apple juice, cool solution to 65 °C, and add 40 ml of 10 % Tegosept in 100 % ethanol. Pour solution into petri dishes (60×15 mm); make approximately 200 plates. Secure these plates to the laying pots with rubber bands.

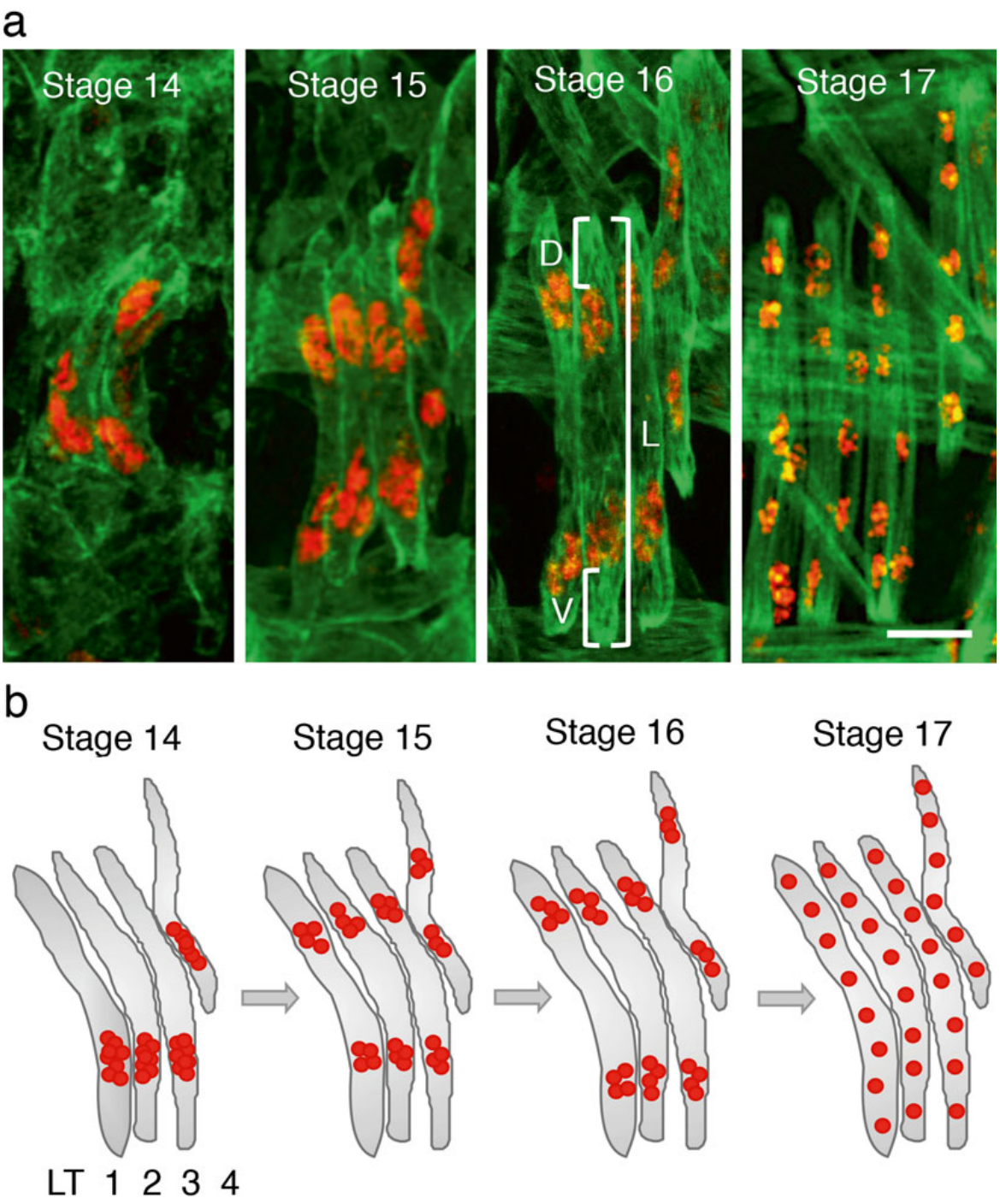


Fig. 2 Myonuclear positioning in the LT muscles during embryonic development. (**A**) Myonuclear position from stage 14 to stage 17. In the images of stages 14–16, the LT muscles are stained with Tropomyosin (*green*) and DsRed (*red*) to show the muscle structure and the nuclei, respectively. In the stage 17 image, the LT muscles are labeled with *Tropomyosin-GFP* (*green*) and the nuclei are labeled with *apterousME::NLSdsRed* (*red*) (*see* Table 2). At stage 16, image measurements are taken: D represents the dorsal measurement, V represents the ventral measurement, and L represents the total length of the muscle. Scale bar, 10 μm. (**B**) Schematic representation of myonuclear movements from stage 14 to stage 17 as shown in panel (**A**). LT muscles 1–3 have 6–8 nuclei each, whereas LT4 has 4–6 nuclei

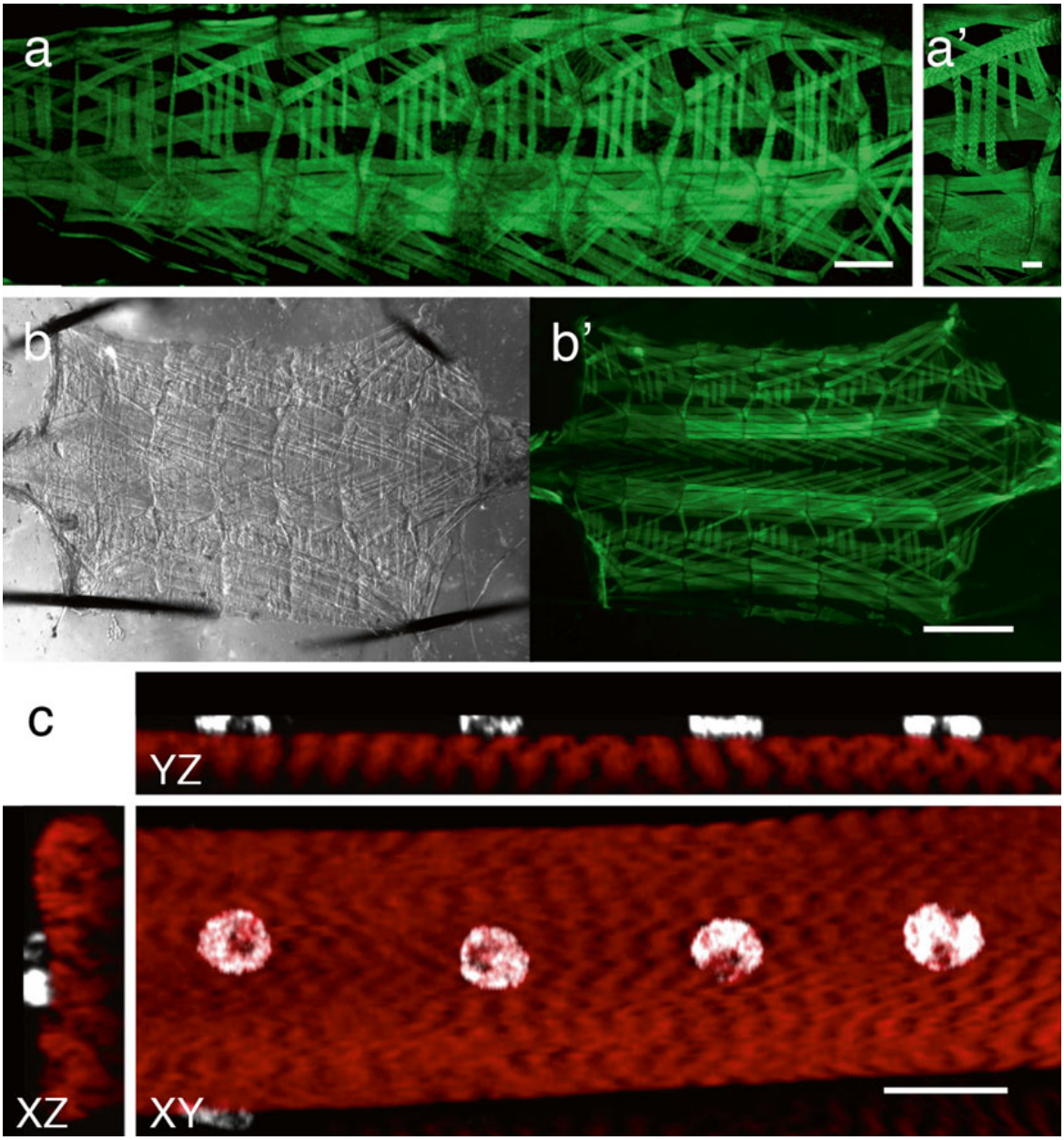


Fig. 3 Larval musculature and myonuclear positioning in a 3rd instar larva. (**A**) Image of a live *Drosophila* 3rd instar larva expressing *Tropomyosin-GFP*, a GFP gene trap that labels all muscles. Note the repeated muscle pattern in each hemisegment. Scale bar, 100 μm. (**A′**) Higher magnification of one hemisegment. Scale bar, 25 μm. (**B**, **B′**) Dissected flat prep of a larva carrying *Tropomyosin-GFP* with all the muscles exposed. Scale bar, 50 μm. (**B**) Bright field image. (**B′**) Wide field fluorescence image. (**C**) Orthogonal view of a ventral longitudinal 4 muscle (VL4). *Red*, actin; *white*, nuclei. Scale bar, 25 μm

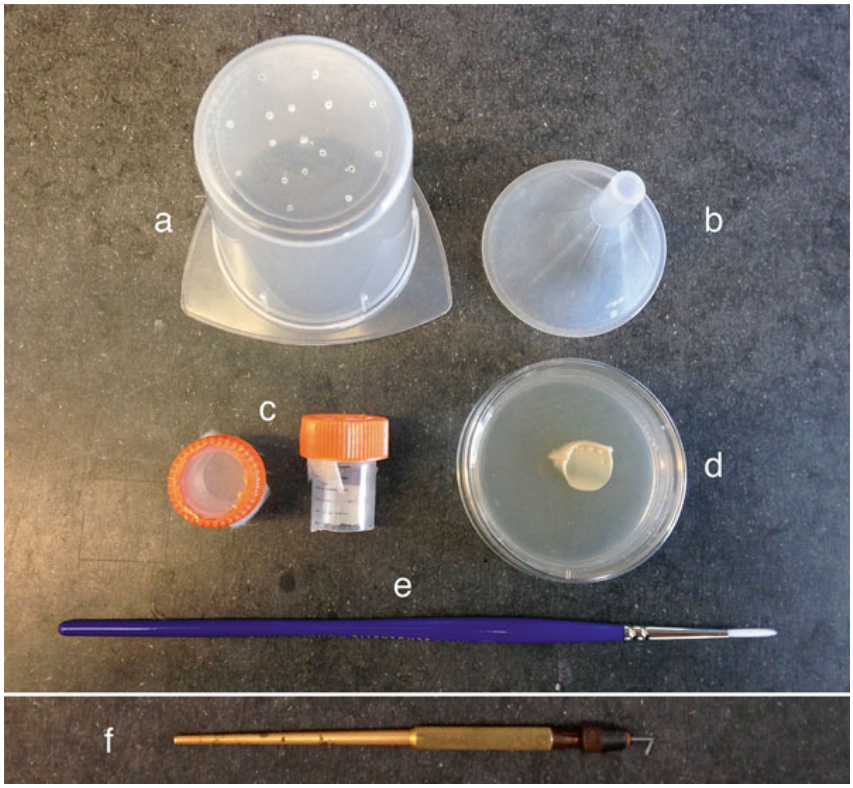


Fig. 4 Materials used for embryo collection. (**A**) Embryo laying pot perforated on the *bottom*. (**B**) Small funnel. (**C**) Collection baskets: *top* and *side* views. (**D**) Yeasted apple juice plate. (**E**) Paintbrush. (**F**) Embryo hook

3. Yeast paste: Distill water plus dry baker's yeast and stir to make a paste. Store at 4 °C.
4. Paintbrush (size 0).
5. Collection baskets: Cut the top off of a 15 ml Falcon tube at approximately the 12 ml line and cut out the center of the tube cap.
6. Nylon membrane (pore size, 140 μm) screwed onto the collection basket with the cap.
7. 3 % sodium hypochlorite (50 % bleach).
8. Small funnel.
9. Eppendorf tubes (1.5 ml).
10. Heptane.
11. Methanol.
12. PFA: 4 % EM grade paraformaldehyde diluted in PBS (phosphate-buffered saline).
13. Platform shaker.
14. Vortex with 1.5 ml Eppendorf tube adaptor.

15. PFA/heptane waste receptacle.
16. Methanol/heptane waste receptacle.
17. Glass Pasteur pipets.

2.1.2 Embryo Staining

1. 3 % Triton X-100: For 200 ml, add 6 ml of Triton X-100 and 194 ml ddH_2O.
2. 10× PBS (phosphate-buffered saline; 0.01 M KH_2PO_4, 0.1 M Na_2HPO_4, 1.37 M NaCl, 0.027 M KCl, pH 7.0).
3. PBT (phosphate-buffered saline containing 0.3 % Triton): For 100 ml, add 10 ml 10× PBS, 10 ml 3 % Triton X-100, and 80 ml ddH_2O.
4. PBT-BSA (phosphate-buffered saline containing 0.3 % Triton and 0.1 % BSA): For 100 ml, add 10 ml 10× PBS, 10 ml 3 % Triton X-100, 1 ml 10 % BSA, and 79 ml ddH_2O.
5. Primary and secondary antibodies of interest. Refer to Table 1 for a suggested list of antibodies and probes routinely used to label *Drosophila* muscle and nuclei.
6. Three-dimensional rotating mixer such as a Nutator.
7. Eppendorf tubes (0.5 ml).
8. Glass Pasteur pipets.

2.1.3 Embryo Mounting

1. Microscope slides.
2. Scotch tape.
3. Cover slips: size 22 × 40 mm with thickness 0.16–0.19 mm.
4. Mounting medium, such as ProLong Gold antifade reagent or Vectashield.
5. Razor blades.
6. Metal washers (any hardware store).

2.1.4 Embryo Imaging

All images in the lab are acquired on a Leica SP5 laser-scanning confocal microscope equipped with a 20× 0.7NA HC PL Apochromat oil objective, 63× 1.4NA HCX PL Apochromat oil objective, and LAS AF 2.2 software. Equivalent microscopes and software may be used.

2.2 Time-Lapse Imaging of Embryonic Muscles

Materials described in Subheading 2.1.1, plus:

2.2.1 Embryo Collection and Mounting (Fig. 5)

1. Plain-tipped applicator (wooden stick).
2. Halocarbon oil 700.
3. Air-permeable Teflon membrane mounted on a circular Perspex frame (designed by E. Wieschaus; [14, 15]).
4. Cover slips: size 22 × 40 mm with thickness 0.16–0.19 mm.

Table 1
Antibodies and probes used to probe *Drosophila* myonuclear positioning[a]

Primary antibodies[b]	Expression detected	Company, reference #
Muscle markers		
Tropomyosin	Actin cytoskeleton	Abcam, ab50567
Myosin heavy chain (MHC)	Myosin, actin motor protein	DSHB, EB165-s
Nuclear markers		
Lamin Dm0	Nuclear envelope	DSHB, ADL67.10
Lamin C	Nuclear envelope	DSHB, LC28.26
Specific muscle nuclear markers		
Even-skipped	DA1	[20]
Vestigial	DA1, DA2, DA3, LL1, VLs1-4	[21]
Others		
DsRed	Red fluorescent protein	Clontech, 632496
GFP	Green fluorescent protein; useful to identify the present of fluorescent balancers (e.g., DGy, CTG)	Clontech, 632381 Invitrogen, A-11120
α-Tubulin	Microtubules	Sigma, T9026
Secondary antibodies	**Expression detected**	**Company, reference #**
Alexa Fluor 488 conjugated		Life Technologies
Alexa Fluor 555 conjugated		Life Technologies
Alexa Fluor 647 conjugated		Life Technologies
Probes antibodies	**Expression detected**	**Company, reference #**
Alexa Fluor 546 conjugated phalloidin	F-actin	Life Technologies, A22283
Hoechst	DNA	Invitrogen, 33342

[a]We refer the reader to several papers for reagents that probe specific proteins involved in myonuclear positioning [2–6, 22]
[b]*See* **Notes 1** and **2**

2.2.2 Embryo Imaging

Mounted embryos are imaged on a Leica SP5 laser-scanning confocal microscope equipped with a 63× 1.4NA HCX PL Apochromat oil objective and LAS AF 2.2 software (for imaging nuclear clusters or individual nuclei [5]) or on a Zeiss AxioPlan2 epifluorescence imaging system with light microscopy with a 40× Plan-NeoFluar 0.75NA objective and AxioVision Rel 4.8 software (for myonuclear movement in the whole embryo; [2]). Equivalent microscopes and software may be used.

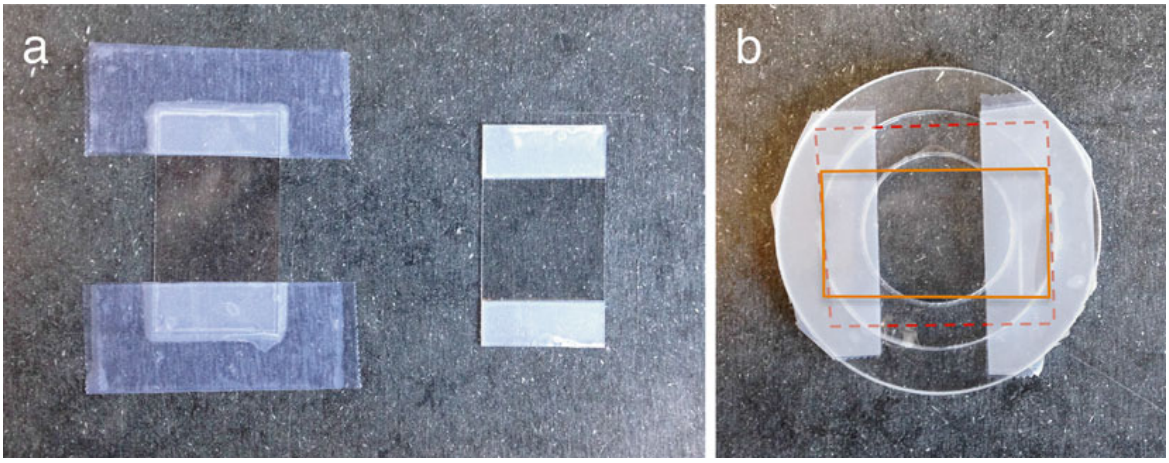


Fig. 5 Materials used for mounting embryos. (**A**) Cover slip with a Scotch tape bridge used to mount fixed embryos for imaging. The image shows a cover slip with two pieces of tape on both ends, before the excess is removed (*left*) and after (*right*). (**B**) Frame used to mount embryos for time-lapse imaging. The image shows an air-permeable Teflon membrane (*red dashed line box*) mounted on a circular Perspex frame. Two pieces of tape provide support for a cover slip bridge where the embryos are placed (*center of the frame*). The orange solid line box represents the cover slip; it is placed on top of both sides of the tape as shown in the image

2.3 Imaging of Formalin-Fixed Larval Muscles

2.3.1 Larvae Collection

1. Laying pot as described in Embryo Collection and Fixation from Imaging of Fixed Embryonic Muscles section (*see* Fig. 4).
2. Lightly yeasted apple juice plates (*see* Subheading 2.1.1, **step 2**).
3. 15 % sucrose solution: sucrose diluted in water.
4. Embryo hook or straight forceps (tip dimensions, 0.1 × 0.06 mm).
5. Dissection microscope equipped with fluorescence.
6. Paintbrush.

2.3.2 Larvae Dissection and Fixation

1. Dissection pins (diameter, 0.1 mm).
2. Two pairs of straight forceps (tip dimensions, 0.1 × 0.06 mm).
3. Dissection plate: petri dish (150 × 15 mm) coated with a thick layer of Sylgard.
4. Vannas spring scissors (sharp tips; non-serrated; cutting edge, 3 mm; tip diameter, 0.05 mm).
5. Cold HL3.1 buffer: 70 mM NaCl, 5 mM KCl, 0.2 mM $CaCl_2$, 20 mM $MgCl_2$, 10 mM $NaHCO_3$, 5 mM trehalose, 115 mM sucrose, and 5 mM HEPES; pH 7.3 [16].
6. 1× PBS.
7. Formalin solution, 10 %.
8. Glass Pasteur pipets.

2.3.3 Larvae Staining and Mounting

As in Subheadings 2.1.2 and 2.1.3, plus:

1. Straight forceps (tip dimensions, 0.1 × 0.06 mm).

2. Kimwipes tissues.
3. Dissection scope.

2.3.4 Heat-Fixed Larvae

1. Water (distilled) at 65 °C.
2. Halocarbon oil or 50 % glycerol.
3. Microscope slides.
4. Cover slips: size 22 × 40 mm with thickness 0.16–0.19 mm.

2.3.5 Larval Imaging

Images are acquired using the 40× 1.25–0.75NA HXC PL Apochromat oil objective of a Leica SP5 laser-scanning confocal microscope and the LAS AF 2.2 software. Equivalent microscopes and software may be used.

2.4 Fly Stocks

The *Drosophila* community has developed a rich collection of genetic reagents to probe various cellular processes, including myonuclear positioning. In addition to classic mutations, there is a wide range of available fly stocks that allow tissue-specific manipulation of a gene of interest. Spatial and temporal manipulation is accomplished using the bipartite GAL4/UAS system [17]. Reagents useful for the study of myonuclear positioning are listed in Table 2. New reagents are constantly being developed, particularly with the development of CRISPR genome-editing approaches in *Drosophila*. We refer the reader to FlyBase (http://flybase.org/), a community resource that provides a comprehensive, searchable compendium of genes, mutations, expression patterns, available stocks, and references.

3 Methods

3.1 Imaging of Fixed Embryonic Muscles

3.1.1 Embryo Collection

1. Set up a laying pot with 60 females/female virgins and 30 males at 22 °C (room temperature), 25 °C, or 29 °C, depending on the experiment (*see* **Note 3**).
2. Label and change the apple juice plates on laying pots, keeping the old ones for embryo collection.
3. Pour enough 50 % bleach to cover embryos on each plate and remove dead flies with a paintbrush. Dechorionate embryos for 4 min at room temperature. During this period, label 1.5 ml Eppendorf tubes and add 500 μl heptane to each.
4. Gently disturb the embryos on the plate with a paintbrush and transfer them to a collection basket using a small funnel. Rinse the plate with water to collect any remaining embryos and transfer them to the collection basket. Rinse the embryos in the collection basket liberally with additional distilled water to remove any traces of bleach.
5. Move the embryos to the Eppendorf tube containing the heptane with the paintbrush.

Table 2
***Drosophila* stocks useful for the study of myonuclear positioning**

Fly stock	Use	Reference
GAL4 lines	Available from stock centers/*Drosophila* labs	
Twist-GAL4	Somatic mesoderm expression from gastrulation to stage 14	[23]
Mef2-GAL4	Somatic mesoderm expression from stage 7 and throughout larval and adult development	[24]
24B-GAL4	Somatic mesoderm expression from stage 7	[17]
MHC-GAL4	Somatic muscle expression—stage 13 throughout larval and adult development	[25]
G7-GAL4	Muscle expression in larvae	[26]
Alpha-GAL4	Muscle expression in larvae	K. Broadie lab, Vanderbilt University
ApterousME-GAL4	LT muscle-specific expression in embryo	[27]
5053-GAL4	VL1 muscle-specific expression in embryo	[28]
Rp298-GAL4	Founder cell-/myotube-specific expression in embryo/pupa	[29]
sns-GAL4	Fusion competent myoblast in embryo/pupa	[30]
UAS lines	Available for gene of interest at *Drosophila* stock centers (i.e., Bloomington or Vienna stock centers) or from individual *Drosophila* labs	
UAS-RNAi	Examples: UAS-DhcRNAi, UAS-SydRNAi	[3, 4]
UAS-fluorescent reporter lines targeted to nuclei or other organelle	Examples: UAS-cytoplasmic GFP, UAS-nuclear localized GFP; UAS-lamin GFP labels nuclear envelope; UAS-EB1-GFP labels microtubule plus ends	[3, 5]
Fluorescent reporter lines		
apterousME::NLSdsRed	Labels all myonuclei in the LT muscles	[2, 27]
Tropomyosin-GFP	GFP gene trap in tropomyosin. Labels all muscles	*Drosophila* FLYTRAP collection
Zasp66-GFP	GFP gene trap in Zasp66. Labels all muscles	*Drosophila* FLYTRAP collection
Gene mutants	Available for gene of interest at stock centers or from *Drosophila* labs: (http://flybase.org/)	

3.1.2 Embryo Fixation

1. Thaw an aliquot of 4 % PFA.
2. Add 500 µl of PFA to the Eppendorf tube containing the heptane and embryos.
3. Using a platform shaker set at 250 rpm, incubate the embryos for 20 min at room temperature.

4. Remove both the PFA and heptane phases, leaving the embryos in the Eppendorf tube.
5. Add 500 µl of fresh heptane and 500 µl of 100 % methanol (for an alternative fixation method to label fixed embryos with phalloidin, *see* **Note 4**).
6. Vortex for 1 min at room temperature. Embryos that have been devitellinized will fall to the bottom of the tube, whereas those that remain at the interface or float are not devitellinized and should be discarded.
7. Remove all liquid.
8. Rinse embryos in methanol three times. To rinse: add solution, invert tube, let settle, remove, and repeat.
9. Add fresh 100 % methanol for storage at −20 °C. Embryos can be stored and used reliably for up to 6 months.

3.1.3 Embryo Staining

1. Transfer embryos to a 0.5 ml Eppendorf tube and remove excess methanol.
2. Rinse three times with PBT-BSA.
3. Add fresh PBT-BSA and incubate for 30 min on Nutator at room temperature. BSA serves to reduce nonspecific binding of antibodies.
4. Add primary antibodies diluted in PBT-BSA (Table 1). As an example, use antibodies directed to tropomyosin or myosin heavy chain to visualize muscles and DsRed to label the nuclei of the lateral transverse (LT) muscles expressing the *apterousME::NLSdsRed* (Figs. 1 and 2). Incubate primary antibodies with the embryos on the Nutator for 1 h at room temperature or overnight at 4 °C.
5. Remove primary antibodies and store at 4 °C (most can be reused up to three times).
6. Rinse embryos with PBT-BSA three times.
7. Wash embryos with PBT-BSA three times for 10 min at room temperature on the Nutator.
8. Remove PBT-BSA and add secondary antibodies (Table 1), diluted in PBT-BSA, to the embryos and incubate on the Nutator for 1 h at room temperature. As fluorescent antibodies are light sensitive, cover them with aluminum foil. From this point forward, keep them covered as much as possible until the staining protocol is finished.
9. Remove and discard secondary antibodies.
10. Rinse embryos with PBT (no BSA) three times.
11. Wash embryos with PBT three times for 10 min on the Nutator at room temperature.

3.1.4 Embryo Mounting

1. While washing the embryos (**step 12** above), prepare slides for mounting. To mount embryos, first make a "tape bridge," comprised of two superimposed pieces of Scotch tape, on two opposite sides of the cover slip (Fig. 5a).
2. Label the slide with date, genotype or cross, and the antibodies used.
3. Place a metal washer on the slide and rest the cover slip on the washer with the tape bridge facing up.
4. Cut 1 cm off of the end of a p200 pipet tip for each sample so that embryos can be pipetted without damage.
5. Remove PBT from the last wash (**step 12** above).
6. Add 80 μl of ProLong Gold antifade reagent to embryos using the truncated p200 tip (ProLong Gold is extremely viscous) and slowly mix them together.
7. Transfer embryos to the cover slip. Remove any visible bubbles.
8. Place a new cover slip over the tape bridge and line up both cover slips to form a sandwich.
9. Store overnight in the dark until the ProLong Gold sets.
10. Remove the washer and tape the cover slip sandwiches to the slide. These slides are ready to be imaged.
11. Slides can be stored at −20 °C for up to 6 months.

3.1.5 Confocal Microscopy

While the data indicate that similar movements and mechanisms are active in other *Drosophila* muscle subsets, our lab has focused on studying myonuclear movements in a subset of muscles, the lateral transverse muscles (LT). Hence, the methodology for confocal imaging described below is focused on this subset.

1. On the confocal microscope, identify an embryo at the correct stage (stages 14–16) positioned with its lateral side facing up using the low-magnification objective. Staging is done based on overall embryo shape, the intensity of DsRed and tropomyosin signal when used, gut morphology, and the morphology of the trachea [2, 3, 18]. At stage 16, a control LT muscle shows two clusters of nuclei (3–4 nuclei in each cluster) near each longitudinal pole of the muscle.
2. After finding a correctly staged embryo for imaging, move to a higher magnification objective, such as the 63× objective, and increase the zoom to 1.5×. On the computer, position the embryo in a horizontal position with four hemisegments visible in the imaging field. Choose hemisegments 3–7 for imaging (*see* **Note 5**).
3. To set the *Z*-stack, begin by selecting the first slice in which the LT muscles are visible, and after moving through the muscle,

stop and select the last slice in which these muscles are no longer visible. The recommended step size is 0.5 μm. The total size of the stack will vary between embryos, but the step size should be kept constant. The gain for each channel should be adjusted according to the intensity of the corresponding signal.

3.1.6 Image Analysis

Multiple software packages, including Volocity Visualization Software 6.1.1 (Improvision), Imaris (Bitplane), and Adobe Photoshop CS4, are used for image processing. ImageJ (NIH) software is used for measurements. With the appropriate plug-in (*bioformats_package*), however, files from Leica or Zeiss confocal microscopes can be opened directly in ImageJ, and all rendering, processing, and analysis can be done within ImageJ. Therefore, the instructions below will refer to ImageJ software:

1. Open your files by dragging them into ImageJ toolbar.
2. For the nuclear positioning analysis, select the extended focus view to visualize whole muscles. Select: Image > Stacks > Z Project and select Standard Deviation as the projection type (*see* **Note 6**). Adjust the number of slices to be included in the final projection.
3. Merge channels by selecting Image > Color and Merge Channels.
4. Brightness and contrast, as well as other settings, can be adjusted by selecting Adjust under the Image menu (Image > Adjust > Brightness/Contrast).
5. For analysis, position the image with the anterior side of the muscle set to the left and dorsal to the top of the viewing field. The image can be rotated by selecting Transform under the Image menu (Image > Transform > Rotate).
6. For measuring nuclear positioning, turn on the segmented line option. To do this, go to the ImageJ toolbar, right-click on the line option (represented as a straight diagonal line), and select Segmented Line.
7. Three different measurements are made for each muscle (Fig. 2a): Dorsal (D)—Distance from the dorsal end of each muscle to the nearest edge of the closest nucleus; Ventral (V)—Distance from the ventral end of each muscle to the nearest edge of the closest nucleus; and Length (L)—Length of each muscle following the curvature of the muscle. The edges of the nuclei and ends of the myofibers are defined by a clear change from signal to background within the relevant viewing channel. Each LT muscle is considered individually in all cases. To register each measurement, hit the M key (a new window will pop up when this is assessed for the first time).
8. For the analysis, a total of three measurements (dorsal, ventral, and length) per muscle, from four muscles per hemisegment in

four hemisegments per embryo, are measured in each of ten embryos per genotype.

9. Copy all measurements to an Excel sheet. To calculate the dorsal and ventral distances, represent each value as a percent of the total muscle length to account for variation in muscle size. This will provide a quantification of the proximity of each cluster to each end of the muscle, which can be compared to control values. To calculate the nuclear spread, use the measurement values in the following formula: $\frac{\text{Length} - \text{Dorsal} - \text{Ventral}}{\text{Length}}$. This quantifies the distance that both clusters have traveled relative to each other and to the muscle length.
10. For statistical analysis, use either Excel or an advanced statistical software, such as SPSS (Statistical Package for the Social Sciences, IBM) or GraphPad Prism. The standard statistical test used is the Student's *t*-test.

3.2 Time-Lapse Imaging of Embryonic Muscles

3.2.1 Embryo Collection and Mounting

1. Follow **steps 1–4** from Subheading 3.1.1.
2. Place the collection basket on a small petri dish and fill it up with water so that the embryos are floating.
3. Dip a wooden stick into halocarbon oil and use the halocarbon oil on the end of the stick to collect the floating embryos from the collection basket. Then transfer them to an air-permeable Teflon membrane mounted on a circular Perspex frame (Fig. 5b). Place two pieces of tape on each side of the embryos to create a bridge that will prevent embryo damage. Place a cover slip on top of both pieces of tape.

3.2.2 Confocal Microscopy

1. For time-lapse imaging of whole embryos, *Z*-stacks are taken with optical sections set at 3 μm on the Zeiss AxioPlan2. To set the stack, the first slice is set when the LT nuclei are in view in multiple hemisegments. The final slice is set below the nuclei. A frame rate of 20 s is used. Only a single Z-section with the greatest number of nuclei in focus is selected for each time point. Images are processed using ImageJ and compiled into a video using QuickTime [2] (*see* **Note 7**).
2. For time-lapse imaging of myonuclear clusters and individual myonuclei, *Z*-stacks of two hemisegments are imaged simultaneously, using a high-magnification objective, such as the 63× 1.4 NA HCX PL Apochromat oil objective (*see* Subheading 2.2.2) and increasing the zoom to 2–2.5×. Set the stack starting slightly above the nuclei and finishing slightly below the nuclei. Set the step size to 0.5 μm and the time interval to be between 20 s and 3 min [5] (*see* **Note 7**).

3. Depending on the types of nuclear movement analyzed, collect data from 10 h (whole embryo) to 60 min (individual nuclear movements). Record a minimum of five time-lapse series per genotype.

3.2.3 Image Analysis

1. Quantification of myonuclear movements and myonuclear morphology changes are completed manually using measurement functions in ImageJ (NIH) as described in Subheading 3.1.6.
2. *Nuclear translocation speed:* The velocity at which myonuclear clusters in the LT muscles separate during stage 15 is assessed by measuring the distance between the dorsal and ventral clusters of nuclei at $t=0$ h and at $t=1$ h and determining the increased distance between the two clusters. By tracking individual nuclei as they moved relative to a fixed position in the embryo over the course of 10 min, the speed of individual myonuclei is determined. One hundred individual myonuclei from five different embryos are assayed for each genotype.
3. *Nuclear rotations:* The number of LT myonuclei that rotate is determined by examining the time-lapse videos. A myonucleus that rotates, stops, and then rotates again is counted as one rotating myonucleus. Two hundred and fifty myonuclei are normally examined.
4. *Nuclear translocation directionality:* The leading edge of a myonucleus is defined as the edge of the myonucleus furthest in the direction of translocation. A myonucleus is judged to have changed direction if it persistently moves a distance of at least one nuclear radius in the opposite direction from its previous direction of translocation. Two hundred and fifty myonuclei are examined.
5. *Nuclear shape changes:* The aspect ratios of moving myonuclei are determined by dividing the length of the dorsal-ventral axis of a myonucleus by the length of the anterior-posterior axis of a myonucleus using ImageJ software (NIH). Aspect ratios are considered to change if a difference of ≥ 0.7 was observed in these measurements. Two hundred and fifty myonuclei are examined with at least ~80 % exhibiting the changes in noted behavior.

3.3 Imaging of Formalin-Fixed Larval Muscles

3.3.1 Larval Collection (Fig. 4)

1. Set up a laying pot with 60 females/female virgins and 30 males at 22 °C (*see* **Note 3**).
2. Label and change the apple juice plates on laying pots, keeping the old ones for embryo collection.
3. Day 0: Under the dissection scope, select stage 16/17 embryos and transfer them to a half-yeasted plate with the help of an embryo hook. Arrange the embryos in a line next to a very thin layer of yeast. This will make it easier to find the 1st instar larvae on the next day.

4. Day 1: Within 24 h, transfer the hatched larvae to a vial with food and store the vial at 25 °C for an additional 3 days or 22 °C for 4 days.
5. On day 4 or day 5 (depending on the temperature), larvae will be 3rd instar larvae. Pour room temperature 15 % sucrose solution in the vial. Gently disturb the food at the bottom of the vial with a spatula. The larvae will float and can be collected using a paintbrush. In the event that some larvae are stuck in the food, release by gentle agitation. Transfer the larvae to an apple juice plate.
6. If larvae expressing a fluorescent protein that was not previously visible in the embryo are desired, select the appropriate larvae under the fluorescence scope before starting dissecting.
7. Prepare separate Eppendorf tubes with PBS for each genotype/cross and keep them in ice.

3.3.2 Larval Dissection and Fixation with Formalin

1. Before starting the dissections, gather at least six dissection pins on the dissection plate.
2. Transfer one larva to the dissection plate and add a drop of cold HL3.1 buffer using a glass pipet. This "relaxing buffer" will slow larval movements.
3. Orient the larva with its dorsal side up (identified by visualization of the main trunks of the trachea) and pin both the anterior and posterior ends of the larva to the plate. Specifically, after securing one end, use the other pin to stretch the larva to its normal length, being careful to not overstretch it, before securing the other end.
4. Using the scissors, make small incisions perpendicular to the length of the larva close to each pin (cutting both trunks of the trachea). Then, cut along the larval body, ideally between the two main trunks of the trachea, to expose the inner organs.
5. With forceps, gently remove the gut, trachea, and neurons, being careful to not damage muscles.
6. Pin each corner of the larval body to the plate, making it flat. Once more, stretch out the tissue, but avoid overstretching. The flatter the larva during preparation, the easier the image acquisition later.
7. Remove the HL3.1 buffer, add a few drops of 10 % formalin, and incubate for 20 min at room temperature.
8. Rinse with cold PBS three times.
9. Add fresh PBS and remove pins.
10. Transfer to an Eppendorf tube with cold PBS.
11. Store at 4 °C for a maximum of 1 week (for optimal staining results). Do not store dissected larvae at –20 °C as this will damage the structure of the muscle.

3.3.3 Larval Staining and Mounting

1. Staining larvae is similar to staining embryos (*see* Subheading 3.1.3), except when using fluorescence-conjugated probes such as phalloidin or Hoechst. If these types of probes are used, there is only one incubation of 1 h at room temperature followed by PBT washes. If antibodies are also used, incubate with primary antibodies first, as in the embryo staining protocol, followed by incubation with appropriate secondary antibodies and the aforementioned probes.
2. After completing the staining, transfer a maximum of six larvae to a microscope slide.
3. Under a dissection scope, position larvae with the head at the top and flatten them by exposing the muscles facing up. Spread out the larvae evenly on the slide. While doing this, do not let larvae dry out. Add more PBT if necessary.
4. Remove any excess PBT by absorbing it with a Kimwipes.
5. Place a drop of ProLong Gold antifade reagent on top of each larva and remove any visible bubbles.
6. Cover with a cover slip and let it dry at room temperature in the dark. Note that there is no bridging of the cover slips for the mounting of larvae.
7. Slides can be stored at −20 °C for up to 6 months.

3.3.4 Confocal Microscopy

1. For formalin-fixed larval muscles, we image the ventral lateral muscles 3 and 4 (VL3 and VL4) because they are easily observed and are more resistant to damage during dissection. For simplicity, it is recommended to focus on VL4, with its single row of myonuclei, rather than VL3, which contains two rows of nuclei.
2. A VL4 muscle should fit in the imaging field on the microscope computer. Set the *Z*-stack, starting a little above the muscle and finishing just prior to the slice when other muscles first become apparent. Set the Z-step size to 0.5 μm. Image six muscles from each of five larvae per genotype.

3.3.5 Image Analysis

As for embryo image analysis (*see* Subheading 3.1.6), different software packages can be used. All the instructions herein will refer to ImageJ software (NIH):

1. Follow **steps 1–4** from Confocal Microscopy in the Imaging of Fixed Embryonic Muscles (*see* Subheading 3.1.6).
2. For assessing myonuclear position in larvae, different types of measurements are made: muscle length, internuclear distance (Fig. 6a, b), nearest neighbor (Fig. 6c), largest gap (Fig. 6d), and myonuclear number.
3. *Muscle length*: Use the straight line option on the ImageJ toolbar and hit the M key to open a new window with the values.

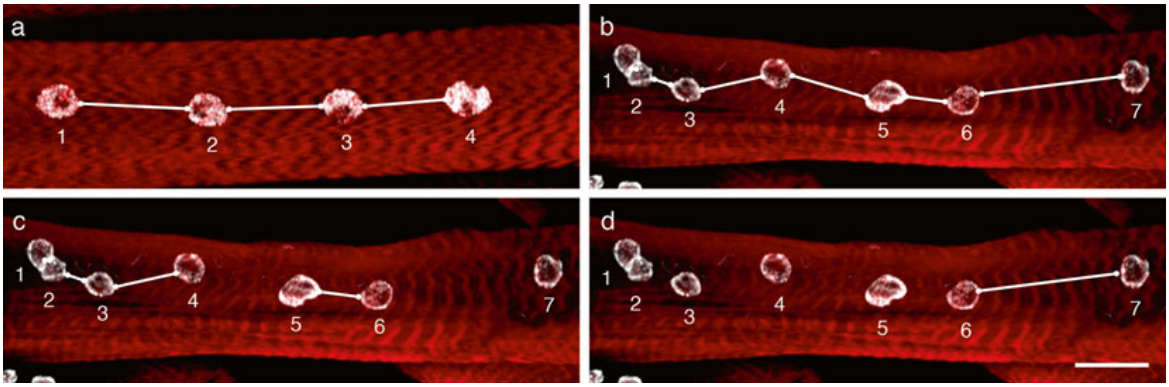


Fig. 6 Myonuclear positioning measurements in larval muscles. In a control VL4 muscle (**A**) and in a VL4 muscle with disrupted myonuclear positioning (**B**–**D**), white lines represent different measurements made to determine myonuclear positioning defects. (**A**) Internuclear distance. Nuclei are approximately equidistant. (**B**) Internuclear distance. The distance between nuclei is variable. (**C**) Nearest neighbor. Two different scenarios: the nearest neighbor of nucleus 5 is nucleus 6 and vice-versa; the nearest neighbor of nucleus 4 is nucleus 3 but the opposite is not the case. Nucleus 2 is the nearest neighbor to nucleus 3. (**D**) Largest gap. In this muscle, the largest gap between two nuclei is the distance between nuclei 6 and 7. Scale bar, 25 μm

4. *Internuclear distance*: Measure the distance between every nucleus. In control muscles or muscles without nuclear clumping, the resulting standard deviation will be very small compared to the measurements from muscles with nuclear clumping.
5. *Nearest neighbor*: Measure the distance to the nearest edge of the closest nucleus from each nucleus. Assume distance equals 0 when two nuclei are touching. The closer the nuclei, the lower the final average will be.
6. *Largest gap*: Measure the longest distance between two nuclei within a given muscle. For more severe defects in myonuclear positioning, this distance is bigger, whereas in muscles with control-like nuclear distribution, this value is smaller.
7. *Number of nuclei per muscle*: A control VL4 muscle contains 7–9 nuclei.
8. Copy all measurements to an Excel sheet. To calculate each of the parameters mentioned above, always consider the length of the muscle and express values as a percentage of muscle length.
9. For statistical analysis, either use Excel or a more advanced statistical software, such as SPSS (Statistical Package for the Social Sciences, IBM) or GraphPad Prism. The standard statistical test used is the Student's *t*-test.

3.4 Heat-Fixed Larvae

An alternative method of fixing larvae for microscopy is heat fixation (adapted from [19]). For this approach, use larvae at any developmental stage. Since there is no staining with this protocol, larvae expressing fluorescent markers in both the muscles and the nuclei are ideal (*see* Table 2):

1. Pick a larva using forceps. Be careful not to damage muscles.
2. Dip the larva in water at 65 °C for 1–2 s.
3. Mount 5–6 larvae in halocarbon oil or 50 % glycerol in a microscope slide.
4. Cover with a cover slip.

4 Notes

1. For antibodies with high levels of nonspecific background staining, preabsorption using fixed control embryos is recommended. For example, some antibodies listed in Table 1, such as anti-Eve, are preabsorbed to obtain better results [6].
2. Due to the formation of the embryonic cuticle at stage 17, antibodies can only penetrate the embryo from the initial stages of embryogenesis until stage 16. For visualizing myonuclear position as well as muscle structure at stage 17, fluorescently tagged proteins that label the myonuclei and the muscles must be examined (*see* Table 2).
3. Although the ideal number of flies in a laying pot is 60 females/female virgins and 30 males, laying pots can be set up with as few as 25 females/female virgins and 15 males. Using a large number of flies in a laying pot is important when collecting large amounts of embryos.
4. For labeling fixed embryos with phalloidin, an alternative fixation method in which methanol is substituted with ethanol should be used. After fixing in heptane and PFA, add 100 % ethanol, vortex for 45 s, discard the ethanol, add 100 % ethanol, vortex for 45 s, collect embryos to a new tube, and store in fresh 90 % ethanol at −20 °C.
5. When imaging embryos, it is recommended to focus on hemisegments 3–7 because these hemisegments are developmentally more similar in age and are less prone to variations in muscle structure.
6. When rendering a *Z*-stack in ImageJ, a number of projection types are available (average intensity, maximum intensity, minimum intensity, sum of slices, standard deviation, and median). The type selected depends on what is being measured. Maximum intensity is suggested if the user is measuring that particular signal. We use standard deviation as it renders an excellent image of the sarcomeric structure in the muscle; however, we are measuring distances between the nuclei.
7. While acquiring time-lapse images, check every 10 min to adjust focus as embryos will move and the nuclei will shift out of focus. However, note that adjusting this focus means restart-

ing the time-lapse sequence. This cannot be done within a time-lapse. After a few adjustments, the focal plane will essentially stabilize and it can be left for hours to get the desired time-lapse sequence.

Acknowledgments

We thank the members of the Baylies Lab for advice, particularly, Krista Dobi, Jonathan Rosen, and Stefanie Windner for providing images for Fig. 3A (Dobi) and 2A Stages 14/15 and Stage 17 (Rosen and Windner, respectively). We also acknowledge our funding agencies, SFRH/BD/52041/2012 (Azevedo), and MDA and NIH NIAMS RO1-068128 (Baylies).

References

1. Romero NB (2010) Centronuclear myopathies: a widening concept. Neuromuscul Disord 20(4):223–228
2. Metzger T et al (2012) MAP and kinesin-dependent nuclear positioning is required for skeletal muscle function. Nature 484(7392): 120–124
3. Folker ES, Schulman VK, Baylies MK (2012) Muscle length and myonuclear position are independently regulated by distinct Dynein pathways. Development 139(20):3827–3837
4. Schulman VK et al (2014) Syd/JIP3 and JNK signaling are required for myonuclear positioning and muscle function. PLoS Genet 10(12):e1004880
5. Folker ES, Schulman VK, Baylies MK (2014) Translocating myonuclei have distinct leading and lagging edges that require kinesin and dynein. Development 141(2):355–366
6. Schulman VK, Folker ES, Baylies MK (2013) A method for reversible drug delivery to internal tissues of Drosophila embryos. Fly (Austin) 7(3):193–203
7. Dobi KC, Schulman VK, Baylies MK (2015) Specification of the somatic musculature in Drosophila. Wiley Interdiscip Rev Dev Biol 4(4):357–375
8. Schulman VK, Dobi KC, Baylies MK (2015) Morphogenesis of the somatic musculature in Drosophila melanogaster. Wiley Interdiscip Rev Dev Biol 4(4):313–334
9. Bourgouin C, Lundgren SE, Thomas JB (1992) Apterous is a Drosophila LIM domain gene required for the development of a subset of embryonic muscles. Neuron 9:549–561
10. Fujioka M et al (2005) Embryonic even skipped-dependent muscle and heart cell fates are required for normal adult activity, heart function, and lifespan. Circ Res 97(11):1108–1114
11. Knirr S, Frasch M (2001) Molecular integration of inductive and mesoderm-intrinsic inputs governs even-skipped enhancer activity in a subset of pericardial and dorsal muscle progenitors. Dev Biol 238(1):13–26
12. Landgraf M, Thor S (2006) Development of Drosophila motoneurons: specification and morphology. Semin Cell Dev Biol 17(1):3–11
13. Demontis F, Perrimon N (2009) Integration of Insulin receptor/Foxo signaling and dMyc activity during muscle growth regulates body size in Drosophila. Development 136(6): 983–993
14. Kaltschmidt JA et al (2000) Rotation and asymmetry of the mitotic spindle direct asymmetric cell division in the developing central nervous system. Nat Cell Biol 2(1):7–12
15. Haseloff J, Dormand EL, Brand AH (1999) Live imaging with green fluorescent protein. Methods Mol Biol 122:241–259
16. Brent JR, Werner KM, McCabe BD (2009) Drosophila larval NMJ dissection. J Vis Exp (24), e1107
17. Brand AH, Perrimon N (1993) Targeted gene expression as a means of altering cell fates and generating dominant phenotypes. Development 118(2):401–415
18. Beckett K, Baylies MK (2007) 3D analysis of founder cell and fusion competent myoblast arrangements outlines a new model of myoblast fusion. Dev Biol 309(1):113–125

19. Schnorrer F et al (2010) Systematic genetic analysis of muscle morphogenesis and function in Drosophila. Nature 464(7286):287–291
20. Frasch M et al (1987) Characterization and localization of the even-skipped protein of Drosophila. EMBO J 6(3):749–759
21. Williams JA, Bell JB, Carroll SB (1991) Control of Drosophila wing and haltere development by the nuclear vestigial gene product. Genes Dev 5(12B):2481–2495
22. Elhanany-Tamir H et al (2012) Organelle positioning in muscles requires cooperation between two KASH proteins and microtubules. J Cell Biol 198(5):833–846
23. Baylies MK, Bate M (1996) Twist: a myogenic switch in Drosophila. Science 272(5267): 1481–1484
24. Ranganayakulu G et al (1998) Divergent roles for NK-2 class homeobox genes in cardiogenesis in flies and mice. Development 125(16):3037–3048
25. Chen EH, Olson EN (2001) Antisocial, an intracellular adaptor protein, is required for myoblast fusion in Drosophila. Dev Cell 1(5):705–715
26. Zhang YQ et al (2001) Drosophila fragile X-related gene regulates the MAP1B homolog Futsch to control synaptic structure and function. Cell 107(5):591–603
27. Richardson BE et al (2007) SCAR/WAVE and Arp2/3 are crucial for cytoskeletal remodeling at the site of myoblast fusion. Development 134(24):4357–4367
28. Ritzenthaler S, Suzuki E, Chiba A (2000) Postsynaptic filopodia in muscle cells interact with innervating motoneuron axons. Nat Neurosci 3(10):1012–1017
29. Dutta D et al (2002) Real-time imaging of morphogenetic movements in Drosophila using Gal4-UAS-driven expression of GFP fused to the actin-binding domain of moesin. Genesis 34(1-2):146–151
30. Kocherlakota KS et al (2008) Analysis of the cell adhesion molecule sticks-and-stones reveals multiple redundant functional domains, protein-interaction motifs and phosphorylated tyrosines that direct myoblast fusion in Drosophila melanogaster. Genetics 178(3): 1371–1383

Published Online: 9 January, 2019 | Supp Info: http://doi.org/10.1083/jcb.201808176
Downloaded from jcb.rupress.org on July 29, 2019

JCB Journal of Cell Biology

ARTICLE

The *Drosophila* Ninein homologue Bsg25D cooperates with Ensconsin in myonuclear positioning

Jonathan N. Rosen[1], Mafalda Azevedo[1,2], David B. Soffar[1], Vitaly P. Boyko[1,3], Matthew B. Brendel[1,3], Victoria K. Schulman[1,4], and Mary K. Baylies[1,4]

Skeletal muscle consists of multinucleated cells in which the myonuclei are evenly spaced throughout the cell. In *Drosophila*, this pattern is established in embryonic myotubes, where myonuclei move via microtubules (MTs) and the MT-associated protein Ensconsin (Ens)/MAP7, to achieve their distribution. Ens regulates multiple aspects of MT biology, but little is known about how Ens itself is regulated. We find that Ens physically interacts and colocalizes with Bsg25D, the *Drosophila* homologue of the centrosomal protein Ninein. Bsg25D loss enhances myonuclear positioning defects in embryos sensitized by partial Ens loss. Bsg25D overexpression causes severe positioning defects in immature myotubes and fully differentiated myofibers, where it forms ectopic MT organizing centers, disrupts perinuclear MT arrays, reduces muscle stiffness, and decreases larval crawling velocity. These studies define a novel relationship between Ens and Bsg25D. At endogenous levels, Bsg25D positively regulates Ens activity during myonuclear positioning, but excess Bsg25D disrupts Ens localization and MT organization, with disastrous consequences for myonuclear positioning and muscle function.

Introduction

In many cell types, nuclei occupy specific subcellular localizations that are functionally important (Gundersen and Worman, 2013). In mammalian muscle, nuclei are positioned at the muscle cell periphery in a manner that maximizes internuclear distance. Myonuclear mispositioning is a feature of certain muscle diseases (Romero, 2010; Folker and Baylies, 2013), and model organisms that are mutant for genes required to position myonuclei exhibit decreased muscle function (Zhang et al., 2010; Elhanany-Tamir et al., 2012; Folker et al., 2012; Metzger et al., 2012; Schulman et al., 2014). These findings argue that correct nuclear positioning is essential for muscle function.

Skeletal muscle development and structure are highly conserved between the fruit fly *Drosophila melanogaster* and humans. In both humans and *Drosophila*, muscle cells are multinucleated and formed from the iterative fusion of muscle precursor cells, each of which contributes a nucleus to the growing myotube. After fusion, myonuclei in each *Drosophila* myotube are present as a single cluster. Subsequently, the myonuclei undergo coordinated movements that ultimately leave them evenly distributed along the length of the muscle cell. The first step of nuclear positioning occurs at stage 14 (10–11 h after egg laying [AEL]), when the myonuclei separate into two clearly defined groups along the myotube's long axis. Then, during stages 15 (11–13 h AEL) and 16 (13–16 h AEL), the two clusters of myonuclei migrate away from the myotube's center toward opposite muscle poles. During stage 17 (16–24 h AEL), the last stage of embryonic development, myonuclei spread out from the two clusters and fill in the myofiber evenly, such that the distance between myonuclei is maximized (Metzger et al., 2012). Finally, this even spacing is maintained, likely by active mechanisms, during the lifetime of the larval myofibers (Elhanany-Tamir et al., 2012; Manhart et al., 2018).

The regulation of myonuclear positioning is poorly understood. A key player in the process is Ensconsin (Ens)/MAP7, a microtubule (MT)-associated protein (MAP). Ens promotes Kinesin-based MT transport by relieving Kinesin from its autoinhibited conformation (Barlan et al., 2013) or by recruiting Kinesin to MTs (Sung et al., 2008). *ens* loss-of-function mutants exhibit a complete block in myonuclear separation and poleward cluster migration through stage 16; at this stage, control myonuclei reside in two clusters near opposite myotube poles, while *ens* mutant myonuclei are present as a single cluster (Metzger et al., 2012). Loss of Kinesin heavy chain (Khc) impairs myonuclear movement (Metzger et al., 2012), as do mutations in the genes encoding the MT minus end–directed motor protein Dynein heavy chain and the motor protein adaptor Sunday driver

[1]Program in Developmental Biology, Sloan Kettering Institute, Memorial Sloan Kettering Cancer Center, New York, NY; [2]Graduate Program in Areas of Basic and Applied Biology, Abel Salazar Biomedical Sciences Institute, University of Porto, Porto, Portugal; [3]Molecular Cytology Facility, Sloan Kettering Institute, Memorial Sloan Kettering Cancer Center, New York, NY; [4]Cell and Developmental Biology, Weill Cornell Graduate School of Medical Sciences, Cornell University, New York, NY.

Correspondence to Mary K. Baylies: m-baylies@ski.mskcc.org.

© 2019 Rosen et al. This article is distributed under the terms of an Attribution–Noncommercial–Share Alike–No Mirror Sites license for the first six months after the publication date (see http://www.rupress.org/terms/). After six months it is available under a Creative Commons License (Attribution–Noncommercial–Share Alike 4.0 International license, as described at https://creativecommons.org/licenses/by-nc-sa/4.0/).

(Folker et al., 2012, 2014; Schulman et al., 2014). Taken together, these findings demonstrate the centrality of MTs and associated proteins to myonuclear positioning. Interestingly, *ens* is the only mutant isolated to date where myonuclear movement appears to be completely blocked. While maternal products may partially ameliorate the phenotypes of *Khc*, *Dhc*, and *syd* zygotic mutants, the uniqueness of the *ens* phenotype raises the possibility that Ens plays additional roles in myonuclear movement beyond its regulation of MT-based transport. Indeed, in other cell types, Ens has been shown to be a MT polymerizing factor (Gallaud et al., 2014). How Ens promotes nuclear movement in muscle, and what other proteins regulate its critical activity, are outstanding questions in the field.

MT networks, which are essential for myonuclear positioning, undergo dramatic changes during muscle development. In mammalian cell culture, following myoblast fusion, centrosomes are lost and centrosomal proteins relocalize to alternative MT organizing centers (MTOCs) in the acentrosomal myotube, most prominently the myonuclear envelopes (Tassin et al., 1985). In *Drosophila*, MTs similarly reorganize during muscle development; starting in the embryonic myotube, most MTs run parallel to the cell's long axis, but by the third-instar stage of larval development, immunofluorescent staining for Tubulin clearly reveals that MT arrays also extend from myonuclear envelopes (Elhanany-Tamir et al., 2012; Metzger et al., 2012; Manhart et al., 2018). Only two genes, *pavarotti* and *RacGAP50C*, have been implicated in the regulation of muscle MT reorganization in the embryo (Guerin and Kramer, 2009). Much more needs to be learned about how this transition occurs.

Proteins that regulate MT networks in other cell types are strong candidates for being factors in muscle MT organization and MT-dependent myonuclear positioning. One such factor is the MT minus end–binding protein Ninein, encoded by the gene *NIN*. Pioneering cell culture experiments showed that Ninein localizes to centrosomes (Bouckson-Castaing et al., 1996) and noncentrosomal MTOCs (Mogensen et al., 2000) and that Ninein anchors MTs to MTOCs and promotes MT nucleation by docking γ-Tubulin (Abal et al., 2002; Casenghi et al., 2005; Delgehyr et al., 2005; Shinohara et al., 2013). More recently, cell culture studies and RNAi-based in vivo approaches have affirmed critical roles for Ninein in regulating MT organization in numerous cell types. Surprisingly, recently generated null *NIN* mutants in invertebrates are relatively normal: *Caenorhabditis elegans* mutants for the *NIN* orthologue *noca*-1 are sterile with defects in the noncentrosomal MT arrays of the germline and epidermis but have grossly normal morphology and develop to adulthood (Wang et al., 2015). Mutants for the *Drosophila NIN* orthologue *Bsg25D* are viable and fertile (Kowanda et al., 2016; Zheng et al., 2016). Loss of Ninein/NOCA-1 in *C. elegans* is partially compensated for by the MT minus end protein Patronin (Wang et al., 2015); no redundant factors have been identified in *Drosophila*. Since *Bsg25D/Ninein* is conserved from invertebrates to humans, *Bsg25D* may have important functions not readily detectable by single mutant analysis. How does Bsg25D function, and what proteins does it interact with in muscle?

In this work, we find that Bsg25D acts with Ens to regulate myonuclear positioning. Muscle-specific *Bsg25D* overexpression caused myonuclear positioning defects in embryonic myotubes, and overexpression of *Bsg25D* and *ens* reciprocally affected the speed and direction of myonuclear movement. In mature myofibers, overexpressed *Bsg25D* caused nuclear positioning phenotypes, MT defects, and reduced muscle stiffness and function. We conclude that Bsg25D, under wild-type conditions, binds to Ens and promotes its activity in myonuclear positioning, whereas when Bsg25D is expressed at high levels, it alters Ens localization and function, phenocopying *ens* mutants, and ultimately disrupts muscle MT networks and muscle function. Our results shed further light on the function of Ens in the process of nuclear movement and find a novel in vivo role for Bsg25D/Ninein, a poorly understood centrosomal protein, in myonuclear positioning.

Results

Bsg25D and Ens interact in vitro and colocalize in embryonic myotubes

We have previously shown that myonuclei in *ens* mutant embryos fail to separate into two clusters and migrate toward muscle poles (Metzger et al., 2012). To better understand the mechanisms underlying myonuclear positioning, we performed a yeast two-hybrid screen to identify proteins that interact with Ens. In addition to clones of *Khc*, which we have previously shown to genetically and physically interact with Ens (Metzger et al., 2012), we recovered numerous clones corresponding to *Bsg25D*, the *Drosophila* homologue of vertebrate *Ninein* (Kowanda et al., 2016; Zheng et al., 2016). The sequence common to all recovered *Bsg25D* clones (nucleotides 1463–1,577/amino acids 487–526, using isoform Bsg25D-PB as a reference) falls entirely within the gene's fourth exon, which is present in all *Bsg25D* alternatively spliced transcripts; thus, the Ens-binding region is present in all Bsg25D isoforms (Fig. 1 A). This region is found in the first of two spans of Bsg25D that contain numerous coiled coil domains. The Ens-binding region is nonoverlapping with the region of Bsg25D thought to be necessary for γ-Tubulin binding, based on alignment between Bsg25D and mouse Ninein, where the latter region was experimentally defined (Delgehyr et al., 2005). The Ens-binding region also does not overlap with the N-terminal Bsg25D region (amino acids 1–353) that has been shown to bind MTs in vitro (Kowanda et al., 2016). The Ens–Bsg25D interaction was validated in S2 cells, where overexpressed Ens and full-length Bsg25D coimmunoprecipitated (Fig. 1 A).

Next, we examined *Bsg25D* expression in vivo. In situ hybridization performed by the Berkeley Drosophila Genome Project showed *Bsg25D* transcripts in embryonic muscle (Tomancak et al., 2002, 2007; Hammonds et al., 2013). By immunofluorescent antibody staining using an existing antibody against Bsg25D (Iampietro et al., 2014), we found that Bsg25D protein was present in discrete puncta in numerous cell types in the embryo. (The Bsg25D signal was absent from *Bsg25D* null mutants [Fig. S1 A].) This punctate expression pattern was expected, as Bsg25D is known to localize to centrosomes in mononucleated cells (Kowanda et al., 2016; Zheng et al., 2016). Notably, it was most strongly expressed in primordial germ cells, as has been previously observed (Zheng et al., 2016; Fig. 1 B, red outlined box).

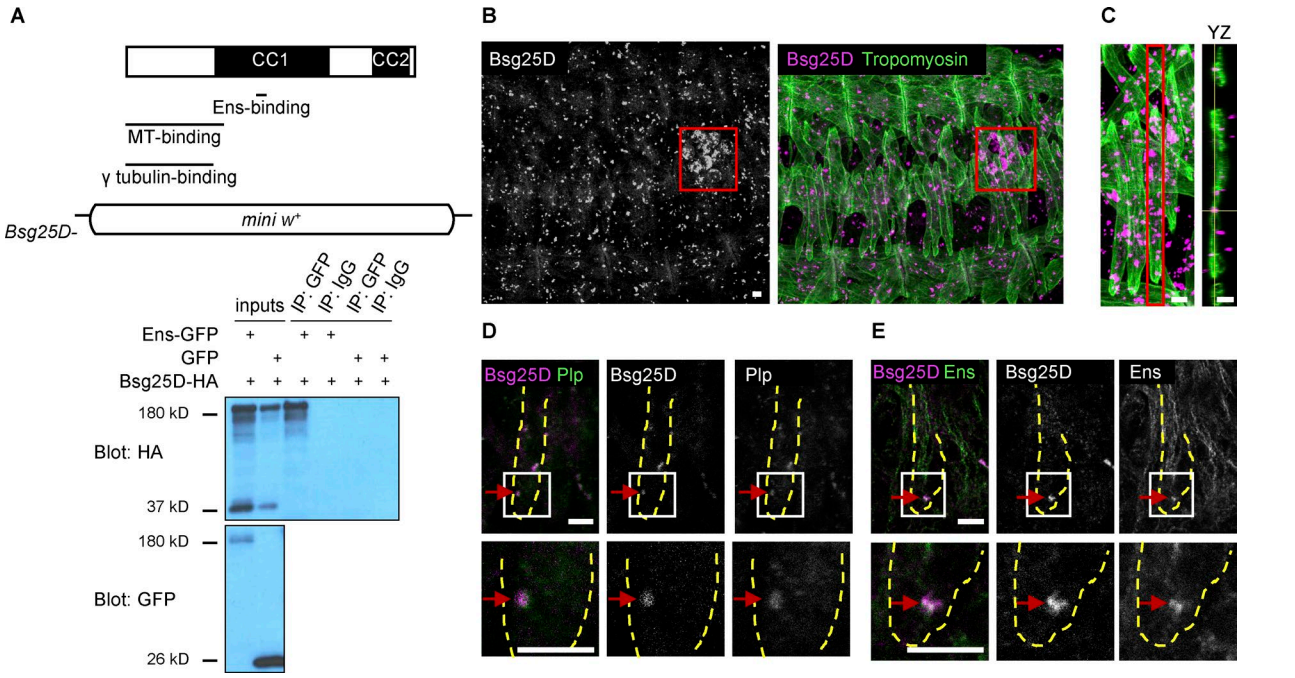


Figure 1. **Bsg25D and Ens physically interact and colocalize in myotubes in vivo. (A)** Top: Map of Bsg25D indicating coiled–coil (CC) domain–rich regions and regions that bind Ens (this work), MTs (Kowanda et al., 2016), and γ-Tubulin (predicted from alignment to mouse Ninein; Delgehyr et al., 2005). In *Bsg25D−*, the entire coding region has been removed and replaced by a mini-white (mini w+) reporter cassette. Bottom: Coimmunoprecipitation of overexpressed Ens-GFP and Bsg25D-HA from S2 cells. The largest Bsg25D-HA band is the main protein species, and smaller bands likely represent cleavage products. IP, immunoprecipitation. **(B)** Bsg25D expression in the stage 16 embryo. Left and right panels are the same image with and without Tropomyosin, a muscle marker. Left: Bsg25D, gray. Right: Bsg25D, magenta; Tropomyosin, green. Red box indicates primordial germ cells. **(C)** Left: Extended focus projection of one stage 16 hemisegment. Right: Orthogonal (YZ) section of indicated (red box) lateral transverse myotube. Crosshairs identify a Bsg25D+ punctum inside myotube. Bsg25D, magenta; Tropomyosin, green. **(D)** Immunofluorescent staining of stage 16 myotube for Bsg25D and Plp. Image is a single slice from a Z-stack. Bsg25D, magenta; Plp, green; colocalization, white (see red arrows). **(E)** Immunofluorescent staining of stage 16 myotube for Bsg25D and Ens. Image is a single slice from a Z-stack. In the merged image, Bsg25D, magenta; Ens, green; colocalization, white (highlighted by arrows). In D and E, images in bottom row are higher magnification views of boxed regions, and dashed lines outline lateral transverse muscles. In all images, scale bars = 5 µm.

Combined immunofluorescent labeling of Bsg25D and the muscle marker Tropomyosin showed that from stage 14 to stage 16, the stages during which myonuclei split into two clusters and migrate toward muscle poles, Bsg25D was broadly but weakly expressed in the cytoplasm and strongly enriched in cytoplasmic puncta of myotubes (Fig. 1 B). Analysis of orthogonal slices of Z-stacks confirmed the presence of Bsg25D puncta inside myotubes (Fig. 1 C). At stage 16, there were between zero and eight Bsg25D puncta per myotube (mode = 1, mean = 2.1). Puncta were excluded from the nucleus but otherwise had no conspicuous localization. Single puncta were also visible in some unfused myoblasts. We used genetic reporters and antibody staining to determine whether the Bsg25D puncta in myotubes reside in various organelles and subcellular structures. We did not observe Bsg25D colocalization with markers of Golgi apparatus, ER, or endosomes, though we did observe that 95% of Bsg25D puncta were in proximity to Arl8 ($n = 60$ myotube puncta), a protein that localizes to lysosomes (Bagshaw et al., 2006; Hofmann and Munro, 2006; Fig. S1 B). Counter to our expectations (Bouckson-Castaing et al., 1996; Mogensen et al., 2000; Kowanda et al., 2016; Zheng et al., 2016), we also failed to detect colocalization between Bsg25D puncta and the MTOC component γ-Tubulin or the MT component α-Tubulin (Fig. S1 B). Interestingly, however, all myotube Bsg25D puncta ($n = 59$) colocalized with the MTOC component Pericentrin-like protein (Plp), the sole *Drosophila* Pericentrin orthologue (Figs 1 D and S1 C). This finding is consistent with physical interactions observed between their mammalian orthologues in cell culture (Chen et al., 2014).

Since we found that Bsg25D and Ens physically interact in vitro, we performed immunofluorescent antibody staining to determine whether they colocalize in embryonic myotubes. While the bulk of Ens protein localized to MTs, as expected for a MAP (Fig. S1 D), there was also Ens protein present in Bsg25D puncta; thus, Ens and Bsg25D colocalize in cytoplasmic puncta in embryonic myotubes (Fig. 1 E). Outside of these puncta, the broad, diffuse cytoplasmic Bsg25D signal was difficult to resolve, so it is possible that Bsg25D and Ens are both present in other parts of the cell as well. Since Bsg25D and Ens bind in vitro and colocalize in myotubes, we hypothesized that *Bsg25D* functions with *ens* during myonuclear positioning.

Loss of Bsg25D enhances *ens* myonuclear positioning defects

To determine whether Bsg25D functions in myonuclear positioning, we generated a null *Bsg25D* mutant. We used an accelerated homologous recombination approach (Baena-Lopez et al., 2013) to remove the entire *Bsg25D* locus, including all predicted alternatively spliced transcripts (Fig. 1 A and Materials and methods). Western blotting showed Bsg25D protein was absent from larval lysates (Fig. 2 A and Materials and methods).

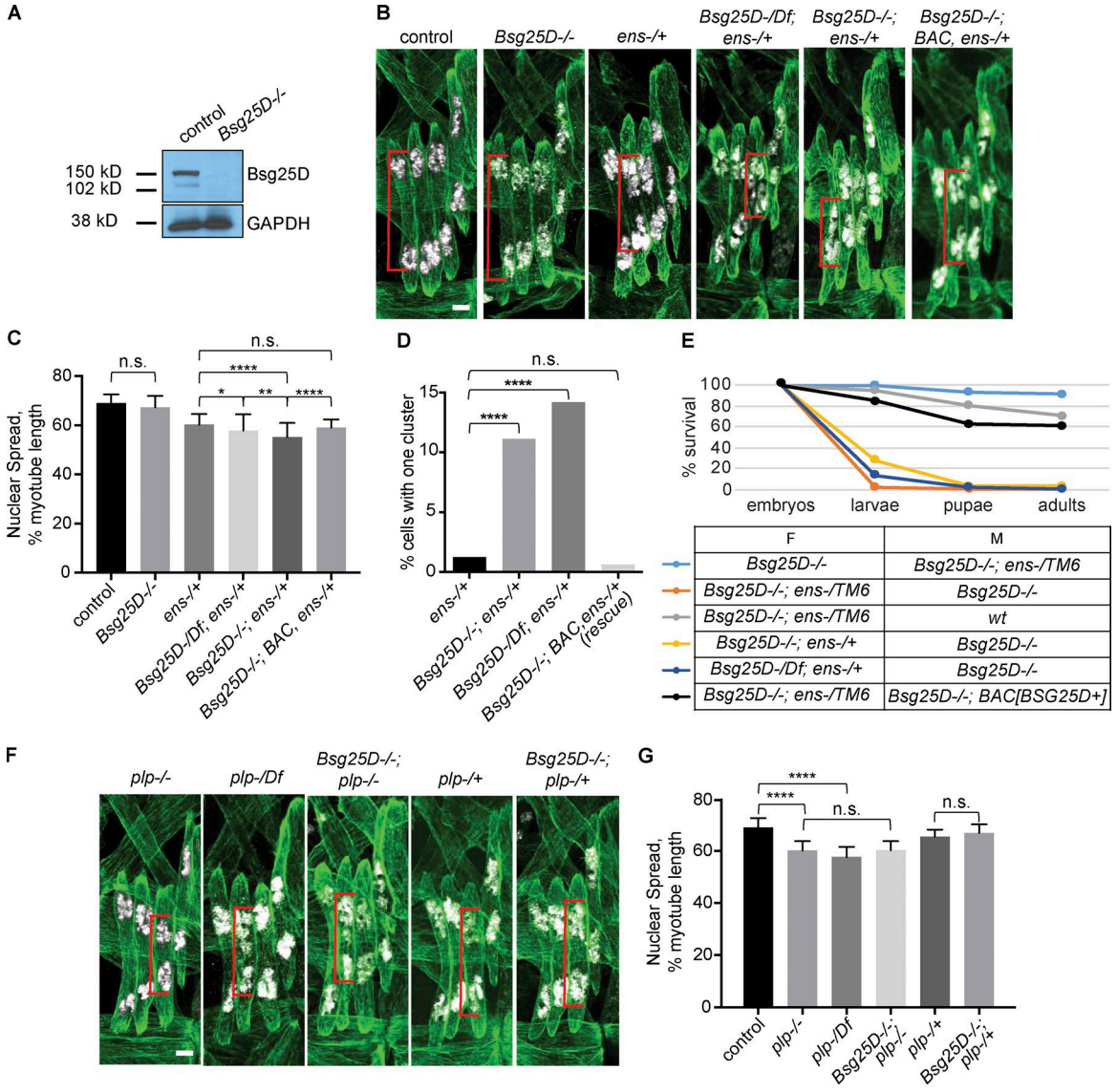


Figure 2. ***Bsg25D*genetically interacts with *ens*, but not *plp*. (A)** Western blot showing loss of Bsg25D protein in *Bsg25D*$^{-/-}$ larval lysates. **(B)** Extended-focus projections of representative stage 16 hemisegments from indicated genotypes. **(C)** Bar graph showing mean nuclear spread and SD. For each genotype, *n* (number of hemisegments) is control, *n* = 39; *Bsg25D*$^{-/-}$, *n* = 61; *ens*$^{-/+}$, *n* = 46; *Bsg25D-/Df;ens*$^{-/+}$, *n* = 43; *Bsg25D;ens*$^{-/+}$, *n* = 71; *Bsg25D*$^{-/-}$*;BAC, ens*$^{-/+}$, *n* = 44. P values were calculated by Student's *t* test. **(D)** Graph showing the percentage of myotubes that have a single nuclear cluster. P values were calculated by Fisher's exact test from contingency tables comparing *ens-/+* to each other genotype. *n* values (number of myotubes for each genotype) are *ens*$^{-/+}$, 239; *Bsg25D*$^{-/-}$*;ens*$^{-/+}$, 296; *Bsg25D-/Df;ens*$^{-/+}$, 176; *Bsg25D*$^{-/-}$*;BAC, ens*$^{-/+}$ (rescue), 160. **(E)** Viability graph showing survival during development for individuals derived from indicated crosses. The following number of individuals were included for each genotype: *Bsg25D*$^{-/-}$×*Bsg25D*$^{-/-}$*;ens*$^{-}$*/TM6*, 140; *Bsg25D*$^{-/-}$*;ens-/TM6*×*Bsg25D*$^{-/-}$, 153; *Bsg25D*$^{-/-}$*;ens-/TM6*×*wt*, 140; *Bsg25D*$^{-/-}$*;ens*$^{-/+}$×*Bsg25D*$^{-/-}$, 113; *Bsg25D-/Df;ens*$^{-/+}$×*Bsg25D*$^{-/-}$, 148; *Bsg25D*$^{-/-}$*;ens-/TM6*×*Bsg25D*$^{-/-}$*;BAC[Bsg25D+]*, 144. F, female; M, male. **(F)** Extended-focus projections of representative stage 16 hemisegments from indicated genotypes. **(G)** Bar graph showing mean nuclear spread and SD. For each genotype, number of hemisegments is *plp*$^{-/-}$, *n* = 47; *plp-/Df*, *n* = 24; *Bsg25D*$^{-/-}$*; plp*$^{-/-}$, *n* = 39; *plp-/+*, *n* = 34; *Bsg25D*$^{-/-}$*;plp-/+*, *n* = 29. P values were calculated by Student's *t* test. The control data in G are the same as in C; for representative image, see first panel in B. *, P < 0.05; **, P < 0.01; ****, P < 0.0001. In all confocal images, red brackets indicate sample nuclear spread measurements. Tropomyosin, green; nuclei, white. Scale bars = 5 µm.

In agreement with recent reports (Kowanda et al., 2016; Zheng et al., 2016), we found that *Bsg25D* homozygous null mutants (*Bsg25D*$^{-/-}$) lacking maternal and zygotic *Bsg25D* were viable and fertile, with a modest decrease in the frequency of survival to adulthood relative to wild-type controls (70% vs. 96%; Fig. S2 A). A standard larval motility assay revealed moderately impaired muscle function (Fig. S2 B). Using a transgenic reporter that labels myonuclei in a specific set of muscles (i.e., the lateral transverse muscles; Richardson et al., 2007), we found that myonuclear positioning in stage 16 *Bsg25D*$^{-/-}$ myotubes was normal (Fig. 2 B). Thus, *Bsg25D* is not essential for viability, fertility, or myonuclear positioning.

We next considered the possibility that *Bsg25D* plays a role in myonuclear positioning but that the pathway it affects is robust enough to withstand the loss of *Bsg25D* if the other components are present at wild-type levels. To investigate this possibility, we generated double mutants in which *Bsg25D* and candidate interactor genes were targeted. We found that *ens*$^{-/+}$ embryos

lacking all maternal and zygotic Bsg25D had significantly more impaired myonuclear positioning than *ens*$^{-/+}$ embryos containing the normal complement of Bsg25D (Fig. 2, B–D): at stage 16, *Bsg25D*$^{-/-}$;*ens*$^{-/+}$ myonuclear clusters traversed less of the distance toward the muscle poles. Further, in some myotubes, myonuclei are present as one cluster, resembling those found in *ens*$^{-/-}$ homozygotes (Metzger et al., 2012). Enhancement of myonuclear positioning defects was also observed when one copy of the null *Bsg25D* allele was replaced by a deficiency removing the gene (Fig. 2, B–D), which argues that the enhancement effect was specific to the *Bsg25D* region. Moreover, we rescued the *Bsg25D*$^{-/-}$;*ens*$^{-/+}$ enhanced phenotype by reintroducing *Bsg25D*$^{+}$ from the large genomic Bacterial Artificial Chromosome (BAC) insertion CH321-49G22 (Fig. 2, B–D). In addition, *Bsg25D*$^{-/-}$;*ens*$^{-/-}$ double mutants showed the *ens*$^{-/-}$ phenotype, which is the most severe clustering phenotype (Fig. S3 A). We conclude that endogenous *Bsg25D* and *ens* likely affect a common pathway that moves myonuclei in embryonic myotubes.

Bsg25D and *ens* genetically interact in nonmuscle cells as well, as embryonic lethality occurred when Bsg25D and Ens were jointly removed in a specific genetic combination. Nearly 100% of embryos derived from *Bsg25D*$^{-/-}$;*ens*$^{-}$/*TM6* mothers and *Bsg25D*$^{-/-}$ fathers failed to hatch (Fig. 2 E). However, embryos derived from the reciprocal cross survived well (Fig. 2 E). *Bsg25D*$^{-/-}$;*ens*$^{-}$/*TM6* females crossed with wild-type males laid eggs that hatched, demonstrating that those females are fertile. We also observed widespread death when the third chromosome balancer *TM6* was replaced by a wild-type chromosome, indicating that the genetic interaction was not due to mutations on the balancer chromosome. The phenotype also persisted when one of the *Bsg25D* alleles was replaced with a deficiency completely uncovering *Bsg25D*. Furthermore, restoring *Bsg25D*$^{+}$ through a BAC transgene achieved nearly complete rescue (Fig. 2 E, compare black and salmon-colored lines in graph). We conclude that *Bsg25D* and *ens* are jointly required to support normal embryonic development. Since genotypes with even the strongest myonuclear positioning defects survive embryonic development (Metzger et al., 2012), the observed lethality must be due to issues in nonmuscle cells.

To gain further insights to the role of *Bsg25D*, we tested for genetic interactions between *Bsg25D* and other genes involved in myonuclear positioning or MT biology. We did not detect interactions between *Bsg25D* and the genes encoding *Khc* and *Dhc* (which are essential for myonuclear positioning) or *patronin* and the γ-Tubulin homologue *γTub23C* (which interact with *Ninein/noca-1* in *C. elegans* [Wang et al., 2015]; Fig. S3, B and C; and data not shown). We also tested *pericentrin-like protein* (*plp*) mutants. Interestingly, *plp*$^{-/-}$ mutants had myonuclear positioning defects; nuclear clusters usually split correctly but failed to move the normal distance toward the muscle poles by stage 16 (Fig. 2, F and G). The same phenotype was observed when one allele of *plp* was replaced by a deficiency uncovering the gene (Fig. 2, F and G). However, loss of *Bsg25D* did not further enhance myonuclear positioning defects in either *plp* homozygotes or heterozygotes (Fig. 2, F and G); thus, although we observed colocalization between the two proteins in myotubes, we did not uncover a role for Bsg25D–Plp interactions in myonuclear positioning. Taken together, these results reveal dosage-sensitive genetic interactions only between *Bsg25D* and *ens*; these are not observed with other genes involved in MT biology or myonuclear positioning.

Muscle-specific overexpression of Bsg25D causes defects in embryonic myonuclear positioning by sequestering Ens

Having demonstrated that *Bsg25D* functions in myonuclear positioning, we next performed gain-of-function analysis with the Gal4/upstream activating sequence (UAS) system (Brand and Perrimon, 1993) using the muscle-specific *Dmef2* promoter to probe the activity of *Bsg25D* in muscle. Strikingly, in stage 16 myotubes overexpressing Bsg25D, myonuclei were present in a single cluster near the myotube center; in contrast, control myotubes at this stage had two nuclear clusters near opposite muscle poles (Fig. 3 A). This suggests that overexpressed Bsg25D blocked myonuclear cluster separation (stage 14) and movement toward the muscle poles (stages 15 and 16).

That *Bsg25D* overexpression phenocopied loss of *ens* (Fig. 3 A; Metzger et al., 2012) led us to hypothesize that overexpressed Bsg25D inhibits or sequesters endogenous Ens in myotubes. In support of this hypothesis, we found that Ens overexpression, but not overexpression of a control protein (GFP), could rescue Bsg25D-induced nuclear positioning defects. In fact, embryos overexpressing Bsg25D and Ens had even greater nuclear spread than control embryos (Fig. 3, A and B). This finding led us to examine the effects of overexpressing Ens in otherwise wild-type embryos. We found that overexpressed Ens caused novel myonuclear positioning defects; nuclear spread was increased and nuclei were often present as individuals rather than as part of clusters (Fig. 3, A and B). In sum, Ens overexpression and Bsg25D overexpression confer reciprocal phenotypes, and Ens overexpression is epistatic to Bsg25D overexpression.

As further support of our hypothesis that overexpressed Bsg25D inhibits or sequesters endogenous Ens, we detected genetic interactions between overexpressed *Bsg25D* and endogenous *ens*. Both loss of one allele of *ens* and overexpression of *Bsg25D* with *rP298-Gal4*, a muscle-specific driver that produces a lower level of gene expression than *Dmef2-Gal4*, conferred reduced poleward movement of nuclear clusters (Fig. 3, A and B). However, in *ens*$^{-/+}$ embryos expressing *rP298>Bsg25D*, a much stronger nuclear positioning phenotype occurred (Fig. 3, A and B). This implies that Bsg25D affects the same pathway as loss of *ens*.

Finally, in support of our hypothesis, we found that overexpressed Bsg25D alters Ens localization. Like endogenous Bsg25D, overexpressed Bsg25D was present both broadly in the cytoplasm and in bright cytoplasmic puncta (Fig. 3 C). Ens normally localizes to MTs (Fig. S1 D), but in Bsg25D-overexpressing myotubes, Ens was strongly enriched at sites of Bsg25D accumulation in the cytoplasm (Fig. 3 C). Outside of Bsg25D^{+} puncta, Ens signal was lower in myotubes overexpressing Bsg25D than in controls overexpressing GFP (Fig. 3, D and E). This argues that overexpression of Bsg25D reduces the amount of Ens on myotubes. Based on our genetic and imaging analyses, we conclude that overexpressed Bsg25D exerts its effect on myonuclear positioning by regulating Ens activity, at least in part by mislocalizing Ens.

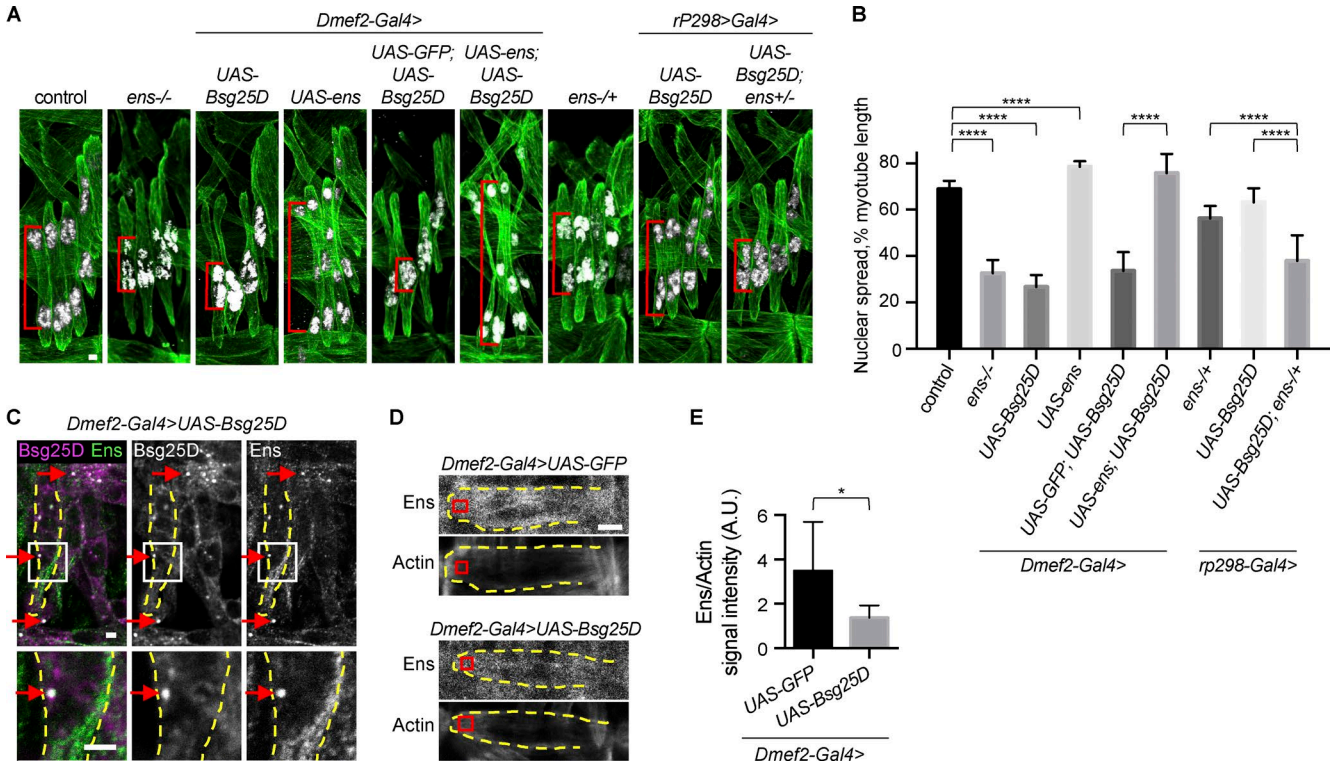


Figure 3. **Overexpressed *Bsg25D* causes nuclear positioning defects in embryonic myotubes by sequestering endogenous Ens. (A)** Extended-focus projections of representative stage 16 hemisegments from indicated genotypes. Green, Tropomyosin; white, nuclei. Red brackets indicate sample nuclear spread measurements. **(B)** Bar graph showing mean nuclear spread and SD. For each genotype, the number of hemisegments is as follows: control, *n* = 22; *Dmef2-Gal4>UAS-Bsg25D*, *n* = 34; *Dmef2-Gal4>UAS-ens*, *n* = 47; *Dmef2-Gal4>UAS-GFP:UAS-Bsg25D*, *n* = 25; *Dmef2-Gal4>UAS-ens;UAS-Bsg25D*, *n* = 42; $ens^{-/+}$, *n* = 37; *rP298-Gal4>UAS-Bsg25D*, *n* = 33; *rP298-Gal4>UAS-Bsg25D;*$ens^{-/+}$, *n* = 37. Control data and the representative image are the same as in Fig. 2. ****, P < 0.0001. **(C)** Immunofluorescent antibody staining for Bsg25D and Ens in an embryo overexpressing Bsg25D. Arrows show examples of colocalization. Dashed yellow lines outline a lateral transverse myotube. In the merged image: magenta, Bsg25D; green, Ens; white, colocalization. Images in the bottom row are higher magnification views of boxed regions. **(D)** Representative images of stage 16 VL1 myotubes from indicated genotypes. Each image is a single slice from a confocal stack. Red boxes show where the signal intensity was quantified. **(E)** Graph showing Ens intensity, normalized to actin intensity. Number of myotubes is six for both genotypes, mean ± SD. *, P < 0.05. Scale bars = 2 µm (A and C) and 5 µm (D).

Bsg25D and Ens levels regulate the dynamics of myonuclear positioning

We hypothesized that modulating Bsg25D and Ens levels affects nuclear positioning at stage 16 by disrupting the normal dynamics of myonuclear movement during stage 15, when nuclear clusters normally move toward muscle poles. To address this hypothesis, we performed time-lapse microscopy during stage 15, as done previously (Folker et al., 2012; Videos 1, 2, 3, 4, and 5). We measured the distance from the dorsal-most nucleus to the ventral-most nucleus (nuclear spread) at the beginning and end of the time-lapse series. We divided the difference between the final and initial nuclear spreads for each cell by the time elapsed and defined this quotient as Δ nuclear spread (Fig. 4 A).

We observed that only 59% of control myotubes exhibited positive Δ nuclear spread over a 1-h period during stage 15. This was initially surprising, because we have previously seen that from stages 14 to 16, nuclear clusters move toward myotube poles (Folker et al., 2012; Metzger et al., 2012). Our interpretation is that nuclear clusters move toward the muscle poles unevenly, with periods where the nuclear spread increases and periods where it decreases. Nuclear clusters all eventually arrive near the muscle poles because the net positive (poleward) movement is greater than negative (toward the center of the muscle) movement; however, during relatively short time-lapse recordings, the nuclear spread in individual cells can decrease quite dramatically.

The percentage of myotubes exhibiting positive versus negative Δ nuclear spread varied with genotype (Fig. 4 B). Embryos with muscle-specific Ens overexpression contained the highest percentage of myotubes with positive Δ nuclear spread (81%) and embryos with muscle-specific Bsg25D overexpression the lowest (21%). In Bsg25D-overexpressing embryos at stage 15, myonuclei were either present in a single cluster or two slightly separated clusters. Negative Δ nuclear spread was due to loosely packed single clusters compacting or barely separated clusters coming back together (for example, Fig. 4 A). Bsg25D-overexpressing cells exhibiting positive Δ nuclear spread had single nuclear clusters that appeared to separate slightly without dividing into two distinct clusters.

We detected a novel behavior in myonuclei from $Bsg25D^{-/-}$;$ens^{-/+}$ embryos. In some cells, two distinct nuclear clusters migrated a considerable distance toward each other and reformed one cluster. In this genotype, there was high variability in dynamic cluster behavior among myotubes; the SD of Δ

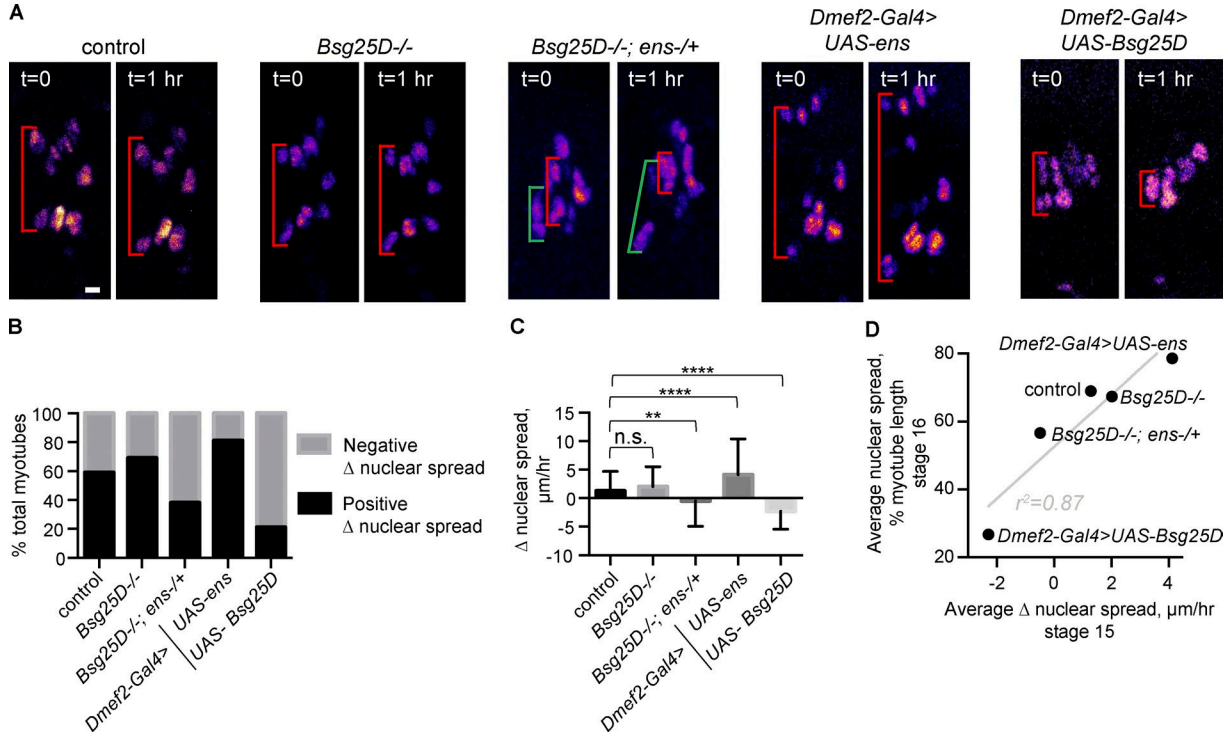


Figure 4. **Dynamics of myonuclear cluster separation are affected by levels of Bsg25D and Ens. (A)** First and last frames from time-lapse series of myonuclear movement during stage 15 in indicated genotypes. Red brackets show change in nuclear spread over time. In *Bsg25D*$^{-/-}$;*ens*$^{-/+}$ images, green and red brackets show adjacent myotubes undergoing opposite Δ nuclear spreads. All images are extended focus projections of Z-stacks. Nuclei are multicolored. Scale bar = 5 µm. **(B)** Graph showing percentages of myotubes undergoing positive versus negative Δ nuclear spread during stage 15. **(C)** Mean and SD of Δ nuclear spread during stage 15. For each genotype in B and C, the number of myotubes is as follows: control, *n* = 112; *Bsg25D*$^{-/-}$, *n* = 72; *Bsg25D*$^{-/-}$;*ens*$^{-/+}$, *n* = 86; *Dmef2-Gal4>UAS-ens*, *n* = 85; *Dmef2-Gal4>UAS-Bsg25D*, *n* = 62. P values were calculated by Student's *t* test. **, P < 0.01; ****, P < 0.0001. **(D)** Correlation between stage 15 mean Δ nuclear spread and stage 16 mean nuclear spread in fixed samples. Linear regression line is in gray; r^2 is the coefficient of determination.

nuclear spread was greater in *Bsg25D*$^{-/-}$;*ens*$^{-/+}$ cells than in controls (4.47 µm/h vs. 3.42 µm/h, P = 0.008; Fig. 4 A).

For each genotype, we averaged Δ nuclear spread for each cell, including both negative and positive values (Fig. 4 C). We found no statistically significant difference between control and *Bsg25D*$^{-/-}$ mutants. Control, *Bsg25D*$^{-/-}$, and Ens-overexpressing cells had a positive average Δ nuclear spread. *Bsg25D*$^{-/-}$;*ens*$^{-/+}$ and Bsg25D-overexpressing cells had a negative average Δ nuclear spread. Across genotypes, there was a strong correlation (r = 0.94) between average Δ nuclear spread at stage 15 and average nuclear spread in fixed embryos at stage 16 (Fig. 4 D). Thus, the rate of nuclear spreading at stage 15 predicts and likely determines the degree of nuclear spread observed at stage 16.

Bsg25D overexpression causes defects in myonuclear positioning in fully differentiated larval muscle that are rescued by addition of Ens

Having characterized the effect of Bsg25D overexpression on embryonic myotubes, we next investigated Bsg25D overexpression in mature myofibers. Myofibers are established in the embryo at stage 17 and continue to grow and function during larval stages. We focused on the third-instar larval stage, a time point when the muscles are amenable to functional analysis and antibody staining (Folker et al., 2012). Using the *Dmef2-Gal4* driver, which becomes active in embryonic muscle and persists through the larval stage, we overexpressed either Bsg25D or GFP (as a control) and measured larval motility as a readout of muscle function. Control larvae outperformed Bsg25D-overexpressing larvae (Fig. 5 A), indicating that Bsg25D overexpression perturbs muscle function. Animals with muscle-specific overexpression of Bsg25D exhibited decreased survival to adulthood, with peak lethality occurring during the pupal stage (Fig. 5 B). Moreover, adult survivors were unable to fly, indicating that overexpressed Bsg25D also perturbs muscle function in adults (data not shown).

After assessing muscle function in Bsg25D-overexpressing larvae, we examined muscle structure. In control larvae with muscle-specific GFP expression, myonuclei were evenly spaced throughout muscle fibers, as expected (Fig. 5 C). In larvae that had developed with sustained muscle-specific Bsg25D overexpression, however, myonuclei were frequently clustered together (Fig. 5 C). This phenotype was highly penetrant and robustly quantifiable by three different analyses. First, the average distance between each nucleus and its nearest neighbor was decreased. Second, the average longest stretch of myofiber devoid of myonuclei was increased. Third, the average SD of the distances between sequential nuclei (SD of internuclear distance) within a myofiber was increased, indicating irregular, uneven positioning of nuclei (Fig. 5 C). Unlike stage 16 myotubes, where Bsg25D-induced myonuclear positioning defects were nearly uniform (i.e., one cluster of myonuclei near the myotube's center), larval muscle fibers overexpressing Bsg25D exhibited nuclear clusters that varied in both nuclear number and position within the fiber

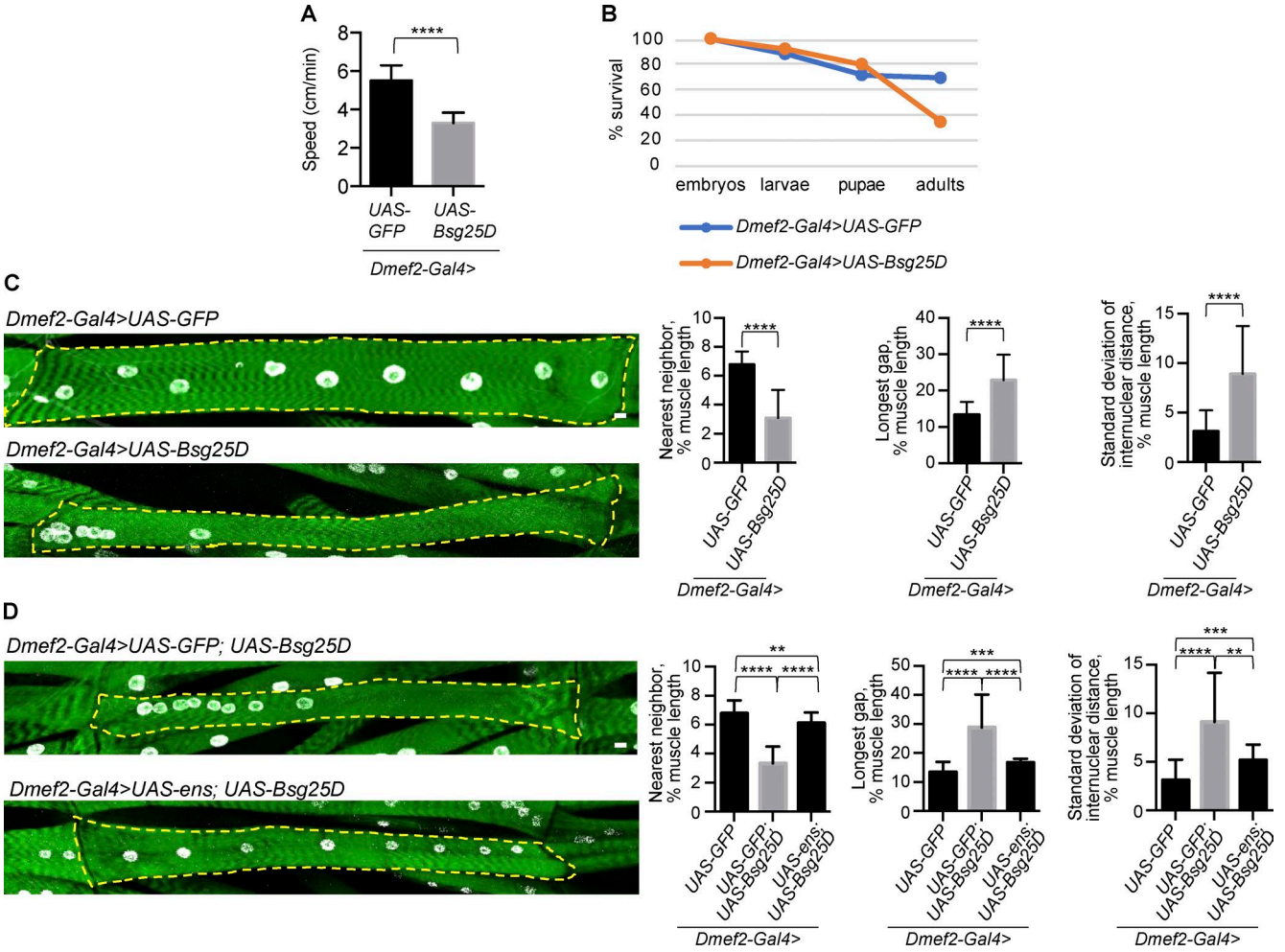


Figure 5. **Bsg25D overexpression induces nuclear positioning defects in larval myofibers that can be rescued by Ens. (A)** Larval motility in larvae overexpressing either GFP (control) or Bsg25D in muscle. For *Dmef2-Gal4>UAS-GFP*, *n* = 30 larvae. For *Dmef2-Gal4>UAS-Bsg25D*, *n* = 12 larvae. P values were calculated by Student's *t* test. **(B)** Viability graph showing survival during development. *n* = 100 individuals for each genotype. **(C and D)** Representative extended focus projections of stained myofibers and nuclear positioning analyses. Green, phalloidin; white, nuclei. Dashed yellow line outlines individual myofibers. Scale bars = 10 µm. Graphs depict mean and SD for three methods for quantifying myonuclear positioning (see Materials and methods). For each genotype, the same images were analyzed with each method. For *Dmef2-Gal4>UAS-GFP*, *n* = 40 myofibers. For *Dmef2-Gal4>UAS-Bsg25D*, *n* = 45. For *Dmef2-Gal4>UAS-GFP;UAS-Bsg25D*, *n* = 23; *Dmef2-Gal4>UAS-ens;UAS-Bsg25D*, *n* = 19. *Dmef2-Gal4>UAS-GFP* data are the same in C and D. P values were calculated by Student's *t* test. **, P < 0.01; ***, P < 0.001; ****, P < 0.0001.

(Figs. 5 C and S4 A). The total number of nuclei present per larval muscle was the same in Bsg25D-overexpressing and control larvae (Fig. S4 B). As with other genotypes affecting myonuclear positioning (Elhanany-Tamir et al., 2012), Bsg25D overexpression conferred a decrease in nuclear size (Fig. S4 C).

Since Ens overexpression restored nuclear spread in Bsg25D-overexpressing embryonic myotubes (Fig. 3, A and B), we hypothesized that "rescued" myotubes would develop into myofibers with normal myonuclear positioning. Indeed, when we overexpressed Ens along with Bsg25D starting in embryonic myotubes, the resulting larval myofibers had nearly normal nuclear positioning; in contrast, control myofibers expressing GFP with Bsg25D had severe nuclear positioning defects (Fig. 5 D). These two genotypes had the same number of myonuclei per myofiber (Fig. S4 D). From these experiments, we conclude that sustained Ens overexpression rescues nuclear positioning defects in Bsg25D-overexpressing mature muscles.

Overexpressed Bsg25D disrupts MT organization in myofibers

Since Bsg25D and Ens have been shown to regulate MT organization in other contexts (Mogensen et al., 2000; Delgehyr et al., 2005; Gallaud et al., 2014; Srivatsa et al., 2015; Kowanda et al., 2016; Zheng et al., 2016), we hypothesized that Bsg25D–Ens interactions control myonuclear positioning by regulating the muscle MT network. However, we did not observe a difference in the density of the MT network in embryonic myotubes among control, *Bsg25D*$^{-/-}$, *Bsg25D*$^{-/-}$*;ens*$^{-/+}$, and *Bsg25D*-overexpressing genotypes (Fig. 6, A and B). Using time-lapse microscopy to follow genetically encoded EB1-YFP, a fluorescently tagged MT plus end–binding protein that tracks the growing ends of MTs, we observed that EB1-YFP "comets" moved with the same speed in control and *Bsg25D*$^{-/-}$ myotubes (control: 0.36 ± 0.12 µm/s, *Bsg25D*$^{-/-}$: 0.37 ± 0.11 µm/s; Videos 6 and 7 and Fig. 6, C and D), indicating that MT polymerization rates were unaffected by complete loss of *Bsg25D*.

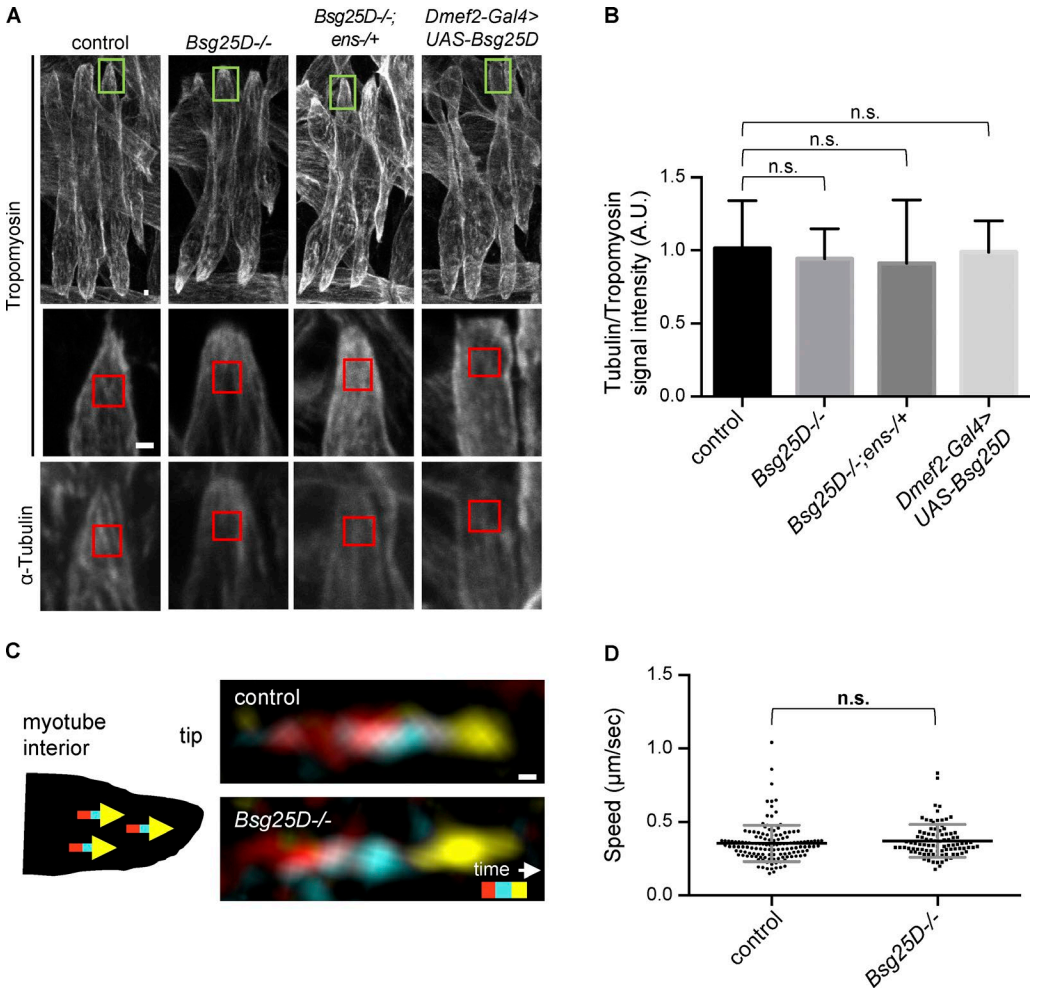


Figure 6. **MT density and dynamics are normal in *Bsg25D*$^{-/-}$ embryonic myotubes. (A)** Representative extended-focus projections of Tropomyosin and α-Tubulin signal in stage 16 lateral transverse myotubes. Green boxes in the top row indicate muscle tips magnified in the second and third rows. Red boxes represent regions where signal intensity was quantified. Scale bar = 1 µm. **(B)** Bar graph showing the mean and SD of the ratio of Tubulin to Tropomyosin signal for indicated genotypes. The number of embryos for each genotype is as follows: control, *n* = 9; *Bsg25D*$^{-/-}$, *n* = 14; *Bsg25D*$^{-/-}$*;ens-/+*, *n* = 11; *Dmef2-Gal4>UAS-Bsg25D*, *n* = 14. P values were calculated by Student's *t* test. The entire experiment was performed twice with similar results; images and graph are from one replicate. **(C)** Representative EB1-YFP comets for indicated genotypes. Schematic shows that comets run toward myotube tips. Images were generated by merging three frames from a time-lapse series, pseudocolored red (t_1 = 0 s), cyan (t_2 = 1.6 s), and yellow (t_3 = 3.2 s). Scale bar = 0.1 µm. **(D)** Scatter plot showing mean speed ± SD (micrometers per second) of EB1-YFP comets. The number of EB1-YFP comets for each genotype is as follows: control, *n* = 140; *Bsg25D*$^{-/-}$, *n* = 94. P value was calculated by Student's *t* test.

Next, we examined the effect of Bsg25D levels on the mature MT organization of larval myofibers. Larval myofibers are advantageous for genetic analysis of MT organization because they are larger, more regularly shaped, and possess a more clearly organized MT network than myotubes. In control muscle fibers, as previously observed (Elhanany-Tamir et al., 2012; Metzger et al., 2012), there were two spatially defined populations of MTs: superficial MTs that emanate from the nuclear envelope of each nucleus, and deeper MTs oriented parallel to the long axis of the fiber. While *Bsg25D* null mutants had normal myonuclear positioning (Fig. S4, E and F) and MT organization (Fig. 7 A), Bsg25D-overexpressing muscle fibers had severe defects in MT organization (Fig. 7 A). Longitudinal MTs were present, but nuclear MT arrays were completely absent. Instead, MTs appeared to grow from Bsg25D-positive ectopic MTOCs in the cytoplasm, as determined by the colocalization of Bsg25D with the centers of star-shaped MT asters (Fig. 7 B). Overexpressed Bsg25D also localized inside myonuclei (Fig. 7 F), as has been seen with overexpressed human Ninein in cell culture. This cell culture localization was linked to posttranslational SUMO modification of Ninein (Cheng et al., 2006), and we observed colocalization of the sole *Drosophila* SUMO protein, SUMO-2, and overexpressed Bsg25D in myonuclei, but not in Bsg25D-positive cytoplasmic puncta (Fig. S5). This is consistent with overexpressed nuclear Bsg25D being sumoylated and raises the possibility that sumoylation is necessary for overexpressed Bsg25D to localize to myonuclei.

Since we have shown that Bsg25D overexpression affects Ens localization in embryonic myotubes (Fig. 3 C), we next determined how it affects Ens localization in mature myofibers. Immunofluorescent staining in control myofibers showed Ens broadly expressed with increased signal around myonuclei,

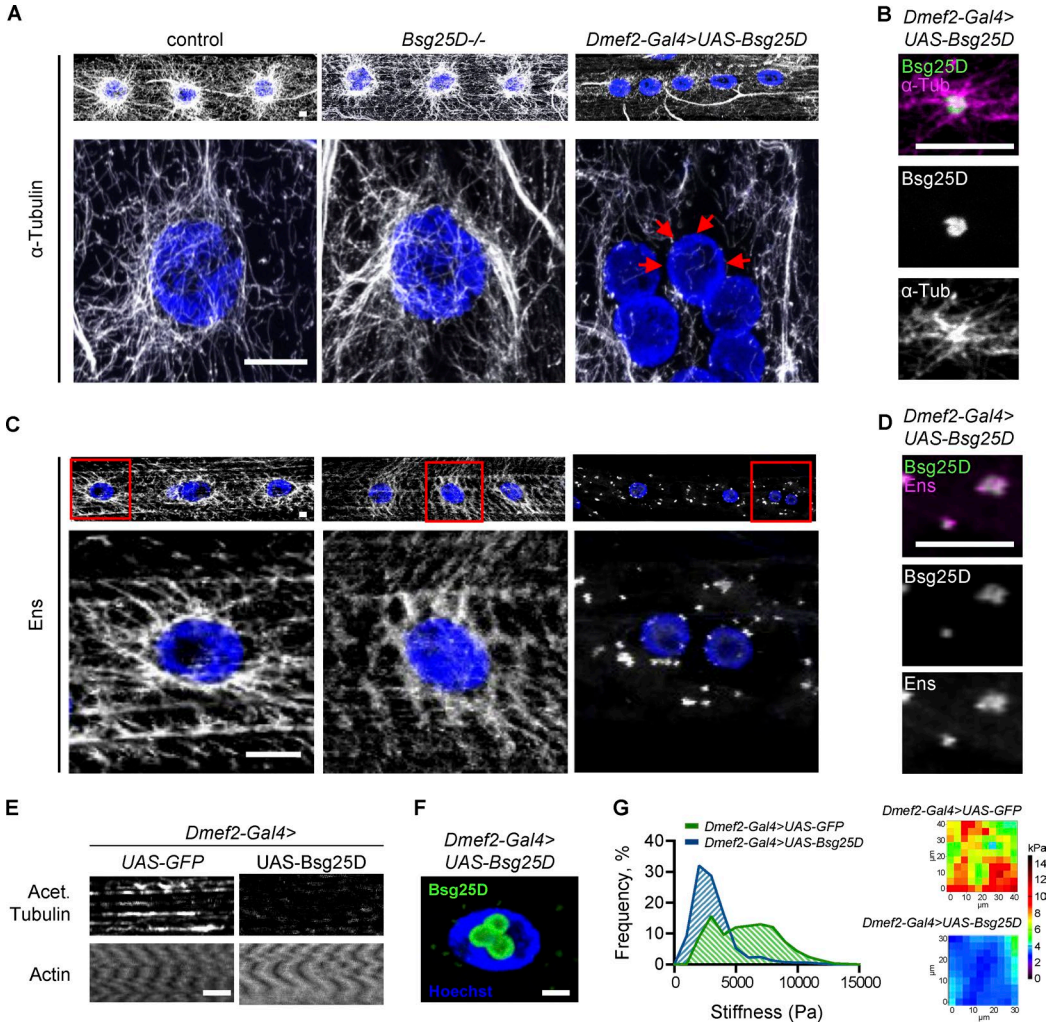


Figure 7. ***Bsg25D* overexpression perturbs normal MT organization and forms Ens-positive MTOCs in larval myofibers. (A)** Top: α-Tubulin signal in extended-focus projections of larval myofibers. Bottom: Higher magnification images of nuclear MT arrays. Gray, α-Tubulin; blue, nuclei. Red arrows show myonuclear envelope without MTs. **(B)** Extended-focus projections of Bsg25D and α-Tubulin signal in a cytoplasmic Bsg25D punctum in *Dmef2-Gal4>UAS-Bsg25D* larval myofiber. Bsg25D, green; α-Tubulin, magenta; colocalization, white. **(C)** Top: Ens signal in extended-focus projections of larval myofibers of indicated genotypes. Bottom: Higher magnification images of nuclei delineated by red boxes. Gray, Ens; blue, nuclei. **(D)** Extended-focus projections of Bsg25D and Ens signal in a cytoplasmic Bsg25D punctum in *Dmef2-Gal4>UAS-Bsg25D* larval myofiber. Bsg25D, green; Ens, magenta; colocalization, white. **(E)** Staining of larval myofibers with phalloidin (labeling Actin) and an antibody against acetylated Tubulin. Images are single slices from Z-stacks, immediately below myonuclei. Staining for actin confirms the presence of intact myofibers. **(F)** Single slice through a *Dmef2-Gal4>UAS-Bsg25D* myofiber nucleus. Blue, Hoechst; green, Bsg25D. In all images, scale bars = 10 µm. In B, D, and F, Bsg25D localization is visualized by Eos, which fluorescently tags the N-terminus of overexpressed Bsg25D. **(G)** Left: Frequency histogram of all stiffness measurements from AFM for indicated genotypes. For *Dmef2-Gal4>UAS-GFP*, $n = 21$ myofibers. For *Dmef2-Gal4>UAS-Bsg25D*, $n = 16$ myofibers. In each genotype, multiple measurements were taken per myofiber; see materials and methods. P value was calculated by Student's *t* test: ****, $P < 0.0001$. Right: Examples of an AFM force map for each genotype.

consistent with Ens (a MAP) being present on MTs (Fig. 7 C). This localization was not affected by loss of *Bsg25D* (Fig. 7 C). However, in myofibers overexpressing *Bsg25D*, Ens was lost from nuclear peripheries and instead colocalized with Bsg25D puncta in the cytoplasm (Fig. 7, C and D). However, Ens did not label the MTs emanating from Bsg25D puncta (Fig. 7, B vs. D). Thus, when Bsg25D is overexpressed, Ens becomes mislocalized from MTs to cytoplasmic Bsg25D puncta.

To further investigate the Bsg25D-induced disruptions to the MT network in larval myofibers, we performed immunofluorescent antibody staining to detect MTs bearing an acetylation modification associated with MT stability. Control muscles exhibited acetylated MTs emanating from the nuclear envelope, as well as in the deeper longitudinal tracts (Fig. 7 E). In Bsg25D-overexpressing myofibers, the antibody against acetylated MTs only weakly labeled longitudinal MTs (Fig. 7 E). This indicates the longitudinal MTs in Bsg25D-overexpressing muscles were hypoacetylated relative to controls. (There was no acetylated tubulin signal around myonuclei, because there were no MTs there.) It was recently shown that MT acetylation in neuronal branches correlates with the subcellular localization of Ens (Tymanskyj et al., 2017), raising the possibility that overexpressed Bsg25D causes MT hypoacetylation by sequestering Ens away from MTs. Taken together, Bsg25D overexpression causes defects in MT organization and posttranslational acetylation; the latter may be indicative of a loss of MT stability.

We next investigated whether Bsg25D overexpression affected the mechanical properties of myofibers by performing atomic force microscopy (AFM) to measure stiffness in control (GFP-overexpressing) and Bsg25D-overexpressing myofibers. We found a significant decrease in the stiffness of Bsg25D-overexpressing myofibers (*Dmef2-Gal4>UAS-GFP* mean ± SD = 5,895 ± 2,646 Pa, *Dmef2-Gal4>UAS-Bsg25D* mean ± SD = 3,167 ± 1,735 Pa, $P < 0.0001$; Fig. 7 G), perhaps due to the changes in MT organization that we documented, although the role of MTs in regulating myofiber stiffness appears to be complex and variable between systems (Collinsworth et al., 2002; Nishimura et al., 2006; Kerr et al., 2015). Alternatively, other cytoskeletal elements such as actin or myosin, which have been shown to be critical for generating stiffness in skeletal muscle (Collinsworth et al., 2002), may have been disorganized or reduced in these muscles. Together, this series of experiments shows that overexpressed Bsg25D causes defects in the intracellular organization and mechanical properties of larval myofibers.

Discussion

Bsg25D functions in myonuclear positioning

The *Bsg25D* null mutants we generated, like those in two recent reports, are viable and fertile (Kowanda et al., 2016; Zheng et al., 2016). Zheng et al. (2016) did not detect any mutant abnormalities, whereas Kowanda et al. (2016) observed a decrease in embryonic hatching and partially penetrant mitotic defects. Our null *Bsg25D* mutant has a lower rate of embryonic death than the mutant generated by Kowanda et al. (2016). The differences between *the* Bsg25D mutant phenotypes generated by different groups likely reflect the sensitivity of *Bsg25D* mutant phenotypes to genetic background. Because our null *Bsg25D* mutant did not have obvious defects, our analysis of *Bsg25D* required other approaches: generation of double mutants and gain-of-function analysis. Through these approaches, we uncovered a role for Bsg25D in myonuclear positioning, where it works with Ens. To our knowledge, Ninein null mice have not been reported; it will be interesting to observe what aspects of Ninein function are conserved in mammals.

Bsg25D and Ens regulate the dynamics of myonuclear movement

Our live imaging of stage 15 embryos yielded unexpected insights about the dynamics of myonuclear movement. We initially thought that nuclear clusters separated at stage 14 and then migrated toward their respective poles in a straightforward fashion. However, in all genotypes tested, we observed both myotubes where the nuclear spread increased during our window of observation and myotubes where nuclear spread decreased. These observations argue for a more complex model of myonuclear positioning in which the forces driving nuclear clusters toward muscle poles (for example, Bsg25D and Ens) are opposed by unknown forces driving clusters toward each other. Thus, the relative levels of these opposing forces during stages 14–16 determine myonuclear spread.

Overexpression of Bsg25D affects multiple aspects of muscle organization and function

Gain-of-function analysis revealed that overexpressed Bsg25D has potent activity in embryonic myotubes and mature myofibers. In myotubes it perturbs myonuclear positioning; in myofibers it perturbs myonuclear positioning, MT organization, muscle stiffness, and muscle function. The severity of these phenotypes suggests it is critical for muscle cells to limit the amount of Bsg25D protein present. In overexpression experiments in the ovary, *Bsg25D* localization and activity is regulated by its 3′ UTR (Kowanda et al., 2016); however, we found that *Bsg25D* overexpression constructs with or without 3′ UTR confer similar phenotypes in myotubes (data not shown), suggesting that the 3′ UTR is not critical to Bsg25D regulation in muscle. Developing muscle presumably employs other mechanisms to limit the levels of Bsg25D.

Unlike in myofibers, Bsg25D overexpression in embryonic myotubes confers no detectable MT defects. Consistent with these observations, overexpressed Bsg25D did not colocalize with α-Tubulin or γ-Tubulin (data not shown). It is unclear how myotubes resist the MT-altering effects of overexpressed Bsg25D that we observed in myofibers and others have observed in other systems (Stillwell et al., 2004; Kowanda et al., 2016; Zheng et al., 2016); perhaps myotubes lack an essential cofactor necessary for Bsg25D to induce ectopic MTOCs. In general, our data support that MTs in developing myotubes have different behaviors from MTs in myofibers and in other tissues.

While overexpressed Bsg25D does not perturb MTs in embryonic myotubes, does endogenous Bsg25D regulate MT organization? We failed to detect differences in MT density and polymerization rate between control and *Bsg25D*$^{-/-}$ myotubes; this is in contrast to the *C. elegans* larval epidermis, where *Bsg25D/Noca-1* mutants were found to have lower-than-normal MT polymerization rates by an EB1-based assay analogous to ours (Wang et al., 2015). There are two caveats to our conclusion that *Bsg25D* does not function in MT regulation in *Drosophila* myotubes. First, we could not draw conclusions about the number of polymerizing MTs in each genotype because the EB1-YFP signal was weaker in mutant cells than control cells, making the number of traceable EB1-YFP comets an unreliable proxy for the number of polymerizing MTs. Second, it remains possible that MT phenotypes in *Bsg25D*$^{-/-}$ myotubes are masked by a redundantly acting factor. Though our negative data do not definitively rule out a role for endogenous Bsg25D in regulating MTs in muscle, the absence of clear MT phenotypes in *Bsg25D*$^{-/-}$ myotubes and myofibers leads us to favor the conclusion that Bsg25D functions in myonuclear positioning without playing a major role in MT regulation.

Ens and Bsg25D exhibit complex interactions

Our work reveals that Bsg25D and Ens work together in myonuclear positioning. It is not clear exactly where in the myotube they interact to promote myonuclear movement. In immunostained embryos, the most conspicuous Bsg25D signal in myotubes is in cytoplasmic puncta, which also stain positive for Ens. However, there is also a broad, low-level Bsg25D signal throughout the cytoplasm that our microscopy techniques cannot further resolve. Given that Ens coats MTs, it is plausible that Bsg25D interacts with Ens broadly on those structures. Indeed, studies have shown Bsg25D/Ninein interacting with the MT network as a cargo (Dammermann and Merdes, 2002; Moss et al., 2007), and a Bsg25D fragment has been shown to directly bind MTs in vitro (Kowanda et al., 2016).

In both myotubes and myofibers, co-overexpression of Ens relieves the myonuclear clustering caused by overexpression of Bsg25D. The mechanisms by which Bsg25D and Ens function likely differ between these two developmental stages. In embryonic myotubes, Bsg25D overexpression phenocopies the *ens* mutant phenotype, so inhibition of Ens by high levels of Bsg25D is sufficient to explain the nuclear positioning defects. However, the nuclear positioning phenotypes in mature larval myofibers caused by long-term overexpression of Bsg25D are more severe than those caused by loss of Ens; thus, inhibition of Ens is not a sufficient explanation for the Bsg25D-induced defects. We propose that Bsg25D causes nuclear positioning defects in larval myofibers through the combined effect of multiple mechanisms, including inhibition of Ens, inhibition of other proteins involved in myonuclear positioning such as Dynein, and disruption of MT organization. Co-overexpressed Ens then suppresses at least some of these Bsg25D activities, restoring normal nuclear positioning.

The finding that embryos with reduced maternal/zygotic *ens* and a total absence of *Bsg25D* fail to survive to larval stages demonstrates that critical Bsg25D–Ens interactions occur outside of the muscle as well. Evidence from the literature raises the possibility that they interact in the female germline, as groups have separately reported overlapping localization patterns for Bsg25D and Ens proteins, with both found at the anterior pole of the developing oocyte during midoogenesis (Sung et al., 2008; Kowanda et al., 2016). Moreover, misexpression of *Bsg25D* and loss of function of *ens* cause common phenotypes: reductions in Dynein and Gurken at the posterior pole and anterior-dorsal corner of the oocyte, respectively, and resulting embryos lacking dorsal appendages (Sung et al., 2008; Kowanda et al., 2016). Thus, it may be the case that forced expression of Bsg25D binds and disrupts endogenous Ens in the female germline as it does in muscle.

Centrosomal proteins participate in myonuclear movement

We find that in addition to Bsg25D, a second centrosomal protein, Plp (the *Drosophila* Pericentrin homologue), is involved in myonuclear positioning. The function of centrosomal proteins in muscle, which lacks centrosomes, has been unclear. Our work suggests that a general function of centrosomal proteins in muscle is to position myonuclei. This hypothesis is supported by the recent finding that the centrosomal protein PCM-1 is required for myonuclear positioning in C2C12 myotubes (Espigat-Georger et al., 2016). These findings underscore the conservation of mechanisms regulating nuclear movement and muscle organization. It is intriguing that although Bsg25D and Plp colocalize in myotubes, and each participates in myonuclear positioning, loss of *Bsg25D* does not enhance myonuclear positioning defects in *plp* mutants. It may be the case that the two proteins ultimately contribute to myonuclear positioning via separate pathways.

Model

We propose that endogenous Bsg25D positively regulates Ens in a manner dependent on their physical interaction (Fig. 8). The critical interaction could either be at Bsg25D–Ens cytoplasmic puncta or on Ens-coated MTs. Bsg25D could conceivably promote Ens activity by affecting its protein levels, subcellular localization, access to binding partners, or posttranslational modification, or by other means. In our model, embryos with the full complement of *ens* have enough Ens activity to withstand loss of the activator Bsg25D without showing diminished myonuclear movement. However, in embryos where Ens activity is limited by loss of one allele of *ens*, loss of Bsg25D further reduces Ens activity and perturbs myonuclear movement.

When Bsg25D is present at high concentrations in myotubes, it confers severe nuclear positioning phenotypes through its interactions with Ens (Fig. 8 B). Overexpressed Bsg25D forms puncta that recruit endogenous Ens away from its normal localization on MTs, leading to a block in Ens-dependent myonuclear movement toward the muscle poles. In myofibers, these Bsg25D- and Ens-positive puncta serve as ectopic MTOCs. MTs are lost from the nuclear envelope, possibly because necessary factors are recruited to the ectopic MTOCs. Nuclei are mispositioned, in part due to altered MT organization, and muscle function is decreased.

Conclusion

We have identified *Drosophila* Bsg25D as a novel Ens interactor and shown that it functions with Ens in myonuclear positioning. We have found that overexpressed Bsg25D blocks myonuclear movements in embryonic myotubes and that sustained Bsg25D overexpression disrupts both myonuclear positioning and MT organization in mature larval myofibers; nuclear positioning defects in embryos and larvae are rescued by cooverexpression of Ens. Thus, Bsg25D–Ens interactions are critical for myonuclear positioning and muscle development. The human homologues of the two proteins have important functions that are illustrated by their association with disease; loss of Ninein causes Seckel syndrome (Dauber et al., 2012), while high levels of MAP7 are associated with types of colon cancer and leukemia (Blum et al., 2008; Fu et al., 2016). The use of model systems to investigate how gain and loss of Ninein/Bsg25D and Ens/MAP7 affect cells in vivo will lend insights to human health.

Materials and methods

Drosophila genetics

Standard *Drosophila* genetics were performed at 25°C. The following stocks were used: *apterous$_{ME}$-NLS::dsRed* (Richardson et al., 2007), *ens^{swo}* (Metzger et al., 2012), *Df-ens$^{\Delta 3277}$* (Sung et al., 2008), khc^{8} (Brendza et al., 1999), *dhc$^{4-19}$* (Gepner et al., 1996), *plp^{5}* (Martinez-Campos et al., 2004), *Dmef2-Gal4* (Ranganayakulu et al., 1998), *rP298-Gal4* (Menon and Chia, 2001), *ubiquitin-Gal4[3xP3-GFP]* (Baena-Lopez et al., 2013), *UAS-Ens-HA* (Metzger et al., 2012), *UAS-2xEGFP* (Halfon et al., 2002), *UAS-EB1-YFP* (Bulgakova et al., 2013), and *patronin$^{\Delta 2}$* (gift from M. Gonzalez-Gaitan, University of Geneva, Geneva, Switzerland). *w^{1118}* (3605), *yw* (1495), *UAS-Rab7.GFP* (42706), UASp-*GFP.Golgi* (30902), *UAS-GFP.KDEL* (9899), *Df(2L)BSC693* (26545), *Df(3L)BSC441* (24945), *hs-FLP, hs-SceI* (25679), *γ-tub23C^{A6-2}* (5728), and *γ-tub23C^{A14-9}* (7041) were obtained from the Bloomington Drosophila Stock Center. P3-83 containing BAC clone CH321-49G22, referred to in the text as *BAC[Bsg25D+]*, was obtained from Gene-

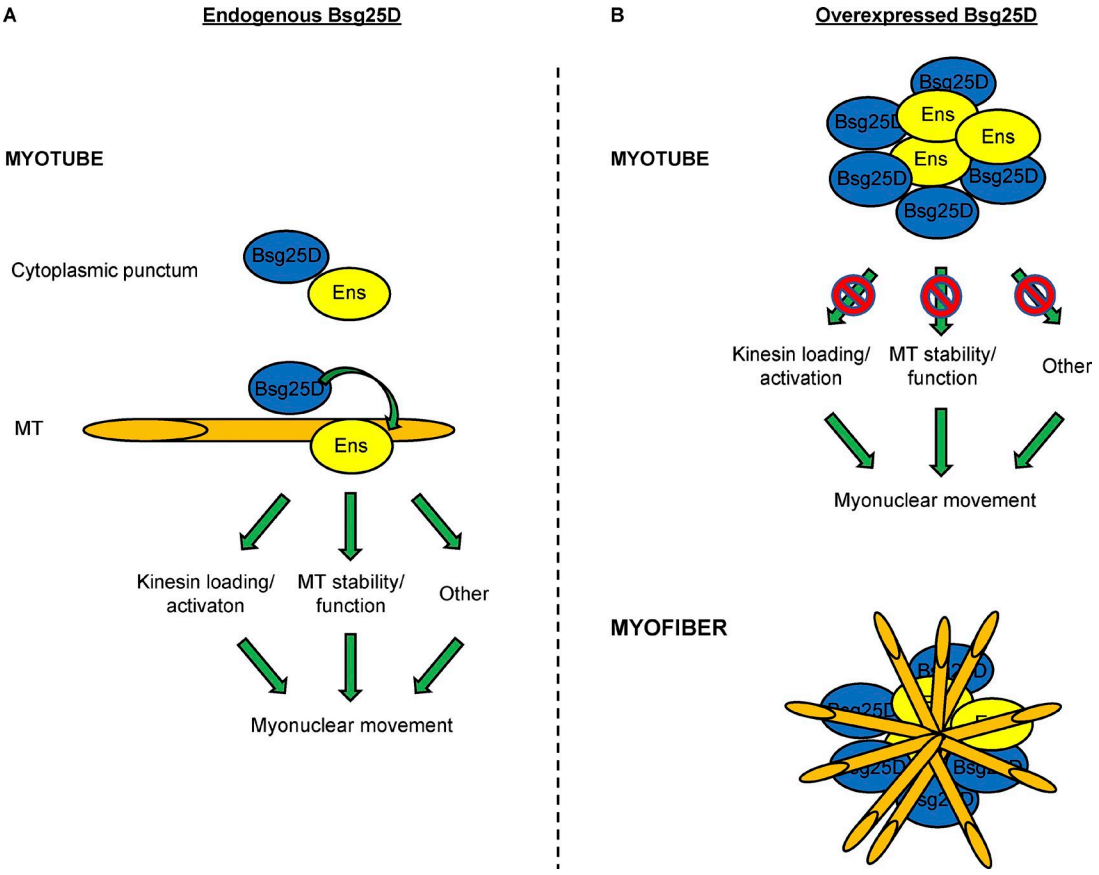


Figure 8. **Model of Bsg25D–Ens interactions. (A)** Model of the Bsg25D–Ens interaction in wild-type myotubes. **(B)** Model of the Bsg25D–Ens interaction when Bsg25D is overexpressed. See Discussion for model details. Bsg25D, blue; Ens, yellow; MTs, orange.

tivision. The following lines were developed for this work (details below): *Bsg25D*^{null}, *UAS-eos::Bsg25D*, and *UAS-ens::EGFP*. *ens*^{swo} and *Df-ens*$^{\Delta 3277}$ homozygotes have the same nuclear positioning phenotype at stage 16 (data not shown). The *Df-ens*$^{\Delta 3277}$ allele was used for genetic interaction experiments with Bsg25D overexpression (the three rightmost panels in Fig. 3 A). All other experiments with *ens* mutants used the *ens*^{swo} allele.

Generation of mutant and transgenic *Drosophila* stocks

Bsg25D^{null} (referred to in this work as *Bsg25D*$^{-/-}$) flies were generated by accelerated homologous recombination without CRISPR/Cas9 (Baena-Lopez et al., 2013). Homology arms 5′ and 3′ of *Bsg25D* were PCR amplified and sequentially cloned into pTV^{Cherry} (gift from J.P. Vincent, Francis Crick Institute, London, UK). The following primers, containing the indicated restriction enzyme sites, were used: 5p homology arm: 5p forward NheI, 5′-GATCGC TAGCAGCCATTCGCCTCGCTCTTC-3′; 5p reverse KpnI, 5′-GATCGG TACCGCTGCCGTTCCAATCGATCG-3′; 3p homology arm: 3p forward BglII, 5′-GATCAG-ATCTGACAAACCTGAGGAGGGAGT-3′; 3p reverse AvrII, 5′-GATCCCTAGGCGTAGAAAGGGTAGAAATAT-3′.

The pTV^{Cherry}-Bsg25D donor cassette was then randomly integrated in *w*^{1118} flies by p-element transformation (Genetic Services, Inc.). Potential transgenic flies were screened for by mini-white expression, and a third chromosome transgenic line was obtained. Following the published accelerated homologous recombination cross scheme (Baena-Lopez et al., 2013), 14 putative mutant lines were recovered. One was validated as *Bsg25D*^{null} by PCR using primers designed to amplify genomic regions specific to either wild-type or mutant chromosomes, followed by sequencing. The *Bsg25D*$^{-/-}$ line used in this study had the mini w+ cassette inserted between bp334 in the Bsg25D 5′ UTR and bp5919 at the beginning of the Bsg25D 3′ UTR based on the published FLYBASE Bsg25D genomic sequence, leading to the removal of all protein coding sequences and, as a result, all protein isoforms (Fig. 2 A). The following PCR primers were used for mutant verification: wild-type-specific *Bsg25D*: 1537 forward, 5′-ACAATACGGACGAGGACCAG-3′; 3907 reverse, 5′-TTCCTTTGC AGCCTTGAGTT-3′; mutant-specific *Bsg25D* pair 1: 7224 forward, 5′-GAGTTGCTGTTGCTGCAGAG-3′; 11081 reverse, 5′-TTGACCTCA GCGTCGTAGTG-3′; mutant-specific *Bsg25D* pair 2: 7326 forward, 5′-TGAAGATACCCCACCAAACC-3′; 10289 reverse, 5′-GCGCAC TCAGCAAAACATTA-3′. Mutant flies were confirmed by Western blotting for Bsg25D multiple times with biological replicates.

UAS-eos::Bsg25D (referred to in this paper as *UAS-Bsg25D*) flies were generated as follows: *Eos* was amplified from pME-eos (gift from D. Raible, University of Washington, Seattle, WA) using the following forward and reverse primers containing restriction sites for NotI and XhoI, respectively: F_NotI_eos_NotI, 5′-CAC CGCGGCCGCATGAGTGCGATTAAGCCAGACATG-3′; R_XhoI_eos_ no_stop_XhoI, 5′-CTCGAGTCGTCTGGCATTGTCAGGCAATCC-3′. The PCR product was cloned into pUAST. Next, *Bsg25D* was amplified from expressed sequence tag clone LD21844 (Drosophila

Genome Resource Center [DGRC]), corresponding to transcript Bsg25D-PB, and cloned into pUAST-eos in frame with the N-terminal Eos. The following primers, both containing *Kpn*I restriction sites, were used for PCR: F-CACC-KpnI-Bsg25D, 5′-CACCGG TACCATGGAGGTATCCGCCGATCCGTAC-3′; R-KpnI-stop-Bsg25D, 5′-GGTACCCTAAGGCATGCCAGGCAGTCCACC-3′. pUAS-eos::Bsg25D was randomly integrated in w1118 flies by p-element transformation (Genetic Services, Inc.). Potential transgenic flies were selected by mini-white expression. The eos::Bsg25D line was used for all fly studies on overexpressed Bsg25D.

UAS-ens::EGFP flies were generated as follows. Full-length *ens* (LD09626; DGRC) was PCR-amplified using the following primers containing EcoRI and BamHI restriction sites, respectively: 5′-GAATTCATGGCGAGTCTTGGGGGCCAACAC-3′ and 5′-GGATCCCAGCAGCGATATATCTTTATTTTCGTG-3′. The PCR product was cloned into pUAST (DGRC) previously modified to contain a C-terminal EGFP tag. pUAS-Ens::EGFP was randomly integrated in w1118 flies by p-element transformation (Best Gene, Inc.), and potential transgenic flies were screened for by mini-white expression.

Protein sequence analysis

Bsg25D protein sequence analysis was performed by InterProScan, which identifies domains by scanning protein sequences against predictive models provided by several different databases (Jones et al., 2014). Alignment of Bsg25D to mouse Ninein was done using the Blastp algorithm (National Center for Biotechnology Information).

Viability assays

Viability assays were done at 25°C essentially as previously described (Schulman et al., 2014). For comparison of GFP- and Bsg25D-overexpressing flies, embryos were bleached and selected at stage 16. For other viability assays, embryos were selected without bleaching under halocarbon oil at stage 5. In all cases, a minimum of 100 embryos were selected over multiple days. The number of hatched and unhatched embryos was counted, and all first-instar larvae were transferred to a vial with fresh food. The number of pupae and adults that eclosed was assessed. Viability is represented as a percentage of the initial number of embryos.

Fluorescent antibody staining

Embryos were prepared for staining as previously described (Richardson et al., 2007). Larvae were dissected and flat mounted in HL3.1 dissecting buffer and fixed for 20 min in formalin. Embryos and larvae were incubated in primary antibody overnight at 4°C or for 1 h at room temperature at the following concentrations: rat anti-Tropomyosin (1:500; Abcam), rabbit anti-DsRed (1:400; Clontech), chicken anti-GFP (1:500; Abcam), mouse anti-α-Tubulin (1:500; Sigma), mouse anti-acetylated α-Tubulin (1:50; Santa Cruz Biotechnology), mouse anti-γ Tubulin clone GTU-88 (1:500; Sigma), guinea pig anti-Bsg25D (Iampietro et al., 2014; 1:400; gift from E. Lecuyer, Montreal Clinical Research Institute [IRCM], Montreal, Canada), rat anti-Ens (1:100; gift from P. Rorth, University of Copenhagen, Copenhagen, Denmark), rabbit anti-Plp (gift from J. Raff, University of Oxford, Oxford, UK), rabbit anti-Arl8 (1:100; Developmental Studies Hybridoma Bank), and mouse anti-SUMO-2 8A2 (1:50; Developmental Studies Hybridoma Bank). Overexpressed eos::Bsg25D was detected either by Bsg25D antibody staining or by Eos signal. For both embryo and larva staining, Alexa Fluor 488–, Alexa Fluor 555–, and Alexa Fluor 647–conjugated secondary antibodies (Invitrogen) were applied 1:400 for 1 h at room temperature. Hoechst and Alexa Fluor-conjugated phalloidin (either Alexa Fluor 488 or Alexa Fluor 555; Life Technologies) were added with the secondary antibody at 1:400 and 1:200, respectively. Samples were mounted in ProLong Gold antifade reagent (Invitrogen).

Fixed sample imaging and analysis

Z-stacks of fixed samples were acquired using a Leica SP5 laser-scanning confocal microscope equipped with the LAS AF software using a 63× 1.4 NA HCX PL Apochromat oil objective and processed in Volocity (Perkin Elmer) or ImageJ (National Institutes of Health). For analysis of nuclear positioning at stage 16, the Line function in ImageJ was used to measure the distances from the dorsal-most nucleus to the dorsal myotube pole, the ventral-most nucleus to the ventral myotube pole, and the total myotube length. "Nuclear spread" was calculated by subtracting the first two values from the third and expressing the difference as a percentage of total myotube length. For statistical purposes, the mean of the four lateral transverse muscles in a hemisegment was considered one sample. Nuclear positioning data were collected from a maximum of four hemisegments (abdominal hemisegments 2–5) per embryo. Embryos were fixed over the course of multiple days and then pooled for staining and analysis. Myonuclear positioning in the ventral longitudinal (VL) 4 muscle of third-instar larvae was also assessed using the Line function in ImageJ. "Nearest neighbor" was defined as the distance between a nucleus and the nearest neighboring nucleus. "Largest gap" refers to the longest stretch of muscle fiber void of myonuclei, and internuclear distance refers to the distance between consecutive myonuclei along the longitudinal muscle axis. All three terms are presented as percentages of muscle length. Statistical analysis of nuclear positioning in larval muscles employed weighted averages to account for different numbers of myofibers analyzed for each larva. *n* refers to the total number of myofibers. MT density was calculated by measuring the intensity of Tubulin and Tropomyosin near the tips of the muscles, essentially as published (Folker et al., 2012). For statistics, the average of Tubulin/Tropomyosin ratios from multiple cells in the same embryo was considered one sample. Student's *t* tests were performed using Prism software or Excel. Analysis of Ens and Phalloidin signal intensities in embryonic VL myotubes were performed in essentially the same fashion from single slices of confocal stacks.

Time-lapse imaging and analysis

Embryos to be subjected to time-lapse imaging of myonuclear movements were prepared as reported previously (Folker et al., 2012). Embryos were bleached for 4 min, rinsed and mounted in halocarbon oil on a custom-made slide with an air-permeable membrane, and covered with a glass coverslip. Time-lapse series of myonuclear movements were acquired on a Zeiss LSM 700 equipped with the ZEN software and using a Plan-Apochromatic 20×/0.8 M27 objective with 1.7× optical zoom. Stacks were

acquired every 3 min for 1 h at 25°C. The line function in ImageJ was used to measure distance between clusters. To calculate Δ nuclear spread, the distance from the dorsal-most nucleus to the ventral-most nucleus in a cell at the beginning of the time-lapse series was subtracted from the same parameter at the end of the series. The difference was then divided by time elapsed to yield Δ nuclear spread, measured in micrometers per hour. Student's *t* tests and correlation analysis were performed using Prism software. F-tests were performed in Excel.

Embryos to be used for EB1-YFP analysis were prepared and mounted as above. Time-lapse series of EB1-YFP comets in the tips of stage 16 lateral transverse muscles were acquired on a Leica TCS SP8 confocal microscope at 25°C using the HCX PL APO 63×/1.30 glycerol lens with 40× optical zoom using the Leica proprietary software. Comets were recorded from 19 cells (control) and 26 cells (*Bsg25D*$^{-/-}$). Z-stacks consisted of ∼10 slices with a step size of 400 nm; stacks were acquired without intervals (i.e., nonstop) at a frame rate of ∼23 frames per second for ∼90 s. Time-lapse datasets were deconvolved by a blind deconvolution algorithm in Autoquant X3 software (Media Cybernetics). EB1-YFP comets were manually tracked in three dimensions using Imaris (Bitplane). For each EB1-YFP comet, the displacement distance between its position in the first and last frames of its run was exported and divided by the time elapsed to determine EB1-YFP comet speed. EB1-YFP speed was compared between groups by Student's *t* test.

Cell culture, coimmunoprecipitation, and Western blotting

For *Drosophila* S2 cell expression studies, pUAS-3xHA::Bsg25D was generated as follows. Full-length *Bsg25D* (LD21844; DGRC) was PCR amplified using the following primers: 5′-CACCATGGAGGTATCCGCGATCCGTAC-3′ and 5′-CTAAGGCATGCCAGGCAGTCCACC-3′. The amplicon was TOPO cloned into pENTR (Life Technologies) and then Gateway cloned using LR Clonase (Life Technologies) into pTHW (DGRC), which contains a UAS followed by an N-terminal 3xHA tag. The generation of pUAS-Ens::EGFP is described above (in Generation of mutant and transgenic *Drosophila* stocks), as the same plasmid was used for transforming flies and driving expression in S2 cells.

Experiments in S2 cells were performed to validate a physical interaction between Ens and Bsg25D detected in a yeast two-hybrid screen previously described (Metzger et al., 2012). S2 cells were cultured in Schneider's media plus 10% FBS using standard procedures. Protein expression was achieved by transfecting a plasmid expressing Gal4 from a constitutively active promoter (Ubiquitin-Gal4) along with pUAS-3xHA::Bsg25D and pUAS-Ens-EGFP or pUAS-3xHA::Bsg25D and pUAS-2xEGFP. Transfections used Effectene (QIAGEN). Cells were lysed 2 d after transfection in lysis buffer (150 mM NaCl, 2 mM MgOAc, 20 mM Tris, pH 7.5, 5% glycerol, 0.5% NP-40, 2 mM DTT, and one Complete Mini tab [Roche]). Following centrifugation, lysate supernatant was collected and protein concentration was determined by Bradford assay (Bio-Rad). 400 µg lysate was incubated with Protein G-Agarose beads overnight at 4°C using rabbit anti-GFP (Torrey Pines Biolab) or rabbit anti-IgG (Santa Cruz Biotechnology) for mock immunoprecipitation controls. Following incubation, beads were washed four times with lysis buffer and boiled in 4× Laemmli buffer. Proteins released from beads and 40 µg (10%) inputs were then subjected to SDS-PAGE, transferred overnight to polyvinylidene difluoride membrane, and blotted with rat anti-HA (Roche), secondary stained at 1:5,000 with anti-rat HRP (Jackson ImmunoResearch), and detected with chemiluminescence (Denville Scientific). Membranes were then stripped according to standard practices and reblotted with mouse anti-GFP antibody (Roche) and HRP-conjugated anti-mouse secondary antibody (Jackson ImmunoResearch) and then developed. Coimmunoprecipitation between 3xHA::Bsg25D and Ens-GFP was demonstrated with multiple biological replicates.

To compare Bsg25D protein expression in control and *Bsg25D*$^{-/-}$ genotypes, *w*^{1118} and *Bsg25D*$^{-/-}$ third-instar larvae were dissected in HL3.1 relaxing buffer. The intestines of the larvae were removed, and the resultant pelts were lysed in lysis buffer (recipe above). Following Bradford determination of protein concentration (Bio-Rad), 80 µg lysate per genotype was loaded on a 7.5% SDS-PAGE protein gel. The gel was transferred to nitrocellulose membrane overnight, blocked with 5% milk (for Bsg25D) or 5% BSA (for GAPDH) in TBS-Tween, and blotted overnight with guinea pig anti-Bsg25D antibody (1:1,000; gift from E. Lecuyer) or mouse anti-GAPDH primary antibody (1:10,000; Abcam). HRP-conjugated secondary antibodies against guinea pig (1:5,000; Jackson ImmunoResearch) or mouse (1:5,000; Jackson ImmunoResearch) were applied before development by chemiluminescence (Kindle Biosciences).

AFM

Larvae were dissected in HL3.1 dissecting buffer and fixed in formalin for 10 min before microscopy. Bright-field images of *Drosophila* larvae, for determination of location of stiffness measurements, were acquired using an inverted microscope (Axio Observer Z1; Zeiss) as the AFM base (LD Plan-Neofluar 20×/0.4 objective). An Asylum Research MFP-3D-BIO Atomic Force Microscope was used to collect force maps from the *Drosophila* larvae tissue. A CP CONT-PS-C (NanoAndMore.com) probe with a 6.1-µm polystyrene bead was used for all measurements. The Asylum Research GetReal calibration method was used for the determination of the spring constant (0.2 N/m). Each force map sampled a 20 × 20-µm to 40 × 40-µm region, depending on muscle width, in a 10 × 10-grid under fluid conditions (PBS). The trigger point was set to 50 nN with an approach velocity of 10 µm/s. The force-indentation curves were fit to the Hertz model for spherical tips using Asylum Research Software to determine the Young's modulus, with an assumed Poisson's ratio value of 0.45 for the sample (Chen et al., 1996). For each genotype, at least three larvae were used; from each larva, at least 400 individual measurements, corresponding to four different muscles, were taken. Force maps of stiffness along with individual stiffness values for each measured point were then exported from Asylum Research Software for analysis. For statistics, the average of all the measurements from a single muscle was considered one sample.

Larval motility assays

Laval motility assays were performed essentially as previously described, either by using a charge-coupled device camera and

Ethovision software (Noldus) to record third-instar larvae crawling and automatically calculate crawling speed (Metzger et al., 2012) or by placing larvae at the center of an apple juice plate surrounded by zones defined by concentric circles and observing which zone they reached in 30 s of crawling at 25°C (Fernandes and Schock, 2014). A minimum of 47 larvae per genotype were used. In all cases, data were acquired over multiple days. P values were calculated by Student's *t* test.

Online supplemental material

Fig. S1 shows the subcellular localization of Bsg25D puncta in developing myotubes. Fig. S2 shows *Bsg25D*$^{-/-}$ viability and larval motility data. Fig.S3 shows myonuclear positioning in *Bsg25D*$^{-/-}$;*ens*$^{-/-}$ myotubes and the lack of genetic interactions between *Bsg25D* and *Khc* or *Dhc*. Fig. S4 shows the effects of Bsg25D overexpression on myonuclear clusters. Fig. S5 shows that overexpressed Bsg25D colocalizes with SUMO-2 in myonuclei. Videos show nuclear movements in control (Video 1), *Bsg25D*$^{-/-}$ (Video 2), *Bsg25D*$^{-/-}$;*ens*$^{-/+}$ (Video 3), Bsg25D overexpression (Video 4), and Ens overexpression (Video 5). Videos 6 and 7 show control and *Bsg25D*$^{-/-}$ EB1-YFP comets, respectively.

Acknowledgments

We thank Eric Lecuyer, Jordan Raff, Pernille Rorth, and the Developmental Studies Hybridoma Bank for antibodies; J.P. Vincent, David Raible, and the DGRC, supported by National Institutes of Health grant 2P40OD010949-10A1, for plasmids; and Marcos Gonzalez-Gaitan, Pernille Rorth, J.P. Vincent, and the Bloomington Stock Center for flies. We also thank Cyrille Alexandre for providing technical advice on the generation of the *Bsg25D*^{null} mutant; members of the Baylies Lab for helpful discussion; and Jennifer Zallen, Kari Lenhart, and Jodi Schottenfeld-Roames for critical reading of the manuscript.

This work was supported by Portuguese Science and Technology Foundation grant SFRH/BD/52041/2012 (to M. Azevedo), National Institutes of Health, National Institute of General Medical Sciences grant GM078318 and National Institute of Arthritis and Musculoskeletal and Skin Diseases grant AR108981 (to M.K. Baylies), and National Cancer Institute Core Grant P30 CA 008748 (to Memorial Sloan Kettering Cancer Center). The funders had no role in the study design, data collection and analysis, decision to publish, or preparation of the manuscript.

The authors declare no competing financial interests.

Author contributions: J.N. Rosen and M.K. Baylies designed the study. J.N. Rosen and M. Azevedo performed the experiments with the help of D.B. Soffar (Western analysis, fly stocks), V.P. Boyko (EB1 tracking experiments), M.B. Brendel (AFM microscopy), and V.K. Schulman (initial training in assessing nuclear position). J.N. Rosen, M. Azevedo, and M.K. Baylies analyzed the data. J.N. Rosen and M.K. Baylies wrote the paper, and all authors participated in generating the final version of the paper.

Submitted: 30 August 2018
Revised: 26 November 2018
Accepted: 28 November 2018

References

Abal, M., M. Piel, V. Bouckson-Castaing, M. Mogensen, J.B. Sibarita, and M. Bornens. 2002. Microtubule release from the centrosome in migrating cells. *J. Cell Biol.* 159:731–737. https://doi.org/10.1083/jcb.200207076

Baena-Lopez, L.A., C. Alexandre, A. Mitchell, L. Pasakarnis, and J.-P. Vincent. 2013. Accelerated homologous recombination and subsequent genome modification in Drosophila. *Development.* 140:4818–4825. https://doi.org/10.1242/dev.100933

Bagshaw, R.D., J.W. Callahan, and D.J. Mahuran. 2006. The Arf-family protein, Arl8b, is involved in the spatial distribution of lysosomes. *Biochem. Biophys. Res. Commun.* 344:1186–1191. https://doi.org/10.1016/j.bbrc.2006.03.221

Barlan, K., W. Lu, and V.I. Gelfand. 2013. The microtubule-binding protein ensconsin is an essential cofactor of kinesin-1. *Curr. Biol.* 23:317–322. https://doi.org/10.1016/j.cub.2013.01.008

Blum, C., A. Graham, M. Yousefzadeh, J. Shrout, K. Benjamin, M. Krishna, R. Hoda, R. Hoda, D.J. Cole, E. Garrett-Mayer, et al. 2008. The expression ratio of Map7/B2M is prognostic for survival in patients with stage II colon cancer. *Int. J. Oncol.* 33:579–584. https://doi.org/10.3892/ijo_00000043

Bouckson-Castaing, V., M. Moudjou, D.J. Ferguson, S. Mucklow, Y. Belkaid, G. Milon, and P.R. Crocker. 1996. Molecular Characterisation of Ninein, a New Coiled-Coil Protein of the Centrosome. *J. Cell Sci.* 109:179–190.

Brand, A.H., and N. Perrimon. 1993. Targeted gene expression as a means of altering cell fates and generating dominant phenotypes. *Development.* 118:401–415. https://doi.org/10.1101/lm.1331809

Brendza, K.M., D.J. Rose, S.P. Gilbert, and W.M. Saxton. 1999. Lethal kinesin mutations reveal amino acids important for ATPase activation and structural coupling. *J. Biol. Chem.* 274:31506–31514. https://doi.org/10.1074/jbc.274.44.31506

Bulgakova, N.A., I. Grigoriev, A.S. Yap, A. Akhmanova, and N.H. Brown. 2013. Dynamic microtubules produce an asymmetric E-cadherin-Bazooka complex to maintain segment boundaries. *J. Cell Biol.* 201:887–901. https://doi.org/10.1083/jcb.201211159

Casenghi, M., F.A. Barr, and E.A. Nigg. 2005. Phosphorylation of Nlp by Plk1 negatively regulates its dynein-dynactin-dependent targeting to the centrosome. *J. Cell Sci.* 118:5101–5108. https://doi.org/10.1242/jcs.02622

Chen, C.T., H. Hehnly, Q. Yu, D. Farkas, G. Zheng, S.D. Redick, H.F. Hung, R. Samtani, A. Jurczyk, S. Akbarian, et al. 2014. A unique set of centrosome proteins requires pericentrin for spindle-pole localization and spindle orientation. *Curr. Biol.* 24:2327–2334. https://doi.org/10.1016/j.cub.2014.08.029

Chen, E.J., J. Novakofski, W.K. Jenkins, and W.D. O'Brien. 1996. Young's Modulus Measurements of Soft Tissues with Application to Elasticity Imaging. *IEEE Trans. Ultrason. Ferroelectr. Freq. Control.* 43:191–194. https://doi.org/10.1109/58.484478

Cheng, T.S., L.K. Chang, S.L. Howng, P.J. Lu, C.I. Lee, and Y.R. Hong. 2006. SUMO-1 modification of centrosomal protein hNinein promotes hNinein nuclear localization. *Life Sci.* 78:1114–1120. https://doi.org/10.1016/j.lfs.2005.06.021

Collinsworth, A.M., S. Zhang, W.E. Kraus, and G.A. Truskey. 2002. Apparent elastic modulus and hysteresis of skeletal muscle cells throughout differentiation. *Am. J. Physiol. Cell Physiol.* 283:C1219–C1227. https://doi.org/10.1152/ajpcell.00502.2001

Dammermann, A., and A. Merdes. 2002. Assembly of centrosomal proteins and microtubule organization depends on PCM-1. *J. Cell Biol.* 159:255–266. https://doi.org/10.1083/jcb.200204023

Dauber, A., S.H. Lafranchi, Z. Maliga, J.C. Lui, J.E. Moon, C. McDeed, K. Henke, J. Zonana, G.A. Kingman, T.H. Pers, et al. 2012. Novel microcephalic primordial dwarfism disorder associated with variants in the centrosomal protein ninein. *J. Clin. Endocrinol. Metab.* 97:E2140–E2151. https://doi.org/10.1210/jc.2012-2150

Delgehyr, N., J. Sillibourne, and M. Bornens. 2005. Microtubule nucleation and anchoring at the centrosome are independent processes linked by ninein function. *J. Cell Sci.* 118:1565–1575. https://doi.org/10.1242/jcs.02302

Elhanany-Tamir, H., Y.V. Yu, M. Shnayder, A. Jain, M. Welte, and T. Volk. 2012. Organelle positioning in muscles requires cooperation between two KASH proteins and microtubules. *J. Cell Biol.* 198:833–846. https://doi.org/10.1083/jcb.201204102

Espigat-Georger, A., V. Dyachuk, C. Chemin, L. Emorine, and A. Merdes. 2016. Nuclear alignment in myotubes requires centrosome proteins recruited by nesprin-1. *J. Cell Sci.* 129:4227–4237. https://doi.org/10.1242/jcs.191767

Fernandes, I., and F. Schock. 2014. The nebulin repeat protein Lasp regulates I-band architecture and filament spacing in myofibrils. *J. Cell Biol.* 206:559–572. https://doi.org/10.1083/jcb.201401094

Folker, E.S., and M.K. Baylies. 2013. Nuclear positioning in muscle development and disease. *Front. Physiol.* 4:363. https://doi.org/10.3389/fphys.2013.00363

Folker, E.S., V.K. Schulman, and M.K. Baylies. 2012. Muscle length and myonuclear position are independently regulated by distinct Dynein pathways. *Development.* 139:3827–3837. https://doi.org/10.1242/dev.079178

Folker, E.S., V.K. Schulman, and M.K. Baylies. 2014. Translocating myonuclei have distinct leading and lagging edges that require kinesin and dynein. *Development.* 141:355–366. https://doi.org/10.1242/dev.095612

Fu, L., H. Fu, L. Zhou, K. Xu, Y. Pang, K. Hu, J. Wang, L. Tian, Y. Liu, J. Wang, et al. 2016. High expression of MAP7 predicts adverse prognosis in young patients with cytogenetically normal acute myeloid leukemia. *Sci. Rep.* 6:34546. https://doi.org/10.1038/srep34546

Gallaud, E., R. Caous, A. Pascal, F. Bazile, J.P. Gagné, S. Huet, G.G. Poirier, D. Chrétien, L. Richard-Parpaillon, and R. Giet. 2014. Ensconsin/Map7 promotes microtubule growth and centrosome separation in Drosophila neural stem cells. *J. Cell Biol.* 204:1111–1121. https://doi.org/10.1083/jcb.201311094

Gepner, J., M. Li, S. Ludmann, C. Kortas, K. Boylan, S.J. Iyadurai, M. McGrail, and T.S. Hays. 1996. Cytoplasmic dynein function is essential in Drosophila melanogaster. *Genetics.* 142:865–878.

Guerin, C.M., and S.G. Kramer. 2009. RacGAP50C directs perinuclear gamma-tubulin localization to organize the uniform microtubule array required for Drosophila myotube extension. *Development.* 136:1411–1421. https://doi.org/10.1242/dev.031823

Gundersen, G.G., and J.H. Worman. 2013. Nuclear positioning. *Cell.* 152:1376–1389. https://doi.org/10.1016/j.cell.2013.02.031

Halfon, M.S., S. Gisselbrecht, J. Lu, B. Estrada, H. Keshishian, and A.M. Michelson. 2002. New fluorescent protein reporters for use with the Drosophila Gal4 expression system and for vital detection of balancer chromosomes. *Genesis.* 34:135–138. https://doi.org/10.1002/gene.10136

Hammonds, A.S., C.A. Bristow, W.W. Fisher, R. Weiszmann, S. Wu, V. Hartenstein, M. Kellis, B. Yu, E. Frise, and S.E. Celniker. 2013. Spatial expression of transcription factors in Drosophila embryonic organ development. *Genome Biol.* 14:R140. https://doi.org/10.1186/gb-2013-14-12-r140

Hofmann, I., and S. Munro. 2006. An N-terminally acetylated Arf-like GTPase is localised to lysosomes and affects their motility. *J. Cell Sci.* 119:1494–1503. https://doi.org/10.1242/jcs.02958

Iampietro, C., J. Bergalet, X. Wang, N.A. Cody, A. Chin, F.A. Lefebvre, M. Douziech, H.M. Krause, and E. Lécuyer. 2014. Developmentally regulated elimination of damaged nuclei involves a Chk2-dependent mechanism of mRNA nuclear retention. *Dev. Cell.* 29:468–481. https://doi.org/10.1016/j.devcel.2014.03.025

Jones, P., D. Binns, H.Y. Chang, M. Fraser, W. Li, C. McAnulla, H. McWilliam, J. Maslen, A. Mitchell, G. Nuka, et al. 2014. InterProScan 5: genome-scale protein function classification. *Bioinformatics.* 30:1236–1240. https://doi.org/10.1093/bioinformatics/btu031

Kerr, J.P., P. Robison, G. Shi, A.I. Bogush, A.M. Kempema, J.K. Hexum, N. Becerra, D.A. Harki, S.S. Martin, R. Raiteri, et al. 2015. Detyrosinated microtubules modulate mechanotransduction in heart and skeletal muscle. *Nat. Commun.* 6:8526. https://doi.org/10.1038/ncomms9526

Kowanda, M., J. Bergalet, M. Wieczorek, G. Brouhard, É. Lécuyer, and P. Lasko. 2016. Loss of function of the Drosophila Ninein-related centrosomal protein Bsg25D causes mitotic defects and impairs embryonic development. *Biol. Open.* 5:1040–1051. https://doi.org/10.1242/bio.019638

Manhart, A., S. Windner, M. Baylies, and A. Mogilner. 2018. Mechanical positioning of multiple nuclei in muscle cells. *PLOS Comput. Biol.* 14:e1006208. https://doi.org/10.1371/journal.pcbi.1006208

Martinez-Campos, M., R. Basto, J. Baker, M. Kernan, and J.W. Raff. 2004. The Drosophila pericentrin-like protein is essential for cilia/flagella function, but appears to be dispensable for mitosis. *J. Cell Biol.* 165:673–683. https://doi.org/10.1083/jcb.200402130

Menon, S.D., and W. Chia. 2001. Drosophila rolling pebbles: a multidomain protein required for myoblast fusion that recruits D-Titin in response to the myoblast attractant Dumbfounded. *Dev. Cell.* 1:691–703. https://doi.org/10.1016/S1534-5807(01)00075-2

Metzger, T., V. Gache, M. Xu, B. Cadot, E.S. Folker, B.E. Richardson, E.R. Gomes, and M.K. Baylies. 2012. MAP and kinesin-dependent nuclear positioning is required for skeletal muscle function. *Nature.* 484:120–124. https://doi.org/10.1038/nature10914

Mogensen, M., M.A. Malik, M. Piel, V. Bouckson-Castaing, and M. Bornens. 2000. Microtubule Minus-End Anchorage at Centrosomal and Non-Centrosomal Sites: The Role of Ninein. *J. Cell Sci.* 113:3013–3023.

Moss, D.K., G. Bellett, J.M. Carter, M. Liovic, J. Keynton, A.R. Prescott, E.B. Lane, and M.M. Mogensen. 2007. Ninein is released from the centrosome and moves bi-directionally along microtubules. *J. Cell Sci.* 120:3064–3074. https://doi.org/10.1242/jcs.010322

Nishimura, S., S. Nagai, M. Katoh, H. Yamashita, Y. Saeki, J. Okada, T. Hisada, R. Nagai, and S. Sugiura. 2006. Microtubules modulate the stiffness of cardiomyocytes against shear stress. *Circ. Res.* 98:81–87. https://doi.org/10.1161/01.RES.0000197785.51819.e8

Ranganayakulu, G., D.A. Elliott, R.P. Harvey, and E.N. Olson. 1998. Divergent roles for NK-2 class homeobox genes in cardiogenesis in flies and mice. *Development.* 125:3037–3048.

Richardson, B.E., K. Beckett, S.J. Nowak, and M.K. Baylies. 2007. SCAR/WAVE and Arp2/3 are crucial for cytoskeletal remodeling at the site of myoblast fusion. *Development.* 134:4357–4367. https://doi.org/10.1242/dev.010678

Romero, N.B. 2010. Centronuclear myopathies: a widening concept. *Neuromuscul. Disord.* 20:223–228. https://doi.org/10.1016/j.nmd.2010.01.014

Schulman, V.K., E.S. Folker, J.N. Rosen, and M.K. Baylies. 2014. Syd/JIP3 and JNK signaling are required for myonuclear positioning and muscle function. *PLoS Genet.* 10:e1004880. https://doi.org/10.1371/journal.pgen.1004880

Shinohara, H., N. Sakayori, M. Takahashi, and N. Osumi. 2013. Ninein is essential for the maintenance of the cortical progenitor character by anchoring the centrosome to microtubules. *Biol. Open.* 2:739–749. https://doi.org/10.1242/bio.20135231

Srivatsa, S., S. Parthasarathy, Z. Molnár, and V. Tarabykin. 2015. Sip1 downstream Effector ninein controls neocortical axonal growth, ipsilateral branching, and microtubule growth and stability. *Neuron.* 85:998–1012. https://doi.org/10.1016/j.neuron.2015.01.018

Stillwell, E.E., J. Zhou, and H.C. Joshi. 2004. Human ninein is a centrosomal autoantigen recognized by CREST patient sera and plays a regulatory role in microtubule nucleation. *Cell Cycle.* 3:923–930. https://doi.org/10.4161/cc.3.7.947

Sung, H.H., I.A. Telley, P. Papadaki, A. Ephrussi, T. Surrey, and P. Rørth. 2008. Drosophila ensconsin promotes productive recruitment of Kinesin-1 to microtubules. *Dev. Cell.* 15:866–876. https://doi.org/10.1016/j.devcel.2008.10.006

Tassin, A.M., B. Maro, and M. Bornens. 1985. Fate of microtubule-organizing centers during myogenesis in vitro. *J. Cell Biol.* 100:35–46. https://doi.org/10.1083/jcb.100.1.35

Tomancak, P., A. Beaton, R. Weiszmann, E. Kwan, S. Shu, S.E. Lewis, S. Richards, et al. 2002. Systematic Determination of Patterns of Gene Expression during Drosophila Embryogenesis. *Genome Biol.* 3:research0088.1. https://doi.org/10.1186/gb-2002-3-12-research0088

Tomancak, P., B.P. Berman, A. Beaton, R. Weiszmann, E. Kwan, V. Hartenstein, S.E. Celniker, and G.M. Rubin. 2007. Global analysis of patterns of gene expression during Drosophila embryogenesis. *Genome Biol.* 8:R145. https://doi.org/10.1186/gb-2007-8-7-r145

Tymanskyj, S.R., B. Yang, A. Falnikar, A.C. Lepore, and L. Ma. 2017. MAP7 Regulates Axon Collateral Branch Development in Dorsal Root Ganglion Neurons. *J. Neurosci.* 37:1648–1661. https://doi.org/10.1523/JNEUROSCI.3260-16.2017

Wang, S., D. Wu, S. Quintin, R.A. Green, D.K. Cheerambathur, S.D. Ochoa, A. Desai, and K. Oegema. 2015. NOCA-1 functions with γ-tubulin and in parallel to Patronin to assemble non-centrosomal microtubule arrays in C. elegans. *eLife.* 4:e08649. https://doi.org/10.7554/eLife.08649

Zhang, J., A. Felder, Y. Liu, L.T. Guo, S. Lange, N.D. Dalton, Y. Gu, K.L. Peterson, A.P. Mizisin, G.D. Shelton, et al. 2010. Nesprin 1 is critical for nuclear positioning and anchorage. *Hum. Mol. Genet.* 19:329–341. https://doi.org/10.1093/hmg/ddp499

Zheng, Y., V. Mennella, S. Marks, J. Wildonger, E. Elnagdi, D. Agard, and T.L. Megraw. 2016. The Seckel syndrome and centrosomal protein Ninein localizes asymmetrically to stem cell centrosomes but is not required for normal development, behavior, or DNA damage response in *Drosophila*. *Mol. Biol. Cell.* 27:1740–1752. https://doi.org/10.1091/mbc.e15-09-0655